

**REMOTE SENSING OF CROP LODGING: A
MULTI-SENSOR APPROACH**

Sugandh Chauhan

REMOTE SENSING OF CROP LODGING: A MULTI-SENSOR APPROACH

DISSERTATION

to obtain
the degree of doctor at the University of Twente,
on the authority of the rector magnificus,
Prof.dr. T.T.M. Palstra,
on account of the decision of the Doctorate Board
to be publicly defended
on Wednesday 11 November 2020 at 12.45 hrs

by

Sugandh Chauhan
born on 27 October 1991
in Bijnor, India

This dissertation has been approved by:

Supervisor

Prof.dr. A.D. Nelson

Co-supervisors

Dr. R. Darvishzadeh

Dr. M. Boschetti

Cover design: Sugandh Chauhan
ISBN: 90-978-365-5075-8
DOI: 10.3990/1.9789036550758
Dissertation no. 386

© 2020 Sugandh Chauhan, The Netherlands. All rights reserved. No parts of this thesis may be reproduced, stored in a retrieval system or transmitted in any form or by any means without permission of the author. Alle rechten voorbehouden. Niets uit deze uitgave mag worden vermenigvuldigd, in enige vorm of op enige wijze, zonder voorafgaande schriftelijke toestemming van de auteur.

**UNIVERSITY
OF TWENTE.**



Graduation Committee:

Chairman/Secretary

Prof.dr. F.D. van der Meer

University of Twente

Supervisor

Prof.dr. A.D. Nelson

University of Twente

Co-supervisors

Dr. R. Darvishzadeh

University of Twente

Dr. M. Boschetti

National Research Council of Italy, Institute
for Electromagnetic Sensing of the
Environment.

Members

Prof.dr.ir. S. Steele-Dunne

Delft University of Technology

Prof.dr. M. Herold

Wageningen University

Prof.dr.ir. A. Veldkamp

University of Twente

Prof.dr. Z. Su

University of Twente

“Fall in love with the process, and the results
will come.”

— *Eric Thomas*

I dedicate this work to my parents and mentors who
pushed me to levels I never thought I would go to.

Acknowledgements

Undertaking this PhD has been truly a life-changing experience for me, and it is my pleasure to acknowledge the roles of several individuals who were instrumental for the completion of my PhD research.

Firstly, I would like to express my sincere gratitude to my promoter, Prof. Andy Nelson, who opened the door for me to work in his department and believed in my potential to be a part of this research project. You created a research environment for me that stimulated original thinking and initiative. The insightful discussions, constructive feedback and brainstorming sessions helped me grow as a person. I thank you for your expert guidance and support during this process. I could not have imagined having a better mentor for my PhD research.

I would also like to extend my tremendous gratitude to my daily co-supervisor Dr. Roshanak Darvishzadeh, who is by far the most ambitious and hardworking person I have ever known. I thank you for your enduring supervision, patience and enthusiasm and for initiating me into the world of science. Your prompt feedback on my work and innumerable comments, thoughts and revisions of my work helped me navigate all the obstacles along the way and achieve my objectives. Your availability that extended beyond the office hours, the constant motivation and reminders to apply for conferences, to attend meetings/workshops and having my back in every situation is much more than I could have ever asked for. You always insisted me to think out of the box and aim higher and I am happy that I got to develop a lifelong cordial relationship with you, which is beyond mere mentoring.

My sincere thanks go to our collaborator Dr. Mirco Boschetti from CNR-IREA, Institute for Electromagnetic Sensing of the Environment, Italy. Thank you for your supervision and involvement throughout my PhD and your support during my stay in Italy. Your expertise in remote sensing helped me shape the research papers in the present form. Your help with the selection of the study site in Bonifiche Ferraresi farm, Italy that matched with my research requirements is greatly appreciated. You facilitated the communication with the employees of the farm whenever the need arose, helped me find relevant contact points, and assisted in the formulation of fieldwork protocol that made the data acquisition process seamless. I also thank the CEO of Bonifiche Ferraresi farm, Dr. Federico Vecchioni, director Ado Guerrini and R&D responsible Francesco Pugliese, who facilitated the logistics for the fieldwork.

I wish to show my gratitude to ITC and University of Twente for providing a lively research environment and to the staff members for their support. I thank Esther Hondebrink for the tremendous help in administrative tasks and for being

such an adorable food enthusiast. I appreciate the friendly assistance provided by Loes Colenbrander in the thesis finalization. I received generous support from Benno and Job during my fieldwork preparation and designing posters for the conferences. I also thank Willem for the technical assistance. Caroline and Kathrin, thank you for assisting me with the lab equipment. I have also had the support and encouragement of all the colleagues in NRS: Michael, Festus, Anton, Thomas, Andrew, Valentijn, Wieteke, Eddy, Iris, Henk, Xin, Abebe, Alby, Louise, Joan, and many more. A special mention of Marga and Carla for the invaluable assistance in the library and giving me access to the papers whenever I needed.

My appreciation also extends to my friends whose assistance was a milestone in the completion of this project. In particular, I would like to acknowledge the contribution of my best friend, Florentina Badea. You have been my most cherished discovery during my stay in Enschede and a literal partner in crime. Without your over the top energy and consistent mental support, I would not have reached where I am today. I am also deeply grateful to Elnaz Neinavaz for being the most generous human being and for supporting me throughout the years, practically and morally. You have helped me find ways to tackle many problems that surfaced during my PhD life. I also thank Xi and Trini for all the memorable moments within and outside ITC. I also wish to express my deepest gratitude to Arka, Sahil and Jagadeesh for all the crazy fun we have had in Mooiehof, for the delicious food we have cooked together and for being the best party crashers. Samer, you have been one of my closest friends in ITC and thank you so much for all the discussions we have had during the coffee breaks and for being the most courteous person. Risham, Arwa, Nidale, Victoria, Evelien, Jurnan, Divyani and Yamini, your friendship and support has been particularly rewarding. Thank you, Alexandra Matei, for being the best badminton buddy and for making my experience in DIOK all the way more memorable. I also thank all my fellow PhDs in ITC: Yifang, Linlin, Xu, Ruosha, Peiqi, Tina, Tonny and so on. Pasqual, a very special thanks to you for your continued and unfailing love, support and understanding. You have helped me grow and evolve as a person and have helped me put things into perspective. Above all, you have been a constant source of inspiration to me in many ways. You showed me ways to make smarter, healthier food choices and instilled in me a lasting passion for life.

Lastly, I would like to recognise the invaluable support and love of my parents and my sister Surbhi. Without your guidance and motivation, none of what I have accomplished would have been possible. Thank you so much for pushing me to do my best and instilling values in me that I will carry on throughout my life.

Table of Contents

Acknowledgements	i
List of Figures	v
List of Tables	x
List of Abbreviations	xii
Chapter-1	1
Introduction	1
1.1. The need for quantifying crop lodging	2
1.2. From conventional methods to remote sensing-based crop lodging assessment ..	3
1.3. Research aim and objectives	4
1.4. Study site	4
1.5. Thesis structure.....	7
Chapter-2	9
Remote sensing-based crop lodging assessment: Current status and perspectives .	9
Abstract.....	10
2.1. Introduction.....	11
2.2. Theoretical background and scope of remote sensing in lodging assessment ...	15
2.3. Review of remote sensing-based studies for crop lodging assessment	21
2.4. Challenges in remote sensing of crop lodging	35
2.5. Research gaps and future scope.....	37
2.6. Outlook on remote sensing sensors and platforms	40
2.7. Conclusions.....	42
Chapter-3	45
Estimation of crop angle of inclination for lodged wheat using RADARSAT-2 and Sentinel-1 SAR data	45
Abstract.....	46
3.1. Introduction.....	47
3.2. Materials and methods	51
3.3. Results	60
3.4. Discussion	66
3.5. Conclusions.....	74
Chapter-4	77
Discriminant analysis for lodging severity classification in wheat using RADARSAT-2 and Sentinel-1 SAR data	77
Abstract.....	78
4.1. Introduction.....	79
4.2. Materials and methods	81
4.3. Results	90
4.4. Discussion	100
4.5. Conclusions.....	106

Chapter-5	109
Understanding wheat lodging using time-series Sentinel-1 and Sentinel-2 data .	109
Abstract.....	110
5.1. Introduction.....	111
5.2. Materials and methods	112
5.3. Results and Discussion.....	121
5.4. Conclusions.....	139
Chapter-6	141
Mapping of wheat lodging susceptibility with Synthetic Aperture Radar data .	141
Abstract.....	142
6.1. Introduction	143
6.2. Materials and Methods	146
6.3. Results.....	156
6.4. Discussion.....	163
6.5. Conclusions	170
Appendix	173
Chapter-7	177
Synthesis: Remote sensing of wheat lodging and its susceptibility	177
7.1. Summary/Introduction.....	178
7.2. Advances in remote sensing of crop lodging	180
7.3. Potential of remote sensing data in detecting crop lodging stages.....	182
7.4. Exploring the information capacity of SAR remote sensing for lodging severity mapping	184
7.5. Contribution of time-series SAR and optical remote sensing data in identifying the time of lodging incidence in wheat	187
7.6. Role of SAR remote sensing in lodging susceptibility mapping	189
7.7. Future opportunities	190
7.8. Research implications	197
Bibliography	201
Summary	221
Samenvatting	223
Multi-Author Declaration	227
Biography	231

List of Figures

Fig. 1.1. An example of a very severely lodged wheat field at the study site in Bonifiche Ferraresi farm, Jolanda di Savoia, Italy.	2
Fig. 1.2. (a) Study region in Italy, (b) Sentinel-1 RGB composite (VV, VH, VH/VV) scene containing the research area and (c) the distribution of daily cumulated precipitation (mm) and daily average wind speed (m/s) at 10 m from the ground during the winter wheat growing season.	6
Fig. 1.3. The structure of the thesis, the relationships between the chapters and list of ISI journal publications.	8
Fig. 2.1. Distribution of the selected peer-reviewed publications on lodging assessment within the last 68 years.	14
Fig. 2.2. Determinants of (a) wind-induced and plant self-weight moment, (b) stem strength and stem lodging and (c) anchorage strength and root lodging.	16
Fig. 2.3. Summary of important factors related to lodging (seasonal susceptibility and risk assessment, lodging detection and its impact on yield loss) and potential contribution of RS.	20
Fig. 2.4. The figure represents the number of reviewed articles based on study type: field/lab-based studies (49) and RS-based studies (22).	32
Fig. 2.5. Summary of important features in (a) optical and (b) microwave regions relevant to crop lodging detection and risk assessment as identified from RS-based crop lodging studies.	34
Fig. 3.1. An example of the change in plant height and crop angle of inclination in the event of lodging for (a) cultivar A and (b) cultivar B, at the same phenological stage.	50
Fig. 3.2. An RGB composite of a Sentinel-1 (R: VH, G: VV, B: VH/VV) scene containing the study area (Bonifiche Ferraresi farm) overlaid with the sampling points over the wheat fields and the farm boundary.	51
Fig. 3.3. (a) Measurement of crop angle of inclination and (b) illustration of different crop lodging stages.	52
Fig. 3.4. Methodological flowchart of the study.	54
Fig. 3.5. The variation in plant height in the healthy plots for different wheat cultivars at the flowering growth stage.	54

Fig. 3.6. Acquisition dates of remote sensing data during the 2018 wheat growing season.	56
Fig. 3.7. Box plots of (a) Sentinel-1 backscattering coefficients, (b) Sentinel-1 coherence, (c) RADARSAT-2 FQ8 backscattering coefficients and (d) RADARSAT-2 FQ21 backscattering coefficients at different polarisations.	62
Fig. 3.8. The CAI values predicted using support vector regression versus field measured crop angle of inclination (CAI) from Sentinel-1 and RADARSAT-2 data.	66
Fig. 3.9. CAI maps predicted from (a) Sentinel-1 data acquired on May 31, 2018, (b) Sentinel-1 data acquired on June 6, 2018, (c) RADARSAT-2 FQ21 data acquired on May 31, 2018, and (d) RADARSAT-2 FQ8 data acquired on June 13 2018.	72
Fig. 4.1. An RGB composite of a Van Zyl decomposed RADARSAT-2 (double bounce, volume, surface scattering) scene containing the study area (Bonifiche Ferraresi farm) overlaid with the sampling points over the wheat sown fields and the farm boundary.	82
Fig. 4.2. (a) Measurement of CAI (b) Depiction of healthy (He) and lodged (L) subplots and plot centres in real field conditions. (c) The plot is divided into four quadrants Q1 to Q4-the lodged area in each quadrant is represented as LA1 to LA4; He1, He2 are the healthy subplots and L1,...L4 are the lodged subplots.	83
Fig. 4.3. Acquisition dates of RADARSAT-2 FQ8, RADARSAT-2 FQ21 and Sentinel-1 data covering the study site during the 2018 wheat growing season.	86
Fig. 4.4. Methodological flowchart of the study.	89
Fig. 4.5. Pearson correlation coefficients between lodging score and metrics derived from (a) RADARSAT-2 FQ8 and (b) RADARSAT-2 FQ21.	92
Fig. 4.6. Pearson correlation coefficients between lodging score and metrics derived from Sentinel-1 in grey.	93
Fig. 4.7. Supervised clustering (left) and estimated and cross-validated AUC-ROC (right) of lodging severity classes using partial least squares discriminant analysis (PLS-DA) with (a), (b) RADARSAT-2 FQ8 data, (c), (d) RADARSAT-2 FQ21 data and (e), (f) Sentinel-1 data.	94
Fig. 4.8. Lodging severity maps generated from (a) Sentinel-1 data acquired on May 31 2018, (b) Sentinel-1 data acquired on June 6, 2018, (c)	100

RADARSAT-2 FQ8 data acquired on May 31, 2018, and (d) RADARSAT-2 FQ21 data acquired on June 13, 2018, using PLS-DA models.

Fig. 5.1. A false-colour RGB composite of a Sentinel-2 scene containing the study area (Bonifiche Ferraresi farm) overlaid with the sampling points over the wheat fields and the farm boundary. 113

Fig. 5.2. Measurement technique of crop angle of inclination (CAI). 114

Fig. 5.3. (a) Illustration of lodged/healthy subplots and the plot centre in real field conditions (b) Division of the plot into four quadrants Q1, Q2, Q3 and Q4. LA1, LA2, LA3 and LA4 correspond to the lodged area in each quadrant. In this scenario, L1, L2, ..., L6 represent the lodged subplots while H1 and H2 are the healthy subplots. 115

Fig. 5.4. Acquisition dates of Sentinel-1 and Sentinel-2 data during the 2018 wheat growing season. 116

Fig. 5.5. (a) Average spectral reflectance variation and (b) continuum removed spectra for healthy wheat plots at the stem elongation, booting, flowering, milking and ripening phenological stages. 122

Fig. 5.6. (a) Average spectral reflectance variation and (b) continuum removed spectra for plots with healthy wheat cultivars: PR22D66, Odisseo, Monastir and Marco Aurelio, at the milking phenological stage. 123

Fig. 5.7. Box plots presenting the reflectance variation in Sentinel-2 bands for healthy wheat plots and wheat plots with different lodging severities (ML, SL and VSL). Observations were taken from the stem elongation stage until the ripening stage. 125

Fig. 5.8. (a) Average spectral reflectance variation and (b) continuum removed spectra for healthy wheat plots and wheat plots with different lodging severities (ML, SL, and VSL) at the milking phenological stage. 128

Fig. 5.9. (a) Average spectral reflectance of plots with healthy wheat cultivars: PR22D66, Odisseo, Monastir and Marco Aurelio, and those with different lodging severities (ML, SL, and VSL) across multiple cultivars at the milking phenological stage. 129

Fig. 5.10. Temporal average reflectance of healthy and lodged wheat plots in (a) red edge (740 nm) and (b) NIR (865 nm) spectral bands, and (c) rainfall and wind speed over Bonifiche Ferraresi farm where wheat was cultivated in 2017-2018. 130

Fig. 5.11. Boxplots presenting the variation in (a) σ_{VH}^o , σ_{VV}^o , $\sigma_{VH/VV}^o$ and (b) μ_{VH}^o and μ_{VV}^o using Sentinel-1 data throughout the stem elongation-ripening 132

phenological stages. (c) σ_{VH}^o , σ_{VV}^o , $\sigma_{VH/VV}^o$ and (d) μ_{VH}^o and μ_{VV}^o corresponds to milking phenological stage.

Fig. 5.12. Temporal average signatures of healthy and lodged wheat plots for (a) σ_{VH}^o , (b) σ_{VV}^o , (c) $\sigma_{VH/VV}^o$, (d) μ_{VH}^o and (e) μ_{VV}^o and (f) rainfall and wind speed over Bonifiche Ferraresi farm where wheat was cultivated in 2017-2018. 136

Fig. 6.1. Schematic diagram of the safety factor against root lodging. 144

Fig. 6.2. An RGB composite of a Sentinel-1 (R: VH/VV, G: VV, B: VH) scene containing the study area (Bonifiche Ferraresi farm) overlaid with the sampling points over the wheat sown fields and the farm boundary. 146

Fig. 6.3. Field photographs of wheat in different phenological stages: (a) stem elongation, (b) booting, (c) flowering and (d) milking. 147

Fig. 6.4. The basic layout of the lodging meter and its demonstration in the field. 149

Fig. 6.5. Process flowchart for the estimation of safety factor against root lodging. 156

Fig. 6.6. Variation of crop biophysical parameters across the growing season. 157

Fig. 6.7. Variation of the field-measured SFA for different cultivar lodging susceptibility scores along the season. 159

Fig. 6.8. Pearson correlation scatter plots of the most significant satellite metrics derived from (a) Sentinel-1, (b) RADARSAT-2 data and the field-measured safety factor against root lodging (SF_A). 161

Fig. 6.9. Scatterplots show the relations between measured and predicted SF_A values obtained using cross-validated regression models for (a) Sentinel-1 and (b) RADARSAT-2 data. 162

Fig. 6.10. Spatial distribution of SF_A in the study area. 163

Fig. 6.11. Distribution of the field measured samples that remained (a) healthy and (b) were lodged at the end of the season versus the field-measured safety factor values. 169

Fig. A6.1. Variation of crop biophysical parameters across the growing season for different wheat cultivars. 173

Fig. 7.1. Flowchart illustrating the research summary. 179

Fig. 7.2. The total number of publications and citations from the RS-based crop lodging studies throughout 1980-2020.	181
Fig. 7.3. The red polygon in (a) shows the location of the wheat fields in the Bonifiche Ferraresi farm where UAV data was acquired, (b) shows the false colour-composite (R:865 nm, G:665 nm, B:560 nm) of the data acquired from the UAV platform, and in (c) are the UAV images classified into different lodging stages.	184
Fig. 7.4. RGB composites (R: VV, G: VH, B: VV) of the two Sentinel-1 images acquired on (a) May 13 2018 (moderately lodged) and (b) May 25 2018 (very severely lodged) showing the variation in the backscattering intensity for the two wheat fields.	186
Fig. 7.5. Boxplot depicting the UAV reflectance at various wavelengths for healthy, moderate, severe and very severe crop lodging stages.	189
Fig. 7.6. Lodging susceptibility map derived from (a) leaf area index (LAI $\text{m}^2 \text{m}^{-2}$), (b) fraction of vegetation cover (fCover %) maps, (c) safety factor against root lodging (SF_A) map and (d) plant density (PD plants m^{-2}).	195
Fig. 7.7. Different stem lodging susceptibility scenarios based on a visual estimate of leaf area index (LAI $\text{m}^2 \text{m}^{-2}$) and the fraction of vegetation cover (fCover %) from the RGB photographs.	197
Fig. 7.8. The market estimation (grouped by the continents) for precision smart farming 2014-2020 is shown. The figures are in billion euros; CAGR is the compound annual growth rate.	198
Fig. 7.9. The proposed framework for developing a web/mobile-based application for lodging detection and risk mapping.	199

List of Tables

Table 2.1. Existing remote sensing studies for crop lodging assessment. The list in the table is sorted based on the platform types (ground-based, airborne, and spaceborne).	22
Table 3.1. Summary statistics of CAI and PH for healthy and lodged plots. Samples were collected throughout the flowering to ripening phenological stages.	53
Table 3.2. Image acquisition parameters for Sentinel-1 and RADARSAT-2 data.	55
Table 3.3. Metrics extracted from RADARSAT-2 SAR data.	57
Table 3.4. Posthoc Tukey's HSD analysis is reported for different classes and sensors.	63
Table 3.5. Pearson correlation coefficients (r) and p -values between CAI and metrics derived from Sentinel-1 data.	63
Table 3.6. Pearson correlation coefficients (r) between CAI and metrics derived from RADARSAT-2 FQ8 and FQ21 data.	64
Table 4.1. Summary statistics of biophysical/biochemical parameters in healthy and lodged samples throughout the flowering to ripening phenological stages.	84
Table 4.2. Cross-validated area under the curve (AUC-CV) statistics for four lodging severity classes using Sentinel-1, RADARSAT-2 FQ8 and RADARSAT-2 FQ21 datasets.	98
Table 4.3. Cross-validated confusion matrix, comparing reference and remote sensing-based lodging severity classes using Sentinel-1, RADARSAT-2 FQ8 and RADARSAT-2 FQ21 datasets.	98
Table 5.1. Summary statistics of measured CAI, LA and LS for all samples throughout the stem elongation to ripening phenological stages.	115
Table 5.2. Summary statistics of measured soil moisture and biophysical/biochemical parameters in healthy and lodged samples throughout the stem elongation to ripening growth stages.	117
Table 5.3. Satellite specifications for Sentinel-1 data. Note that the range of the incidence angle is specific to the location of the study site within the swath.	118

Table 5.4. Specifications of the Multi-Spectral Imager (MSI) onboard the Sentinel-2 satellite.	119
Table 5.5. Average biophysical/biochemical properties of plots with healthy wheat cultivars: PR22D66, Odisseo, Monastir, and Marco Aurelio, at the milking phenological stage.	123
Table 5.6. Kruskal Wallis p -value statistics for Sentinel-2 spectral bands.	126
Table 5.7. Post-hoc Tukey's HSD p -value statistics of different lodging severities for Sentinel-2 spectral bands.	126
Table 5.8. Kruskal Wallis p -value statistics for Sentinel-1 metrics.	133
Table 5.9. Post-hoc Tukey's HSD p -value statistics of different lodging severities for Sentinel-1 metrics.	133
Table 6.1. Summary statistics of field measurements.	150
Table 6.2. The dates for the acquisition of Sentinel-1 and RADARSAT-2 images over Bonifiche Ferraresi farm, Jolanda di Savoia, Italy during the wheat growing season March-June 2018 are outlined.	151
Table A6.1. Pearson correlation coefficients and p -values between metrics derived from Sentinel-1 data and the safety factor against root lodging at a crop angle of inclination of 30°.	174
Table A6.2. Pearson correlation coefficients and p -values between metrics derived from RADARSAT-1 data and the safety factor against root lodging at a crop angle of inclination of 30°.	174
Table A6.3. Comparisons within and across wheat cultivars demonstrating the agreement of lodging susceptibility predicted based on safety factor (high/low) and the actual crop condition (lodged/non-lodged) observed on the field at specific growth stages.	175

List of Abbreviations

AHDB	Agriculture and Horticulture Development Board
ASC	Ascending
AUC-ROC	Area Under the Curve-Receiver Operating Characteristics
BBCH	Biologische Bundesanstalt, Bundessortenamt und Chemische Industrie
BD	Band Depth
BMI	BioMass Index
BOA	Bottom Of Atmosphere
CAI	Crop Angle of Inclination
CCD	Coherence Change Detection
COA	Copernicus Open Access
CSI	Canopy Scattering Index
DB	Dry Biomass
DEM	Digital Elevation Model
DMC	Disaster Monitoring Constellation
DoY	Day of Year
DSC	Descending
EO	Earth Observation
ESA	European Space Agency
ϵ-SVR	Epsilon-Support Vector Regression
ETM	Enhanced Thematic Mapper
FB	Fresh Biomass
fCover	Fraction of vegetation cover
FQ	Fine Quad-pol
FTP	File Transfer Protocol
GLCM	Grey-Level Co-occurrence Matrix
GRD	Ground Range Detected
GS	Growth Scale
He	Healthy
HH	Horizontal-Horizontal polarisation
HSD	Honest Significant Difference
HV	Horizontal-Vertical polarisation
ISI	Institute of Scientific Information
IW	Interferometric Wide-swath
LA	Lodged Area
LAI	Leaf Area Index
LiDAR	Light Detection And Ranging
LS	Lodging Score
LSS	Lodging Susceptibility Score
MDA	MacDonald Dettwiler Associates Ltd

ML	Moderate Lodging
MLA	Mean Leaf Angle
MSI	MultiSpectral Imager
NCA	Neighbourhood Component Analysis
NEON	National Ecological Observatory Network
NIR	Near-InfraRed
NRT	Near-Real Time
OLI-TIRS	Operational Land Imager -Thermal InfraRed Sensor
PCA	Principal Component Analysis
PGR	Plant Growth Regulator
PH	Plant Height
PLS	Partial Least Squares
PLS-DA	Partial Least Squares-Discriminant Analysis
PWC	Plant Water Content
R-2	RADARSAT-2
RADAR	Radio Detection And Ranging
RE	Red Edge
RFDI	Radar Forest Degradation Index
RGB	Red Green Blue
RMSEC	Calibrated Root Mean Square Error
RMSECV	Cross-Validated Root Mean Square Error
RPAS	Remotely Piloted Aircraft System
RS	Remote Sensing
RVI	Radar Vegetation Index
S-1	Sentinel-1
S-2	Sentinel-2
SAM	Sustainable Agriculture Management
SAR	Synthetic Aperture Radar
SDGs	Sustainable Development Goals
SfM	Structure from Motion
SL	Severe Lodging
SLC	Single Look Complex
SOAR	Science and Operational Applications Research
STICS	Simulateur multIdisciplinaire pour les Cultures Standard
SVM	Support Vector Machine
SVR	Support Vector Regression
OA	Overall Accuracy
UAV/UAS	Unmanned Aerial Vehicles/Systems
VENμS	Vegetation and Environment monitoring on a New MicroSatellite
VIS-SWIR	VISible-Short Wave InfraRed
VH	Vertical-Horizontal polarisation
VSI	Volume Scattering Index
VSL	Very Severe Lodging

VSSC	VEN μ S Superspectral Camera
VV	Vertical-Vertical polarisation
XGB	eXtreme Gradient Boosting

Symbols

α	Alpha angle
A	Anisotropy
σ^0	Backscattering coefficient
H	Entropy
μ^0	Interferometric coherence
K	Kappa coefficient
G	Genetic
E	Environment
M	Management
SF_A	Safety factor against root lodging
S_A	Anchorage strength
M_P	Self-weight moment of the whole plant
H_P	Plant height
h_P	Height at the center of gravity
FB_P	Fresh biomass
R^2_{Cal}	Calibrated coefficient of determination
R^2_{CV}	Cross-Validated coefficient of determination
$RMSE_{Cal}$	Calibrated Root Mean Square Error
$RMSE_{CV}$	Cross-Validated Root Mean Square Error
r	Pearson correlation coefficient

Chapter-1

Introduction

1.1 The need for quantifying crop lodging

Crop lodging is the permanent displacement of crop stems from the upright position (Pinthus, 1974) and is common in staple cereals such as wheat (Fig. 1.1). Lodging can occur either due to root failure (root lodging) or stem failure (stem lodging) (Sterling et al., 2003). The incidence of lodging in wheat is most likely to occur during the two or three months before harvest and is caused due to complex interactions between genetic (G), environmental (E, i.e. weather – precipitation/hail and wind) and management factors (M, such as sowing date, sowing density, nitrogen application rate etc.) (Berry et al., 2004).



Fig. 1.1. An example of a very severely lodged wheat field at the study site in Bonifiche Ferraresi farm, Jolanda di Savoia, Italy. The wheat is in the milking phenological stage (May 25, 2018).

Lodging can cause drastic yield losses in wheat due to the destruction of the crop morphology and reduction in the photosynthetic capability of the plant (Berry and Spink, 2012). The level of yield loss depends upon how severe lodging is. The lodging severity is a function of numerous factors such as the crop phenological stage at which lodging occurs, the crop angle of inclination (CAI) and the spatial area that is lodged (Acreche and Slafer, 2011). For instance, Berry and Spink (2012) reported a reduction of 61% in wheat yield when wheat lodged at the CAI of 90° from the vertical. Lodging also deteriorates grain quality (reduced grain weight), increases drying costs and makes harvesting difficult, thus reducing the likelihood of achieving a premium market price. Continued intensification of cereal production (more production per unit area of land) coupled with the effects of climate change (increased frequency and intensity of extreme rainfall events and storms) will likely increase the occurrence of lodging and its impacts on yield. A quantitative evaluation of lodging susceptibility and timely detection of its incidence can control the effects of lodging and decisions regarding expected yield, crop-price, or insurance pay-outs can be made effectively.

1.2 From conventional methods to remote sensing-based crop lodging assessment

Conventional measures to assess lodging rely on either visual ratings or mathematical/mechanistic crop growth models. The problem with solely relying on visual ratings of lodging is that they require the on-site availability of a person for the visual assessment. This makes the measurements point-based, time-consuming and subjective, depending on the skill and self-consistency of the observer or complexity of the lodging event (Bock et al., 2010). The problem with mathematical/mechanistic crop growth models is their dependency on detailed field measurements of soil and crop parameters, which makes them input-intensive and challenging to apply over large areas.

Remote sensing (RS) technology offers a very promising alternative to these conventional methods for automated monitoring of crop lodging at local, regional and global scales in near-real-time (NRT). The last three decades have witnessed a rapid evolution in RS methods and technologies, with satellite imagery now being routinely used for agricultural applications (Davies, 2009). Fine resolution RS data, coupled with data from ground surveys, are useful for monitoring crops at multiple spatial scales (Ozdogan et al., 2010). Agriculture monitoring using RS has been addressed from various viewpoints – based on i) specific applications (e.g., crop type mapping, biophysical parameter retrieval, phenology monitoring), ii) specific RS platforms (ground-based, airborne or satellite) or specific sensors (e.g., active vs passive, wavelength domain) and iii) particular locations and climate contexts (e.g., dryland, country, continent). In terms of the specific applications, the scientific literature on crop lodging assessment using RS is still in a nascent stage. Our published review (Chauhan et al., 2019a), in addition to the studies published subsequently, shows that there are only 44 peer-reviewed studies since 1951 that have focused on the use of RS for crop lodging assessment (with most of them limited to qualitative lodging assessment).

An extensive analysis of these studies shows that features derived from optical sensors embedded on ground-based (such as smartphones) and airborne RS platforms (such as unmanned aerial vehicles/systems (UAV/UAS) and air balloons) have been used for lodging detection in many crops such as wheat (Hufkens et al., 2019; Wang et al., 2018), buckwheat (Murakami et al., 2012), maize (Acorsi et al., 2019; Chu et al., 2017; Han et al., 2018), rice (Ding et al., 2019; Han et al., 2017; Yang et al., 2020), spearmint (Vargas et al., 2020), canola (Mardanisamani et al., 2019) and barley (Wilke et al., 2019). However, timely

information about crop condition over vast and remote areas has become available due to the increased availability of free, high-resolution satellite data such as data from Sentinel 1, 2 and 3. While most studies have focused on optical imagery, synthetic aperture radar (SAR) platforms such as Sentinel-1 and RADARSAT-2 provide a rich set of features in dual (VV, VH) and fully polarimetric modes (HH, HV, VH and VV), that can help characterise complex agricultural ecosystems and more specifically the often heterogeneous patterns of lodging.

Our thorough review of the literature and the limited number of existing studies (Gu et al., 2019; Kumpumäki et al., 2018; Shu et al., 2019) have demonstrated that there is no conceptual framework nor methodology for using satellite-based RS images to assess crop lodging. This research addresses that gap.

1.3 Research aim and objectives

This research aims to investigate the potential of spaceborne RS data for lodging detection, characterisation and mapping lodging susceptibility in wheat. To achieve this aim, we formulated five specific objectives as follows:

- a. To carry out a systematic literature review that relates field/lab-based lodging assessment approaches to RS-based methods, characterises the relative strengths, assesses the operational feasibility and identifies potential RS-based research gaps.
- b. To evaluate the performance of Sentinel-1 and RADARSAT-2 time series in estimating the crop angle of inclination (CAI) as a measure of crop lodging stage.
- c. To distinguish and classify lodging severity based on a lodging score using time-series of Sentinel-1 and RADARSAT-2 data.
- d. To investigate the capability of Sentinel-1 and Sentinel-2 time series in detecting the time of lodging incidence in wheat and to understand the effect of lodging on the RS signal.
- e. To estimate a safety factor against root lodging as a measure of root lodging susceptibility by exploiting time-series of Sentinel-1 and RADARSAT-2 data.

1.4 Study site

The study was carried out in the Bonifiche Ferraresi farm (Fig. 1.2b), situated in Jolanda di Savoia (central coordinates 44°52'59"N, 11°58'48"E), a commune in

the province of Ferrara, Italy (Fig. 1.2a). Bonifiche Ferraresi is an agri-food company and one of the largest farm holdings in Italy, with over 6500 ha of land spread across the municipalities of Jolanda di Savoia, Arborea, Mirabello and Santa Caterina. More than 60% of the area is in Jolanda, covering approximately 3,850 ha. The study region is mainly covered by arable land. The main crops are durum wheat (*Triticum durum*), soft wheat (*Triticum aestivum*), rice (*Oryza sativa*), corn (*Zea mays*), barley (*Hordeum vulgare*), soybean (*Glycine max*) and potatoes (*Solanum tuberosum*), among several other horticulture and medicinal plants. These crops are typically grown in rotation in consecutive years.

In 2017, winter wheat was sown between October 21-November 4 on almost 600 ha area and was harvested by June 30, 2018. Several wheat cultivars were sown, with a wide range of lodging susceptibility scores (LSS) ranging between 0-9, with 0 being least susceptible and 9 being highly susceptible to lodging. The farm provided the LSS data of each cultivar which is derived from technical sheets of the cultivars and historical cultivar tests carried out in Bonifiche. The cultivars were PR22D66 (LSS: 1.5), Marco Aurelio (LSS: 2.5), Massimo Meridio (LSS: 3), Rebelde (LSS: 3), Claudio (LSS: 4), Monastir (LSS: 5), Odisseo (LSS: 6.5), Giorgione (LSS: 7) and Senatore Capelli (LSS: 9).

The size of the wheat fields in the farm varied between 2.38 and 84.86 ha. Winter wheat is dormant in the first few months after sowing due to low temperatures (from October to Feb). It is not until spring (from March onwards in this site) that wheat breaks its dormancy and resumes vegetative growth. We used a standard BBCH growth scale or GS (Biologische Bundesanstalt, Bundessortenamt und Chemische Industrie) of 0-99 (Bleiholder et al., 2001), to quantify the phenological growth stages throughout the work. The BBCH GS is based on ten principal phenological growth stages in wheat: germination (GS00-09), leaf development (GS10-19), tillering (GS20-29), stem elongation (GS30-39), booting (GS40-49), heading (GS50-59), flowering (anthesis) (GS60-69), milking (GS70-79), dough development (GS80-89) and senescence or ripening (GA90-99). Our study focused on several stages that are critical to lodging in wheat.

In the study site, wheat was mainly cultivated over clayey and silty soils in a warm and temperate climate. During the wheat growing season of 2017-18, the daily cumulated precipitation and average wind speed, as measured from a local automatic weather station, ranged between 0-65 mm and 0.5-6.4 m/s respectively (Fig. 1.2c).

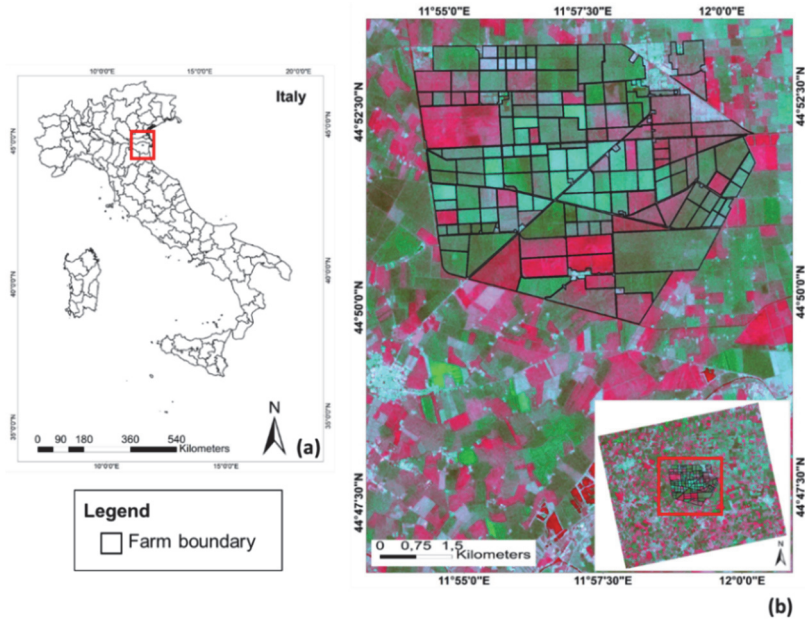


Fig. 1.2. (a) Study region in Italy, (b) Sentinel-1 RGB composite (R: VV, G: VH, B: VH/VV) scene acquired on March 26, 2018, containing the research area (Bonifiche Ferraresi farm, a red polygon in the lower-left map) overlaid with the farm boundary (black outline) and (c) illustrates the distribution of daily cumulated precipitation (mm) and daily average wind speed (m/s) at 10 m from the ground during the winter wheat growing season from October 19, 2017-June 30, 2018. The period selected for this study ranges from March 14-June 30, 2018.

1.5 Thesis structure

The thesis consists of seven chapters, including an introduction, five core chapters and a synthesis. Each core chapter has been published in or submitted to a peer-reviewed ISI journal (Fig. 1.3). The seven chapters have been structured as follows:

Chapter 1 (This chapter) introduces the importance and relevance of the research topic, gives an overview of the limitations of field-based methods and perspectives on how RS can address these limitations for lodging assessment, defines the research objectives, introduces the study area and outlines the thesis structure.

Chapter 2 presents a systematic overview of current approaches for crop lodging assessment and evaluates their strengths and weaknesses in the context of operational applications. It also identifies the challenges, research gaps and the potential contribution of RS within the current framework of field/lab-based crop lodging assessment studies. Several of these challenges and research gaps are addressed in chapters 3 to 6.

Chapter 3 develops an approach for the evaluation of crop lodging stages through RS-based estimation of crop angle of inclination. This is achieved by relating field measurements with RS-based metrics derived from Sentinel-1 data and low incidence and high incidence angle RADARSAT-2 data.

Chapter 4 presents an approach for the classification of lodging severity based on a lodging score assessment. This is done by exploring the potential of RS-based metrics derived from Sentinel-1 data and low incidence and high incidence angle RADARSAT-2 data.

Chapter 5 investigates the potential of Sentinel-1 and Sentinel-2 time-series data to detect the time of lodging incidence in wheat and understand the effect of lodging on RS-based metrics.

Chapter 6 demonstrates the use of RS-based metrics derived from Sentinel-1 data and multi-incidence angle (low and high combined) RADARSAT-2 data for estimating a safety factor against root lodging as a simple measure of root lodging susceptibility in wheat.

Chapter 7 provides a synthesis of the main findings of the research. Future opportunities and research implications for technology transfer to potential end-users are also outlined. The market potential and the relevance of the research findings for the attainment of Sustainable Development Goals (SDGs) are also discussed.

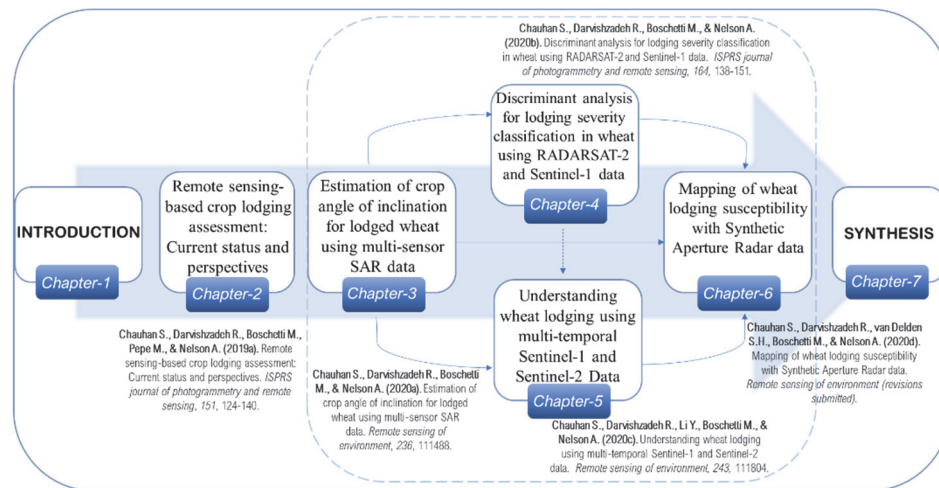


Fig. 1.3. The structure of the thesis, the relationships between the chapters and list of ISI journal publications.

Chapter-2

Remote sensing-based crop lodging assessment: Current status and perspectives*

*This chapter is based on:

Chauhan, S., Darvishzadeh, R., Boschetti, M., Pepe, M., & Nelson, A., (2019a). Remote sensing-based crop lodging assessment: Current status and perspectives. *ISPRS journal of photogrammetry and remote sensing*, 151, 124-140. <https://doi.org/10.1016/j.isprsjprs.2019.03.005>

Abstract

Rapid and quantitative assessment of crop lodging is important for understanding the causes of the phenomena, improving crop management, making better production and supporting loss estimates in general. Accurate information on the location and timing of crop lodging is valuable for farmers, agronomists, insurance loss adjusters and policymakers. Lodging studies are performed to assess the impact of lodging events or to model the risk of occurrence, both of which rely on information that can be acquired by field observations, from meteorological data and RS. While studies applying RS data to assess crop lodging dates back three decades, there has been no comprehensive review of the status, potential, current approaches and challenges in this domain. In this position paper, we review the trends in field-/lab-based and RS-based studies for crop lodging assessment and discuss the strengths and weaknesses of current approaches. We present a theoretical background on crop lodging and review and discuss the scope of RS in assessing plant characteristics associated with lodging. The review focuses on RS-based studies, grouping them according to the platform deployed (i.e., ground-based, airborne and spaceborne), with an emphasis on analysing the pros and cons of the technology. Finally, we present the challenges, research gaps and perspectives for future research. We also offer an outlook on new sensors and platforms to provide state-of-the-art and future potential of RS in lodging assessment. Our review reveals that the use of RS techniques in crop lodging assessment is still in an experimental stage. However, there is increasing interest within the RS scientific community (based on the increased rate of publications over time) to investigate its use for crop lodging detection and risk mapping. The existing satellite-based lodging assessment studies are very few, and the operational application of the current approaches over large spatial extents seems to be the biggest challenge. We identify opportunities for future studies that can develop quantitative models for estimating lodging severity and mapping lodging susceptibility and risk using RS data.

2.1 Introduction

2.1.1 Lodging and its impact on agricultural production

Lodging, which is the displacement of a crop stem from its upright position (stem lodging) or failure of root-soil anchorage system (root lodging) (Pinthus, 1974), is a major yield-reducing factor in staple cereal crops such as wheat, rice, barley, maize and oats (Islam et al., 2007; Wu and Ma, 2016). It is induced by strong winds or heavy precipitation/hail and is exacerbated by improper crop management practices such as excessive nitrogen applications or high planting density (Duy et al., 2004). Studies conducted by Berry and Spink (2012) and Berry et al. (2013) report that yield losses in cereal crops and oilseed rape in the UK could be as high as 75% if lodging occurs close to the grain-filling period. In a severe lodging year, such losses are estimated at £105 and £64 million for wheat and oilseed rape, respectively (Berry, 2013). Lodging also causes several knock-on effects such as deterioration in grain quality, destruction in plant morphology, physiological disruptions, etc. (Norberg et al., 1988; Setter et al., 1997). Therefore, proper monitoring of lodging, its impact, seasonal susceptibility and risk assessment is of interest for farmers, agronomists, insurance loss adjusters, and policymakers.

2.1.2 The role of remote sensing

The past few decades have witnessed considerable growth in the use of sensors on-board Earth Observation (EO) systems for agricultural monitoring applications. Today, crop biophysical properties such as leaf area index (LAI) can be estimated globally at the high spatial resolution, providing reliable inputs to crop growth models. RS estimates of crop lodging are also an important component of crop growth models and can help us make better crop production/loss estimates.

Agronomists and plant physiologists have studied the problem of crop lodging for decades. For example, several studies have developed models to simulate and assess seasonal lodging risk (Baker et al., 2014, 1998; Sposaro et al., 2010) and to understand lodging-related morphological traits (Berry et al., 2002; Islam et al., 2007; Kong et al., 2013). These studies rely on the field- or lab-based methods and visual ratings for lodging assessment. Conventionally, visual lodging evaluation is done by assigning a lodging score to a crop, based on the lodged area and crop angle of inclination (CAI) (Fischer and Stapper, 1987). However,

such methods are likely to be constrained by limited coverage, high labour consumption, poor accessibility, and unfavourable weather conditions. RS is capable of providing consistent and continuous data in the spatial and temporal domains; however, to date, there are few examples of the use of RS for crop lodging assessment. This is mainly due to the complexity of the lodging process. While it may be straightforward to associate the increase in near-infrared (NIR) reflectance to biomass increment, the assessment of lodging is more complicated. It requires knowledge of local crop management practices and an understanding of crop biophysical variable dynamics and the physical processes involved in lodging. Given the complexity, our literature search revealed that there are only 22 peer-reviewed articles - published between 1951 and 2018 - that focus on the use of RS to assess lodging damage or its risk. It suggests that the scientific consensus on RS-based lodging assessment is still evolving.

The way vegetation responds to changing ecological and climatological conditions is reflected by an immediate or slow change in its biophysical and biochemical properties (Hong et al., 2007). The retrieval of such plant properties by RS methods has been well established and documented (Battude et al., 2016; Moran et al., 1994; Zarco-Tejada et al., 2012) and can be extended further to extract lodging-related information. An RS-based approach to study crop lodging requires i) understanding of specific plant traits, which make a plant susceptible to lodging or can help to assess the occurrence of lodging; and ii) identification of appropriate modelling approaches. Such information can help predict the occurrence of lodging (risk) and map its severity.

The existing RS-based lodging assessment studies have focused on two broad application areas: lodging detection (Liu et al., 2014; Yang et al., 2015) and lodging risk mapping (Coquil, 2004). These studies have been conducted as improvements to or complements to field-/lab-based assessment methods. However, there is no systematic review that relates field-/lab-based approaches to RS-based methods and characterises the relative strengths, assess the operational feasibility and identifies potential RS-based research gaps. This paper addresses the existing gap by exploring the current and potential application of RS for lodging damage and seasonal risk assessment. The objectives of this study are to:

- a) Present the contribution of RS within the current framework of field-/lab-based crop lodging assessment studies.

- b) Present a methodical overview of current approaches for assessing crop lodging and evaluate their strengths and weaknesses in the context of operational applications.
- c) Identify the challenges, research gaps and provide perspectives on the potential use of RS for crop lodging assessment research and applications.

2.1.3 Review approach

We browsed several scientific citation databases - Google Scholar, Scopus, ISI Web of Science, and Crossref - to search for field-/lab-based and RS-based articles on crop lodging, with keywords/expressions such as: crop lodging OR lodging AND husbandry; crop lodging OR lodging risk AND yield loss; remote sensing AND crop lodging OR plant lodging, etc. To refine the search in each category we altered or added more keywords, e.g., we searched for papers focusing on lodging (or its risk) in specific crops such as wheat, barley, and rice, or we substituted “remote sensing” with specific sensor types/names such as Remotely Piloted Aircraft System (RPAS), thermal, multispectral, radar, RADARSAT-2, etc. During the search, we came across very few ISI publications (22) that focused on the use of RS technique to assess lodging, which suggests that the use of this technology for crop lodging assessment is still in a nascent stage. To ensure that we covered all the studies, we also searched for the cited references individually.

On the other hand, we retrieved more than 5000 field-/lab-based studies based on the set criteria (e.g., “crop lodging” OR “lodging risk” AND “husbandry”; “crop lodging” OR “lodging risk” AND “yield loss”). We focus on significant peer-reviewed articles (field-/lab-based) on lodging published post-1951 since they have formed an important basis in the understanding of lodging phenomenon. We further pruned the number of field-/lab-based studies (to 49) to include modelling or observational studies where RS can have a contribution. We derived the descriptive statistics from a set of 71 studies (field-/lab-based – 49, RS-based – 22). Fig. 2.1 illustrates the trend of field-/lab-based and RS-based publications over the past 68 years.

While the focus of our review was to examine the progress made in RS-based assessment of crop lodging and to explore future potential areas, most RS-based studies have built upon numerous field-/lab-based experiments, hence their inclusion here. The RS-based studies have mainly highlighted the application of RS for lodging detection in cereal crops (Liu et al., 2012; Ogden et al., 2002;

Yang et al., 2017; Zhao et al., 2017) and to our knowledge, only one study has explored the complex interactions between environmental and crop management factors to map (or predict) the risk of lodging (Coquil, 2004).

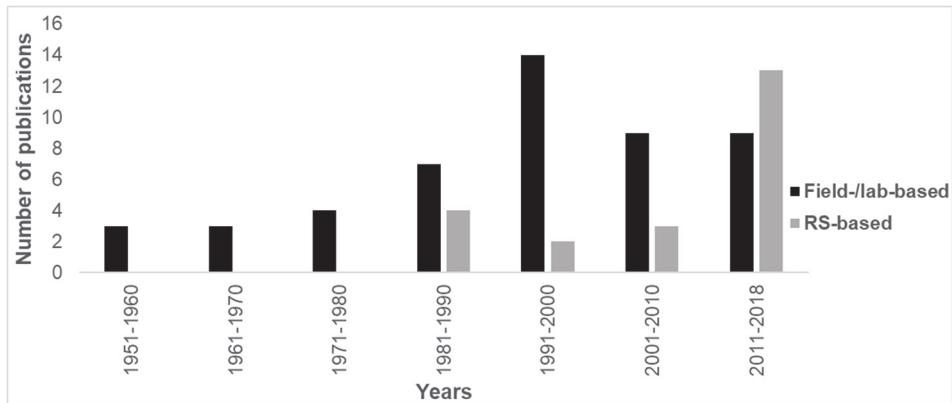


Fig. 2.1. Distribution of the selected peer-reviewed publications on lodging assessment within the last 68 years. The figure synthesizes the publications retrieved using controlled searches on Crossref, ISI Web of Science, Scopus and Google Scholar databases. These publications include significant lodging studies that have formed the basis of current lodging research and are important from an RS perspective. These studies are published as complete research articles in peer-reviewed journals or as book chapters or in conference proceedings between 1951 and 2018. The trend in field-/lab-based studies is based on the selected studies only.

The remainder of the paper is structured as follows: Section 2 provides a theoretical background on lodging and briefly discusses the scope of RS within the current framework of field-/lab-based studies for crop lodging assessment. The review of field-/lab-based studies aims to understand: (i) the mechanics and factors that cause lodging; (ii) impact of lodging on yield loss; and (iii) methods/models for crop lodging assessment. Section 3 gives an overview of the status of RS-based lodging assessment at different scales and a variety of methods for assessing lodging. The advantages, drawbacks, and potential of each method are also highlighted. Section 4 discusses the challenges of RS-based crop lodging assessment. In section 5, we examine the research gaps in existing approaches and provide recommendations to undertake future studies. We provide an outlook on the new and upcoming sensors/platforms having potential for lodging assessment in section 6, and in the final section, we conclude the main findings.

2.2 Theoretical background and scope of remote sensing in lodging assessment

2.2.1 Background and mechanics of lodging

Before we proceed, it is important to understand the conceptual differences between the two terms: susceptibility and risk. In the case of lodging, susceptibility means the degree to which the crop is prone to lodging. It captures the fact that the host (the plant) reacts variably to lodging, some plants do better than others even if the exposure to a certain external factor is the same. Heavy rain increases the risk of lodging, but the amount and severity of lodging that occurs will be (partially) determined by how susceptible each plant is to lodging.

From a mechanical perspective, the susceptibility of a crop to lodge depends on two factors: (i) bending strength of the stem and its resistance to buckle (Neenan and Spencer-Smith, 1975) and (ii) the anchorage strength of the root system (Crook and Ennos, 1993). The cultivar, environment, management practices and their complex interactions, strongly influence these factors due to their effects on the crop structure (Berry et al., 2004). A study of all these factors together can form part of a comprehensive lodging risk assessment.

The bending strength of a stem can be quantified by the amount of force needed to break it and is an essential determinant of lodging resistance. Baker (1995) expressed this force as a wind-induced base bending moment (leverage force) and illustrated its significance in comprehending the mechanics of stem (Fig. 2.2b) and root (Fig. 2.2c) lodging. Crook and Ennos (1995, 1994) approximated these wind-induced forces into a plant self-weight moment. Plant self-weight moment is a moment induced at the plant base by the weight of the aerial parts of the plant (such as leaves, head, and stem). It is governed by the plant's height at the centre of gravity, fresh aerial biomass of the plant, in addition to the CAI (illustrated in Fig. 2.2).

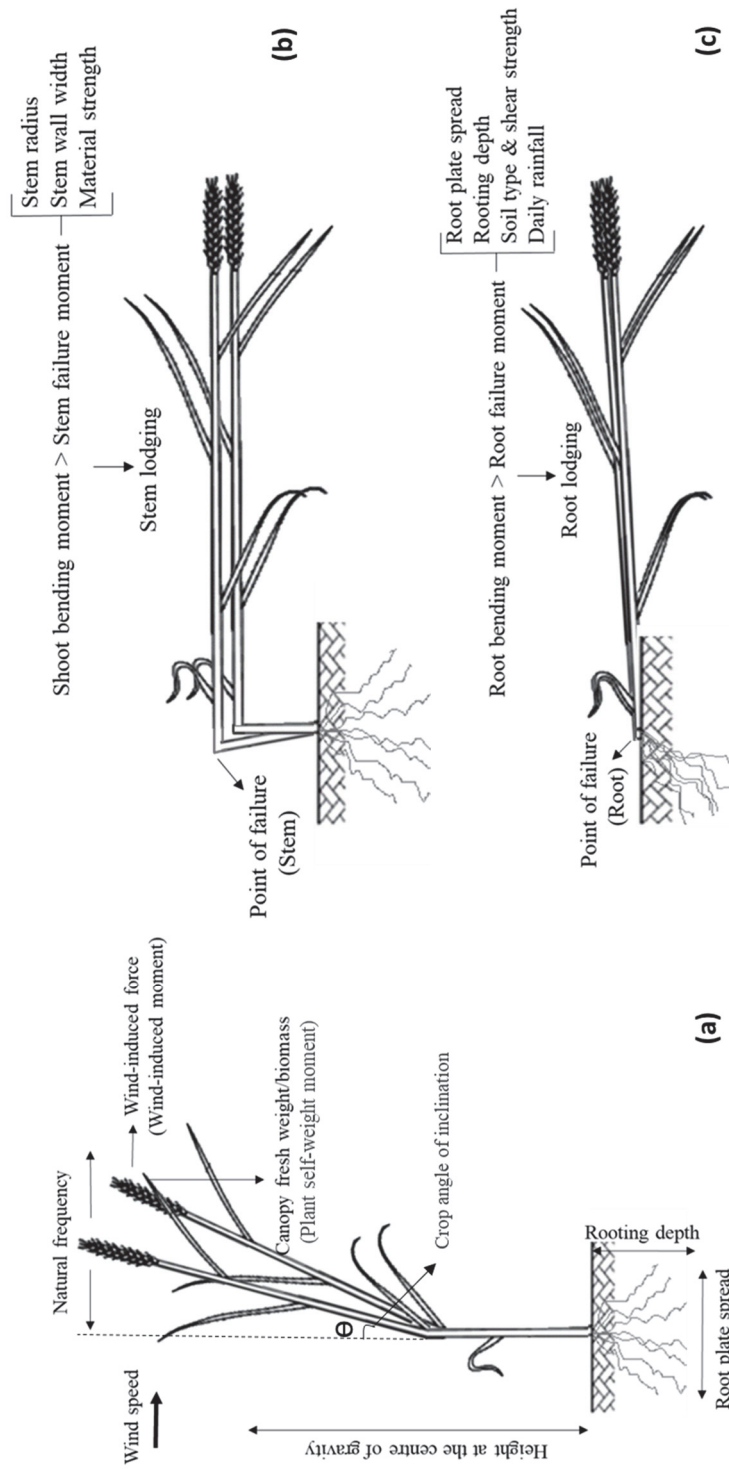


Fig. 2.2. Determinants of (a) wind-induced and plant self-weight moment, (b) stem strength and stem lodging and (c) anchorage strength and root lodging (Modified after Berry et al. (2002)).

Timely and quantitative measurement of the variation in plant self-weight moment (or its determinants such as fresh aerial biomass) can help assign safety factors to a crop to reduce stem/root lodging and more importantly, can indicate the lodging susceptibility in future. A large body of literature spanning almost five decades has shown that RS technology has the potential to study the complex interactions in the crop canopy by providing detailed spatio-temporal information on plant response to the local environment and management practices (Asrar et al., 1985; Jackson, 1986; Lemaire et al., 2008).

2.2.2 Factors affecting crop lodging

The lodging risk of a crop is altered by the genetic, crop management and environmental factors, as shown in Fig. 2.3 (Berry et al., 2000; Hanley et al., 1961). The effect of these factors on lodging is difficult to quantify due to the complexity of the lodging process. According to the practical guidelines issued by the Agriculture and Horticulture Development Board (AHDB, 2005), lodging risk can be scored on a scale of 1 to 9 (a higher score means higher resistance to lodging). To assess lodging risk, the cultivar lodging resistance score (determined through crop cultivar trials) is adjusted for the effect of wind speed, rainfall, LAI, crop nitrogen content, soil nitrogen supply, sowing date, and plant population density.

Weather is an important aspect affecting lodging. Even 6-11 mm rain in a day can cause root failure by decreasing the soil strength, thereby increasing the risk of root lodging (AHDB, 2005). The study by Sylvester-Bradley et al. (1990) suggests that prolonged rainfall can also increase the plant self-weight moment on the stem base. Heavy rain, when accompanied by strong winds, can significantly increase the lodging risk, too (Niu et al., 2016).

Apart from environmental factors, the crop management plan can be designed such that it minimises a plant's susceptibility and ultimately, the risk of lodging. Sowing date, for instance, can affect the lodging susceptibility in winter wheat (Green and Ivins, 1985). Early sowing makes a plant more susceptible to lodging as it increases the residual soil nitrogen uptake efficiency, which results in profuse vegetative growth (Fischer and Stapper, 1987; Kirby et al., 1985; Spink et al., 2000). RS can provide reliable methods to monitor plant phenology and delineate spatio-temporal phenological patterns across large areas in a timely and accurate way (Boschetti et al., 2017; Manfron et al., 2017; Sakamoto et al., 2005). While numerous methods have been proposed to detect the timing of vegetation

green-up, maturity, senescence, and dormancy (e.g., Funk and Budde (2009); Zhang et al. (2003)), only a few have related phenological information derived from RS time-series to determine actual sowing dates (e.g. Jain et al. (2016); Marinho et al. (2014)).

Lodging due to high plant population density is also prevalent in many crops such as wheat (Webster and Jackson, 1993), corn (Sangoi et al., 2002; Van Roekel and Coulter, 2011) and barley (Kirby, 1967). High seed rates lead to dense plant tillering and competition for limited resources (nutrients, space, etc.). According to AHDB guidelines (AHDB, 2005), an increase of 50 plants/m² in winter wheat can lower the cultivar root and stem lodging resistance score by 1 and 0.5, respectively. High plant nitrogen and soil nitrogen supply can also increase lodging in cereals by either promoting vegetative growth (i.e., biomass) or by increasing stem height and thereby the plant self-weight moment (Chalmers et al., 1998; Tripathi et al., 2003). Accurate measurement of plant population density and nitrogen content during the growing season is a key to the targeted application of resources (such as fertilisers or plant growth regulators) as well as for mapping seasonal lodging susceptibility. Several studies have shown that RS signal (e.g., reflectance or backscatter) is a potential source for estimating plant population density (Patel et al., 2006) and characterising the plant/soil nitrogen status (Sorenson et al., 2017).

Structural crop parameters, such as plant height can also affect the lodging resistance of a cultivar and have been a central focus of seasonal crop lodging risk management (Pinthus, 1974). In the event of lodging, the plant structure is destroyed such that the stem is inclined at a certain angle, thus reducing the plant height (basically the distance between the plant head and the soil surface) (Murakami et al., 2012; Setter et al., 1997; Zhu et al., 2016). Setter et al. (1997) reported a reduction of 75% in rice canopy height under lodged conditions, which consequently lowered the photosynthesis rate by 60-80% relative to non-lodged rice. Thus, a rapid, continuous and in-season availability of plant height data is essential for developing lodging classification models and seasonal risk mapping applications. Structure-from-Motion (SfM) photogrammetry using high-resolution RPAS data (Holman et al., 2016), crop surface models derived from LiDAR data (Eitel et al., 2016) and polarimetric-interferometric capabilities of SAR data (Erten et al., 2016) have been applied successfully to estimate plant height (in non-lodged conditions) throughout the growing season. The measurement of LAI at the beginning of stem elongation (GS30-31), together

with ancillary information on the cultivar lodging resistance score and the yield potential, can also enable lodging risk prediction and formulate subsequent plant growth regulator (PGR) programme (BASF, 2011). Using RS, LAI products can be produced at local, regional and global scales. For instance, LAI has been derived from high spatial resolution (10-30m) data such as MSI and ETM+/OLI-TIRS on-board Sentinel-2 and Landsat respectively (Campos-Taberner et al., 2016; Fang et al., 2003), as well as from coarse to moderate resolution data (1 km) such as MODIS, SPOT/VEGETATION, AVHRR and PROBA-V sensors (Gao et al., 2008).

2.2.3 Crop yield response to lodging

The response of crop yield to lodging has been explored in a large number of studies, but only at field or lab scale (Baylis and Wright, 1990; Easson et al., 1993; Lang et al., 2012; Sisler and Olson, 1951). The outcome of these studies indicates that lodging severity impacts the extent of lodging-induced yield loss (Fig. 2.3). The studies also show that three factors govern lodging severity: the lodging stage (defined based on crop angle of inclination), the lodged area and time of its occurrence (phenological stage). A crop with a high CAI, lodged on a large surface area and close to the grain-filling growth stage depicts the most severe form of lodging (Caldicott and Nuttall, 1979; Laude and Pauli, 1956; Stanca et al., 1979). Determination of lodging severity has long been pursued via conventional field-based methods (Fischer and Stapper, 1987; Piñera-Chavez et al., 2016).

RS has demonstrated to be a superior alternative for measuring 3D vegetation structure across different scales (e.g., Gao et al. (2013)). While several studies have assimilated RS data into crop growth models to improve crop yield estimates (Dente et al., 2008; Fang et al., 2008), further work is required to incorporate lodging severity into yield prediction models. We present a summary of important factors related to seasonal lodging risk assessment, lodging detection and yield loss in Fig. 2.3. The figure also illustrates the potential contribution of RS in estimating lodging-related parameters related to different factors.

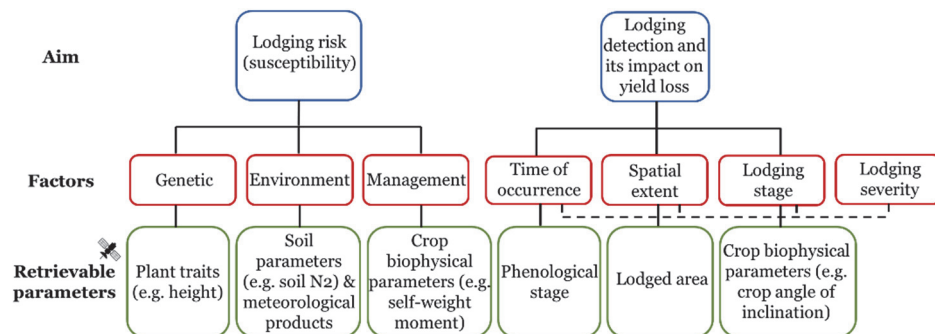


Fig. 2.3. Summary of important factors related to lodging (seasonal susceptibility and risk assessment, lodging detection and its impact on yield loss) and potential contribution of RS.

2.2.4 Field-/lab-based methods for crop lodging assessment

Based on the selected studies, we found that lodging has been studied most extensively in wheat (Sterling et al., 2003) followed by barley (Stanca et al., 1979; White, 1991) and rice or cereals in general (Lang et al., 2012) (Fig. 2.4). Several methods and models of lodging assessment have been developed for these crops (Baker et al., 1998; Berry et al., 2006). For instance, Caldicott and Nuttall (1979) adapted the prior work of Caldicott (1966) and Caldicott and Nuttall (1968), to develop a field-based visual/*in situ* assessment method for determining the lodging score in cereals. The score, on a scale of 1 (completely lodged) to 10 (no lodging), accounts for both; the lodged area and the stage (CAI) of lodging. Retrieval of the lodging score is an interesting application from RS perspective since current approaches are solely based on visual ratings.

In another study, Baker (1995) made the first attempt to develop a theoretical model for the windthrow (i.e. uprooting or breakage by wind) of cereals and forest trees. The model was extended by Baker et al. (1998) to develop a quantitative lodging risk model for wheat. Sterling et al. (2003) and Berry et al. (2003b) further refined and validated the model to obtain more accurate model parameters. The fundamental assumption of these models is the depiction of a crop as a simple damped harmonic oscillator. These works have formed a basis of the methodology that is now being used to guide farmers and agronomists in many countries (such as the UK) on ways to reduce lodging risk in wheat.

The applicability of these models has also been tested on other crops. For instance, Berry et al. (2006) extended the wheat-lodging model to barley. The authors suggest that a minor modification is needed to adapt the wheat root-

lodging model to barley. In contrast, the stem-lodging model needs to be changed substantially, owing to the less erect nature of barley ears, greater stem height, and increased flexibility. Similarly, Sposaro et al. (2010) developed a mathematical lodging model for sunflower based on existing models for wheat and barley. A more generalized model was developed by Baker et al. (2014) to calculate crop lodging risk. The authors tested the model on barley, oats, and oilseed rape and found varying levels of uncertainties in the lodging risk for each crop. Mi et al. (2011) and more recently, Brune et al. (2017) also developed models to predict lodging risk in maize.

While these mathematical models are promising and provide an understanding of the lodging process, they are data-intensive, complex and computationally expensive. They also require prior knowledge and understanding of the input data for proper calibration and fine-tuning. Moreover, model formulations are primarily based on empirical data and artificially induced or controlled lodging conditions. These models, therefore, need to be optimized before they can be extended on a larger scale. More straightforward methods are needed that can rapidly assess the biophysical parameters of crops and provide accurate lodging-related information.

2.3 Review of remote sensing-based studies for crop lodging assessment

The traditional techniques for crop lodging assessment are visual ratings/*in situ* assessment and the use of complex field-/lab-based physical models. Visual rating is a direct way to evaluate the extent and degree of lodging damage in crops, but it has its drawbacks as discussed previously. The field-/lab-based models, on the other hand, are data-intensive and largely based on empirical data. RS can complement the traditional methods and has the potential to extend our knowledge of crop lodging in space and time (Branson, 2011). The past decade has seen an increase in the use of RS for crop lodging assessment, although the research in this domain is still at an early stage. Broadly, we have grouped the current RS studies into three categories based on the monitoring platform deployed: ground-based, airborne and spaceborne. Table 2.1 lists the studies that demonstrate the use of different RS platforms for crop lodging assessment in terms of the aim, crops studied, extent, scale and significant findings.

Table 2.1. Existing remote sensing studies for crop lodging assessment. The list in the table is sorted based on the platform types (ground-based, airborne, and spaceborne). For a higher resolution version please refer to <https://www.sciencedirect.com/science/article/abs/pii/S0924271619300747>

	configuration	frequency	period of study	site
1	Fanochromatic Ground-based	Kodak Plus-X panchromatic film used, Polarizing filter at 0°, 45°, 90° and 135°, 8-bit resolution	Crop(s): common wheat, barley, durum wheat Year: 1982	California Local
2	Microwave Ground-based	Scatterometer with X-band VV, HH polarization, incidence angles: 10° to 80°	Repeated measurements at 2.5 days interval of 1-4 days.	Wageningen, Rotterdam, Dromen Local
3	Microwave Ground-based	Scatterometer with X-band VV, HH polarization, incidence angles: 10° to 80°	Repeated measurements at 2-5 days the interval of 1975-1981	Wageningen, Rotterdam, Dromen Local
4	Microwave Ground-based	Scatterometer with X-band VV, HH polarization, incidence angles: 10° to 80°	Repeated measurements at the interval of 2-5 days.	Test farm in Wageningen, Rotterdam, Dromen Local
5	VNIR Ground-based	Motor driven cameras with shutter speed: 1/60; F: 2.8, 4, or 5.6 depending on the light condition	Crop(s): rice Year: 1991	Japan Local (26 sites)
6	VNIR Ground-based	Two Nikon digital cameras (RGB and NIR band-pass filter), auto flash inside	Crop(s): rice, barley Year: 2007	Toyama and Tsukuba, Japan Experimental
7	VNIR-SWIR (hyperspectral) Ground-based	ASD FieldSpec Pro FTSM Spectroradiometer with spectral range from 250 nm to 2500 nm, spectral: 3 nm to 10 nm	2 times repeated measurements with the interval of 4 days.	Heilongjiang and Zhejiang provinces, China Local (92 sites)
8	VIS Ground-based and airborne	Nikon D80 and D90 (l1 Phantom series	2 times repeated measurements with the interval of 4 days.	Timisoara, Romania Scale Local

The spatial mean value of linear polarization decreased for barley but increased for both kinds of wheat due to lodging

Information is lost while extracting the image arrays from photographs; image correction procedure assumes the light reflected from greyscale to be unpolarized

Understand linear polarization response to lodging

Assess the main backscatter influencing factors in crops

Backscatter (σ^0) at 20° decreased by 2 dB with the lodging of potato

Badly: Increase in σ^0 at medium and high angles of incidence (by 2 dB) caused by lodging more polarization.

Assess the main backscatter influencing factors in crops

Understand the backscatter response to lodging at different incidence angles

Backscatter (σ^0) at 20° decreased by 2 dB with the lodging of potato

Badly: Increase in σ^0 at medium and high angles of incidence (by 2 dB) caused by lodging more polarization.

Ons: Increase in σ^0 at low angles of incidence and a small increase at medium angles

Understand the backscatter response to lodging at different incidence angles

Predict lodging scores

Increase in VV backscatter caused by lodging in barley.

Heavily dependent on data quality such as the pixel values

Pixel values along the transects across images can enable prediction of lodging scores (Lodging severity/stage)

Lodging detection/assessment/ classification

Indices such as green NDVI and Night time relative brightness index in NIR are sensitive to lodging

Simple digital camera with small modification can record temporal profiles of indices on a field scale

Wheat: Low spectral values in R and G channels (and higher in B) as compared to healthy crops

Barley: low RGB spectral values as compared to healthy crops

#	Reference	Platform	Spectral-domain	Sensor/system configuration	Data acquisition frequency	Crops and period of study	Location/ study site	Scale	Aim	Results/findings	Our remark(s)
9	Gerten and Wise (1987)	Airborne	VNIR	Apple IIC microcomputer with a digitizer and interfaced to an RCA video camera	3 times repeated measurements with the interval of 15 days.	Crop(s): winter wheat Year: 1983	Eastern Washington	Local (7 fields)	Lodging detection/ damage assessment/ classification	The video image analysis of colour and NIR photographs detected lodging from 2 to 32% of the total area of each field based on differences in light intensity	The lodged areas were highly underestimated during video image analysis from original photographs
10	Bouman and Hoekman (1993)	Airborne	Microwave	Scatterometer with six frequency bands: L, S, C, C, K ₁ , K ₂ at VV, HH polarization, incidence angles: 10° to 60°	Single image acquisition.	Crop(s): winter wheat Period: 1987-88	Southern Plevoland, Netherlands	Local (35 fields)	Understand backscatter response of crops	Lodging increased the backscatter in all angles of incidence with higher frequencies (X- to K ₂ bands) being most sensitive to the canopy architecture	The field sample size was not sufficient for a statistically significant solution
11	Murakami et al. (2012)	Airborne	VIS	Panasonic Lumix FX-40 camera with 12 million pixels (4000 × 3000)	4 times repeated measurements with the interval of 14 days.	Crop(s): buckwheat Year: 2010	Iwate, Japan	Experimental (single field of ~ 235 m ²)	Lodging detection/ damage assessment/ classification	Lodging easily distinguished in 3D images based on texture and colour. Digital canopy height used as an index of lodging severity/stage	Significant underestimation of plant height at the harvesting stage
12	Chapman et al. (2014)	Airborne	VNIR (red-edge and thermal)	Remotely-piloted aerial system (RPAS) with Mircle thermal camera, RICOH cameras with a 10 million pixel CCD image sensor, Thermoteknix MIRACLE 307 K with ≤ 50 mK sensitivity (excluding optics) and 56.3° horizontal field of view RPAS with photo3S optical camera and ADC-lite (NIR) camera	Single image acquisition.	Crop(s): irrigated wheat Year: 2012	Southern Queensland	Local (90 plots)	Lodging detection/ damage assessment/ classification	NIR (red-edge) band more sensitive to lodged areas; Crop height used as a measure to detect lodged areas; Canopy temperature of lodged areas is higher than the non-lodged areas	The platform cannot be purchased as "ready-to-fly," miniaturization of the imaging platform can result in a low-cost system
13	Zhang et al. (2014)	Airborne	VNIR	RPAS with Canon Power Shot G16, resolution: 3000 × 4000; Terras an ADC Litar multispectral camera	Single image acquisition.	Crop(s): wheat, soybean, barley, oats, canola Period: 2013-14 Year: 2014	North-eastern Ontario, Canada	Local (45 plots)	Lodging detection/ damage assessment/ classification	Large contrast in lodged and non-lodged areas in the infrared image	Critical to set up a routine procedure for image capture and processing due to high costs
14	Liu et al. (2014)	Airborne	VNIR	RPAS with Canon Power Shot G16, resolution: 3000 × 4000; Terras an ADC Litar multispectral camera	Single image acquisition	Crop(s): wheat Year: 2014	Yangzhou, China	Experimental	Lodging detection/ damage assessment/ classification	Combination of spectral and textural features resulted in highest classification accuracy of lodged and non-lodged fields (Lodging detection)	The texture of wheat lodging is very close to that of bare land resulting in the mixing of these two classes. The small sample size makes it difficult to arrive at robust conclusions.
15	Chu et al. (2017)	Airborne	VNIR	RPAS with 4 cameras with array size of 4048 × 3048, 4000 × 3000, 4000 × 3000, and 4608 × 3456 pixels, respectively	19 times repeated measurements with the interval of 1-10 days.	Crop(s): corn Year: 2016	Texas	Experimental (single field < 100 m ²)	Lodging detection/ damage assessment/ classification	Mathematical grid-based lodging assessment based on plant height can enable the detection and estimation of the number of lodged plants per unit area	Less accurate for heterogeneous crop angles of inclination resulting in under/ overestimation
16		Airborne	VNIR				Hokkaido, Japan				

Remote sensing-based crop lodging assessment: Current status and perspectives

#	Reference	Platform	Spectral-domain	Sensor/System configuration	Data acquisition frequency	Crops and period of study	Location/ study site	Scale	Aim	Results/findings	Our remark(s)
	Du and Noguchi (2017)			RPAS with SONY ILCE-6000 digital camera	8 times repeated measurements with the interval of 7 days	Crop(s): wheat Year: 2015		Experimental (3.2 ha)	Lodging detection/ damage assessment/ classification	Visually interpreted lodging patterns in the orthomosaic colour images	Visual interpretation is error-prone since it is neither quantitative nor objective
17	Yang et al. (2017)	Airborne	VMIR	RPAS with Samsung NX200 digital camera with 20.3-megapixel APS-C CMOS sensor, the image size of 23.5 mm × 15.7 mm	Single image acquisition.	Crop(s): rice Year: 2014	Chianan Plain and Taibao City, Taiwan	Local (3 ha)	Lodging detection/ damage assessment/ classification	Used a decision tree classifier to classify lodged rice from an image composite of spectral (RGB) and texture information, also calculated lodging ratio for each field	
18	Coquil (2004)	Space- and airborne	VMIR (multi- and hyperspectral)	Spot satellites, Infoerra's AISA Eagle with 11 VNIR channels/CASI/MVIS sensors	2 times repeated measurements with the interval of 24 days	Crop(s): wheat, winter barley, corn, potato, soybean, rapeseed Period: development since 1996, operational in France since 2002	France, UK, Germany, Australia, Canada	Regional (800,000 ha)	Lodging risk mapping	LAI, plant nitrogen, plant population, and crop biomass used to estimate the lodging risk	Estimation of biophysical parameters relies on the combined use of SPOT and airborne sensors, due to limited spectral bands in SPOT
19	Yang et al. (2015)	Spaceborne	Microwave	SLC C-band fully polarimetric, Radarsat-2 data, fine quad mode	2 times repeated measurements with the interval of 24 days.	Crop(s): wheat Year: 2013	Mongolia, China	Regional (Farm of ~ 3000 ha)	Lodging detection/ damage assessment/ classification	Polarimetric ratios such as $\sigma_{hh}^0/\sigma_{vv}^0$, $\sigma_{hv}^0/\sigma_{vh}^0$, $\sigma_{hh}^0/\sigma_{vv}^0 + \sigma_{hh}^0/\sigma_{vv}^0$, $\sigma_{hh}^0/\sigma_{vv}^0 + \sigma_{hh}^0/\sigma_{vv}^0 + \sigma_{hh}^0/\sigma_{vv}^0$ can be used to distinguish lodged fields from normal ones	Solely relying on the backscatter and polarimetric characteristics to identify lodging and is merely qualitative.
20	Chen et al. (2016)	Spaceborne	Microwave	SLC C-band fully polarimetric, Radarsat-2 data	6 times repeated measurements with the interval of 24 days.	Crop(s): irrigated sugarcane Year: 2013	Guangdong Province, China	Local (700 fields based on field survey and empirical selection, 3000 pixels)	Lodging detection/ damage assessment/ classification	HV backscatter, T22, T33, and polarimetric features such as double and volume scattering are capable of lodging detection in sugarcane	Trends in polarimetric features are influenced by a composite of plant variables related to crop growth and not just lodging; lack of quantitative estimates
21	Zhao et al. (2017)	Spaceborne	Microwave	The SLC-C band fully polarimetric, Radarsat-2 data in POI-8 mode with a central incidence angle of 38°	5 times repeated measurements with the interval of 6-12 days	Crop(s): wheat, canola Year: 2013	Erguna, China,	Local (2-47 ha)	Lodging detection/ damage assessment/ classification	Reflection asymmetry and reduced extinction coefficient observed for wheat but not for canola. Increased WV, decreased HH and increased depolarization degree observed for wheat.	More detailed <i>in situ</i> measurements needed to reduce uncertainty in the crop growth analysis at different lodging stages and moisture levels
22	Han et al. (2017)	Spaceborne	Microwave	Chand, WV, VH polarization, incidence angle: 30, 47-45, 98°	3 times repeated measurements with the interval of 6-12 days	Crop(s): corn Year: 2017	The experimental area in National Precision Agriculture Research and Demonstration Base, Beijing.	Regional (2500 acres)	Lodging detection/ damage assessment/ classification	VH backscatter is sensitive to the plant height before lodging while WV, VH to the plant lodging. The height difference before and after lodging is used to classify the degree of lodging: mild, moderate and severe	The model only applies to tasselling corn stage.

2.3.1 Remote sensing platforms for crop lodging assessment

2.3.1.1 Ground-based platforms

RS-based agricultural applications have particular spatial, radiometric and temporal resolution requirements. For example, timely availability of diagnostic information on a crop's biophysical and ecophysiological status (such as LAI) is critical in the context of precision farming (Doraiswamy et al., 2004), while high spatial resolution is mandatory when observing fragmented crop fields or for assessing within-field variability (Cushnie, 1987). The motivation behind using ground-based or proximal sensing systems is mainly threefold: i) ground conditions can be manipulated or conditioned to examine the effects of specific crop parameters; ii) the mixed-pixel impact is reduced and iii) high spatial resolution information is not constrained by weather conditions or platform revisit frequency, thus enabling the timely implementation of required remedial action (Moran et al., 1997). Our literature review shows that most of the studies (10) have applied proximal sensing to analyse the RS signal from lodged crop canopies (Fig. 2.4). Of these, only a few deal with lodging as the central focus (e.g., Ogden et al. (2002)), while the majority provide some valuable interpretations about the behaviour of the RS signal in response to crop lodging (e.g., Bouman and van Kasteren (1990a), Fitch et al. (1984), Sakamoto et al. (2010); see Table 2.1).

When a plant is lodged, the signal that is reflected or backscattered at different wavelengths is affected by the changes in plant geometry and structure (LAI, leaf angle of inclination and CAI) (Hosoi and Omasa, 2012); plant morphology (plant height and biomass) (Murakami et al., 2012) and plant biochemical properties (such as chlorophyll content) (Baret et al., 2007; Clevers, 1986). Multispectral data have been exploited to assess these changes in most of the investigations. Earlier work by Fitch et al. (1984) examined the linear polarisation of light reflected from wheat and barley to determine its potential in detecting the differences in crop morphology. The spatial mean value of polarisation showed a decreasing trend for barley, but an increase for wheat due to lodging.

In another study, Ogden et al. (2002) employed motor-driven cameras in paddy fields to investigate the use of textural information from digital images to measure the extent of lodging. However, studies suggest that textural information alone fails to give effective classification results (Berberoglu et al., 2000) as different image characteristics, due to differences in vigour, soil type or phenology etc.

may produce contradicting results (Sims and Gamon, 2002). Therefore, more research should be conducted to validate the applicability of texture-based approaches for lodging assessment.

The use of hyperspectral measurements for distinguishing lodged and non-lodged rice has also been demonstrated by Liu et al. (2012). They observed that the shape of the spectral signature of lodged rice is similar to that of non-lodged. However, there is a significant increase in the spectral amplitude. Broadly, it can be concluded that studies employing proximal optical sensors mostly rely on the spectral reflectance-based measures to assess lodging state, but this approach has some contradictions. For example, Yang et al. (2015) state that the success of using spectral methods is limited to ideal situations only since the change in spectral features due to lodging is relatively weak. It is often drowned out in the complex mixed spectrum of features that optical data is sensitive to (like moisture stress, pesticide stress or pigment content). Thus, more conclusive results are needed to comment on the utility of optical RS data for crop lodging assessment.

The feasibility of studying geometric or structural characteristics of a crop canopy with synthetic aperture radar (SAR) data has long been recognised and is well documented (Brown et al., 2003; McNairn and Brisco, 2004). Since crop structural changes are evident in the event of lodging, observations made from SAR data can be useful in crop lodging assessment since lodged crops exhibit asymmetric polarimetric behaviour, in contrast to the symmetric behaviour portrayed by standing vegetation in the azimuth direction (Freeman et al., 1994). Ground-based SAR systems (such as scatterometers) can be instrumental in investigating the response of radar data to crop lodging due to the availability of a wide range of sensor configurations (such as multi-polarisation, multi-frequency, etc.). For instance, Bouman and van Kasteren (1990a, 1990b) estimated lodging-induced changes in radar backscattering with multi-parametric scatterometer data. The main findings of these studies are presented in Table 2.1. In another study, Bouman (1991a) suggested that a sudden increase in radar backscatter from wheat could indicate lodging. These studies also state that for a given crop type, the satellite incidence angle and state of polarisation can contribute to high variability in the backscatter signal obtained from lodged crops. Our review suggests that there has been no detailed investigation of the suitability of different radar configurations (for example, the sensitivity of satellite incidence angle to lodging) and polarimetric data to detect lodging.

With the increasing pressure and growing demand for efficient crop monitoring methods to improve management, there is a need to transfer the research from these scientific studies to agricultural practices. Proximal sensing is particularly suited for such applications, as it allows an “on-the-go” monitoring of the crop with high temporal resolution. However, there are some limitations to its commercial use in agriculture at this moment. For instance, the spatial coverage of proximal monitoring equipment is poor, even if mounted on fixed poles or moving vehicles (Maes and Steppe, 2012). In such scenarios, multiple sensors are required to view entire fields, which can be prohibitively expensive. With advances in ground-based sensors, it is now possible to mount some sensors directly on the operating tractor (e.g., GreenSeeker active canopy sensor; Trimble, Sunnyvale, CA, USA) and map the variability within a field during mechanisation activities.

2.3.1.2 Airborne platforms

Recent advancements in the development of RPAS, commonly known as drones, together with robotics, electronics and computer vision, have led to new opportunities in airborne RS (Nebiker et al., 2008). The fine spatial resolution and NRT monitoring ability of airborne RS suggests that it is well suited for applications that characterise changes in crop attributes over time. Airborne video imaging systems, LiDAR/RADAR data and RPASs have been applied to agricultural disaster (and post-disaster) assessment applications to meet the need for timely observational data (Huang et al., 2010; Hunt et al., 2005). Except for a few early applications, it is only in the last decade that the use of airborne platforms for lodging assessment has gained momentum. About 85% of these studies were published after 2010, emphasising the growing interest of the RS scientific community in the subject (Fig. 2.1).

The earliest efforts can be traced back to the work of Gerten and Wiese (1987), and Hoekman and Bouman (1993). Gerten and Wiese (1987) employed an aerial video camera to identify lodging in winter wheat. They reported high underestimation of the lodged areas due to problems in density slicing and lack of a microcomputer with enhanced graphics capabilities. Hoekman and Bouman (1993), on the other hand, analysed the angular backscattering behaviour of lodged wheat at different frequencies using airborne scatterometer data.

With the development of miniature imaging instruments (such as scanning detectors and cameras) and an expanding pool of commercial vendors facilitating

data acquisition and analysis, there has been a shift from aircraft towards relatively low-cost systems such as RPASs. In comparison to proximal sensors, RPAS platforms can carry out surveys at a faster rate without disturbing the canopy cover (Burkart et al., 2015) and are more flexible than aircrafts and satellite-based systems, in terms of flight planning. They are increasingly being deployed as RS platforms for retrieving biophysical/biochemical parameters (Thenkabail et al., 2000), detecting environmental stress (Sullivan et al., 2007) and, more recently, for extracting lodged areas and estimating lodging severity (Liu et al., 2014; Yang et al., 2017).

The importance of using airborne multispectral data has been reported by some studies. For instance, Constantinescu et al. (2017) studied the normalised reflectance RGB spectra of wheat and barley cultivars and identified distinct spectral features that differed notably across different bands. In lodged wheat, the normalised reflectance in red and green bands was lower than that in the blue band while in lodged barley; the reflectance in all the three bands was lower than the reflectance in non-lodged barley. They also employed Euclidean distance-based cluster analysis (between RGB bands), which yielded distinct clusters of lodged and non-lodged crops. Furthermore, Zhang et al. (2014) performed a qualitative analysis of lodging (in the VIS-NIR region) in wheat and found that the lodged areas could be detected as a bright red tone in the IR image. Chapman et al. (2014) reported similar results and additionally highlighted the significance of thermal images in detecting lodged areas. They found that the lodged areas appear hotter (higher surface temperature) in both day and night thermal images.

Textural features such as Grey-Level Co-Occurrence Matrix (GLCM)-based measures (Liu et al., 2014) have also been adopted in airborne RS for improving the classification accuracy of crop lodging. Texture usually provides supplementary information about the object properties, which can help in the assessment of heterogeneous crop fields (Pacifici et al., 2009), although they are highly dependent on image quality, resolution and have high computational cost. Factors such as phenological stage, canopy structure, planting patterns and plant population density mainly define the textural pattern of the crops at a parcel-scale. Combining spectral and textural features often increases the accuracy of lodging classifications (Yang et al., 2017). According to Liu et al. (2014), incorporating texture information improved the lodging classification accuracy by up to 8-9%. However, in hierarchical classification scenarios, selective application of textural information for specific classes becomes crucial since not all classes are separable

based on a single textural measure (Yang et al., 2017). Also depending on the crop and its phenological stage, the textural information can lead to contradictory results (Stroppiana et al., 2018). With a limited number of studies, it is difficult to conclude the significance of textural features for lodging classification.

As discussed in section 2.2.2, changes in crop morphological status affect the RS signal. While most of the studies rely on spectral changes and spatial variations to detect the occurrence of lodging, only a few studies have used plant traits (such as plant height) to detect lodging. For instance, Murakami et al. (2012) used digital canopy model-derived plant height as an index to detect lodging in buckwheat, with smaller height values implying severe lodging. Broadly, two approaches have been demonstrated for detecting lodging using height information derived from RPAS or aerial stereo images: (1) height thresholding and (2) grid-based thresholding. Chapman et al. (2014) calculated the average height of lodged and non-lodged crops from a DEM and used a height threshold (50 cm, based on the variance in pixel heights) to identify lodged areas. The successful delineation of 10 to 70% of the lodged area using this approach seems to confirm the validity of using height information for lodging stage detection. In a more recent study, Chu et al. (2017) investigated the potential of the grid-based thresholding approach to detect lodging. This method divides the image into grids and applies thresholds to each grid to detect the occurrence of lodging and can also be used to estimate the number of lodged plants. While this approach was applied successfully to detect lodging, the number of lodged plants were highly under/overestimated. The authors suggest that such uncertainties can be due to the existence of mixed grids (where leaves from a non-lodged grid extend into a lodged grid) and estimation errors introduced by seed count (which ultimately affects the stand count and the number of lodged plants). In summary, substantial research efforts are still required to develop transferrable crop lodging detection algorithms to facilitate proper remedial actions.

As the initial trials have demonstrated promising results towards crop lodging assessment, the introduction of such portable RPASs opens up several research directions (discussed in the later sections). In comparison to the point measurements provided by proximal sensors, airborne sensors possess the capability to offer additional information associated with the patterns of lodging, thus allowing exploration of lodging events on a larger scale. Despite some interesting results, the quality of data from RPASs relies heavily on sky conditions and is affected by intervening atmospheric disturbances, cloud or

snow cover, and solar radiation. Moreover, even though these systems deliver high spatial resolution data, radiometric responses can differ between the acquired frames, thereby generating artefacts in vegetation condition. This could be due to the inability of the automatic systems to find homologous points between frames when creating orthomosaics. Finally, commercial and research RPAS can potentially be cost-prohibitive for regional or large-scale applications.

2.3.1.3 Spaceborne platforms

Spaceborne/satellite-based platforms can monitor the textural and spectral characteristics of vegetation at varying spatial and temporal scales. They provide local to global coverage while offering data at different intervals: monthly (ERS, ASAR, RADARSAT-2), biweekly (Landsat), near-weekly (Sentinel-1 and Sentinel-2) or approximately daily (NOAA-AVHRR, SPOT-VEGETATION, MODIS, PROVA-V and Sentinel-3). The spatial, temporal, spectral, and radiometric resolution of spaceborne RS sensors is continuously improving through technical improvements in sensor technology, while access to imagery is improving through increased public and private investments in satellite platforms.

The availability of optimal resolution data actively governs the accuracy with which within-field spatial variabilities of lodging can be mapped. While moderate resolution sensors (e.g. AVHRR or MODIS) provide global coverage at daily intervals, their coarse spatial (>1km), spectral (5/6 bands) and radiometric (10/12 bits) resolution cannot capture such variabilities. Satellites such as Landsat- 7/8 with 30 m spatial resolution (and 8/11 spectral bands, 9/12-bit radiometric resolution), on the other hand, have lower revisit times (~ 16 days) which are impractical for lodging-related applications. The spatial resolutions have improved in some recent satellite sensors such as Sentinel-2 (10 or 20 m), Sentinel-1 (20×22 m) (from the European Space Agency), or commercial providers such as Worldview-4 (31 cm in the panchromatic and multispectral at 1.24 m) and IKONOS-2 (1 m). However, free access to high spatial resolution temporal spaceborne images becomes crucial if operational satellite-based quantitative applications are to be developed.

In our review, we found very few studies that have utilized RS data acquired from spaceborne platforms to address the problem of crop lodging (Fig. 2.4). To the best of our knowledge, the first study that demonstrated the capability of satellite data (SAR) to address the problem of lodging was performed in 2015 on a farm-scale extending over 3000ha (Yang et al., 2015). Until then, the potential of SAR

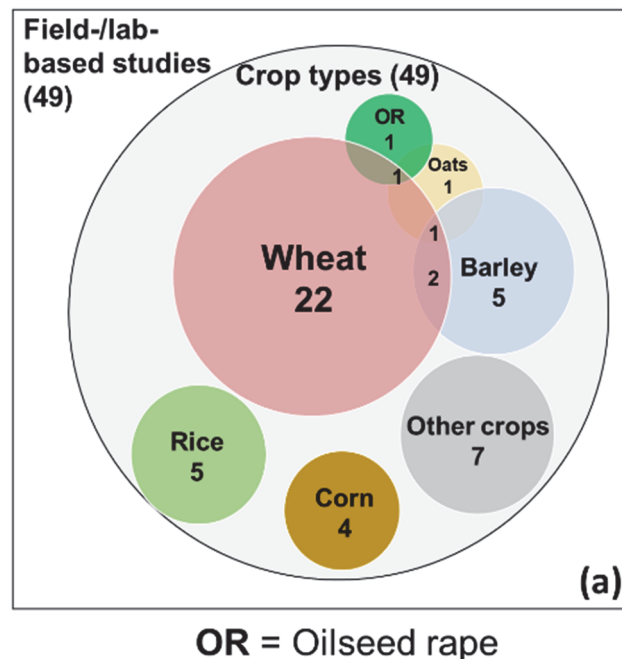
satellite data for crop lodging assessment was undetermined. Building upon the findings of earlier studies that have established the unique sensitivity of SAR to vegetation structural changes (McNairn et al., 2009; Ulaby et al., 1984), some subsequent studies have explored the potential of RADARSAT-2 quad-polarimetric data to assess lodging in wheat and sugarcane (Chen et al., 2016; Yang et al., 2015; Zhao et al., 2017). These studies suggest that advanced polarimetric parameters such as scattering ratios, circular-pol correlation coefficients, etc. and time-series data can enhance the discrimination of lodged areas from non-lodged.

However, the existing studies address lodging qualitatively and do not provide quantitative estimates of lodging (e.g., crop angle of inclination or CAI). Such estimates are important in predicting the yield losses or assessing grain quality. For instance, Fischer and Stapper (1987) demonstrated that the yield losses incurred at a CAI of 80° are almost 2-4 times than those at 45° in wheat. Furthermore, the selected sites in these studies comprise of relatively homogeneous fields. It remains a challenge to address lodging in areas with complex and fragmented agricultural fields. While a few studies have exploited the advanced capabilities of RADARSAT-2 satellite data (a single platform, commercial data source with limited revisit frequency), we found only one study that used freely accessible satellite data with a high temporal resolution to map lodging. Recently, Han et al. (2017) built a quantitative lodging classification model for maize using height information derived from Sentinel-1 data. It is a first step towards the use of satellite data for quantitative modelling of lodging.

Still, the main problem for the farmers is their inability to predict where and when lodging is likely to occur. An early-season assessment of lodging susceptibility and risk can support more accurate and cost-effective targeting of lodging control measures. While most of the studies using spaceborne data have focused on lodging detection problem, there is only one study which mentions the use of satellite images for seasonal lodging risk mapping at a regional scale. Coquil (2004) describes the FARMSTAR commercial service that was launched successfully in France in 2002. It is a decision support tool for sustainable crop management; seasonal lodging risk mapping is one of its application. The service is based on the integration of RS images (satellite, aircraft or UAVs), agronomic expertise and meteorological data, and is still operational. It exploits SPOT-6/7 satellite images to measure crop biophysical parameters (LAI, chlorophyll content and biomass) which are then analysed and transformed into seasonal

lodging risk maps for the second plant growth regulator (PGR) spray. The product has been tested on different crop types: wheat, corn, soybean, barley, potatoes, etc. and it is being transferred to other countries: such as Germany, UK, Spain, Canada and Australia. However, a challenge is posed by the spectral bands of SPOT-6/7 for the estimation of chlorophyll content and LAI, since more bands are required to decouple the absorption features of these biophysical parameters from other physical effects. As a result, highly accurate *a priori* information needs to be fed into the model inversion process, making the model data intensive. FARMSTAR also relies on the combined use of SPOT-6/7 and airborne sensors (CASI, AISA Eagle, and MIVIS) to ensure better spatial and spectral coverage for an accurate estimation of crop parameters. The applicability of spaceborne RS for lodging can thus be constrained by limited spectral bands, in addition to lower revisit times, coarser spatial resolutions and high acquisition/processing costs (in most cases).

In the view of these studies, we have categorised the RS contributions for crop lodging assessment in terms of crop type, RS platform and sensor spectral range, as illustrated in Fig. 2.4b.



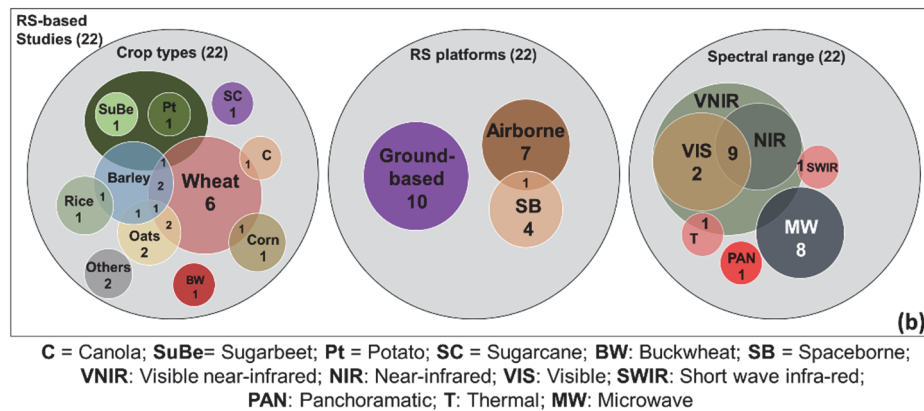


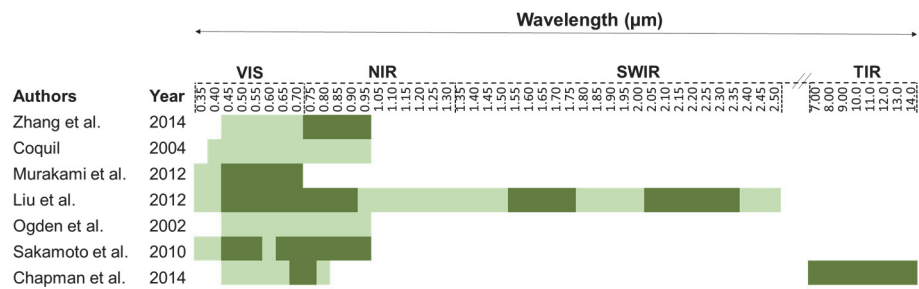
Fig. 2.4. The figure represents the number of reviewed articles based on study type: field/lab-based studies (49) and RS-based studies (22). Field/lab-based studies are further categorised based on crop type, while RS-based studies are divided into three categories: crop type, deployed RS platform and sensor spectral range.

2.3.2 Important wavelength regions and remote sensing parameters

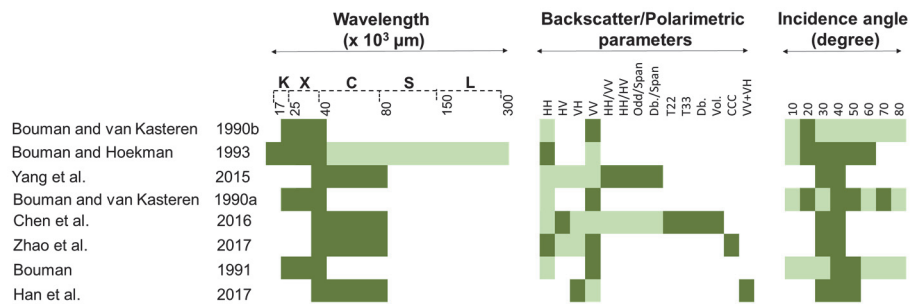
The findings of the above studies underline the importance of different wavelength regions in detecting lodging and assessing its risk (e.g., Yang et al. (2015), Zhang et al. (2014)). Fig. 2.5 summarises important wavelength regions and other RS parameters retrieved from the major RS-based crop lodging studies. Fig. 2.5a reveals that the important wavelength intervals (marked as dark green) mainly correspond to the absorption bands of plant pigments and water, thus corroborating the hypothesis that they are the main components of lodging detection in VIS-SWIR region. Some studies have highlighted the significance of the near-infrared (NIR) and red-edge regions for lodging assessment. For instance, Chapman et al. (2014) and Sakamoto et al. (2010) discuss the relevance of NIR reflectance in detecting lodging in wheat since a strong increase in the reflectance from wheat leaves and stems is recorded in NIR region (and relatively less from the underlying soil as lodged crops entirely cover it).

Crop lodging information from SAR data mainly relates to crop structural parameters such as CAI and plant height. The estimation of these features depends on the SAR wavelength, the incidence angle, as well as polarisation modes, in addition to terrain and weather conditions. The SAR wavelength governs the penetration depth of a signal through the crop canopy, with shorter wavelengths (e.g. K-, X-, C-band) interacting mainly with the top canopy and longer-wavelengths (e.g., L-, P-band) penetrating deeper through the canopy and

yielding backscatter from both vegetation and soil (Ulaby et al., 1984). Concerning the selection of optimal SAR wavelength for crop lodging assessment, studies show that shorter wavelengths, namely X- to Ku2-bands are more suitable for assessing lodging (Bouman and Hoekman, 1993; Bouman and van Kasteren, 1990a). Similar conclusions regarding the potential of C-band for studying lodging in “narrow-leaf” crops such as wheat have been made by Yang et al. (2015) and Han et al. (2017). These results are summarised in Fig. 2.5b.



(a)



(b)

Selected features
 Total range considered
H: Horizontal; **V:** Vertical; **Odd:** Odd/single bounce scattering;
Db.: Double bounce scattering; **Vol.:** Volume scattering;
T22, T33: Components of Pauli decomposition;
Span: Total scattering power; **CCC:** Circular-pol corr. coeff.

Fig. 2.5. Summary of important features in (a) optical and (b) microwave regions relevant to crop lodging detection and risk assessment as identified from RS-based crop lodging studies. Light green indicates the entire wavelength range of the respective sensors, the total number of backscatter/polarimetric parameters and the range of incidence angles that were tested in the selected studies. Dark green indicates the specific wavelength

region, backscatter/polarimetric parameters and incidence angles that have been found to be sensitive to lodging (according to the results of these selected studies).

Apart from emphasising the importance of specific wavelengths in assessing lodging, some studies also outline the additional information obtained from different polarisations and incidence angles (Bouman, 1991b; Zhao et al., 2017). Yang et al. (2015) suggest that the backscatter from a single channel (HH or HV or VV) cannot distinguish the lodged wheat parcels from non-lodged ones while a polarimetric index based on ratios can enhance the detection capability (Fig. 2.5b). Chen et al. (2016), on the other hand, found that HV backscatter intensity alone could distinguish lodged and non-lodged sugarcane fields, in addition to other polarimetric features. More recently, Zhao et al. (2017) studied the sensitivity of correlation coefficients (co-, cross-, and circular-pol) to lodging in wheat and canola. They found that co-pol and circular-pol correlation coefficients are uniquely sensitive to lodging in wheat but not in canola. As reflection asymmetry described by the circular-polarisation coefficient is an identifiable feature of lodged wheat, this observation seems to be very promising for lodging detection.

2.4 Challenges in remote sensing of crop lodging

The contribution of RS data to operational crop monitoring systems is increasing (Atzberger, 2013). However, several challenges have prevented the integration of RS data into routine crop lodging assessment. Primarily it is the unavailability of high spatial resolution data at low costs. The heterogeneous distribution of lodging directly affects our ability to detect it using RS. In general, to map lodging accurately, the spatial resolution of the sensor must be smaller than the size of the field and the lodged area. However, high spatial resolution alone is not sufficient. High temporal resolution information is also important to improve lodging detection and to identify the phenological stage at which lodging occurs (to quantify yield loss estimates). With coarse resolution data, more frequent observations are available but with pronounced mixed-pixel effects. For instance, consider a single MODIS 250 m pixel, which corresponds to an area of 6.25 hectares, while a Sentinel-2 10/20 m pixel covers 0.01/0.04 hectares. In this case, the lodged area would fall in only a fraction of the coarse spatial resolution pixel of MODIS, while in the latter case; there is a possibility to extract a unique signature from lodging. Moreover, the selection of optimal spectral bands (optical) or polarisations (radar) that are uniquely sensitive to lodging is also challenging. For example, while several indices have been tested for retrieving

crop biophysical parameters (e.g. crop biomass), the cause of their spatio-temporal variations, whether due to crop growth or lodging, is much less straightforward and hence more difficult to determine.

The accuracy assessment of lodging severity and lodging risk maps poses another issue, given the absence of a standard reference scale or terminologies to represent lodging. There is also no consensus about the most appropriate way of producing and validating lodging maps. For instance, the term ‘lodging detection’, used until now, is reasonably broad and merely means identifying the presence or occurrence of lodging in an area. Based on our review and the gathered insights, we propose three terms that can further characterise lodging detection, through the quantification of i) *lodging stage* (i.e. moderate, severe or very severe lodging based on crop structural parameters such as crop angle of inclination (CAI)); ii) *lodging severity* (i.e. moderate, severe or very severe lodging based on an index called lodging score which combines CAI and lodged area at a particular phenological stage) and iii) *lodging incidence* (i.e. when lodging occurs based on time-series analysis of lodging score). As mentioned in section 2.2.1, we also differentiate between the terms susceptibility and risk mapping in the context of lodging. Genetic traits (such as plant height) and crop management factors (such as self-weight moment, LAI, etc.) determine how susceptible a plant is to lodging. On the other hand, a model encapsulating the impact of external environmental factors (such as rainfall and wind speed) on the genetic and crop management factors could contribute to a comprehensive lodging risk assessment. We believe that the above distinction can serve as a framework or a standard reference for future studies.

The collection of ground truth data (such as plant height, CAI, lodged area) to assess lodging damage can itself be a daunting task, due to unfavourable weather conditions, irregular plant structures, lack of expertise and absence of field methods/equipment to carry out the measurements. A considerable investment in time and resources is required to plan and perform such campaigns. Furthermore, the acquisition of RS data coincident to specific dates, especially from spaceborne platforms, may not always be feasible. This can consequently hinder the application of RS data close to the onset of the lodging event, making it difficult to capitalise on the current lodging information being reported (e.g., lodged area) and *in situ* data (e.g., plant height) being collected. Seasonal lodging susceptibility and risk mapping, on the other hand, requires specific phenological stages to be monitored so that in-season remedial actions can be undertaken. For

instance, the crop nitrogen status and plant population density at the start of stem elongation (GS30-31) in wheat can be indicative of the fertility of a field and therefore its propensity to lodge. An assessment of these attributes with RS (directly) can be crucial to map the potential susceptibility and risk of lodging and target proper management strategies.

2.5 Research gaps and future scope

Active engagement of the RS community with crop physiologists is important for successful integration of EO products into lodging assessment. The Earth Science Decadal Survey (Board and NRC, 2007) emphasises the need to form a stronger linkage between RS scientists and end-users to define data requirements in a better way and disseminate knowledge to the users to be able to apply the EO data to specific applications. The end-users, for instance, loss adjusters, could provide real case scenarios, to have an overview of and determine the intensity of lodging damage. This data can then be shared with the interested parties, such as the farmers whose crops are damaged or the Agriculture Development Authorities providing support to farmers in the event of crop damage. Moreover, end-users should be engaged, in future, in the provision of crowdsourced lodging information directly from the field, thus promoting Citizen Science initiatives, and exploiting smart technologies, such as those used by Dickinson et al. (2012) and Fritz et al. (2009) in ecology and land cover mapping, respectively. This kind of interaction can be fruitful, not only for the collection of a large amount of data but also for raising user awareness regarding the use of RS information for crop management. Providing web-based GIS solutions for lodging susceptibility/risk mapping as well as enhancing data visualisation and decision making by using the data from RS sensors and field surveys can facilitate collaboration between stakeholders involved in farm risk management.

RS can be a convenient and efficient method to monitor crop lodging, but its use within operational lodging detection or seasonal susceptibility or risk assessment faces some challenges. In this review, we made the first attempt to consolidate research progress in the field of RS while categorising different studies into major groups. We found only 22 publications that explored the potential of RS to study lodging. The early work on the assessment of crop lodging with RS date back to the 1980s; however, significant progress has been made post-2000. Nevertheless, there are still many prospective research areas that merit further investigation.

2.5.1 Lodging detection

The current literature on RS-based lodging assessment suggests that a large group of studies (68%) have focused on either lodging identification or evaluating crop lodging stage based on plant height. However, most of these studies focus on the qualitative analysis of lodging. Although timely identification of lodging can be beneficial to plan harvest operations, such qualitative analyses can be of limited use since the yield losses or deterioration in grain quality cannot be directly quantified. There is scope to develop quantitative approaches for estimating lodging stages as well. Moreover, the use of plant height for the interpretation of lodging stages is highly influenced by the crop cultivar and the phenological stage, making it less reliable. The CAI, on the other hand, is independent of these variables and can also be used to predict crop lodging scores, which are otherwise evaluated by visual assessment of lodged fields. The potential of radar polarimetry and suitability of different radar configurations in characterising crop structural properties (Gherboudj et al., 2011) should also be further explored.

A potentially interesting avenue for future research is to explore how lodging severity and lodging rate (i.e., number of lodged plants per unit area) can be estimated remotely close to a lodging event. This information can enable a farmer or a loss adjuster to evaluate crop loss, quantitatively support damage assessment and aid in agricultural disaster relief compensation. For instance, according to the regulations of the Agricultural Natural Disaster Relief system in Taiwan, if lodging in a sampled area exceeds 20%, it is considered a disaster area. A sampling accuracy of > 90% is required in these cases to allocate funds and restore the damaged crop (Yang et al., 2017). Furthermore, the images analysed before harvesting can enable assessment of the lodged patches in a field and can practically result in navigation maps to guide the drivers or autonomous harvesting vehicles to adjust their speeds based on the lodging situation. Another research gap is NRT identification of lodging incidence (when lodging occurs) using the dense time-series analysis of the satellite data. In this context, Sentinel-1 and Sentinel-2 data have high potential and should be explored.

We also found that the re-occurring method for crop lodging detection is the use of spectral and textural indices from optical imagery. In this context, the drawback of using a spectral index is that the change/variability in such features may be caused by a composite of factors other than lodging, such as soil conditions, water or nutritional stresses, leaf pigment concentrations, canopy structure, pests, diseases, etc. (Schaepman et al., 2009). Therefore, it is difficult

to automatically detect and recognise the evidence of lodging amongst these factors, unless their effect is characterised in combination with lodging. More diagnostic measures that are strongly sensitive to lodging should be investigated, though some attempts have been made by Zhao et al. (2017) and Chapman et al. (2014) in this direction. Another finding of our review is that there are very few examples of characterising crop lodging over large areas. Bridging the gap between current approaches and crop lodging assessment over large spatial extents is still one of the major challenges in this field. From 22 reviewed cases, only five studies (as shown in Fig. 2.4) explored lodging using satellite data (e.g., (Chen et al., 2016; Yang et al., 2015). Furthermore, the utility of thermal and hyperspectral datasets for lodging assessment seems to be under-examined. We found only one study that examined the utility of thermal dataset (Chapman et al., 2014). The data from spaceborne thermal sensors may not offer fine spatial resolution but can be integrated into ensemble sensor fusion/multi-sensor cross-calibration frameworks to derive lodging information over large geographical extents.

2.5.2 Lodging susceptibility and risk mapping

Mapping lodging susceptibility is an essential component of a comprehensive risk assessment for lodging (and it does not yet exist). Complex mathematical models based on the underlying physics of plant structure have been formulated to predict lodging risk quantitatively (Baker et al., 1998; Berry et al., 2003a). However, their complexity and reliance on intensive field measurements of input parameters make it difficult to apply them widely. The mapping capabilities of RS can be used to quantify simple lodging susceptibility indicators such as safety factors, crop nitrogen, plant population density, etc. so that remedial treatments can be targeted more efficiently. Studies show that a safety factor can be used to predict both root and stem lodging susceptibilities of a plant and correlates well with the observed lodging (Crook and Ennos, 1994), even though the external wind or precipitation/hail-induced forces are not accounted. RS-based lodging risk assessment, on the other hand, has been reported by only one study (Coquil, 2004), although the results are still not conclusive. Research along these lines would require building upon earlier efforts (Berry et al., 2006; Crook and Ennos, 1994; Sposaro et al., 2010) that have modelled the risk of lodging in various crops (such as wheat, barley, and sunflower) using intensive ground measurements. In our view, future studies should develop stand-alone geo-information products/models for the provision of seasonal lodging susceptibility and risk maps to facilitate proper crop recommendations and management. It is envisioned

that such seasonal lodging susceptibility/risk models could also contribute to climate change resilience of agricultural practices since lodging susceptibility/risk is directly associated with the increased frequency of extreme rainfall and wind events.

2.6 Outlook on remote sensing sensors and platforms

Timely and accurate monitoring of crop lodging at multiple scales can provide insights into its spatial and temporal dynamics. The need for large and fine-scale analysis for agricultural applications has boosted the ongoing efforts in developing high-end sensors and monitoring platforms. Recent developments in RS have resulted in new satellite missions such as the Sentinel series, which provides free data while continuously mapping the Earth at short time intervals. Other missions such as RADARSAT-2 and COSMO-SkyMed (constellation of four satellites), RapidEye (five-satellite constellation), DigitalGlobe (constellation of Worldview and GeoEye high-resolution satellites), DMC (Disaster Monitoring Constellation) and Planet (with 175+ satellites in orbit) also provide flexible monitoring options, imaging the Earth's landmass at monthly to daily time intervals.

Until recently, the availability of spectral data from the red-edge region, which is highly sensitive to crop's biophysical parameters such as biomass (Mutanga and Skidmore, 2004), and indirectly to lodging, was limited to certain hyperspectral sensors. The scenario changed with the launch of RapidEye (in 2008), Worldview-2 (2009), Worldview-3 (2014), and more recently with Sentinel-2A (2015), Worldview-4 (2016) and Sentinel-2B (2017). There is little research on whether broadband red-edge, satellite data (>10 nm) can detect high biomass values or lodging-induced changes in crops. Although local-scale studies may benefit with very high spatial resolution data from commercial missions such as Worldview (2-4), availability of freely available satellite data (such as from Sentinel) can be a motivation to investigate such approaches on a larger scale. The VSSC (VEN μ S Superspectral Camera) onboard the VEN μ S (Vegetation and Environment monitoring on a New MicroSatellite) spacecraft launched in 2017, is another sensor providing red-edge data at high spatial resolution (5.3 m) and two-days' revisit time. Other ongoing/future missions such as PRISMA (2019, 237 spectral bands), JAXA's HISUI (2019, 20 m), EnMAP (2020, 228 spectral bands), Capella (2019, <1 m), ICEYE mission (2018, 1-3 m), RADARSAT Constellation Mission (2019, 5-30 m), HypSIRI (2022, 60 m), SHALOM (2022,

8-10 m) will deliver super-spectral information at moderate (60 m) to high (8 m) spatial resolutions and have the potential for regional-scale applications.

Lodging occurs in adverse climatic conditions and the all-weather data capability of SAR data can contribute to developing operational applications. Among the satellite sensors, studies have predominantly used RADARSAT-2 for assessing crop lodging. RADARSAT-2, with its ability to acquire data in quad-polarisations (HH, HV, VH, VV), reduces the need to acquire data over several dates. Moreover, data from recently launched SAR missions such as L-band ALOS-2 (2014) and C-band Sentinel-1A and B (2014, 2016) have not yet been explored for lodging assessment (except by Han et al. (2017)). Although the limited feature space of Sentinel-1 data (dual-pol data) may not characterise the heterogeneous patterns of lodging in the same way as RADARSAT-2, free data access and high temporal resolution make it particularly relevant for developing operational applications. Furthermore, the frequency (5.4 GHz) of Sentinel-1, unlike ALOS-2 (1.2 GHz), is more sensitive to the phenological changes and volume scattering from crops, such as wheat with moderate plant height, providing an excellent contrast in the dynamic range of backscatter response from a crop and the underlying soil cover. Also, the multi-sensor fusion of Sentinel-2 with either Sentinel-1 or RADARSAT-2 data should be investigated due to the complementary nature of microwave and optical signals.

We are confident that field-level research on the application of airborne multi/hyperspectral as well as microwave data for crop lodging assessment will continue. The availability of airborne data is slowly reaching an operational level and can be obtained over large spatial extents, as exemplified in the national ecological observatory network (NEON, <http://www.neoninc.org>) (Keller et al., 2008). RPASs may become even more powerful, due to continued improvements in spatial and spectral resolution of the onboard sensors and their ability to provide information to meet specific temporal requirements. RPAS data can be used either directly as a dataset to assess lodging on local scales or can serve as additional reference information for satellite or airborne datasets. The second solution is more viable when large areas have to be mapped. RPAS reference data can provide detailed information on lodging extent or crop properties such as stem diameter and shoot numbers, which could then serve as explanatory variables to interpret the success or failure of lodging detection or seasonal susceptibility/risk mapping algorithms using coarser RS data.

2.7 Conclusions

The accurate and timely detection of lodging, its susceptibility and risk is a challenging prospect. In this paper, we made the first attempt to review the progress towards this goal and at classifying different studies in some major groups. Given the demand for rapid and quantitative evaluation of crop lodging (and its risk), with evidence from 22 studies, RS data has been explored for lodging assessment during the last three decades. RS measurements of crop lodging are needed for crop models; however, the methodology has not yet reached sufficient maturity in an operational context. Here we attempt to fill the current gap in RS reviews by placing a focus on crop lodging assessment. The main findings of the review are:

- (i) A comprehensive review of 71 studies showed that lodging is one of the major yield-reducing factors in crops and is a global phenomenon. Viable solutions for its detection and seasonal susceptibility and risk mapping require knowledge of crop biophysical parameters (such as self-weight moment, plant height, crop nitrogen, LAI, etc.) during the growing season and meteorological products potentially derived from RS data and processing chains that can contribute to the development of practical applications.
- (ii) The number of RS-based studies focusing on crop lodging assessment has increased in the last decade, but the research is still at an early stage. We found only 22 RS-based articles that studied lodging, of which 15 were lodging-detection driven investigations, six focused on understanding the response of RS signal under lodged conditions, while only one study explored the capability of RS technique for seasonal lodging risk mapping (see Table 2.1).
- (iii) Studies using satellite imagery for large-scale monitoring of the agricultural areas are still sparse (only five studies). To date, there is no rapid method available for the quantitative evaluation of crop lodging over large areas. With the ongoing developments in sensor technologies and reducing data acquisition costs, the satellite data (such as from Sentinel missions) has great potential in the context of operational applications.
- (iv) The results from existing RS studies are mostly qualitative. For instance, the focus of most of the studies was to analyse the response of the RS signal to lodged and non-lodged crops. There are several other research areas that remain unexplored. The goal of the future studies should be to develop empirically tested

robust quantitative models that can support estimation of crop lodging stages, lodging severity, lodging incidence and prediction of seasonal susceptibility and lodging risk. The models can be enhanced by assimilation of crop biophysical parameters (such as crop angle of inclination, plant self-weight moment, LAI and chlorophyll content) and phenological information (e.g. sowing date) derived from RS data. This may provide an alternative to complex models that need extensive parameterisation and a huge amount of ground data. The studies should focus on investigating representative/diagnostic measures of crop lodging from RS.

(v) Most research on crop lodging has been conducted using optical RS data, with an emphasis on the VIS-NIR region of the electromagnetic spectrum. Very few studies have examined other spectral regions such as SWIR bands, TIR or microwaves, which might be due to the constraints on data access or lack of expertise. For instance, before the advent of Sentinel-1 data, SAR data was available only from commercial (RADARSAT, ALOS, COSMO) or scientific space agency platforms (e.g. ASAR from ENVISAT of ESA) with biweekly or monthly frequencies, making it difficult to study lodging phenomena. Future research efforts should investigate ensemble sensor fusion approaches to extract lodging information.

(vi) The greatest number of RS-based lodging studies have been carried out for wheat and barley, through the development of lodging detection models and the identification of different bands/indices/wavelengths that are sensitive to lodging. This has underpinned most of the current understanding of the response of RS variables to wheat and barley lodging. There are few RS-based studies on other crops such as corn, oats, rice, canola, and sugarcane. Genetic, structural and physiological differences, as well as crop-specific management practices, may influence the incidence and intensity of lodging in different crops. For instance: in comparison to wheat, barley stems are more flexible and the ears are less erect with the presence of awns, which can affect the lodging model parameters significantly; the pods in canola provide a high degree of randomness to the canopy structure, which causes the scattering properties to be significantly different from other crops. These differences suggest that (a) genetic, environmental and management differences should be accounted for when considering the relevance of observed relationships between RS information and lodging between one crop production situation and another and (b) a need for

Remote sensing-based crop lodging assessment: Current status and perspectives

further RS studies of lodging across diverse crops, including studies of multiple crops with the same imagery.

Chapter-3

Estimation of crop angle of inclination for lodged wheat using RADARSAT-2 and Sentinel-1 SAR data*

*This chapter is based on:

Chauhan, S., Darvishzadeh, R., Boschetti, M., & Nelson, A. (2020a). Estimation of crop angle of inclination for lodged wheat using multi-sensor SAR data. *Remote sensing of environment*, 236, 111488. <https://doi.org/10.1016/j.rse.2019.111488>

Chauhan, S., Nelson, A. D., Darvishzadeh, R., & Boschetti, M. (2019c). Detecting crop lodging stage using SAR-derived crop angle of inclination. In *ESA Living Planet Symposium*, Milan 2019

Abstract

Lodging - bending of crop stems or failure of root anchorage, reduces the quantity and quality of cereal crop yields. Early quantification of crop lodging is vital to prevent further losses and to facilitate harvesting operations. Crop angle of inclination (CAI); an important structural parameter for lodged crops, is a quantitative measure of the lodging stage and is a component of lodging severity/score. To our knowledge, no study has yet explored the potential of satellite RS for estimating CAI. In this study, we investigated the performance of two satellite sensors: RADARSAT-2 at different incidence angles (R-2 FQ8-27° and R-2 FQ21-41°) and Sentinel-1 (S-1) for estimating CAI. We collected temporal crop biophysical/structural parameters (CAI and plant height) and meteorological data (rainfall and wind speed) throughout May 1-June 30, 2018 in a very large commercial farm located in Jolanda di Savoia, Ferrara, Italy. We defined non-lodged/healthy (He) and different crop lodging stages (moderate lodging (ML), severe lodging (SL) and very severe lodging (VSL)) based on field-measured CAI. We then established quantitative relationships between field-measured CAI values and the RS-based metrics derived from S-1 and R-2 using support vector regression (SVR) models. The R-2 FQ8 model estimated CAI most robustly with an R^2_{CV} (cross-validated R^2) of 0.87 and an $RMSE_{CV}$ (cross-validated RMSE) of 8.89° while the performance of the S-1 and R-2 FQ21 models were comparable with an $RMSE_{CV}$ of 11.35° and 11.63° respectively. Low incidence angle R-2 data were particularly sensitive to high CAI values (VSL) while high incidence angle data were useful for predicting lower CAI (ML and SL). While the R-2 FQ-8 model outperformed the other two, the S-1 model still explained 78% of the CAI variability in the study site, which is important in the context of operational crop lodging stage assessment. This is the first study to demonstrate the utility of SAR RS data for estimating CAI as a measure of the lodging stage and a component of lodging severity.

3.1 Introduction

Crop lodging is the permanent bending of plant stems from the vertical or displacement of the root anchorage, causing destruction of canopy structure, degradation of grain quality, slowed harvest, increased drying costs and severe yield reductions (up to 75%) (Berry et al., 2004; Pinthus, 1974). Crop lodging is caused by the complex interaction between crop's genetic, environmental and management factors, making every lodging event unique with different onset, duration and intensity (Nafziger, Wax, & Brown, 1986; Zhu et al., 2016; Piñera-Chavez et al., 2016). The assessment of lodging on large scales is challenging due to these complex interactions and many other factors: the heterogeneous and random distribution of lodging within a field, the absence of a standard scale to represent it and the lack of statistics to validate lodging (e.g. year wise statistics of percentage area lodged for different crops at a local, regional or global scale).

Plant physiologists and agronomists have studied crop lodging intensively (Baker et al., 1998; Easson et al., 1993; Lang et al., 2012; van Delden et al., 2010) but the scope is mainly limited to breeding trials (i.e. producing lodging resistant cultivars) and agronomic management (i.e. agronomic practices that can reduce lodging risk). The results of these studies, as reviewed by Chauhan et al. (2019a) show that three main factors - the CAI, the lodged area and the time when lodging occurs (phenological stage) control lodging severity and govern the extent of yield loss. CAI is defined as the angle made by the crop stem with respect to the vertical (Fig. 3.1). During the process of lodging, a crop undergoes a series of stages (hereafter referred to as lodging stages) starting with a slight lean from the vertical (CAI $\sim 0^\circ$) and ending with the crop lying close to horizontal (CAI $\sim 90^\circ$). CAI is, therefore, an important metric to describe the physical structure of a lodged crop or the lodging stage (an index based on CAI-moderate, severe or very severe).

Accurate estimation of CAI can contribute to the estimation of crop yield losses. For instance, Fischer and Stapper (1987) demonstrated that the yield losses in wheat incurred at a CAI of 80° were almost 2-4 times than those at 45° . CAI, when combined with lodged area estimates, can also help assign lodging scores (a lodging severity index combining CAI and lodged area) to a crop. Quantitative estimates of CAI can thus be beneficial to farmers (to plan remedial actions, for example, to minimise the harvesting losses and settle compensation disputes) and insurance loss adjusters (to get an estimate of the extent of damage). The conventional methods to measure CAI and assess lodging stages rely on intensive

manual ground measurements and visual ratings. As with most ground measurement strategies, such methods are time consuming and severely restrict their application for monitoring large areas repeatedly. In addition, high spatial variability associated with lodging makes it challenging to capture this variability via ground measurements.

Remotely sensed imagery offers an efficient way to obtain timely information on the temporal trends and spatial distribution of lodging. This is possible with frequent acquisitions of high-resolution imagery during the crop growth period or at least during the critical phenological stages. High-quality optical RS data may not be consistently available due to cloud, rain and haze interference. In this context, synthetic aperture radar (SAR) sensors offer a clear advantage since microwaves are less affected by the atmosphere and can image the Earth's surface successfully irrespective of weather conditions. Also, the unique sensitivity of microwave scattering to crop structure has led to many studies utilizing the SAR data for crop monitoring (Chauhan et al., 2019c, 2018; Lopez-Sanchez et al., 2011; Nelson et al., 2014a; Yuzugullu et al., 2017). However, a recent review by Chauhan et al. (2019a) revealed that only eight peer-reviewed articles published between 1951-2018 have focused on the use of SAR data for lodging assessment, four of which utilized data acquired from spaceborne platforms (Chen et al., 2016; Han et al., 2017; Yang et al., 2015; Zhao et al., 2017). Most of these studies have investigated the behaviour of RS signals with respect to the condition of the lodged crop (lodging detection), but there is limited knowledge on the use of SAR data for the quantitative assessment of crop parameters associated with lodging.

Multi-parametric (multi-incidence angle, multi-polarisation and multi-temporal) data from RADARSAT-2 (hereafter abbreviated as R-2) satellite has made it possible to address crop lodging in more effective ways. For instance, a correlation analysis between RS-based metrics derived from R-2 data and lodging in wheat by Yang et al. (2015) showed that polarimetric ratios, especially those based on odd/double scattering and span (i.e. Odd/Span, Double/Span) could distinguish non-lodged and lodged wheat fields, while a single-channel backscattering coefficient (σ^0) such as σ^0_{HH} , σ^0_{HV} or σ^0_{VV} cannot separate the two classes efficiently. However, given the sensitivity of the polarisation of microwaves to crop structure and dielectric properties (Srivastava et al., 2009), the capability of PolSAR in crop lodging assessment is highly dependent on the crop type (Mascolo et al., 2016). Zhao et al. (2017) performed a study to test this hypothesis. The authors examined σ^0 and polarimetric features derived from R-2

data to distinguish lodging in wheat and canola fields. Some features such as σ°_{VV} , σ°_{HH} , the depolarisation degree and the circular-pol correlation coefficient were highly sensitive to lodged wheat, unlike canola, whose canopy structure is highly random. In another study, Chen et al. (2016) showed that σ°_{HV} , as well as features such as those referring to the double bounce scattering, volume scattering and the T22 and T33 matrix elements derived from R-2 data, are capable of detecting lodging in sugarcane. Unfortunately, these studies do not provide quantitative estimates of lodging-related crop parameters.

To date, quantitative assessment of lodging using RS was also hampered by the lack of dense time-series data at high spatial resolution. An analysis of dense time series data over the crop-growing season has the potential to detect when lodging occurs in NRT. A new era started with the launch of Sentinel-1 (hereafter abbreviated as S-1), offering a unique opportunity to monitor lodging systematically. In a recent study, Han et al. (2017) used S-1 data to classify lodging into different stages (mild, moderate and severe) using plant height as a proxy variable. Although their model demonstrated some potential to identify and classify lodging stages, it was tested over a single phenological stage (tassel) and did not exploit dense time-series data. Furthermore, the use of plant height for the interpretation of lodging stages is highly dependent on the crop cultivar and the phenological stage. This is exemplified in Fig. 3.1. As the crop inclines at a certain angle (θ) during lodging, the effective plant height, which is defined as the distance from the soil surface to the tip of the head of the longest tiller, also changes (van Delden et al., 2010). However, it is highly probable that at a specific phenological stage, the non-lodged plant height ($h_H = 150\text{cm}$) of a wheat cultivar A can be higher than that of wheat cultivar B ($h_H = 90\text{cm}$). In the event of lodging, the lodged height (h_L) will, therefore, be different in both cases (say at 45° , $h_L = 75\text{cm}$ for cultivar A and $h_L = 45\text{cm}$ for cultivar B, respectively). This variation makes plant height a poor indicator of lodging since there is too much of “natural” variation to use it to distinguish between lodged and non-lodged targets (hereafter abbreviated as He or healthy), without additional information. CAI, on the other hand, is independent of the crop cultivar and the phenological stage, as evident in Fig. 3.1.

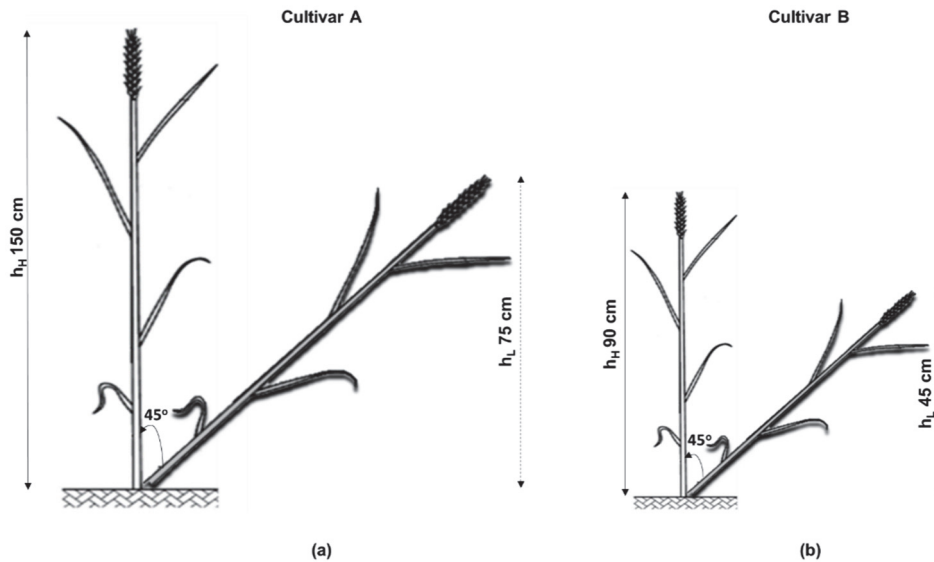


Fig. 3.1. An example of the change in plant height and crop angle of inclination in the event of lodging for (a) cultivar A and (b) cultivar B, at the same phenological stage. h_H is the height before lodging, while h_L is the height of the lodged crop (figures not to scale).

Estimation of crop biophysical properties from active RS data has been investigated using several modelling approaches. These models have evolved from regression and machine learning approaches such as multiple linear regression, neural networks and decision trees (Kumar et al., 2018; Prasad et al., 2012) to sophisticated radiative transfer models (Blaes et al., 2006). While these process-based models are theoretically sound in interpreting SAR data (Erten et al., 2016), the inversion of crop variables is still challenging due to inherent complexity, limited operational usage and intensive data requirement (Wang et al., 2009). Among the machine learning approaches, support vector machine regression (SVM-R or SVR) has shown excellent generalization capabilities (Blanzieri and Melgani, 2008; Tuia et al., 2011).

To the best of our knowledge, there is no research on the use of SAR data for estimating CAI of lodged wheat. Therefore, the main objective of this study is to compare the performances of S-1 and R-2 data (at different incidence angles) for estimating CAI. The CAI estimation has been achieved by implementing SVR as a regression tool with different sets of RS-based metrics derived from the two SAR sensors.

3.2 Materials and methods

3.2.1 In situ measurements

We performed stratified random sampling and identified 76 sample plots (Fig. 3.2) using six information strata (elevation, seed density, soil type, soil pH, crop cultivar and sowing date). Care was taken to ensure that the samples were collected from various stratum and that the entire geographical area was well represented while also considering the spatial distribution of the points. We chose the plot size of 60×60 m in this study since larger plots considerably reduce the negative impact of the potential edge effects on the stability and magnitude of RS-based metrics (Frazer et al., 2011) and exhibit less inter-plot variance (Zeide, 1980). Furthermore, to capture the structural variability and heterogeneity of CAI within the plots, we sampled three subplots of 2×2 m in fully healthy plots ($0^\circ < \text{CAI} < 5^\circ$, $n=51$) and increased the number of subplots to 4-8 in lodged plots ($6^\circ < \text{CAI} < 90^\circ$, $n=67$), depending on the lodged area. We averaged the subplot values such that they were representative of the crop condition at the plot level.

We started revisiting the plots three times from March 2018 onwards (when the crop was in GS30-39) to detect when lodging occurred. It was only around May 1 (i.e. amidst the 2nd round of sampling when the crop was approaching GS40) that we recorded the first few instances of lodging. Therefore, for this study, we considered the observation period as of May 1-June 30, 2018, which resulted in a subset of 118 samples covering three phenological stages– flowering, milking and ripening.

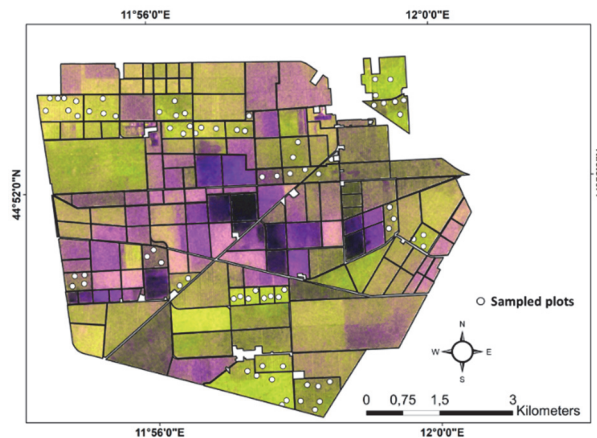


Fig. 3.2. An RGB composite of a Sentinel-1 (R: VH, G: VV, B: VH/VV) scene acquired on June 6, 2018 containing the study area (Bonifiche Ferraresi farm) overlaid with the sampling points (white dots) over the wheat fields and the farm boundary (black outline).

Since there is no definite method in the literature, we developed a simple technique to measure CAI. For each subplot, we measured CAI indirectly using a plumb bob (Fig. 3.3a), measuring tape and some trigonometric calculations (eq. 3.1). We suspended the string of the plumb bob from the top of the plant head until the tip touched the ground. The heavyweight at the bottom ensured accurate measurement of the vertical height from the point of suspension (Fig. 3.3a). We then used the total length of the suspended string (h_s) and the height of the plumb bob (h_w) to calculate the vertical height (h_L) (Fig. 3.3a). For lodged plants, we measured the slant height (h_{sl}) with a measuring tape. We derived CAI (θ) from the vertical based on the measurements shown in Fig. 3.3a and equation 3.1. Subsequently, we defined the lodging stages based on CAI from the vertical (Fig. 3.3b) to carry out an exploratory discriminative analysis. We categorised the plots with an average CAI of 1-5° as healthy (He, $n=51$) plots and classified those with the average CAI ranging between 6-90° into moderate lodging (ML, $n=12$), severe lodging (SL, $n=25$) and very severe lodging (VSL, $n=30$) stages (Fig. 3.3b).

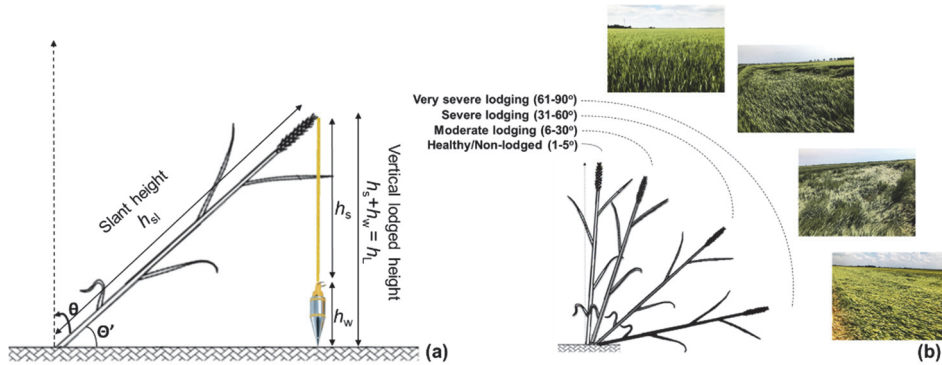


Fig. 3.3. (a) Measurement technique for crop angle of inclination using a vertical plumbbob. θ and θ' are the crop angle of inclination (CAI) with respect to the vertical and soil surface, respectively. h_s and h_w are the height of the string and the heavyweight at the bottom of the plumbbob, respectively, h_L ($h_s + h_w$) is the total vertical height of the lodged plant, h_{sl} is the slant height of the plant measured from the soil surface to the tip of the head of the longest tiller with a measuring tape and (b) illustration of different crop lodging stages: healthy/non-lodged, moderate, severe and very severe lodging, along with the field photographs.

$$\theta \text{ (degree)} = 90^\circ - \sin^{-1} \frac{h_L}{h_{sl}} \quad (3.1)$$

Where, θ is the crop angle of inclination (CAI) from the vertical, h_L and h_{sl} are the height of the lodged plant and slant height of the plant, respectively.

In addition, we also took replicate measurements of soil moisture in each plot using a Stevens Hydra Probe. We quantified the crop phenological stages using the BBCH scale. In each plot, we also recorded the point of plant failure (stem or root lodging) and other structural/morphological parameters (such as plant height, leaf area index (LAI), biomass, etc.) to facilitate interpretation of the results. Additionally, we continually recorded the daily cumulated precipitation (mm) and daily average wind speed (10 m from the ground) through a local automatic weather station (44°5'22.9"N, 11°57'51.0"E). The summary statistics of important field measurements are presented in Table 3.1 and the methodological flowchart of the study is presented in Fig. 3.4. Lastly, we also analysed the variation in plant height (PH) for healthy cultivars at a specific (flowering) growth stage to demonstrate the point we made earlier in Fig. 3.1. Our field records show that for healthy plots, the CAI remained stable at 3-5° during the flowering stage. On the other hand, as we can see in Fig. 3.5, the PH varied from 0.70 to 1.22 m, which shows that CAI is a better proxy variable for lodging stage assessment than PH as there is a lot of “natural” variation in PH to use it to distinguish between lodged and non-lodged targets.

Table 3.1. Summary statistics of CAI and PH for healthy (He, $n=51$) and lodged plots (L, $n=67$). Samples were collected throughout the flowering to ripening growth stages. COV is the coefficient of variation.

Data	Mean		Min		Max		Std. Dev.		COV (%)	
	He	L	He	L	He	L	He	L	He	L
CAI (°)	4.84	50.79	3.00	9.36	5.00	79.50	0.53	18.76	0.11	0.37
PH (m)	0.86	0.49	0.70	0.18	1.22	0.94	0.08	0.19	0.10	0.38

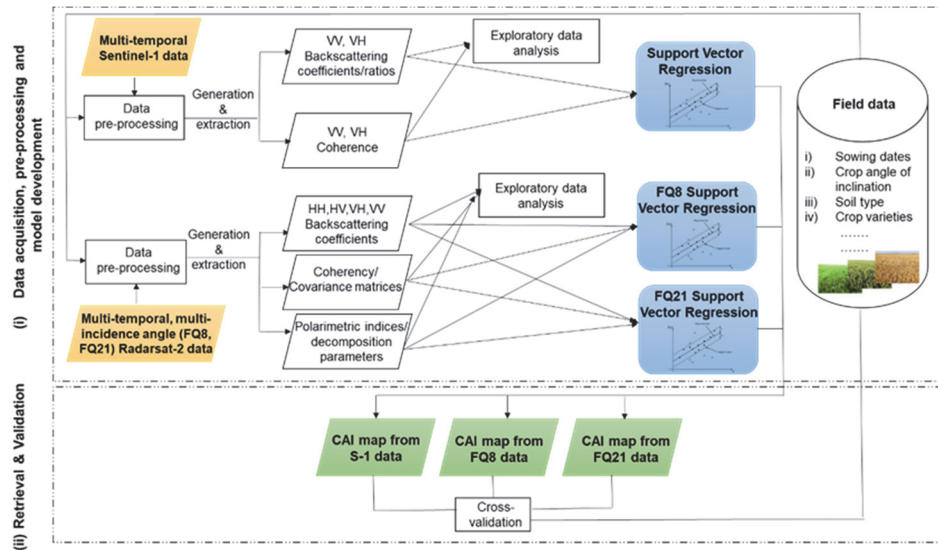


Fig. 3.4. Methodological flowchart of the study. The inputs are colour-coded in yellow, the model used is in blue and primary outputs are in green.

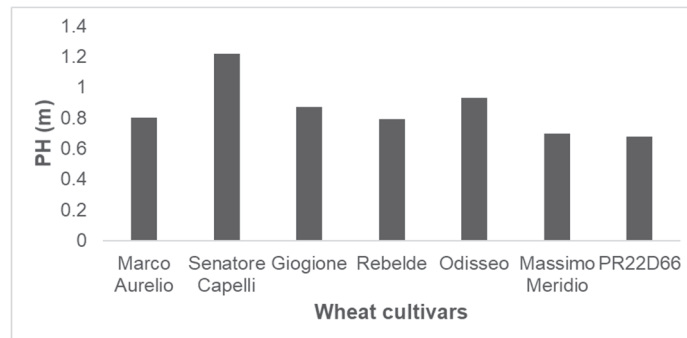


Fig. 3.5. The variation in plant height (PH) in the healthy plots for different wheat cultivars at the flowering growth stage.

3.2.2 Remote sensing data acquisition

We selected the satellite images synchronous to the dates of the field data acquisition. We acquired a total of five R-2 images in single look complex (SLC) fine quad-polarimetric (FQ) mode from the Canadian Space Agency through the SOAR (Science and Operational Applications Research) program. We selected two-beam modes (FQ8-27° and FQ21-41°) to study the effect of incidence angle on the estimation of CAI and to increase the temporal data availability.

We also procured 11 S-1A/B images in Interferometric Wide-swath (IW) dual-polarimetric (VV and VH) mode. We used the data in both Level-1 ground range detected (GRD) and SLC formats to extract backscattering coefficients (σ^0) and coherence (μ^0), respectively. The GRD products consist of focused SAR data that has already been detected, multi-looked and projected to ground-range using the WGS84 Earth ellipsoid model. SLC products, on the other hand, consist of focused SAR data and are provided in slant-range geometry. Table 3.2 shows some key characteristics of the acquired S-1 and R-2 images. Fig. 3.6 gives an overview of the image acquisition dates of S-1, R-2 FQ8 and R-2 FQ21 images. In our study, we could acquire only two R-2 FQ8 and three R-2 FQ21 images (as opposed to 11 Sentinel-1 images) available during the observation period. Thus, only 57 and 61 field samples could be used for the analysis of R-2 FQ8 and R-2 FQ21 data, respectively, while for S-1 data, all field samples ($n=118$) were analysed.

Table 3.2. Image acquisition parameters for Sentinel-1 (S-1) and RADARSAT-2 (R-2) data. Note that the incidence angle is based on the location of the study site within the swath.

Sensor	Data format/Beam mode/Polarisation	Incidence angle range (deg.)	Pixel spacing in Range (m) \times Azimuth (m)	Pixel resolution in Range (m) \times Azimuth (m)	Nominal swath width (km)	Orbit direction
R-2	SLC FQ8 HH, HV, VH, VV	26.9-28.7	4.78×4.78	10×10	25×25	ASC
	SLC FQ21 HH, HV, VH, VV	40.2-41.6	4.73×5.12	7×7	25×25	DSC
S-1	IW-GRD VV, VH	39.7-40.4	10×10	15×15	250×250	ASC
	IW-SLC VV, VH	39.7-40.4	2.3×14.1	15×15	250×250	ASC

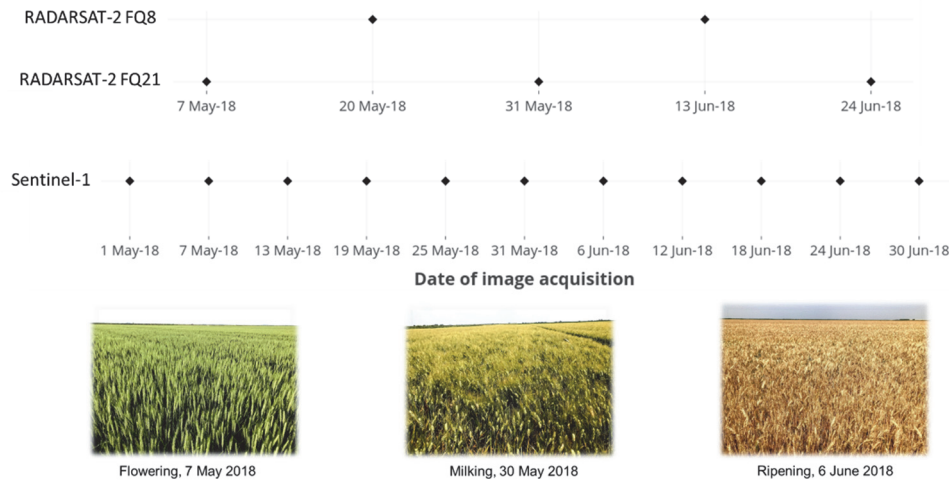


Fig. 3.6. Acquisition dates of remote sensing data during the 2018 wheat growing season.

3.2.3 Remote sensing data pre-processing

3.2.3.1 RADARSAT-2

We performed the linear backscatter processing of R-2 in SARscape 5.5 and extracted the polarimetric parameters in SNAP 6.0 software. To eliminate the orbital error in R-2 images, we applied the definitive orbit files obtained from the FTP repository of MacDonald Dettwiler Associates Ltd. (MDA) on the SLC images. We subset and co-registered the images using a high-resolution (10 m) digital elevation model (DEM) provided by Tarquini et al. (2007). We then spatially co-registered and resampled the image pixels to compensate for the relative translational shift, rotational and scale differences (Farghaly et al., 2019). The targets under observation can have translational and rotational motion relative to the data collection platform. Uncompensated translational motion can result in target signatures being degraded by large frequency phase errors (Werness et al., 1990) and hence need to be accounted for. For rotating targets too, it is crucial to obtain a satisfactorily focused target image whose dimensions in azimuth are known (Werness et al., 1990). We then used the De Grandi spatio-temporal filter to remove speckle from the images. The filter works in a combined time-space domain and preserves the temporal signature (De Grandi et al., 1997). We used the approach outlined in Nelson et al. (2014b) for further processing to get normalised σ^0 values (in dB).

Table 3.3. Metrics extracted from RADARSAT-2 SAR data. * denotes metrics referring to double bounce scattering, ** denotes metrics referring to volume scattering and *** denotes metrics referring to surface scattering.

Method/Index	Parameters/Formulation	Reference
Backscattering coefficients	$\sigma_{HH}^o, \sigma_{HV}^o, \sigma_{VH}^o, \sigma_{VV}^o$	(Lee and Pottier, 2017)
Sinclair decomposition	$ \sigma_{VV}^o ^2, (\sigma_{HV}^o + \sigma_{VH}^o)/2 ^2, \sigma_{HH}^o ^2$	(Krogager et al., 1997)
Pauli decomposition	Pauli_T11, Pauli_T22, Pauli_T33	(Cloude and Pottier, 1996)
Freeman-Durden decomposition	Freeman_double*, Freeman_volume**, Freeman_surface/odd***	(Freeman and Durden, 1998)
Yamaguchi decomposition	Yamaguchi_double*, Yamaguchi_volume**, Yamaguchi_surface/odd***, Yamaguchi_helix	(Yamaguchi et al., 2005)
H-a Alpha decomposition	Entropy (H), Anisotropy (A), Alpha	(Lee and Pottier, 2017)
Cloude decomposition	Cloude_double*, Cloude_volume**, Cloude_surface/odd***	(Cloude and Pottier, 1996)
Touzi decomposition	Psi, Tau, Alpha, Phi	(Touzi, 2007)
Van Zyl decomposition	VZ_double*, VZ_volume**, VZ_surface/odd***	(Van Zyl et al., 2011)
Coherency matrix elements	T11, T22, T33	(Cloude and Pottier, 1996)
Covariance matrix elements	C11, C22, C33	(Cloude and Pottier, 1996)
Span	$ \sigma_{HH}^o ^2 + 2 \sigma_{HV}^o ^2 + \sigma_{VV}^o ^2$	(Lee and Pottier, 2017)
Pedestal height	$\frac{\text{Maximum eigenvalue}}{\text{Minimum eigenvalue}}$	(Lee and Pottier, 2017)
Radar vegetation index (RVI)	$\frac{8\sigma_{HV}^o}{\sigma_{HH}^o + \sigma_{VV}^o + 2\sigma_{HV}^o}$	(Kim and van Zyl, 2009)
Radar forest degradation (RFDI)	$\frac{(\sigma_{HH}^o - \sigma_{HV}^o)}{(\sigma_{HH}^o + \sigma_{HV}^o)}$	(Mitchard et al., 2012)
Canopy scattering index (CSI)	$\frac{\sigma_{VV}^o}{\sigma_{VV}^o + \sigma_{HH}^o}$	(Pope et al., 1994)
Biomass index (BMI)	$\frac{(\sigma_{HH}^o + \sigma_{VV}^o)}{2}$	(Pope et al., 1994)
Volume scattering index (VSI)	$\frac{\sigma_{HV}^o}{\sigma_{HV}^o + BMI}$	(Pope et al., 1994)

The normalisation of the σ^o helps in compensating for the range variations and is intended to empirically correct the dependency of the backscatter signal on the incidence angle. We also computed the polarimetric indices, polarimetric decomposition parameters, covariance (C3) and coherency matrix (T3) elements from each R-2 image (Table 3.3). We generated a total of 42 metrics from each beam mode, as listed in Table 3.3.

3.2.3.2 Sentinel-1

We performed the entire processing of S-1 data in SARscape 5.5. The methodology of extracting linear σ^o from GRD data was similar to that explained in Nelson et al. (2014b). We subset and co-registered the images and applied a De Grandi multi-temporal filter to remove the speckle. For the generation of geocoded coherence maps, we used the coherence change detection (CCD) processing chain of SARscape. Coherence is a function of additive noise, systemic spatial de-correlation and scene de-correlation that occurs between two acquisition dates. It is sensitive to changes in either phase or amplitude of an image pixel. For instance, dielectric (wet vs dry soil) or backscattering properties both due to natural processes (e.g. crop growth) and due to abrupt changes (e.g. harvest or destruction of a crop morphology during lodging) can result in coherence loss. The interferometric coherence (μ^o), which ranges from 0-1 (1 being the perfect coherence), refers to the amplitude of the complex correlation coefficient between the two complex SAR images (s_1 and s_2) and is formulated as follows:

$$\mu^o = \frac{|\langle s_1 s_2^* \rangle|}{\sqrt{(\langle s_1 s_1^* \rangle \langle s_2 s_2^* \rangle)}} \quad (3.2)$$

Where μ^o is the interferometric coherence, s^* is the complex conjugate of s ; $|\cdot|$ represents the absolute values and $\langle \rangle$ is the ensemble average (Touzi et al., 1999). CCD chain operates in a series of steps: i) importing the master and slave SLC data which are already corrected using the precise orbit files, ii) importing a DEM to estimate the multi-looking factors, iii) μ^o estimation and iv) geocoding. We used a high-resolution (10 m) DEM provided by Tarquini et al. (2007) in steps (ii) and (iv) to geocode and correct for topographic variations. The coherence was calculated for every adjacent image pair from an ascending pass (e.g. date-1 and date-2, date-2 and date-3, ... date-n-1 and date-n) to achieve the lowest possible temporal baseline (six days). It was assumed that there was no change in the crop lodging condition during the six-day interval (i.e. He

remained He, ML remained ML and so on). Thus, we computed five metrics (σ°_{VV} , σ°_{VH} , $\sigma^{\circ}_{VH/VV}$, μ°_{VH} , μ°_{VV}) from S-1 data.

3.2.4 Exploratory statistical data analysis

Given limited knowledge of the spatio-temporal dynamics of lodging, we carried out a preliminary exploratory statistical data analysis in MATLAB 2018b. Firstly, we analysed the behaviour of σ° (and μ° from S-1 data) metrics derived from both satellites and interpreted them using *in situ* CAI measurements for different lodging stages (He, ML, SL and VSL).

We also calculated the Pearson correlation coefficients (r) between CAI and the 47 metrics (42 from R-2 and five from S-1 data). We checked the normality with the Shapiro-Wilk test and used Levene's test to check the homogeneity of variances between different lodging stages. We used the Kruskal Wallis rank-sum test (Kruskal and Wallis, 1952) to assess the statistical differences of the sample means among the groups. Subsequently, we used a post hoc Tukey's Honest Significant Difference (HSD) test to find significant pairwise differences between the categorical variables.

3.2.5 Support Vector Regression analysis

Support vector regression (SVR) is a non-parametric machine-learning tool that relies on kernel functions which project the input data into a new (higher dimensional) hyperspace where complex non-linear trends can be represented in a simple manner (Brereton and Lloyd, 2010; Williams, 2011). SVR aims to build an optimal hyperplane in the new hyperspace in a way that it fits the data with minimal error and complexity of the modelling function. The main advantages of SVR are (i) its ability to generalize from limited training data, (ii) convexity of the cost function allowing it to identify the optimal solution consistently, thus making it resilient to being trapped in local minima, (iii) it is independent of the statistical distribution of the data, (iv) does not have the problem of local optimal and multicollinearity and (v) it minimises the risk of overfitting (Bhatia and Yu-Wei, 2017).

In this study, we implemented three epsilon-SVR (ϵ -SVR) models to estimate CAI using input metrics from S-1 ($n=118$), R-2 FQ8 ($n=57$) and R-2 FQ21 ($n=61$) datasets. We trained and cross-validated the models using the partial least squares toolbox v8.7 from Eigenvector Research, Inc., with Multivariate Image Analysis toolbox v3.0 add-on in MATLAB 2018b (Wise et al., 2007). We used a Venetian

blinds cross-validation procedure with 10 data splits to preserve the class proportion in each cross-validation group (Allison et al., 2009). We operated the toolbox in default mode where it utilizes a grid search and cross-validation to select the optimal SVR parameters (such as cost, epsilon and gamma) and then build a model using those values.

The type of kernel function also governs the performance of SVR. The purpose of using a kernel function is to transform linearly inseparable data to linearly separable one by applying them on each data instance. The original (non-linear) observations are then mapped into higher-dimensional space (in which they become separable). This transformation is applied to the data before the model is trained. We used a Gaussian or Radial Basis Function since it is known to produce better results, than other functions such as sigmoid or linear, and has fewer parameters to tune (Zuo and Carranza, 2011). We evaluated the model performance using the coefficient of determination (R^2_{CV}) as a measure of goodness-of-fit (between predicted and measured CAI) and root-mean-square error ($RMSE_{CV}$). We applied the cross-validated models on two S-1 (May 31 and June 6), one R-2 FQ8 (June 13) and one R-2 FQ21 (May 31) satellite images to map CAI in all the wheat fields. We selected the S-1 and R-2 images with the least temporal gap to enable comparative analysis of the performance of the two sensors.

3.3 Results

We observed the first few instances of lodging when the crop was approaching the end of the booting stage or was in the early flowering stage. Lodging became more severe as the crop approached its maturity. During this period, the CAI varied significantly from 3° in the *He* plots to a maximum of 79.5° in VSL plots (Table 3.1). Since PH also changes during lodging, we performed a preliminary analysis to understand its variability as well. Over the same observation period, the PH changed from a maximum of 1.22 m in *He* plots to the minimum of 0.18 m in lodged plots (Table 3.1) and was negatively correlated with CAI ($r=-0.55$) (not shown). PH, however, did not correlate well with the RS-based metrics. We also carried out a detailed time series analysis of S-1 derived metrics for different lodging stages to understand the effect the rainfall, wind speed and other crop parameters (such as LAI) (not shown).

3.3.1 Scattering characteristics of different lodging stages

We present the scattering behaviour for different lodging stages using the σ° (and μ°) metrics derived from S-1 and R-2 data in Fig. 3.7. Table 3.5 and 3.6 indicates the Pearson correlation coefficients for all the metrics.

We found significant differences in the variation of mean values of the metrics across the lodging stage groups. It can be seen in Fig. 3.7a that the σ°_{VV} and σ°_{VH} derived from S-1 increased as lodging became severe. The increase was more prominent in VH polarisation with a difference of 1.3 dB, 2 dB and 4.2 dB for ML, SL and VSL stages respectively w.r.t. He stage. In contrast, the σ°_{VV} variation was smaller (2.7 dB difference between He and VSL) (Fig. 3.7a). The average σ°_{VH} and σ°_{VV} for He stage was around -19 dB and -12.5 dB respectively, whereas for VSL, it was around -14.8 dB and -9.8 dB, respectively (Fig. 3.7a). The change in S-1 derived $\sigma^\circ_{VH/VV}$ was very gradual, while no significant variations were observed for R-2 data. As we can see in Fig. 3.7a, the average $\sigma^\circ_{VH/VV}$ values for He, ML and SL stages are almost the same while for VSL stage, the value increased by 1.4 dB (w.r.t. He). From Fig. 3.7b, we also see that μ°_{VV} dropped substantially when lodging occurred. This is also evident from Table 3.5, where CAI has a low negative correlation with μ°_{VV} ($r = -0.34$) and μ°_{VH} ($r = -0.31$). However, the variation in μ° was statistically insignificant across all the groups (Table 3.4).

In the case of R-2 data, we investigated the scattering mechanisms at low/shallow (R-2 FQ8) and high/shallow (R-2 FQ21) incidence angles by interpreting the SAR data behaviour for different lodging stages. Fig. 3.7c and 3.7d compare the σ°_{HH} , σ°_{HV} , σ°_{VH} and σ°_{VV} values observed at approximately 27° and 41° incidence angles over different lodging stages in wheat. The average σ°_{HV} and σ°_{VH} values were almost the same since natural targets (e.g. agricultural fields) follow the assumption of reciprocity (Larranaga et al., 2012; Lee and Pottier, 2017). R-2 derived σ°_{VH} was thus not included in the subsequent analysis. In general, studies show that σ° decreases over a crop field with moderate surface roughness as the angle of incidence increases (McNairn and Brisco, 2004). This is noticeable in the He stage, as the incidence angle increased from 27 to 41°, the overall σ° decreased by ~0.6 dB. The σ° measurements showed distinct behaviours at the two incidence angles (Fig. 3.7c, 3.7d). For instance, the average σ°_{HH} moderately increased (by 1.5 dB) as CAI increased at 27° while it decreased steadily at 41° (1.6 dB). We also noticed remarkable differences in the HV band. At low incidence angle (Fig. 3.7c), we observed a sharp increase in σ°_{HV} (5.3 dB) as

lodging progressed from He to VSL, whereas at higher angles, we witnessed a relatively small increase (1.4 dB) from He to ML stage, after which the σ_{HV}^0 saturated.

While the Kruskal Wallis test revealed statistically significant differences between the He, ML, SL and VSL classes for most of the metrics, the post hoc Tukey’s analysis showed significant differences only between some of them (Table 3.4). For instance, in the case of S-1 derived σ_{VV}^0 , the He class was significantly different from the lodging classes (ML, SL and VSL). Still, the separability among the lodging classes was not significant (Table 3.4). On the other hand, significant differences were observed among the lodging classes (ML and VSL, SL and VSL) with S-1 derived σ_{VH}^0 (Table 3.4). With R-2 data, the results confirmed that the σ_{HV}^0 in FQ8 beam mode was favourable for distinguishing most of the classes (He-SL, He-VSL, ML-VSL, SL-VSL) while σ_{HH}^0 (He-VSL) and σ_{VV}^0 (He-SL, He-VSL) resulted in reasonable detection of only few of them. The results are presented in Table 3.4.

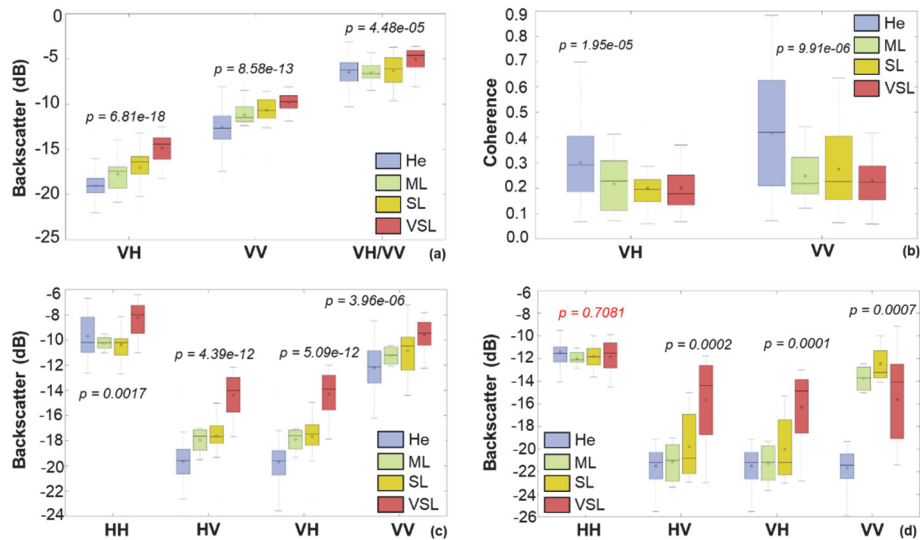


Fig. 3.7. Box plots showing the variation of (a) Sentinel-1 derived backscattering coefficients ($n=118$), (b) Sentinel-1 derived coherence ($n=118$), (c) RADARSAT-2 FQ8 derived backscattering coefficients ($n=57$) and (d) RADARSAT-2 FQ21 derived backscattering coefficients ($n=61$) at different polarisations. The p -values calculated using the Kruskal Wallis test (at 0.01 level of significance) are displayed adjacent to the box plots. Red p -values are non-significant at $p=0.01$ level of significance.

Table 3.4. Posthoc Tukey's HSD analysis is reported for different classes and sensors. * and ** indicate significant values at $p = 0.05$ and 0.01 levels of significance respectively.

S-1						
Class1	Class2	σ°_{VH}	σ°_{VV}	μ°_{VH}	μ°_{VV}	$\sigma^{\circ}_{VH/VV}$
He	ML	0.2400	0.0057**	0.9958	0.9955	0.6470
He	SL	0.0015*	0.0000**	0.9970	0.8467	0.6212
He	VSL	0.0000**	0.0000**	0.9980	0.9613	0.0641
ML	SL	0.9202	0.9661	0.9858	0.9907	0.9871
ML	VSL	0.0012**	0.1361	0.9877	0.9511	0.0393*
SL	VSL	0.0001**	0.0854	1.0000	0.6529	0.0069**

R-2 FQ8					
Class1	Class2	σ°_{HH}	σ°_{HV}	σ°_{VH}	σ°_{VV}
He	ML	0.8336	0.2815	0.2505	0.4107
He	SL	0.7432	0.0059**	0.0058**	0.0118*
He	VSL	0.0000**	0.0000**	0.0000**	0.0000**
ML	SL	0.9966	0.9896	0.9947	0.9774
ML	VSL	0.0110*	0.0080**	0.0070**	0.3200
SL	VSL	0.0000**	0.0001**	0.0001**	0.1818

R-2 FQ21					
Class1	Class2	σ°_{HH}	σ°_{HV}	σ°_{VH}	σ°_{VV}
He	ML	0.7598	0.9892	0.9821	0.5832
He	SL	0.8011	0.1838	0.1481	0.0048**
He	VSL	0.7661	0.0000**	0.0000**	0.8146
ML	SL	0.9923	0.6921	0.6793	0.6198
ML	VSL	0.9953	0.0002**	0.0003**	0.3064
SL	VSL	0.9999	0.0004**	0.0006**	0.0024**

Table 3.5. Pearson correlation coefficients (r) and p -values between CAI and metrics derived from Sentinel-1 data. *** denotes significant values at $p = 0.001$ level of significance.

	Satellite metrics	r	p -value
1	σ°_{VH}	0.67	1.81e-31***
2	σ°_{VV}	0.48	1.28e-14***
3	μ°_{VH}	-0.31	9.75e-07***
4	μ°_{VV}	-0.34	9.18e-08***
5	$\sigma^{\circ}_{VH/VV}$	0.25	1.06e-04***

Table 3.6. Pearson correlation coefficients (r) between CAI and metrics derived from RADARSAT-2 FQ8 and FQ21 data. Backscattering coefficients are expressed in dB and the covariance/coherency matrix elements are in a linear scale. *, ** and *** denote significant values at $p = 0.05, 0.01$ and 0.001 levels of significance, respectively.

	Satellite metrics	r R-2 FQ8	p -value	r R-2 FQ21	p -value
1	σ_{HH}^o	0.19	0.03*	-0.42	3.98e-06***
2	σ_{HV}^o	0.74	1.42e-22***	0.40	1.75e-05***
3	σ_{VV}^o	0.48	1.71e-08***	-0.27	0.005**
4	Span	0.30	0.0007***	-0.23	0.01**
5	Pedestal height	0.57	8.78e-12***	0.21	0.02*
6	RVI	0.55	8.79e-12***	-0.11	0.24
7	RFDI	-0.49	1.12e-08***	-0.24	0.01**
9	CSI	0.22	0.0135*	0.30	0.001***
9	VSI	0.48	2.53e-08***	0.17	0.07
10	BMI	0.17	0.06	-0.21	0.02*
11	Sinclair_1	0.41	2.52e-06***	-0.020	0.83
12	Sinclair_2	0.65	0.84e-16***	-0.005	0.95
13	Sinclair_3	0.15	0.0903	-0.37	6.08e-05***
14	Pauli_T11	0.30	7.10e-04***	-0.33	4.56e-04***
15	Pauli_T22	0.65	0.84e-16***	-0.006	0.95
16	Pauli_T33	0.24	0.008**	-0.15	0.11
17	FD_dbl	-0.40	3.43e-06***	-0.42	3.92e-06***
18	FD_vol	0.67	2.25e-17***	0.00	0.94
19	FD_surf	-0.54	9.31e-11***	-0.15	0.09
20	Yamaguchi_dbl	-0.40	4.97e-06***	-0.53	1.69e-09***
21	Yamaguchi_vol	0.69	1.34e-18***	0.05	0.55
22	Yamaguchi_surf	-0.45	0.41e-07***	-0.26	0.006**
23	Yamaguchi_hlx	-0.20	0.02*	-0.08	0.38
24	VZ_dbl	-0.45	1.36e-07***	-0.53	1.85e-09***
25	VZ_vol	0.66	0.16e-16***	0.03	0.73
26	VZ_sur	-0.11	0.20	-0.08	0.35
27	Cloude_dbl	-0.05	0.52	-0.43	2.52e-06***
28	Cloude_vol	0.62	3.10e-14***	-0.07	0.44
29	Cloude_surf	0.22	0.01**	0.23	0.01**
30	Entropy	0.52	9.20e-10***	0.26	0.005**
31	Anisotropy	-0.33	1.54e-04***	-0.39	2.56e-05***
32	Alpha	0.34	1.19e-04***	0.18	0.05*
33	Psi	0.18	0.041*	-0.01	0.89
34	Tau	0.12	0.18	-0.09	0.33
35	Alpha_touzi	0.11	0.20	0.07	0.42
36	phi	-0.26	0.004**	-0.25	0.008**
37	T11	0.27	0.003**	-0.14	0.14
38	T22	0.35	6.07e-05***	-0.30	0.001***

39	T33	0.72	7.20e-21***	0.02	0.76
40	C11	0.24	0.007**	-0.20	0.03*
41	C22	0.42	1.05e-06***	-0.16	0.07
42	C33	0.44	3.57e-07***	-0.06	0.52

3.3.2 Estimating CAI using support vector regression

We conducted a preliminary test, employing a neighbourhood component analysis (NCA) feature selection method, to select the most important features and compare the performance of SVR for two cases: the model with the whole set of RS-based metrics and the one with subset features. The results were quite similar, with lower RMSE in the former case, which confirmed that multicollinearity was dealt within the SVM and the complementary effect of the interaction among the predictor variables contributed to increased accuracy of the model. Therefore, the whole set of features were used in the final regression models.

We evaluated the SVR models for estimating CAI using RS-based metrics as inputs from (a) S-1 (S-1 model), (b) R-2 FQ8 (FQ8 model) and (c) R-2 FQ21 (FQ21 model) images. We calibrated and cross-validated the models using Gaussian radial basis functions and calculated the overall accuracy and error statistics. The utility of the S-1 derived metrics was confirmed by a good linear relationship that was established throughout the growth cycle ($R^2_{CV} = 0.78$; $RMSE_{CV} = 11.63^\circ$) (Fig. 3.8a), with only a minor underestimation at higher CAI values ($>70^\circ$). The model performance considerably improved with the FQ8 model. It performed most robustly, accounting for 87% of the observed variance in CAI while the $RMSE_{CV}$ dropped by almost 24% in comparison to the S-1 model (Fig. 3.8b). However, a slight underestimation was again recorded in the FQ8 model, which was most evident at the medium CAI values (50-60°) (see Fig. 3.8c). The performance of the FQ21 model, was comparable to the S-1 model as it explained close to 81% of the variance in the plot level measurements, with some underestimated values at high CAI values ($>70^\circ$). In contrast to the FQ8 estimations, the $RMSE_{CV}$ increased by 28%.

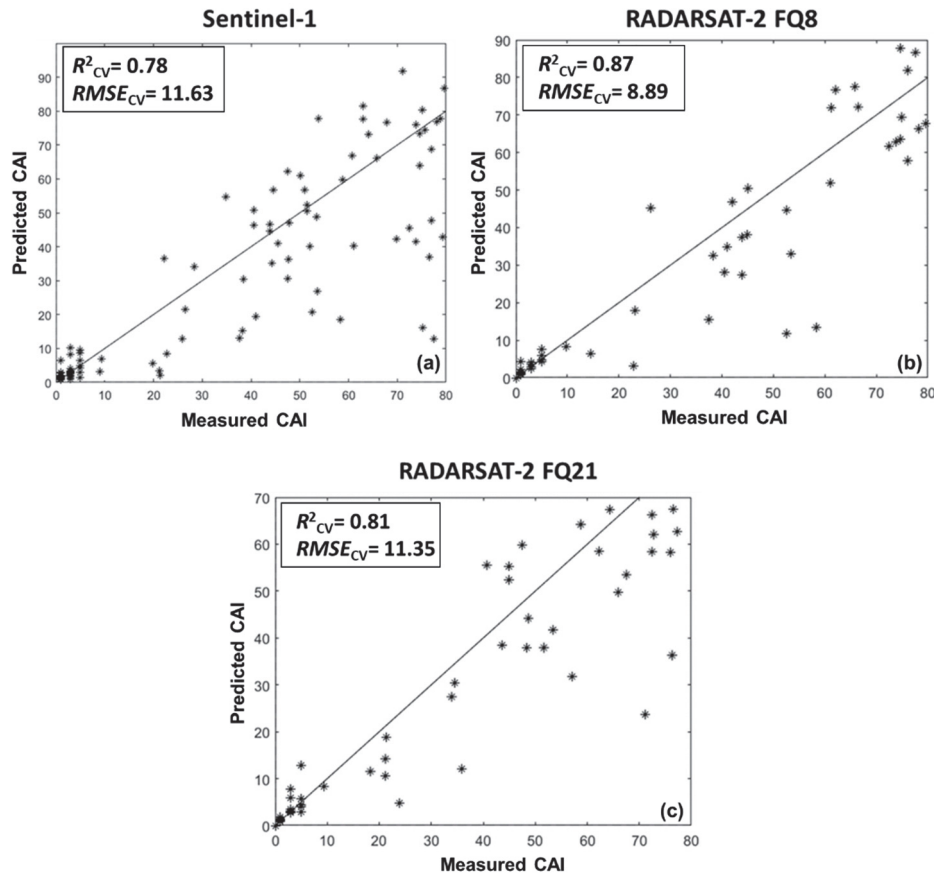


Fig. 3.8. The CAI values predicted using support vector regression versus field measured crop angle of inclination (CAI) from (a) Sentinel-1 ($n=118$), (b) RADARSAT-2 FQ8 ($n=57$) and (c) RADARSAT-2 FQ21 data ($n=61$).

3.4 Discussion

This study investigated the performance of S-1 and R-2 data for estimating CAI in wheat. We first assessed the scattering behaviour of metrics derived from SAR satellite data across different lodging stages. Further, we established quantitative relationships between CAI measured in the field and RS-based metrics. Finally, we used those relationships to map CAI in 26 wheat fields in the study site. The important findings are discussed in this section.

3.4.1 Scattering characteristics of SAR metrics for different lodging stages

The wavelength of S-1 and R-2 satellites (~ 5.5 cm) is comparable to the size of some of the wheat plant constituents such as grain heads and leaves, which makes them particularly useful for wheat monitoring (Ferrazzoli et al., 1997). In section 3.3.1, we saw how the σ^o (and μ^o from S-1) derived from the two sensors with different configurations vary across different lodging stages. In the case of S-1, the relative change in σ^o_{VV} was smaller than that in σ^o_{VH} as lodging became severe (Fig. 3.7a). This could be due to the increased attenuation in the VV polarisation. The Pearson coefficient values in Table 3.5 also confirm our interpretation that σ^o_{VV} and σ^o_{VH} increase significantly with CAI (positive r). $\sigma^o_{VH/VV}$, on the other hand, was particularly sensitive to the VSL stage (Fig. 3.7a). The $\sigma^o_{VH/VV}$ is known to be strongly correlated with PH and represents the randomness of scattering mechanisms (Canisius et al., 2018). During lodging, the PH reduces with an associated increase in CAI. The reduction in PH is more drastic in the VSL stage (mean PH = 0.37 m) and it seems that $\sigma^o_{VH/VV}$ is sensitive to this change.

We did not observe meaningful differences in the variation of μ^o across different lodging stages. The change was statistically insignificant (Table 3.4). This may have been due to the unavailability of field observations every six days. With a six-day temporal baseline, the μ^o was low over the vegetated fields. However, we found an inverse relationship between CAI and μ^o (for both μ^o_{VV} and μ^o_{VH} see Fig. 3.7b), i.e. the μ^o declined as the CAI increased (Fig. 3.7b). A probable explanation for this is that a lodged crop screens the ground more effectively, resulting in higher backscatter from vegetation that decorrelates more quickly than that from the underlying soil (Engdahl et al., 2001). Simplistically, coherence can be explained as the summation of the incoherent and coherent scattering from the soil surface as well as the vegetation (Blaes and Defourny, 2003). In the case of a healthy crop, it is possible that mainly coherent scattering from the soil constitutes the backscattering and results in higher coherence values than that from a lodged crop. However, due to a limited amount of data (every six days) and lack of literature (for the six-day interval), it is difficult to comment on how the underlying soil moisture and surface roughness affect the soil scattering in healthy and lodged areas in this study. Precipitation also results in temporal decorrelation, thus complicating the interpretation of coherence (Tamm et al., 2016). Our meteorological records show that in cases where rainfall coincided with the date of image acquisition (e.g. May 13 – 2.6mm and June 6 – 7.6mm), it might have resulted in increased soil moisture. Besides, the antecedent soil

moisture conditions on other dates (due to few other rainfall events) could also have resulted in a decrease in the coherence values, thus impeding its use for detecting the lodged event. Therefore, repeated observations across several growing seasons are necessary to confirm the potential exploitation of coherence as a key source of information for lodging assessment.

Some interesting findings were also generated from high (41°) and low incidence angle (27°) R-2 data. High incidence angle is known to maximize the contribution of vegetation scattering due to increased path length (of the signal) through the crop canopy. In contrast, low incidence angle is less sensitive to vegetation attenuation and maximizes the contribution from ground scattering in the return signal (Srivastava et al., 2009). At both angles, the σ°_{HH} was higher than that in σ°_{VV} (Fig. 3.7c, 3.7d). This finding is consistent with the findings of Brown et al. (2003) and Mattia et al. (2003a) for healthy wheat. This is primarily due to stronger attenuation of the *V* wave by the vertical stems on both forward and returns propagation paths (Xu et al., 2014). The angular variation was particularly evident between He and VSL stages (Fig. 3.7c, 3.7d). Due to the reduced path length of a radar signal through vegetation at low incidence angle (Brown et al., 2003), it is possible that as CAI increases, this path length through the lodged crop is further reduced, resulting in higher scattering from the ground.

The σ°_{HH} increased as lodging became severe, as the soil return dominates the σ°_{HH} (Mattia et al., 2003b). At low incidence angle, a sharp increase was witnessed in σ°_{HV} from He to VSL stage (5.3 dB) (Fig. 3.7c), which could be due to the contributions from both volume and double bounce scattering mechanisms. At low incidence angle, σ°_{HV} had a good correlation with CAI ($r=0.74$) while at the high incidence angle, a moderate relationship existed ($r=0.40$) (Table 3.6). The ability of σ°_{HV} to distinguish most of the lodging stages at low incidence angle (Table 3.4) can be explained by the strong impact of ear-bending/ear orientation on σ°_{HV} (Ferrazzoli, 2002). The Pearson coefficient values in Table 3.6 also confirm our interpretation that volume scattering indicators increase significantly with CAI (positive r). In contrast, the double bounce indicators show a negative trend (negative r).

Lodging mainly results in the irregular appearance of crop canopy and changes the orientation of the canopy elements. In a healthy plot, the crop canopy stands erect with the horizontal orientation of the ears. When lodging occurs, the stems and the ears bend downwards and incline against each other. This effect is more

pronounced in VSL stage. Radar σ^o is sensitive to these structural changes and hence can explain the variability in different stages of lodging (Fig. 3.7a-d). The variation is more considerable at the low incidence angle (Fig. 3.7c). Thus, the box plots in Fig. 3.7 provide some evidence for the potential application of RS (or specifically C-band SAR) to distinguish different stages of lodging. We recommend that future studies explore simple electromagnetic models to better understand the behaviour of different polarisations in the event of lodging.

3.4.2 Estimation of CAI

Microwave scattering from vegetation is dependent on the SAR frequency/wavelength, incidence angle and polarisation (Soria-Ruiz et al., 2009). Apart from this, the spatial resolution and radiometric quality also affects the backscatter response (Bovenga et al., 2018) and may provide different and/or complementary information. We achieved satisfactory results when we modelled the field measured CAI values using SVR. Overall, the SVR models fitted with inputs from R-2 data performed better than the S-1 model. Even though these two sensors have the same frequency, some of the other characteristics such as their polarisation (dual vs quad), incidence angle (27° vs $41^\circ/40^\circ$), radiometric quality and spatial resolution are considerably different resulting in a better performance for R-2.

Among the input variables from R-2, the metrics referring to volume scattering derived from low incidence angle data were highly correlated with CAI ($0.62 < r < 0.69$). In contrast, the metrics relating to double bounce scattering had a weak negative relationship with CAI at a high angle of incidence (FQ21) ($-0.30 < r < -0.53$) (see Table 3.6). Pedestal height and RVI also proved to be important indicators of CAI at a low incidence angle ($r = 0.57, 0.55$) (Table 3.6). The height of the pedestal determines the degree of polarisation of the scattered wave. The signatures with high pedestal height are characteristic of targets that are dominated by volume scattering (McNairn et al., 2002). Pedestal height is also reported to be directly proportional to vegetation density or the vegetation cover (Evans et al., 1988), which increases with the increase in lodging percentage (Sher et al., 2018). RVI (ranges from 0 to 1), on the other hand, is a measure of randomness of scattering. The average RVI for the healthy vegetation was close to 0.6 while for the VSL crop, RVI was considerably higher (>0.96) at a low incidence angle (see Table 3.6). The high RVI values could be explained by the displacement of some of the individual plant scatterers during lodging, due

to which several scattering mechanisms arise from the target resulting in an increased degree of random scattering.

The findings also revealed that low incidence angle data is particularly sensitive to high CAI ($>60^\circ$) while high incidence angle can be useful for predicting lower CAI values (Fig. 3.8b, 3.8c). The underestimation of the FQ8 model for SL stage could be due to the non-homogeneous distribution of the number of samples in different lodging classes. It could be that the SVR model did not have enough cases in the SL class to be more robust. Also, in our case, the samples for the SL class comes from two images, while those for VSL comes from one image which could also have been a potential source of error. The reason being that during cross-validation, the model has to estimate VSL on the same target condition. At the same time, SL can correspond to different target conditions according to the acquisition dates. For S-1 data, σ°_{VH} and σ°_{VV} had a reasonable correlation with CAI ($r = 0.67$ and $r = 0.48$, respectively) while coherence values were poorly correlated with CAI ($r < -0.4$) (Table 3.5). The performance of the S-1 model was almost comparable to FQ21 model, which suggests that the potential of S-1 data; considering the significance of free data for operational needs, cannot be ignored.

It is also important to note here that the acquisition of S-1 and R-2 FQ8 data in the ascending pass (evening time) (Table 3.2) ensured that the possible early morning dew effects on the backscatter values were non-existent. Due to user conflicts and acquisition constraints, the R-2 FQ21 images were, however, acquired in the descending pass (morning 5 am). Therefore, the morning dew could be a source of error in the analysis of these images. However, a study done by Wood et al. (2002) suggests that there is a significant correlation between the backscatter of ascending and descending orbits, which implies that although absolute backscatter increases in the presence of dew, relative differences remain very similar. Also, the effect of azimuth angle or orientation on the polarimetric response of wheat crop could be neglected in this study since for C-band (contrary to lower frequencies such as L-band), the scattering value is independent of azimuth angle as shown by Stiles et al. (2000).

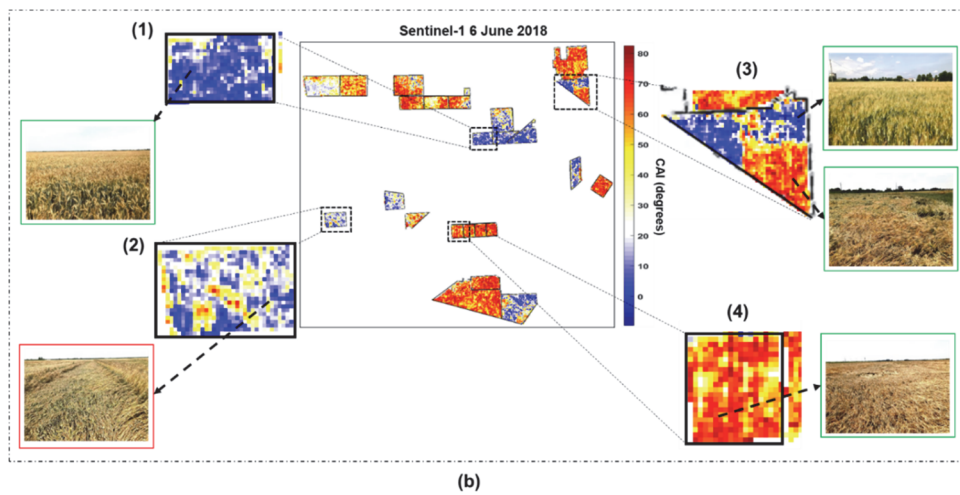
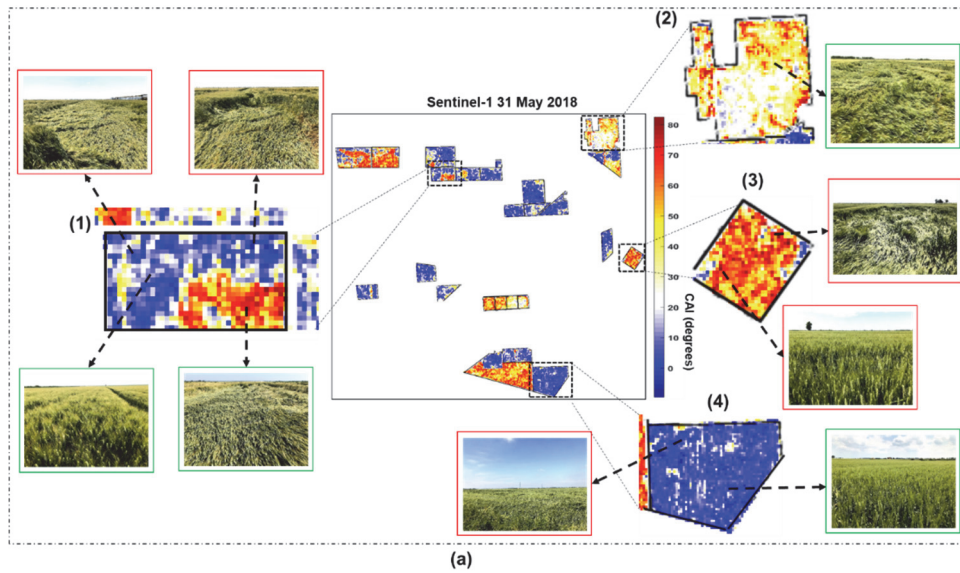
3.4.3 Mapping of CAI

To map CAI, we applied the SVR models on two S-1 and two R-2 images. We masked out the non-wheat areas and the resulting maps are shown in Fig. 3.9. We derived the maps when the crop was in the milking stage (May 31), early ripening stage (June 6) and mid-ripening stage (June 13). The healthy areas are mapped

with CAI values close to 0° , while the most severe ones are close to 90° . The maps indicate that lodging was widespread across the wheat fields with more severely lodged areas detected in the ripening stage as expected. Since field observations were used to assess the mapping results qualitatively, the obtained CAI maps should be considered as qualitative indicators of the within-field spatio-temporal variability of lodging. However, patterns provided by different models show the convergence of CAI results, supporting the general qualitative validity of the produced maps.

The closest acquisition dates between S-1 and R-2 images were considered for comparing the outputs. For instance, Fig. 3.9a and 3.9c show the S-1 and R-2 FQ21 predicted CAI maps, respectively for May 31. While the S-1 model mapped the entire field 4 as He (Fig. 3.9a), the FQ21 model could capture the ML areas as well (Fig. 3.9c). Also, in field 1 (Fig. 3.9c), the S-1 model overestimated the healthy patches. The better performance of FQ21 model can be attributed to its high spatial resolution that allowed for the assessment of spatial variability at both field and plot scale. The FQ8 image from June 13 could also capture the spatial variabilities of CAI quite effectively. These spatial maps can serve as a valuable baseline for assessing the performance of the models across stages of lodging progression and have potential applications for crop management and precision agriculture. For instance, the CAI maps generated before harvesting can contribute to in-field navigation routes to guide drivers or autonomous driving vehicles to adjust their speeds based on the lodging condition and thus minimise the harvesting losses.

Estimation of crop angle of inclination for lodged wheat



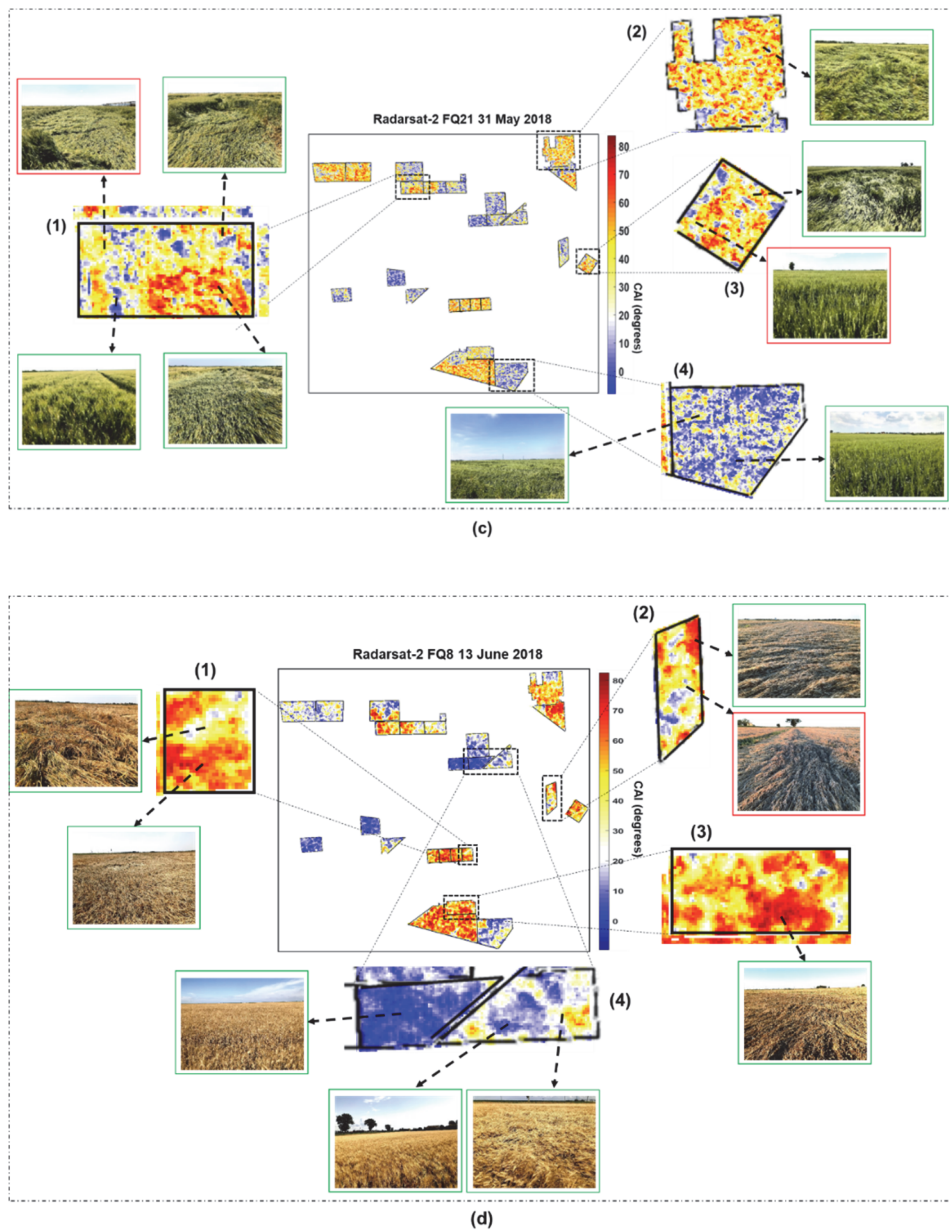


Fig. 3.9. CAI maps predicted from (a) Sentinel-1 data acquired on May 31, 2018, (b) Sentinel-1 data acquired on June 6, 2018, (c) RADARSAT-2 FQ21 data acquired on May 31, 2018 and (d) RADARSAT-2 FQ8 data acquired on June 13, 2018. Field photographs from several plots have been used to assess the maps qualitatively. The correctly mapped areas are supported with field photographs marked in green while the others are marked in red. "RADARSAT-2 Data and Products. MacDonald, Dettwiler and Associates Ltd. (2018) – All Rights Reserved. RADARSAT is an official trademark of the Canadian Space Agency."

3.5 Conclusions

In this study, we introduced a new method to assess crop lodging stages based on the crop angle of inclination (CAI) derived from Sentinel-1 and RADARSAT-2 data. We first demonstrated the potential of metrics derived from these datasets to distinguish between different lodging stages: non-lodged/healthy (He), moderate lodging (ML), severe lodging (SL) and very severe lodging (VSL). The performance of different support vector regression models (SVR) was then evaluated for estimating CAI from RS-based metrics. The main conclusions of the study are summarised below:

1) Among the different SVR models developed to establish quantitative relationships between field-measured CAI values and RS-based metrics, the R-2 FQ8 (low incidence angle) performed most robustly with an R^2_{CV} of 0.87 and $RMSE_{CV}$ of 8.89° . The performance of S-1 and R-2 FQ21 (high incidence angle) models were comparable with an $RMSE_{CV}$ of 11.35° and 11.63° , respectively. The differences in sensor configuration (mainly the incidence angle and spatial resolution) had a primary influence on the model performance. At the same time, the increased dimensionality of R-2 data seemed to play a secondary role. However, we believe that the combination of the two can improve the ability to monitor CAI throughout the crop growth cycle.

2) Low incidence angle data was found to be particularly sensitive to high CAI ($>60^\circ$) while high incidence angle predicted the lower CAI values more accurately.

3) Among the polarimetric decomposition parameters that were derived from R-2 data, the volume scattering parameters (such as FD_vol, Yamaguchi_vol, VZ_vol, Cloude_vol) derived from low incidence angle data were highly correlated with CAI ($0.62 < r < 0.69$) while double bounce scattering parameters (such as FD_dbl, Yamaguchi_dbl, VZ_dbl, Cloude_dbl) had a stronger negative relationship with CAI at a high angle of incidence ($-0.30 < r < -0.53$).

4) The S-1 model explained 78% of the CAI variability in the area showing that the dense time series high-resolution S-1 data can be exploited for lodging stage assessment. The unprecedented amount of free S-1 data guaranteed with the next generation of Sentinel up to or probably beyond 2030, presents a unique opportunity to monitor lodging in crops in NRT.

5) In summary, this study provides evidence of the potential of high-resolution SAR RS data in estimating CAI as a measure of assessing lodging stages, which to the best of our knowledge, has not been documented in the literature.

Chapter-4

Discriminant analysis for lodging severity classification in wheat using RADARSAT-2 and Sentinel-1 SAR data*

*This chapter is based on:

Chauhan, S., Darvishzadeh, R., Boschetti, M., & Nelson, A. (2020b). Discriminant analysis for lodging severity classification in wheat using RADARSAT-2 and Sentinel-1 data. *ISPRS journal of photogrammetry and remote sensing*, 164, 138-151. <https://doi.org/10.1016/j.isprsjprs.2020.04.012>

Chauhan, S., Darvishzadeh, R., Boschetti, M., & Nelson, A. (2020e). Understanding of crop lodging induced changes in scattering mechanisms using RADARSAT-2 and Sentinel-1 derived metrics, In *The International Archives of Photogrammetry, Remote Sensing and Spatial Information Sciences*, 43, 267-274.

Abstract

Crop lodging - the bending of crop stems from their upright position or the failure of root-soil anchorage systems - is a major yield-reducing factor in wheat and causes deterioration of grain quality. The severity of lodging can be measured using a lodging score (LS)- an index calculated from the crop angle of inclination (CAI) and the lodged area (LA). The information derived from RS-based estimates of LS could improve estimates of crop yield losses, ensure timely insurance pay-outs and influence management decisions for subsequent seasons. This research - conducted in the 600 ha wheat sown area of the Bonifiche Ferraresi farm, located in Jolanda di Savoia, Ferrara, Italy - evaluated the performance of RADARSAT-2 (R-2) and Sentinel-1 (S-1) data to distinguish and classify lodging severity based on LS. We measured temporal crop characteristics related to lodging (e.g. lodged area, CAI, plant height) and collected relevant meteorological data (wind speed and rainfall) throughout May 1-June 30, 2018. We used LS to distinguish healthy (He) wheat from lodged wheat with different degrees of lodging severity (moderate, severe and very severe). We acquired the low (FQ8-27°) and high (FQ21-41°) incidence angle R-2 images in combination with high incidence angle S-1 (40°) images. As a part of our data exploration, we performed a correlation analysis between the RS-based metrics and LS. Next, we developed a multi-temporal discriminant analysis approach, including a partial least squares (PLS-DA) model to classify lodging severities. Results show that (1) volume scattering components were highly correlated with LS at low incidence angle while double and surface scattering was more prevalent at high incidence angles; (2) lodging severity was best classified using low incidence angle R-2 FQ8 data (overall accuracy 72%) and (3) the S-1 classification model was able to correctly identify 60% of the lodging severity cases in the study site. The results from this first study on classifying lodging severity using satellite-based SAR platforms suggests that SAR-based metrics can capture a substantial proportion of the observed variation in lodging severity. This is important in the context of operational crop lodging assessment in particular, and sustainable agriculture in general.

4.1 Introduction

Food production will have to increase by 70% by 2050 (FAO, 2014) to ensure that global food supply meets the demands of the world's growing population. Raising the productivity of wheat, a staple crop that contributes to 20% of global dietary calories, will be fundamental in achieving this goal (Reynolds et al., 2012; Shiferaw et al., 2013). Multiple factors limit or reduce wheat productivity. Lodging - the bending of crop stems from their upright position, or the failure of crop root-soil anchorage systems (Pinthus, 1974) - is a major yield-reducing factor in wheat. A complex interaction between genetic, environmental and management factors affects the incidence and severity of lodging. Lodging limits wheat productivity directly by reducing photosynthetic efficiency due to disruption of crop morphology (Berry and Spink, 2012), and indirectly through breeding by boosting the amount of dry matter (Berry et al., 2007). Methods to detect lodging and estimate its severity can be incorporated into agricultural management practices to reduce losses, boost productivity and make more efficient use of resources.

A standard, quantitative measure of the severity of crop lodging is the lodging score (LS) (Piñera-Chavez et al., 2016). LS has two components: the angle of displacement or crop angle of inclination (CAI) from the vertical and the lodged area (LA) (Fischer & Stapper, 1987; Oplinger & Wiersma, 1984). In-season assessment of LS can indicate plant health status, lodging severity, improve estimations of yield loss, facilitate targeted and early harvesting operations (Oplinger et al., 1967; Wu and Ma, 2019). The conventional methods to evaluate LS rely on visual ratings on a scale of 0-1, 1-9 or 0-100 where 1, 9 or 100 refer to instances when crop in the entire plot is lying horizontally on the ground. Such evaluations are i) sparse and may not cover all lodged areas, ii) biased and subjective since they depend on the skill or self-consistency of the observer and the complexity of the lodging event, and iii) time consuming and expensive to implement (Bock et al., 2010). As with many ground-based observation methods, such assessments cannot provide consistent and comparable estimates of lodging severity over vast areas from season to season. Thus, LS is difficult and time consuming to measure manually meaning that information on lodging occurrence and severity is limited and sparse.

Alternatively, RS provides a timely, synoptic and reliable way of obtaining crop lodging information across large and diverse areas. RS has been used for crop lodging assessments, albeit with a focus on detecting lodging in individual fields

rather than at regional scales (Chauhan et al., 2019a). The earliest work dates back to 1980s to identify lodging in winter wheat using microcomputer-assisted video image analysis (Gerten and Wiese, 1987). Subsequent work that focused on lodging assessment using optical data provided examples of where lodging could be detected, and where the variability in inter/intra-field lodging could be captured by airborne or satellite-based information (Vargas et al., 2020; Yang et al., 2020; Zhou et al., 2020). For instance, Zhang et al. (2014) and Chapman et al. (2014) showed that infrared and thermal images respectively could be useful in identifying lodged patches in a field. The potential of synthetic aperture radar (SAR) data for lodging assessment has particularly been emphasised in the literature due to its all-weather availability and unique sensitivity to plant structure (Chen et al., 2016; Zhao et al., 2017).

Recently, more widespread access to images and advanced data processing platforms have substantially reduced the cost of obtaining and (pre-)processing images. For instance, georeferenced Sentinel-1/2 data is now available for free via the Copernicus Open Access Hub and can be rapidly mosaicked and composited in the Sentinel Hub or Google's Earth Engine platform (Gorelick et al., 2017). For instance, Han et al. (2017) utilised the plant height information derived from S-1 data to build a quantitative lodging stage classification model. More recently, Shu et al. (2019) used S-1 data to develop a method based on the change in plant height before and after lodging to estimate CAI and monitor the lodging stages. However, the use of height variation is not a reliable diagnostic of lodging without additional information as it is sensitive to the crop cultivar and phenological stage (Chauhan et al., 2020a). On the other hand, the metrics retrieved from commercial RADARSAT-2 (hereafter referred as R-2 data) fully polarimetric data - such as HV backscatter and the ratios of the span, double bounce scattering and single-bounce scattering - have also shown promising results for lodging detection in wheat (Yang et al., 2015; Zhao et al., 2017).

LS-based discrimination between healthy and different lodging severity classes (such as moderate, severe and very severe) from RS has still not become widespread due to a combination of factors including (i) unavailability of high spatio-temporal resolution data at low cost; (ii) absence of a standard scale to represent lodging which hinders accuracy assessment; (iii) a lack of consensus on the most appropriate way to produce and validate lodging maps; (iv) a lack of statistics/data related to lodging (unlike crop yield) on local/ regional/global scales; and (v) the daunting task of collecting field data related to lodging, due to

its heterogeneous distribution. Among the few limited studies, our previous research investigated the utility of RS for detecting lodging stages in wheat-based on CAI (Chauhan et al., 2020a). However, CAI alone is not a representative and quantitative measure of crop lodging. LS, which combines CAI and LA, provides a more comprehensive assessment of lodging-related damage. Our review (Chauhan et al., 2019a) also shows there is no prior published research that demonstrates the potential of RS-based information for classifying crop lodging severity based on LS. This study aims to fill this gap by developing a new approach for lodging severity classification and building on the positive outcomes of our previous research on CAI estimation via non-parametric regressive analysis of SAR metrics (Chauhan et al., 2020a).

Among several methods applied for discriminant analysis and image classification, partial least squares discriminant analysis (PLS-DA) has shown to be a promising tool when dealing with the complexities of high dimensional datasets (Boulesteix and Strimmer, 2006). While the use of PLS-DA has mainly been limited to regression-based analysis, such as for predicting canopy biomass in wheat (Hansen and Schjoerring, 2003) or estimating forest structural parameters (Wolter et al., 2009), only a few have examined the utility of PLS for discriminant analysis and classification purposes (Peerbhay et al., 2013).

In this context, we present an approach that integrates CAI and LA as a way to assess and classify crop lodging severity. We evaluate the performances of R-2 (at different incidence angles) and S-1 data for classifying non-lodged/healthy (He) wheat and wheat with different degrees of lodging severity (moderately lodged (ML), severely lodged (SL) and very severely lodged (VSL)) using partial least squares discriminant analysis (PLS-DA).

4.2 Materials and methods

4.2.1 In situ measurements

We implemented stratified random sampling using six information strata (elevation, sowing date, crop cultivar, soil type, seed density and soil pH) and identified 76 sample plots (60×60 m). The spatial distribution of these plots is shown in Fig. 4.1. We started inspecting the plots frequently from March 2018 onwards to record the first instance of lodging. The first few instances of lodging were observed close to the end GS40 (around May 1, amidst the 2nd round of sampling). Therefore, we considered the observation period from May 1 onwards

until June 30, 2018, when the crop was harvested. A total of 118 samples were collected during this period which spanned three phenological stages - flowering, milking and ripening. The field and satellite image data were collected synchronously between May 1-June 30, 2018.

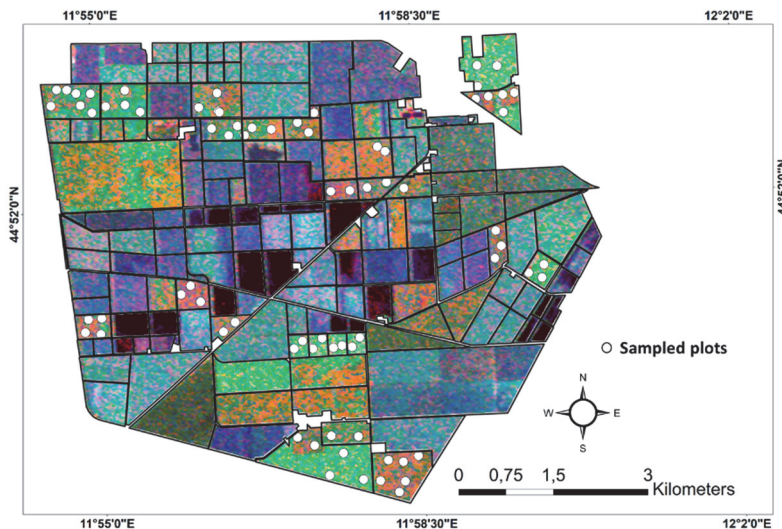


Fig. 4.1. An RGB composite of a Van Zyl decomposed RADARSAT-2 (double bounce, volume, surface scattering) scene acquired on May 31, 2018, containing the study area (Bonifische Ferraresi farm) overlaid with the sampling points (white dots) over the wheat sown fields and the farm boundary (black outline). “RADARSAT-2 Data and Products. MacDonald, Dettwiler and Associates Ltd. (2018) – All Rights Reserved. RADARSAT is an official trademark of the Canadian Space Agency.”

We calculated a normalised lodging score index (LS, [0-1]) (see Eq. (4.2), modified after Fischer and Stapper (1987) for each plot based on CAI (θ , [0-90°]) (see Eq. 4.1) and lodged area (LA%, [0-100%]). We measured and calculated the CAI from the vertical using a plumb bob, measuring tape and some trigonometric calculations (Eq. 4.1). The detailed approach for CAI estimation is mentioned in Chapter-3. We assessed the LA (0-100%) using a quadrant method. From the plot centre, we visually assessed the LA in four quadrants (Fig. 4.2c) and averaged the readings. A scenario is depicted in Fig. 4.2b and 4.2c, illustrating the distribution of He and lodged subplots in real field conditions.

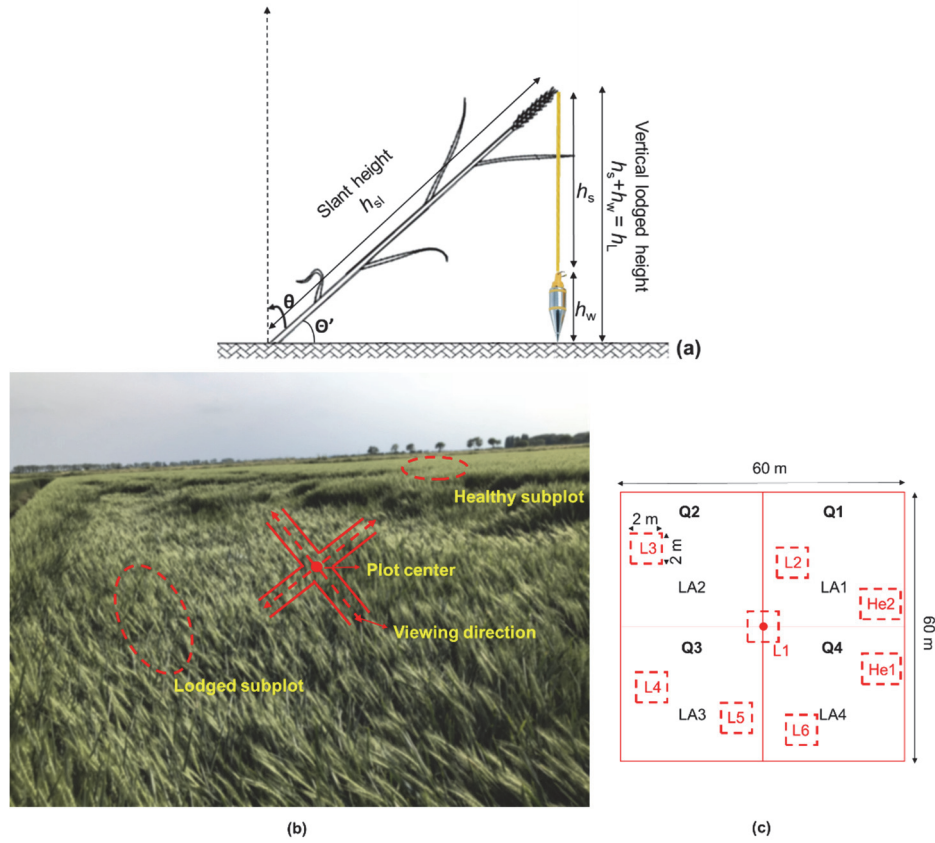


Fig. 4.2. (a) Measurement technique for crop angle of inclination using a vertical plumbob (Chauhan et al., 2020a). θ and θ' is the crop angle of inclination (CAI) with respect to the vertical and soil surface, respectively. h_s and h_w is the height of the string and the heavyweight at the bottom of the plumbob, respectively, h_L ($h_s + h_w$) is the total vertical height of the lodged plant, h_{sl} is the slant height of the plant measured from the soil surface to the tip of the head of the longest tiller with a measuring tape (θ) (b) Depiction of healthy (He) and lodged (L) subplots and plot centres in real field conditions. (c) The plot is divided into four quadrants Q1 to Q4-the lodged area in each quadrant is represented as LA1 to LA4; He1, He2 are the healthy subplots and L1,...L4 are the lodged subplots.

$$\theta \text{ (degree)} = 90^\circ - \sin^{-1} \frac{h_L}{h_{sl}} \quad (4.1)$$

$$LS = \frac{LA\%}{100} * \frac{CAI}{90^\circ} \quad (4.2)$$

Table 4.1. Summary statistics of biophysical/biochemical parameters in healthy (*He*, *n*=51) and lodged samples (*L*, *n*=67) throughout the flowering to ripening phenological stages. *COV* is the coefficient of variation.

Parameter	Mean		Min.		Max.		Std. Dev.		COV	
	He	L	He	L	He	L	He	L	He	L
CAI (deg)	4.84	50.79	3.00	9.36	5.00	79.50	0.53	18.76	0.11	0.37
Lodged area (%)	0.00	87.71	0.00	20.00	0.00	100.00	0.00	18.26	0.00	0.21
Lodging score	0.00	0.52	0.00	0.02	0.00	0.88	0.00	0.23	0.00	0.45
Fresh biomass (t/ha)	4.42	4.98	2.10	1.23	8.01	12.85	1.45	2.21	0.33	0.45
Dry biomass (t/ha)	1.26	2.07	0.49	0.26	2.10	5.30	0.39	0.84	0.31	0.41
Plant height (m)	0.86	0.49	0.70	0.18	1.22	0.94	0.08	0.19	0.10	0.38

The plots with $LS=0.0$ were categorised as healthy (He, $n=51$) while the lodged plots ($LS>0.0$) were divided into three lodging severity classes: moderately lodged (ML) ($0.0<LS\leq 0.30$, $n=12$), severely lodged (SL) ($0.31<LS\leq 0.60$, $n=25$) and very severely lodged (VSL) ($0.61<LS\leq 1.0$, $n=30$) to capture the heterogeneity of LS. The determination of lodging has been partly derived and modified after the works of Caldicott and Nuttall (1979), Chauhan et al. (2020b), Fischer and Stapper (1987) and Nottingham and User (1998). In He plots, we chose three subplots of 2×2 m to carry out the crop biophysical measurements. In lodged plots, we increased the number of subplots to 4-8 (depending on the LA within each plot) to capture the heterogeneity caused by lodging and then averaged the readings. The summary statistics of these parameters are presented in Table 4.1.

Furthermore, to investigate lodging in relation to crop condition, we measured several biophysical/biochemical parameters (such as plant height, biomass). The meteorological data (daily cumulative precipitation (mm) and average daily wind speed 10 m from the ground) were recorded through a local automatic weather station at the farm. For biomass measurements, we destructively sampled the plants in 0.2×0.2 m² area in each subplot and used a high-precision digital scale to measure the weight. We then placed the samples in a zip-locked plastic bag and transported to the laboratory where we dried them in an oven at 60°C for 72 hours and then weighed the dry mass. We calculated the fresh and dry biomass (t/ha) using the fresh and dry weights divided by the surface area. Lastly, we used a measuring tape to measure plant height. The summary statistics of these parameters are presented in Table 4.1 for He and lodged samples. Additionally, we used a standard BBCH phenological scale to identify the phenological stages.

4.2.2 Remote sensing data acquisition

We acquired a set of five R-2 and eleven S-1 A/B images over the study area (Fig. 4.3). We selected the S-1 and R-2 images that were synchronous to the dates of the ground truth data acquisition. We procured single look complex (SLC) R-2 data in fine-quad pol (FQ) beam mode from the Canadian Space Agency through the SOAR (Science and Operational Applications Research for RADARSAT-2) program. We selected two-beam modes: low/steep incidence angle FQ8 or R-2 FQ8 (resampled to 10 m spatial resolution with $\sim 27^\circ$ incidence angle, 25 km swath, ascending mode) and medium/shallow incidence angle FQ21 or R-2 FQ21 (resampled to 7 m spatial resolution, $\sim 41^\circ$ incidence angle, 25 km swath, descending mode). Also, we obtained S-1A/B images in the Interferometric Wide

(IW) swath mode with dual polarisation (VV and VH) from the Copernicus Open Access Hub. In this study, we used both SLC as well as ground range detected (GRD) images (resampled to 15m spatial resolution with $\sim 40^\circ$ incidence angle, 250 km swath and ascending mode) for polarimetric as well as backscatter intensity analysis, respectively. Fig. 4.3 gives an overview of the acquisition dates of S-1, R-2 FQ8, and R-2 FQ21 images. In our study, we could acquire only two R-2 FQ8 and three R-2 FQ21 images (as opposed to 11 Sentinel-1 images) available during the observation period. Thus, only 57 and 61 field samples could be used for the analysis of R-2 FQ8 and R-2 FQ21 data, respectively, while for S-1 data, all field samples ($n=118$) were analysed.

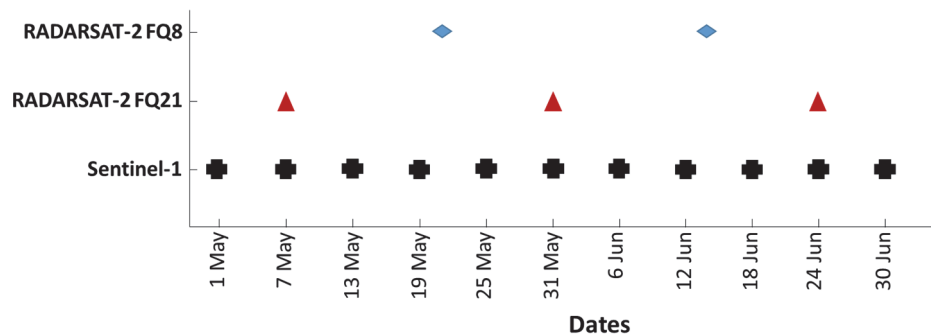


Fig. 4.3. Acquisition dates of RADARSAT-2 FQ8, RADARSAT-2 FQ21 and Sentinel-1 data covering the study site during the 2018 wheat growing season.

4.2.3 Remote sensing data pre-processing

4.2.3.1 RADARSAT-2

We performed the backscatter processing of R-2 data in SARscape 5.5 and extracted the polarimetric parameters using SNAP 6.0. After applying the orbit file correction, we obtained the normalised backscattering coefficient (in dB) using the approach outlined in Nelson et al. (2014b). In order to extract the polarimetric parameters, we first performed radiometric calibration on the subset images so that the pixel values could be directly related to the target radar backscatter. We then extracted the polarimetric parameters such as span (Lee and Pottier, 2017), pedestal height (Lee and Pottier, 2017), radar vegetation index (RVI) (Kim and van Zyl, 2009), radar forest degradation index (RFDI) (Mitchard et al., 2012), canopy scattering index (CSI) (Pope et al., 1994), biomass index (Pope et al., 1994), and volume scattering index (VSI) (Pope et al., 1994) and geocoded the co-registered datasets using a high-resolution (10 m) DEM (Tarquini et al., 2007).

For polarimetric decomposition, we first applied a Refined Lee polarimetric speckle filter with a 5×5 window size to reduce speckle in the images while preserving the complex information. With several polarimetric decomposition methods, we decomposed the scattering matrix into different components that could be physically interpreted. We used Sinclair decomposition (Krogager et al., 1997), which represents the symmetric scattering matrix in the form of a three-element target vector where the elements are associated with the HH, HV and VV polarimetric channels. We used the Pauli decomposition (Cloude and Pottier, 1996), which denotes the vector representation of linear combinations of the elements of the scattering matrix. We used an eigenvector-eigenvalue based- $H/\alpha/A$ decomposition proposed by (Cloude and Pottier, 1997) to calculate H (entropy), α (alpha angle) and A (anisotropy) parameters. The H represents the heterogeneity of the scattering, ranging from 0 (for dominant scatterers, e.g. corner reflectors) to 1 (a random mix of scattering mechanisms, e.g. in vegetation canopy). The α indicates the type of scattering, ranging from the surface ($\alpha \sim 0^\circ$), to random volume/dipole scattering through anisotropic particles (e.g. tree crowns, $\alpha \sim 45^\circ$), moving into double bounce scattering mechanisms (e.g. urban areas, α up to 90°). The A enables further understanding of the secondary backscattering mechanisms occurring in the resolution cell (or a pixel). Finally, we also used model-based decomposition methods such as Freeman-Durden (Freeman and Durden, 1998), Yamaguchi (Yamaguchi et al., 2005), Cloude (Cloude and Pottier, 1996), Touzi (Touzi, 2007) and Van Zyl (Van Zyl et al., 2011), which decompose the scattering matrix into different scattering mechanisms (e.g., surface, double bounce or volume). The decomposed images were co-registered and geocoded with the high-resolution DEM. Thus, a total of 36 metrics were generated from each beam mode.

4.2.3.2 Sentinel-1

We extracted the normalised VH (σ_{VH}^0), VV (σ_{VV}^0) and VH/VV ($\sigma_{\text{VH/VV}}^0$) backscattering coefficients/ratios (in dB) from the GRD S-1 datasets in SARscape 5.5 using the approach outlined by Nelson et al. (2014b). The metrics were extracted for each sample plot by averaging the pixel values in a 3×3 window. For polarimetric decomposition, we first applied the orbit file correction on the SLC S-1 images in SNAP 6.0. We then used the TOPSAR Split operator to extract the sub-swath with our area of interest. We then radiometrically calibrated the output product and deburst it to produce a continuous image in terms of azimuth time. The deburst operation is required to remove the black-fill demarcation lines as well as the redundant lines between the bursts. We then

applied a Refined Lee speckle filter with a 5×5 window and performed H/ α /A polarimetric decomposition to extract H, α and A parameters for all the sample plots. Similar to R-2 data, the decomposed products were then co-registered and geocoded. Thus, a total of six metrics (σ°_{VH} , σ°_{VV} , $\sigma^{\circ}_{VH/VV}$, H, α and A) were generated from S-1 images.

4.2.4 Statistical analysis

4.2.4.1 Partial least squares discriminant analysis (PLS-DA)

As a part of our data exploration, we first calculated the Pearson correlation coefficients (r) and p -values between each RS-based metric and our field measured lodging score (LS) to understand the relationship between them. This analysis was done to enable the interpretation of the results. We then carried out a partial least squares discriminant analysis (PLS-DA) for discriminating He from other LS-derived lodging severity classes. All these steps were performed in MATLAB 2018b. The methodological flowchart of the study is presented in Fig. 4.4.

PLS-DA is an adaptation of classical PLS regression methods to the problem of supervised clustering and classification (Wold et al., 2001). In an application where the response variable (Y) is related to the predictor variables (X), PLS regression aims to provide dimensionality reduction while dealing with multicollinearity (Abdullah et al., 2018). The response variable is categorical and expresses the class membership (Galtier et al., 2011) by transforming the categorically dependent variable into a binary dummy variable “0” and “1”. In our case, the categorical variable, i.e. lodging severity had four levels/classes (He, ML, SL, VSL) and therefore, four dummy variables were required to represent those classes. PLS-DA aims to sharpen the separation between groups of observations by rotating Principal Component Analysis (PCA) components to obtain maximum class separation and to understand which variables separate the classes in the best way. The model is developed in a way that the chosen latent variables retain the most information from the predictor and response variables.

In this study, we developed three classification models (for R-2 FQ8, R-2 FQ21, S-1) for distinguishing He from other LS-derived lodging severity classes using PLS-DA algorithm. The principal components were used as new predictors and regressed on lodging severity classes to determine the optimum separation between the lodging classes. With the increase in the number of predictor

variables/components, the predictive capacity of PLS-DA model increases, as many variables tend to contain more information than a few (Whelehan et al., 2006). However, in general, due to the presence of many correlated variables in a PLS model, it is essential to identify the optimal number of components to minimise the risk of overfitting (Wold et al., 2001). We optimised the parameters of all the three classification models using 10-fold Venetian blinds cross-validation (Wolter et al., 2008). The optimisation involved adding each component progressively to the model until the further addition did not reduce the CV error rate. Since PLS is known to deal with multicollinearity (Serrano-Cinca and Guti rrez-Nieto, 2013), we fed all the metrics as inputs to the respective models. We performed the modelling using partial least square (PLS) toolbox v8.7 from Eigenvector Research, Inc., with the Multivariate Image Analysis (MIA) toolbox v3.0 add-on (in MATLAB 2018b) (Wise et al., 2007).

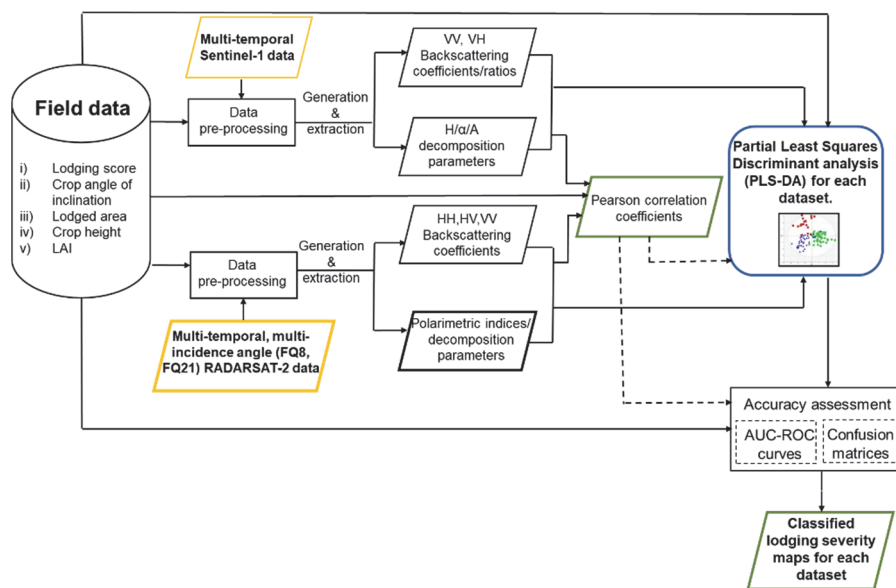


Fig. 4.4. Methodological flowchart of the study. Inputs are in yellow, method/model in blue, and primary/intermediate outputs in green. The dashed line represents that the output is used for interpretation.

4.2.4.2. Accuracy assessment

For the accuracy assessment of the PLS-DA classification results, we used two methods: Area under the curve-Receiver Operating Characteristics (AUC-ROC) and a cross-validated confusion matrix. These are important metrics for

evaluating the performance of multi-class classifiers (Comber et al., 2012; Narkhede, 2018). For validation, we used a Venetian blinds cross-validation procedure (Wolter et al., 2008) with 10 data splits as this method is useful in preserving the class proportion in each cross-validation group and guarantees that both training and validation sets span across the entire data range (Allison et al., 2009). This involved dividing the datasets randomly into ten subgroups, each with approximately 10% of the samples from each class. We trained the model with 90% of the reference data and applied it to the remaining 10% (i.e. validation set). After ten repetitions, we aggregated the results.

AUC-ROC is a powerful tool to evaluate classifiers over all the possible thresholds and is particularly useful for problems with skewed class distribution and differing classification errors costs (Fawcett, 2006). ROC is a probability curve, while AUC is a measure of separability. Higher the AUC, better the model at predicting class A as A and class B as B. An AUC=1 is an ideal diagnostic test since it results in 100% specificity as well as 100% sensitivity (Estes et al., 2010). The AUC-ROC quantitatively represents the trade-offs between omission (true positive rate or sensitivity) and commission (false positive rate or 1-specificity) error. AUC>0.5 signify classifiers performing better than chance. In this study, we created the estimated and cross-validated ROC response curves for all the three datasets. When used in conjunction with the confusion matrix, ROC can enable the selection of an optimal threshold for the latter (Alatorre et al., 2011). The confusion matrix allows identification of confusion between the classes and the accuracy is measured in terms of overall accuracy (OA), producer's accuracy (PA), user's accuracy (UA) and kappa coefficient (K). We computed a cross-validated confusion matrix to evaluate the classification accuracy.

4.3 Results

4.3.1 Field observations

The first round of lodging occurred when the crop was approaching the end of the booting stage (around May 1, 2018). Lodging subsequently became more severe as the crop approached maturity (June 10 onwards). During this period, CAI varied significantly from 3-5° in *He* plots to 9-79.5° in lodged plots with a COV of 0.11-0.37 (see Table 4.1). LA also varied dramatically from 0% (*He*) to 100% (VSL) with a COV of 0.0-0.21 (Table 4.1). LS varied from 0.00 (*He*) to 0.88 (VSL), with a standard deviation of 0.00-0.23 and COV of 0.00-0.45.

4.3.2 Correlation analyses of the backscattering coefficients and polarimetric parameters with lodging score

We first calculated the Pearson correlation coefficients (r) between each RS-based metric and LS to investigate the capability of RS to classify lodging severity. This further enabled us to interpret the classification results. A majority of the metrics obtained from R-2 data had a significant correlation with LS (Fig. 4.5). In general, higher correlations between LS and R-2 metrics were obtained at a low incidence angle (R-2 FQ8) than those at a high incidence angle (R-2 FQ21). Among the backscattering coefficients, σ°_{HV} had the highest correlation with LS ($r = 0.77$) while σ°_{HH} and σ°_{VV} were moderately correlated to LS at a low incidence angle ($0.50 < r < 0.70$) (Fig. 4.5a). On the contrary, at a high incidence angle, σ°_{HV} had a moderate correlation with LS ($r = 0.67$) while with σ°_{HH} and σ°_{VV} , the correlation was not significant (Fig. 4.5b).

Among the polarimetric parameters, Span computed from low incidence angle data resulted in a positive, moderate correlation ($r = 0.54$) with LS. At the same time, CSI had a negative, moderate correlation at high incidence angle ($r = -0.52$) (Fig. 4.5). In both cases, a negative, low correlation was obtained between RFDI values and LS ($r = -0.31$ and -0.34 , respectively). The parameters generated from different decomposition methods had contrasting r values at low and high incidence angle (Fig. 4.5). At low incidence angle, the volume scattering components (such as FD_vol, Yamaguchi_vol) were highly correlated with LS ($r \sim 0.75$ in most cases) while at high incidence angle, double and surface scattering mechanisms had higher correlations (Fig. 4.5). The double bounce scattering components (such as FD_dbl, Yamaguchi_dbl) were negatively correlated while the surface scattering components (such as FD_surf, Yamaguchi_surf) had positive correlations with LS (Fig. 4.5). On the other hand, in the case of S-1 data, the backscattering coefficients were more significantly correlated with LS ($r = 0.65$) than the polarimetric parameters ($r < 0.36$) (Fig. 4.6).

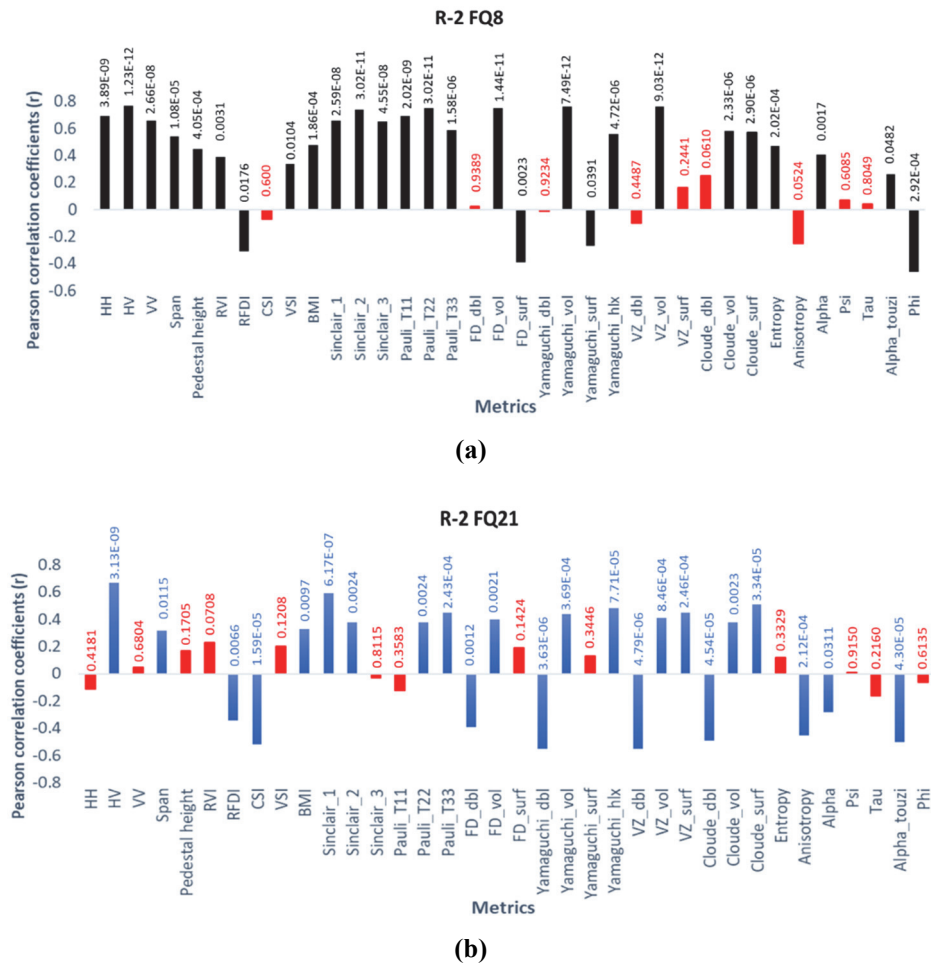


Fig. 4.5. Pearson correlation coefficients (r) between lodging score (LS) and metrics derived from (a) RADARSAT-2 FQ8 ($n=57$) in black and (b) RADARSAT-2 FQ21 ($n=61$) in blue. p -values are indicated at the end of the bars. Metrics with non-significant p -values (at 0.05 level of significance) are marked red.

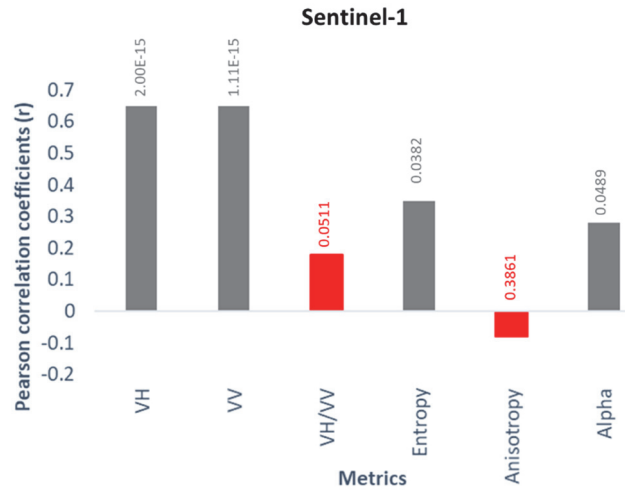
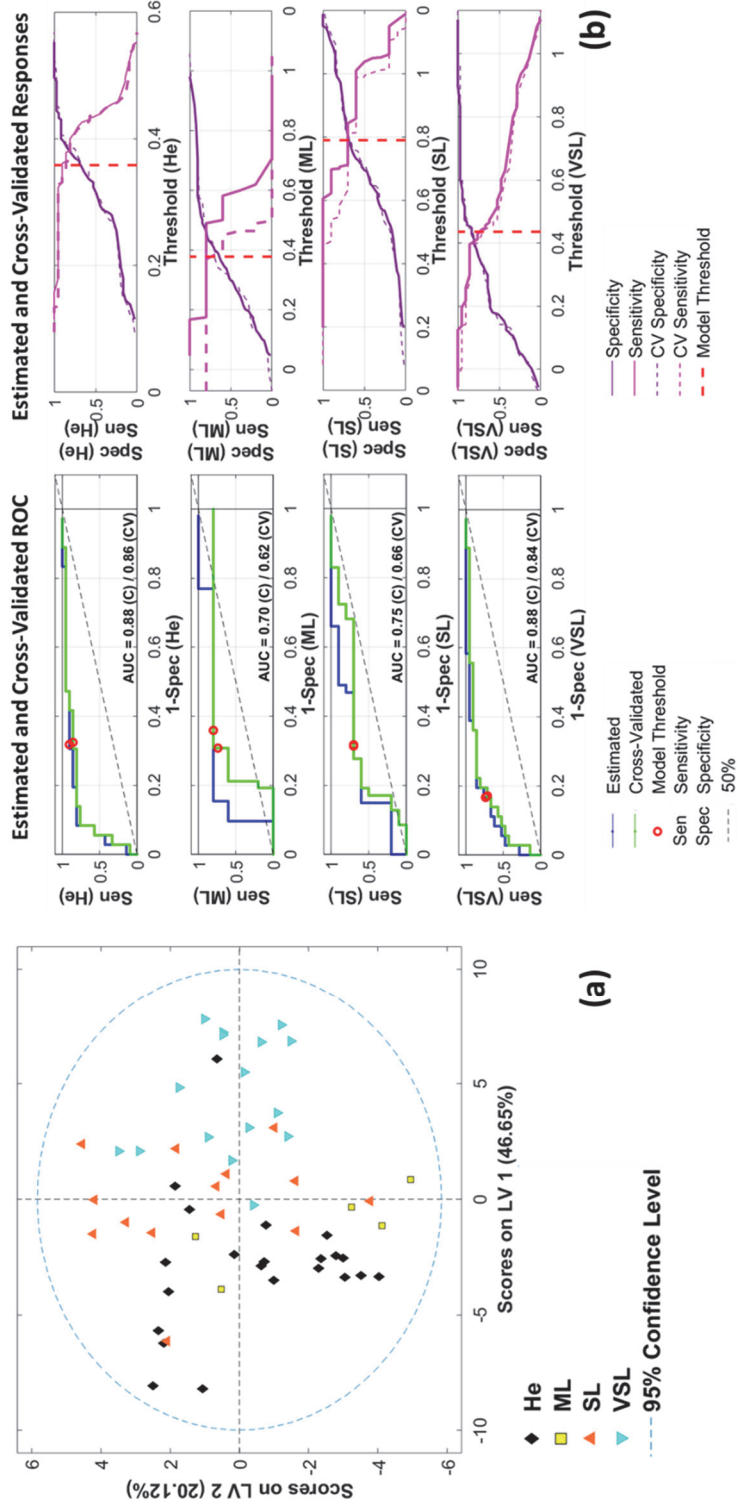


Fig. 4.6. Pearson correlation coefficients (r) between lodging score (LS) and metrics derived from Sentinel-1 ($n=118$) in grey. p -values are indicated at the end of the bars. Metrics with non-significant p -values (at 0.05 level of significance) are marked red.

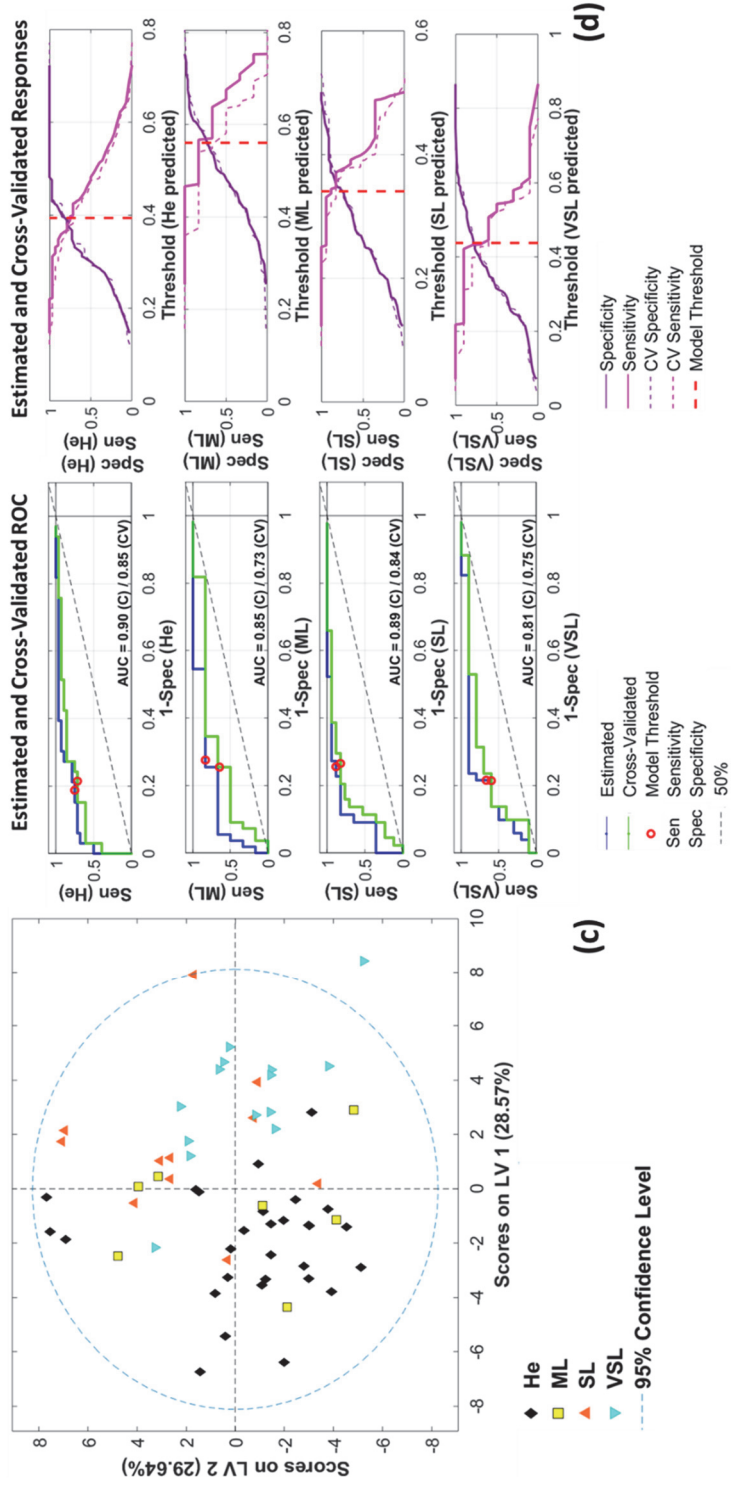
4.3.3 PLS Discriminant analyses (PLS-DA) and accuracy assessment

We used six metrics derived from S-1 data as an input to the model, while for the R-2 data, we used 36 metrics as the input. Fig. 4.7(a, c, e) shows a scatter plot of the classes grouped according to the first two PLS components for R-2 FQ8 (incidence angle 27°), R-2 FQ21 (41°) and S-1 (40°) datasets, respectively. The ellipse surrounds the observations that are within the 95% confidence interval. The sensitivity (true positive rate) and 1-Specificity (false positive rate) as functions of the varying thresholds associated with each class are shown in Fig. 4.7(b, d, f) for different datasets. The graphs present both estimated and cross-validated ROC curves over ten training and test partitions at varying thresholds. If both the sensitivity and specificity at the threshold of x is high, it indicates excellent discrimination power at that threshold. Furthermore, the corresponding cross-validated AUC(CV) are presented in Table 4.2. Generally, the AUCs in the training and test data did not differ much, suggesting little overfitting in the LS classification.

R-2 FQ8



R-2 FQ21



S-1

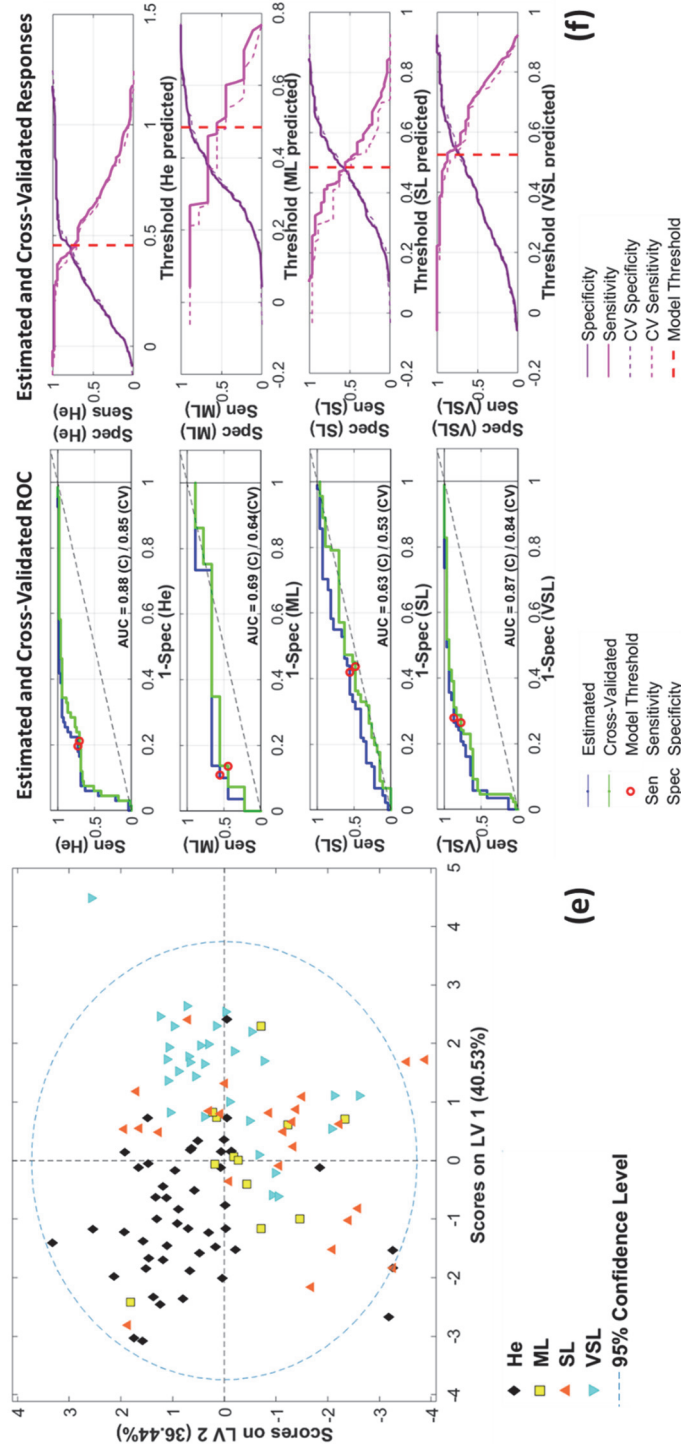


Fig. 4.7. Supervised clustering (left) and estimated and cross-validated AUC-ROC (right) of lodging severity classes using partial least squares discriminant analysis (PLS-DA) with (a), (b) R-2 FQ8 data ($n=57$), (c), (d) R-2 FQ21 data ($n=61$), and (e), (f) S-1 data ($n=118$). He represents healthy samples, ML is moderately lodged, SL is severely lodged, and VSL corresponds to very severely lodged samples. In (a), (c) and (e) the scores of the first two principle components are plotted on the x and y axis. In (b), (d) and (f) AUC-ROC graphs are on the left and the model threshold selection is shown on the right for different severity classes.

Although distinct clusters were not evident for any class, the predictive capability of the models can be ranked roughly as fail ($0.5 < \text{AUC} \leq 0.6$), poor ($0.6 < \text{AUC} \leq 0.7$), fair ($0.7 < \text{AUC} \leq 0.8$), good ($0.8 < \text{AUC} \leq 0.9$) and excellent ($0.9 < \text{AUC} \leq 1.0$) (Swets, 1988). One can note that for the classifier based on He and VSL observations, the predictive capability of the models was “good” and “fair”, respectively in terms of AUC(CV) (Table 4.2). It is apparent that most of the He and VSL samples are distinctly grouped for S-1, R-2 FQ8 and R-2 FQ21, with an AUC(CV) > 0.74 . However, as seen in the scatter plots of Fig. 4.7, there was moderate to extreme mixing among the other lodging severity classes (mainly ML and SL) with the AUC(CV) ranging between 0.53 (fail) to 0.73 (fair), except for the SL class modelled with R-2 FQ21 data (AUC(CV) = 0.84).

The S-1 model classified the ML class with a poor AUC(CV) value (0.64) while the SL class had the lowest separability (Fig. 4.7e). The mixing among the lodging severities (more extreme in ML and SL) is evident in Fig. 4.7e as well. The separability of the SL class enhanced by 25% (Table 4.2) with R-2 FQ8 model (with respect to the S-1 model) while the AUC(CV) for the ML class was comparable to the S-1 model. In contrast, the AUC(CV) values for ML and SL increased considerably by 17% and 26% with the inputs from the R-2 FQ21 model (with respect to the R-2 FQ8 model). The R-2 FQ21 model, however, performed fairly in terms of distinguishing the VSL class from the other classes (AUC(CV) = 0.75) in comparison to the other models (Fig. 4.7c, Table 4.2).

We further assessed the classification accuracy for all the models using confusion/error matrices. We used cross-validated data to construct the standard confusion matrices for each dataset (Table 4.3). We converted the data in each cell of the matrix into percentages by dividing the number of pixels in each cell by the total number of pixels. The percentage figures in the matrix allow a straightforward comparison between the measurements derived from field reference data and the RS-based estimates. While it is apparent that some classes are more reliably classified than others (indicated via PA and UA), the OA and K are used to make quantitative comparisons of different models (Table 4.3).

The first evaluation of the classifier results shows that the ability of PLS-DA to distinguish between He and VSL accurately is consistent across all the datasets. These results are in line with the ROC curves. The S1-based model had the lowest OA of 60% with a K of 0.42, ranging from PA of 22.2% for the SL class to 80.4% for the He class (Table 4.3). We can note that the SL class had the lowest PA

(22.2%) and UA (35.3%). Using the R-2 FQ8 and R-2 FQ21 data, the OA increased by 20% and 10%, with K of 0.60 and 0.49, respectively (Table 4.3). The low PA and UA of the ML class are consistent across all the datasets, with significant mixing with other classes.

Table 4.2. Cross-validated area under the curve (AUC-CV) statistics for four lodging severity classes using Sentinel-1, RADARSAT-2 FQ8 and RADARSAT-2 FQ21 datasets.

Data	He	ML	SL	VSL
S-1	0.85	0.64	0.53	0.84
R-2 FQ8	0.86	0.62	0.66	0.84
R-2 FQ21	0.85	0.73	0.84	0.75

Table 4.3. Cross-validated confusion matrix, comparing reference and RS-based lodging severity classes using Sentinel-1 (He: $n=51$, ML: $n=12$, SL: $n=25$, VSL: $n=30$), RADARSAT-2 FQ8 (He: $n=22$, ML: $n=5$, SL: $n=14$, VSL: $n=16$) and RADARSAT-2 FQ21 (He: $n=29$, ML: $n=7$, SL: $n=11$, VSL: $n=14$) datasets. Figures are in percentages. OA is the overall accuracy and K is the kappa coefficient

		Reference data				
		R-2 FQ8				
Classified data		He	ML	SL	VSL	Sum
	He	31.58	8.77	3.51	0.00	43.86
	ML	1.75	3.51	1.75	0.00	7.02
	SL	5.26	1.75	19.30	1.75	28.07
	VSL	1.75	0.00	1.75	17.54	21.05
	Sum	40.35	14.04	26.32	19.30	100
	PA	78.26	25.00	73.33	90.91	
	UA	72.00	50.00	68.75	83.33	
	OA	72%		K	0.60	

		Reference data				
		R-2 FQ21				
Classified data		He	ML	SL	VSL	Sum
	He	39.34	3.28	1.64	0.00	44.26
	ML	4.92	1.64	3.28	0.00	9.84
	SL	4.92	4.92	13.11	4.92	27.87

	VSL	3.28	1.64	1.64	11.48	18.03
	Sum	52.46	11.48	19.67	16.39	100
	PA	75.00	14.29	66.67	70.00	
	UA	88.89	16.67	47.06	63.64	
	OA	66%		K	0.49	

Reference data							
S-1							
Classified data		He	ML	SL	VSL	Sum	
		He	31.36	0.85	5.93	0.85	38.98
		ML	0.85	4.24	2.54	3.39	11.02
		SL	5.08	0.85	5.08	3.39	14.41
		VSL	5.93	1.69	9.32	18.64	35.59
		Sum	43.22	7.63	22.88	26.27	100
	PA	72.55	55.56	22.22	70.97		
	UA	80.43	38.46	35.29	52.38		
	OA	60%		K	0.42		

Lastly, we applied the PLS-DA models on two R-2 (R-2 FQ21: May 31, R-2 FQ8: June 13) and two S-1 (May 31, June 6) images to map the lodging severity on those dates. We chose the closest acquisition date between R-2 and S-1 images to facilitate comparison. We masked out the non-wheat areas and generated four classified maps, as shown in Fig. 4.8. The four classes correspond to He, ML, SL and VSL categories. The maps indicate that lodging was widespread in the study site with more severely lodged patches in June when the crop was approaching maturity, thus agreeing with the general trends observed during our fieldwork.

As illustrated in Fig. 4.8d, the FQ8 image from June 13 captured the spatial variability in lodging severity most effectively (OA = 72%). Fig. 4.8a and 4.8c show the lodging severity mapped with S-1 and R-2 FQ21 models, respectively for May 31. Table 4.3 and the classified maps reveal that with R-2 FQ21 data, variability in lodging severity is more effectively captured (OA = 66%) in comparison to the S-1 model which overestimated the healthy patches in some areas with an OA of 60%.

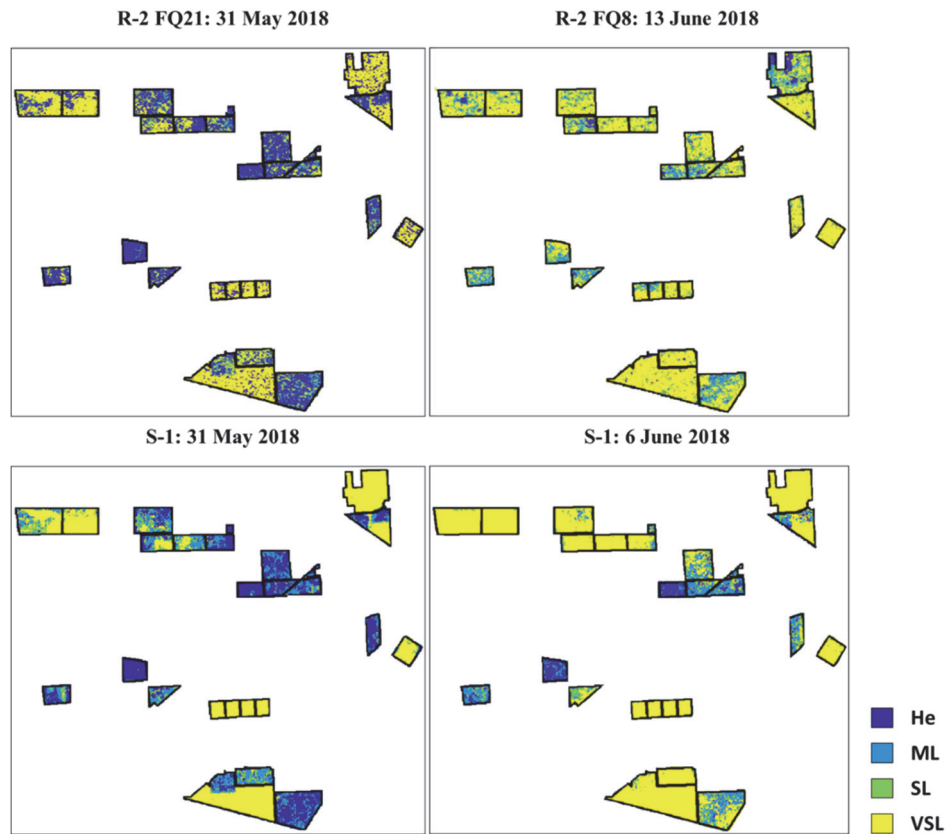


Fig. 4.8. Lodging severity maps generated from (a) Sentinel-1 data acquired on May 31, (b) Sentinel-1 data acquired on June 6, (c) RADARSAT-2 FQ8 data acquired on May 31 and (d) RADARSAT-2 FQ21 data acquired on June 13 using PLS-DA models. He represents healthy samples, ML is moderately lodged, SL is severely lodged, and VSL corresponds to very severely lodged samples. “RADARSAT-2 Data and Products. MacDonald, Dettwiler and Associates Ltd. (2018) – All Rights Reserved. RADARSAT is an official trademark of the Canadian Space Agency.”

4.4 Discussion

In this paper, we presented the first comparative study on lodging severity classification based on lodging score using data from two sensors (R-2 data at different incidence angles and S-1 data). As a part of our preliminary data analysis, we studied the correlation between RS-based metrics and lodging score. We then used the input metrics generated from different SAR configuration satellites separately in a PLS-DA algorithm for classifying the lodging severity based on lodging score. The important findings are discussed below.

4.4.1 General characteristics of the backscattering coefficients and polarimetric parameters with respect to the lodging score

SAR backscattering coefficients are primarily a function of crop structure (such as size, orientation and density of scatterers in the plant) and the dielectric properties of crop canopy as well as underlying soil moisture (particularly at initial phenological stages when the vegetation is scarce and more soil surface is exposed) (Chauhan et al., 2018; Forkuor et al., 2014). The trends vary from crop to crop and change with crop condition. In the study area, healthy wheat grew to its maximum biomass (up to 8.01 t/ha) during May before it reached the milking stage. The intensity of σ°_{HV} at this time was close to -6.4 dB (R-2 FQ8) with an entropy of 0.94 (R-2 FQ8). It has been shown that the interaction of the incident waves with the top leaf layer in this scenario produces more surface/single bounce and double bounce scattering due to the dense canopy structure while random orientation results in volume scattering due to depolarisation (Jiao et al., 2014). By mid-June, wheat reached the senescence stage and the plants were dead and dry. This implies that there are fewer vegetative components available for attenuation. The σ°_{HV} dropped significantly to -12.7 dB (R-2 FQ8) with an entropy of 0.37 (R-2 FQ8) as fresh biomass reduced.

We can also make several insights on the sensitivity of multi-angular data to crop lodging based on the Pearson correlation analysis of backscattering coefficients and polarimetric parameters with LS. The strong correlation (>0.74) of volume scattering components (e.g., σ°_{HV} , Yama_vol, VZ_vol, FD_vol, VSI, entropy) with LS at a low incidence angle indicates that an increase in lodging severity (or LS) leads to an increase in the amount of multiple scattering which causes the signal to depolarise, thus increasing the volume scattering (Fig. 4.5a). On the other hand, a moderate negative correlation of double bounce scattering components at a high incidence angle (R-2 FQ21, Fig. 4.5b) suggests that destruction of the vertical structure of the canopy after lodging results in a decrease in the double bounce scattering from the soil surface and upright stems. This decrease is mainly driven by the CAI component of LS, as also shown by Chauhan et al. (2020b). Contrarily, the positive correlation of surface scattering components with LS at a high incidence angle (R-2 FQ21, Fig. 4.5b) seems to depend on the LA component of LS. As the LS increases or lodging becomes very severe, the crop area is lodged flat on the ground resulting in more surface scattering.

As expected, CSI (ratio of σ°_{VV} and $\sigma^{\circ}_{VV} + \sigma^{\circ}_{HH}$) which is an indicator of the relative importance of vertical versus horizontal vegetation structure (Pope et al., 1994), had a negative correlation with LS ($r = -0.52$) at high incidence angle (Fig. 4.5b). Since σ°_{HH} favours double bounce scattering (Pope et al., 1992), this implies that crop structures dominated by vertical stems (and low double bounce) will lead to higher CSI values. The BMI parameter, which is known to respond to changes in crop biomass, had a moderate correlation with LS at low ($r = 0.48$) and high ($r = 0.33$) incidence angle (Fig. 4.5). Field observations show that the average fresh biomass of He wheat (LS = 0) during the period was 4.42 t/ha, while for lodged wheat, the average fresh biomass was close to 4.98 t/ha (Table 4.1). The moderate correlation can be explained by the small change in the average fresh biomass of lodged wheat. Pedestal height which is characteristic of volume scattering and is directly proportional to vegetation density or the vegetation cover (Evans et al., 1988; McNairn et al., 2002), had a moderate correlation with LS ($r = 0.45$) (Fig. 4.5). At the time of lodging, the vegetation cover increases due to an increase in the LA (Sher et al., 2018). The RFDI index (ratio of $\sigma^{\circ}_{HH} - \sigma^{\circ}_{HV}$ and $\sigma^{\circ}_{HH} + \sigma^{\circ}_{HV}$), on the other hand, decreased with the increase in LS at both low ($r = -0.31$) and high ($r = -0.34$) incidence angle (Fig. 4.5). RFDI assesses the strength of double bounce scattering and decreases with increasing lodging severity since the σ°_{HH} term (in RFDI index) is sensitive to both volume and double bounce scattering (Mitchard et al., 2012) while σ°_{HV} is sensitive to volume scattering.

4.4.2 Performance of PLS-DA models for lodging severity classification

The results of this study demonstrate that the classification of lodging severity (based on LS) using SAR RS data is feasible. We applied the models developed using PLS-DA on two R-2 images with different incidence angles and two S-1 images. Each dataset has varying spatial resolution and a different number of polarimetric channels.

The consistent performance of the PLS-DA algorithm is demonstrated by the class-specific accuracies (Table 4.3). The models classified the He and VSL classes with high PA and UA while there was some degree of mixing in the ML and SL classes (higher in case of S-1 data). The high accuracy of the He and VSL classification can be attributed to the wide separation in the range of the LS values for both classes (0.0 and 0.61-1.0), which correspond to distinct crop structural attributes (e.g. CAI, plant height, etc.) which reduces the probability of erroneous

placements of validation pixels to any other class. However, in the case of ML, our field records show that at least 50% of the healthy crop in ML plots had turned yellow, the plant water content was very low while the lodged patches suffered from a phenological delay. This might have attributed to the confusion between ML and other classes. This observation is, in particular, coherent with the commission error that occurs mainly in the SL class. Considering the level of detail (different lodging severities) and complexity (random and heterogenous lodging distribution) in the lodged crop canopy, the achieved accuracies assured by rigorous cross-validation of PLS-DA models are very promising. AUC-ROC and confusion matrices contributed differently to the accuracy assessment of the classification models. Since the class distribution was skewed in this study, the ROC curve proved to be a better measure of the classification performance. We suggest that in general, AUC values can be considered as a measure to indicate the discriminability between different class pairs while the OA derived from the confusion matrices can be used to evaluate the overall performance of the models.

Overall, the use of low incidence angle R-2 FQ8 data outperformed high incidence angle R-2 FQ21 and S-1 data for classifying lodging severity. This ranking of performance can be explained as follows. Microwave scattering from a crop canopy is dependent on many sensor parameters such as SAR wavelength, polarisation and incidence angle (Soria-Ruiz et al., 2009). Besides, the spatial resolution and radiometric quality of the data also affects the backscatter signal (Bovenga et al., 2018). This can result in the contribution of different and/but complementary information. Although both S-1 and R-2 (FQ8/FQ21) sensors operate at C-band, differences in other characteristics such as polarisation (dual and quad-pol), incidence angle (40° and $27^\circ/41^\circ$), radiometric accuracy (1 dB and <1 dB) and spatial resolution (15×15 m and 10×10 m/ 7×7 m) resulted in better performance of R-2 data. The higher accuracy of R-2 FQ8 model contrary to that of R-2 FQ21 indicates that the incidence angle has a higher impact on lodging detection than spatial resolution of the radar image.

In this study, we tested a new approach to map lodging severity with both commercial and freely available satellite imagery. S-1 data shows potential for crop lodging monitoring at the global, national and regional scales. The unprecedented availability of dense time-series of SAR data with a high spatial resolution with no acquisition costs presents a new opportunity for operational assessment of lodging severity in NRT. This potential was not explored to date. A key question is a degree to which the high temporal observation density of S-

1 dual-polarised SAR data can compensate for the lower sensitivity to detect lodging severity when compared to quad-polarimetric R-2 SAR data. Our results show that relatively small but abundant changes in crop lodging condition, such as changes in moderately or severely lodged areas, could not be detected by S-1 as efficiently as R-2 FQ8 data. The R-2 FQ8 data (with higher spatial resolution, higher range of incidence angles with more polarimetric information) quantified and mapped these changes at a fine spatial resolution.

Furthermore, the classified maps (Fig. 4.8) can serve as a valuable baseline for evaluating the utility of SAR data for mapping lodging severity in wheat. The identification of lodging severities within agricultural fields can be used by the farmers or insurance adjusters to support insurance claims, can contribute to in-field navigation routes to minimise harvesting losses and deliver accurate crop lodging inventories with consistency and reliability. Studies also show that an accurate assessment of LS can enable prediction of lodging-induced yield losses (Xiao et al., 2015). If the number of days that the crop has been lodged is known, LS can be multiplied with this number to get the lodging duration. Yield is estimated to reduce by 1% for every two days of lodging duration in the milking stage (Stapper et al., 2007).

Future efforts can be aimed at improving the overall accuracy of classifying lodging severity based on LS with the following points in mind. We believe that the simplicity of our approach for measuring the crop lodged area visually in the field (quadrant method) could have been a potential cause of error due to factors such as omission and misstatement. A more robust and objective methodology might be needed to get better estimates of the lodged area in the plot size as big as 60×60 m. Secondly, the backscatter recorded by a radar system contains information about dielectric properties and geometrical structure of the crop, which makes it challenging to interpret SAR images (Xu et al., 2012). Moreover, being a coherent measuring system, the signal received by the radar system is affected by high coherent noise (speckle), which degrades image quality, reducing the classification accuracy (Gallego et al., 2008; Wang et al., 2015). The substantial spatial heterogeneity caused by the random distribution of lodged patches further aggravates the problem as there are chances of the noise being misinterpreted as crop lodging. It is also possible that the speckle filtering operations might result in loss of information related to spatial heterogeneities caused by lodging.

Model accuracy could be further improved by combining SAR and optical data (especially hyperspectral observations) in a multi-sensor approach, to account for risks associated with adverse atmospheric conditions and ensure continuity of data acquisition (Kussul et al., 2013; McNairn et al., 2009). For instance, McNairn et al. (2009) integrated SAR and optical data in a decision tree, neural network and supervised Gaussian Maximum-Likelihood Classifier (MLC) for crop classification. The study showed that the overall accuracies increased with MLC for SAR-optical classification, especially when limited optical images are available. The almost daily availability of Capella, ICEYE and RADARSAT Constellation Mission (RCM) SAR data and high temporal resolution of EnMap and PRISMA (in combination with all available sets of Sentinel-1 and Sentinel-2 images) will help to overcome the problem of the image gap.

While there have been a few studies that have utilised surface reflectance from airborne optical sensors to produce crop lodged area estimates (Sun et al., 2019), there is no research on the use of SAR data for the same. For instance, a study by Liu et al. (2018) has shown that incorporation of structure, texture and thermal information from time-series optical data can result in higher accuracy of crop lodged area estimation with R^2 values greater than 0.90. In another study, Wilke et al. (2019) reported the R^2 of 0.96 (RMSE=7.66%) while estimating crop lodged area based on RGB images with a slight overestimation of 2%. The authors used differentiated canopy height variations to determine thresholds to detect lodged areas. Unfortunately, these estimates are available for only very fine spatial resolution data (in the order of a few centimetres) and limited surface area (1-2 ha) as acquired from aerial platforms such as UAVs. Data from the EO satellites can play an important role in delivering this information over large geographic areas at relatively low cost. There are no studies employing data (optical and SAR) from satellite-based platforms for quantitative estimation of crop LA. Nevertheless, there is no shortage of research on large scale crop area estimates mainly based on the spectral theory of green plants from coarse resolution MODIS data (Potgieter et al., 2013) to high-resolution Landsat-5/TM and RapidEye data (Gallego et al., 2014), which can be used as a reference for building algorithms for retrieving lodged area estimates.

In our study, the temporal offset between the satellite images and the ground reference data ranged from 0-4 days, and therefore, this may also represent a potential error source. Another thing to note here is that the S-1 and R-2 FQ8 images were acquired in the ascending pass (evening time) while due to user

conflicts and acquisition constraints, R-2 FQ21 data was obtained in the descending pass (morning time). Thus, while the effect of early morning dew on the backscatter was non-existent in the former case, it might have been a potential source of error in the latter case. Nonetheless, Wood et al. (2002) suggest that the presence of dew can cause an absolute increase in the backscatter. Still, the relative differences remain similar due to a high correlation between the backscatter of ascending and descending orbits.

Overall, our work opens up a new avenue for research to explore the use of RS-based information for crop lodging. This has the potential for tactical and strategic applications to help manage and mitigate crop lodging, which is a major yield-reducing factor in cereal crops cultivation.

4.5 Conclusions

Existing information on lodging severity is scarce, which limits actions to address this important yield-limiting factor. Satellite-based RS data allows monitoring of the status and variation in crop condition during the growing season. In particular, microwave data can capture information related to structural and dielectric plant properties. The assessment of crop lodging is nevertheless challenging due to the unavailability of frequent microwave data at high spatial resolution. To the best of our knowledge, this study represents the first attempt to compare the performance of high-resolution satellite data acquired from different sensors to assess lodging severity using a quantitative crop lodging score.

We presented a discriminant analysis approach that integrated a partial least squares method (PLS-DA) and metrics derived from satellite data to distinguish between different lodging severities (He, ML, SL and VSL). We assessed the accuracy of the cross-validated models for each dataset using AUC-ROC and confusion matrices and applied them to classify and map lodging severity.

Our results show that at low incidence angle (R-2 FQ8), volume scattering components had a higher correlation with LS ($r \sim 0.75$ in most cases). In contrast, double bounce and surface scattering were more prominent at high incidence angle (R-2 FQ21). The polarimetric parameters such as CSI, BMI, pedestal height and RFDI had a moderate correlation with LS. Among the applied models, the low incidence angle R-2 FQ8 (27°) model discriminated different class pairs with the highest AUC and resulted in the highest OA and Kappa (72% and 0.60, respectively) values. The performance of S-1 (40°) and R-2 FQ21 (41°) were

comparable with OAs of 60% and 66% respectively. High PA and UA for He and VSL classes were consistent across the three datasets while there was considerable mixing between the ML and SL classes. These results are important in the context of operational crop lodging assessment in particular, and sustainable agriculture in general.

Chapter-5

Understanding wheat lodging using time-series Sentinel-1 and Sentinel-2 data*

*This chapter is based on:

Chauhan, S., Darvishzadeh, R., Lu, Y., Boschetti, M., & Nelson, A. (2020c). Understanding wheat lodging using multi-temporal Sentinel-1 and Sentinel-2 data. *Remote Sensing of Environment*, 243, 111804.

<https://doi.org/10.1016/j.rse.2020.111804>

Chauhan, S., Darvishzadeh, R., Lu, Y., Stroppiana, D., Boschetti, M., Pepe, M., & Nelson, A. (2019b). Wheat lodging assessment using multispectral UAV data. *ISPRS - International Archives of the Photogrammetry, Remote Sensing and Spatial Information Sciences*, XLII-2/W13, 235–240. <https://www.int-arch-photogramm-remote-sens-spatial-inf-sci.net/XLII-2-W13/235/2019>

Abstract

Identifying the time of crop lodging incidence is essential for facilitating crop pricing and informing crop management decisions for sustainable agricultural production. While a few studies have demonstrated the potential of optical and SAR data for crop lodging assessment in general, large-scale identification of the time of lodging incidence in wheat has been hampered by the unavailability of dense satellite time-series data. The unprecedented availability of free Sentinel-1 and Sentinel-2 data may provide a basis for operational detection and monitoring of crop lodging. In this context, this study aims to investigate the potential of time-series Sentinel-1 and Sentinel-2 data for identifying the time of lodging incidence in wheat and understanding the effect of lodging on the remote sensing signal. We measured the crop biophysical parameters in the field for both healthy and lodged plots from March to June 2018 in a study site in Ferrara, Italy, and processed the corresponding Sentinel images. We further categorised the lodged plots into different lodging severity classes (moderate, severe and very severe) based on lodging score. We studied the temporal profiles of backscatter, coherence, reflectance and continuum removed spectra for healthy and lodging severity classes throughout the stem elongation to ripening phenological stages. We used Kruskal Wallis and posthoc Tukey tests to analyse if there were significant differences between different classes. Our results showed that red edge (740 nm), NIR (865 nm) and the VH backscatter could best distinguish healthy from lodged wheat. In contrast, VV and VH/VV backscatter were complementary in distinguishing the maximum number of classes. Moreover, with the time-series analysis of Sentinel-1 and Sentinel-2 data, it was possible to indicate a plausible window of the main lodging event, thus demonstrating the potential of Sentinel data for near real-time identification of the time of lodging incidence and severity of lodging in wheat. To the best of our knowledge, no study has contributed to this application.

5.1 Introduction

Lodging, defined as the permanent displacement of plant shoots from their upright position (stem lodging) or destruction of the root anchorage (root lodging), is a major yield-limiting factor in cereal crops, including wheat (Zhang et al., 2017). Apart from reducing grain yield (Fischer and Stapper, 1987; Tripathi et al., 2005), lodging can cause several knock-on effects such as increased drying costs, deterioration of grain quality and slowed harvest (Berry et al., 2004). Accurate and timely detection of crop lodging can help farmers improve crop yield forecasts, guide harvest operations and contribute to optimum crop pricing (Ceballos et al., 2019; Shah et al., 2017). Field-based approaches – that use visual inspection- are the most common methods to assess lodging and detect the time of its incidence (Chauhan et al., 2019a), but are infeasible for areas larger than a few hundred hectares. Moreover, the accuracy of these methods is subjective to the skill, experience and consistency of the observer (Bock et al., 2010). RS offers a more cost-effective and scalable approach (Yang et al., 2015).

Only a few studies have explored the use of optical and SAR data for crop lodging assessment. For instance, Ogden et al. (2002) and Liu et al. (2014) used airborne optical data to investigate the role of spectral and textural information to measure the extent of lodging and improve lodging classification accuracy. Chauhan et al. (2019b) analysed the spectral variability between different lodging stages using high-resolution multispectral data acquired by UAVs. However, to date, no study has utilised satellite-based optical time-series data to identify the time of lodging incidence and its severity.

The earliest works that used SAR data for lodging assessment can be traced back to the works of Bouman and van Kasteren (1990b) and Bouman (1991b). They analysed the temporal backscatter trends of X-band scatterometer data to study lodging-induced changes in wheat. In a recent study, Shu et al. (2019) investigated the potential of Sentinel-1 satellite data for quantitative assessment of maize lodging. The results showed that the VH/VV ratio was sensitive to non-lodged maize, while VV backscatter was sensitive to lodged maize. A few studies have also demonstrated the ability of polarimetric SAR to distinguish lodged and healthy areas (Chen et al., 2016; Yang et al., 2015; Zhao et al., 2017). For instance, Chauhan et al. (2020b) explored the potential of Sentinel-1 and RADARSAT-2 SAR data for estimating crop angle of inclination (CAI) as a measure of lodging stage in wheat. The study highlighted the importance of Sentinel-1 time series data, in the context of the operational assessment of CAI-

based lodging stage, as it could explain 78% of the variability in CAI. These studies have primarily focused on the detection, classification and quantitative assessment of lodging; however, large-scale identification of the time of crop lodging incidence has been hindered by the lack of high spatial resolution dense time-series SAR data. The analysis of dense time-series satellite data may further improve our understanding of how lodging affects spectral and backscatter signals from the crop canopy and how RS data can be used to identify the time of lodging incidence.

Identifying the time of lodging incidence and its severity from RS is challenging due to a combination of factors such as the unavailability of low-cost, high spatio-temporal resolution data and the absence of a standard scale to represent lodging. Moreover, collecting field data related to lodging damage can be a daunting task due to its heterogeneous distribution within and across fields. The Sentinel-1 and Sentinel-2 missions provide fine spatial resolution imagery with revisit times that offer an unprecedented capacity for land surface monitoring applications such as identifying the time of lodging incidence. In this context, the main objectives of this study are to assess the capability of Sentinel-1 and Sentinel-2 time series data for detecting when lodging occurs in wheat and understanding the change in backscatter/coherence and reflectance spectra due to lodging. Our study benefits from measurements performed in actual lodged field conditions.

5.2 Materials and methods

5.2.1 In situ measurements

We identified 76 plots (Fig. 5.1), each measuring 60×60m, based on a stratified random sampling and the wheat planting plans of the farm. Several cultivars of winter wheat were planted in 600 of the 3,850 hectares: Altamira, Bologna, Claudio, Giorgione, Marco Aurelio, Massimo Meridio, Monastir, Odisseo, PR22D66, Rebelde and Senatore Capelli. We collected field data from each plot between March 14 and the end of June 2018 when the crop was harvested. Each plot was revisited three times during this period, resulting in 228 samples. Five important phenological stages were covered during this period: stem elongation, booting, flowering, milking and ripening. The first few instances of lodging were recorded towards the end of the booting stage.

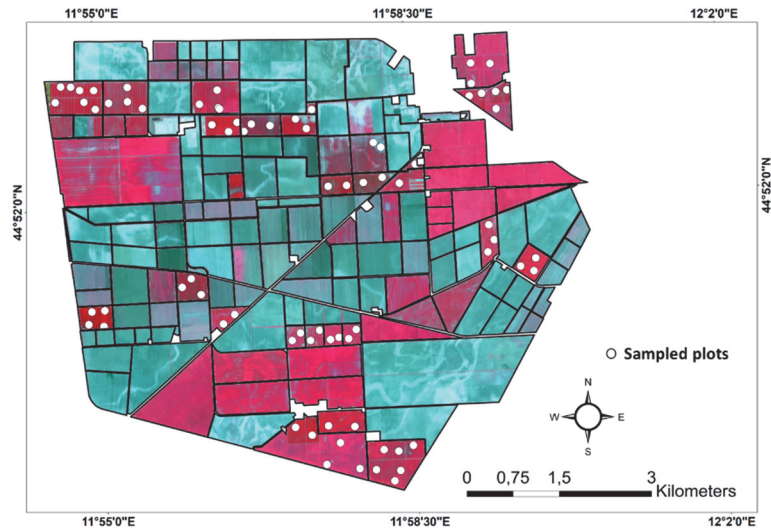


Fig. 5.1. A false-colour RGB composite of a Sentinel-2 scene acquired on April 19, 2018 containing the study area (Bonifiche Ferraresi farm) overlaid with the sampling points (white dots) over the wheat fields and the farm boundary (black outline).

We measured the crop angle of inclination from the vertical (CAI, [0-90°]) and lodged area (LA [0-100%]) in each plot to determine if the plot was healthy (He) or lodged. We measured CAI from the vertical using a plumb bob, a measuring tape and trigonometric calculations (Chauhan et al., 2020a). We suspended the string of the plumb bob from the top of the plant head such that the tip of the plumb bob just touched the ground, ensuring accurate measurement of the vertical height (h_v) (Fig. 5.2). For lodged plants, we used a measuring tape to measure the slant height (h_{sl}). We then calculated CAI from the vertical using the measurements shown in Fig. 5.2 and in equation 5.1.

We also visually assessed LA using a quadrant method (Chauhan et al., 2020b). From the centre of each plot, we visually assessed the percentage of LA in each of the four quadrants (Fig. 5.3b) and averaged them to obtain a representative LA for the plot. A scenario is illustrated in Fig. 5.3 for a lodged plot, depicting the distribution of lodged and He subplots. In He plots, we carried out the crop biophysical measurements in three subplots (2×2m) while in lodged plots, we increased the number of subplots to 4-8 (depending on the LA) to account for the spatial heterogeneity of lodged patches.

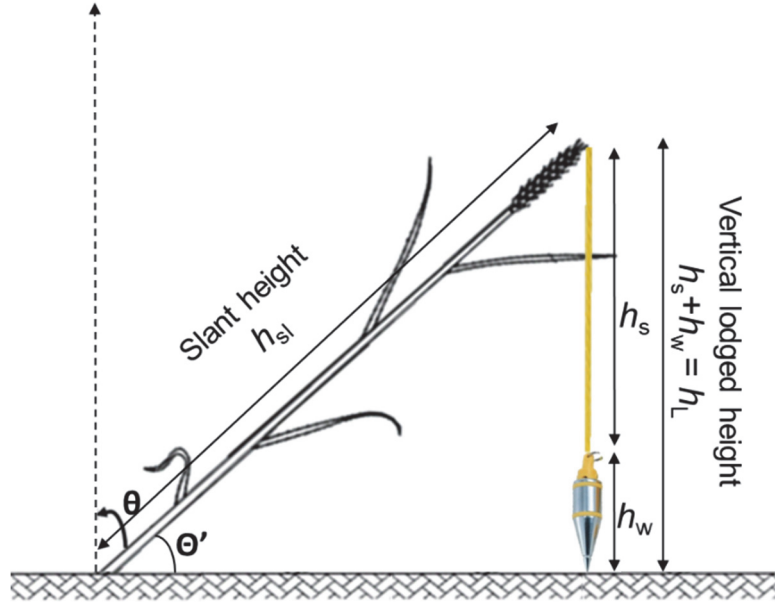


Fig. 5.2. Measurement technique for crop angle of inclination using a vertical plumbob (Chauhan et al., 2020a). θ and θ' is the crop angle of inclination (CAI) with respect to the vertical and soil surface, respectively. h_s and h_w is the height of the string and the heavyweight at the bottom of the plumbob, respectively, h_L ($h_s + h_w$) is the total vertical height of the lodged plant, h_{sl} is the slant height of the plant measured from the soil surface to the tip of the head of the longest tiller with a measuring tape (θ)

$$\theta \text{ (degree)} = 90^\circ - \sin^{-1} \frac{h_L}{h_{sl}} \quad (5.1)$$

We then calculated a normalised lodging score index (LS, [0-1]) combining CAI and LA to define healthy and lodging severity classes (equation 5.2) as also mentioned in Chauhan et al. (2020b). If no lodging was observed within a plot, then we labelled the plot as He (LS = 0.0, $n=160$). In the event of lodging, the plots were categorised as moderately lodged (ML) ($0.0 < LS \leq 0.30$, $n=12$), severely lodged (SL) ($0.31 < LS \leq 0.60$, $n=25$) and very severely lodged (VSL) ($0.61 < LS \leq 1.0$, $n=31$). The summary statistics of these parameters are shown in Table 5.1.

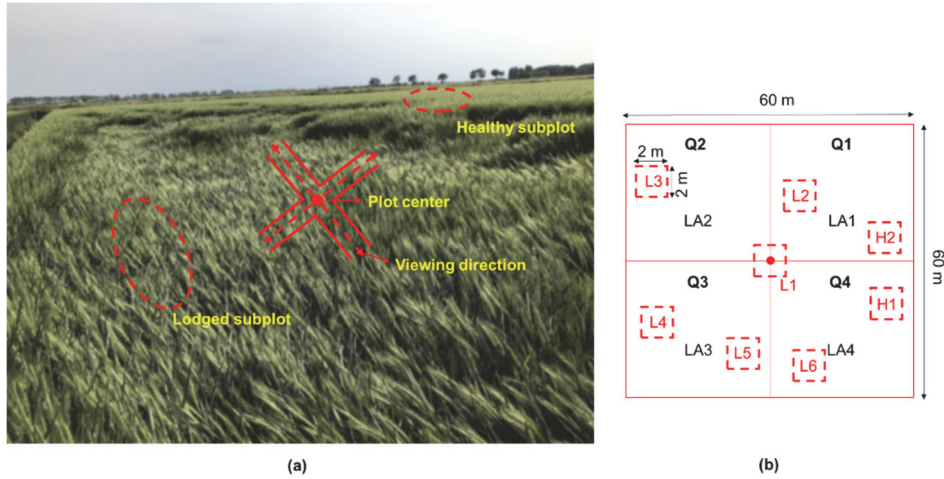


Fig. 5.3. (a) Illustration of lodged/healthy subplots and the plot centre in real field conditions (b) Division of the plot into four quadrants Q1, Q2, Q3 and Q4. LA1, LA2, LA3 and LA4 correspond to the lodged area in each quadrant. In this scenario, L1, L2, ..., L6 represent the lodged subplots while H1 and H2 are the healthy subplots. The CAI is calculated by averaging the sampled CAI and LA estimated in the six lodged subplots and in each quadrant, respectively.

$$LS = \frac{LA\%}{100} * \frac{CAI}{90^\circ} \quad (5.2)$$

Table 5.1. Summary statistics of measured CAI, LA and LS for all samples (healthy ($n=160$) and lodged ($n=68$)) throughout the stem elongation to ripening phenological stages. *COV* is the coefficient of variation.

Parameter	Mean	Min.	Max.	Std. Dev.	COV
CAI (°)	17.33	1.00	79.50	25.83	1.49
LA%	25.53	0.00	100.00	40.83	1.60
LS	0.162	0.00	0.88	0.28	1.76

We also collected other biophysical parameters such as plant height, leaf area index (LAI), mean leaf angle (MLA), SPAD readings, fresh/dry biomass (FB/DB), plant water content (PWC) and soil moisture and obtained meteorological data (daily-cumulated rainfall and windspeed) from a local automatic weather station (located at 44°51'22.9"N, 11°57'51.0"E) to facilitate interpretation of the results. The summary statistics of these parameters are shown in Table 5.2. We measured the LAI non-destructively using an LAI-2200 Plant Canopy Analyser. In each subplot, we made two above-canopy and six below-

canopy radiation measurements using a view restrictor of 45° with the sun behind the operator and then we averaged the readings from the subplots. We also made chlorophyll measurements using a SPAD-502, which measures the transmittance in the red (650 nm) and NIR (920 nm) regions. We took readings from 10 leaves; representing the dominant crop state in each subplot and averaged them. We measured average soil moisture using a calibrated Stevens Hydra Probe. For measuring biomass, we destructively sampled the plants in each subplot (0.2×0.2 m²). We placed the samples in a zip-locked plastic bag, transported them to the on-farm laboratory and processed them on the day of collection. We measured the FB using a high-precision digital scale. We then dried the samples in the oven for 72 hours at 60°C and weighed the DB.

5.2.2 Remote sensing data acquisition and pre-processing

We acquired a set of 19 Sentinel-1 (A/B) and eight Sentinel-2 (A/B) images over the study area between March 14 (day of the year or DoY 73) and June 30, 2018 (DoY 181) (Fig. 5.4). The Sentinel-1 (hereafter referred to as S-1) images were acquired in Interferometric Wide swath dual-polarisation (VV and VH) mode from the Copernicus Open Access (COA) Hub of the European Space Agency (ESA, 2015). We obtained both ground range detected (GRD) and single look complex (SLC) formats to extract backscatter intensity (σ^0) and interferometric coherence (μ^0) respectively.

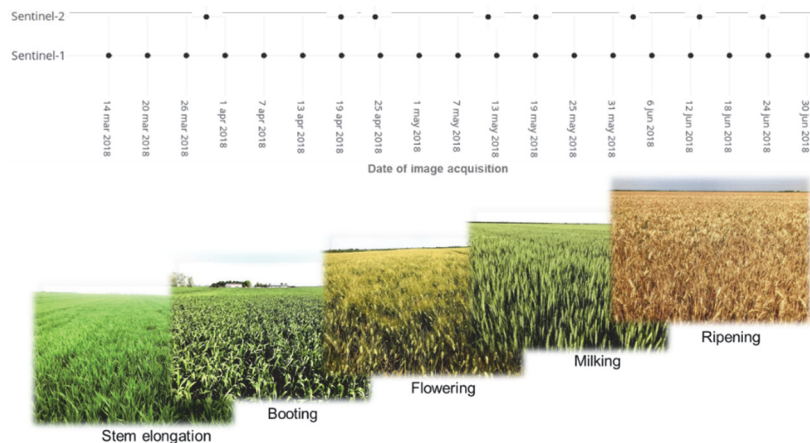


Fig. 5.4. Acquisition dates of Sentinel-1 and Sentinel-2 data during the 2018 wheat growing season.

Table 5.2. Summary statistics of measured soil moisture and biophysical/biochemical parameters in healthy ($n=160$) and lodged samples ($n=68$) throughout the stem elongation to ripening growth stages. COV is the coefficient of variation. *The statistics for soil moisture exclude the readings from fully saturated plots.

Parameter	Mean		Min.		Max.		Std. Dev.		COV	
	He	L	He	L	He	L	He	L	He	L
LAI	3.18	3.02	0.695	1.20	6.54	6.58	1.36	1.22	0.43	0.41
MLA (°)	35.74	46.93	18.00	27.00	50.00	60.00	4.87	6.14	0.09	0.14
CAI (°)	2.69	50.85	1.00	9.36	5.00	79.50	1.75	18.64	0.65	0.37
SPAD	40.62	24.98	5.00	2.50	51.00	47.80	7.84	13.80	0.19	0.57
FB (t/ha)	3.27	4.99	1.09	1.23	8.01	12.85	1.78	2.19	0.55	0.44
DB (t/ha)	0.72	2.06	0.10	0.26	2.10	5.30	0.51	0.84	0.72	0.41
PWC (%)	77.86	55.15	26.19	13.37	95.86	82.22	12.83	15.75	0.17	0.29
Crop height (m)	0.58	0.50	0.16	0.18	1.22	0.94	0.28	0.20	0.47	0.40
Soil moisture* (%)	42.50	42.56	22.00	22.00	83.00	69.00	9.40	10.88	0.22	0.26

Studies reveal that early morning dew can increase the backscatter from a crop and hence should be considered when extracting quantitative crop information from SAR imagery (Wood et al., 2002). To address this, we selected the S-1 images only from the ascending (ASC) pass (acquired at approximately 5:00 PM local time). Other satellite specifications are shown in Table 5.3.

For GRD image pre-processing, we first updated the orbit information of the images and then co-registered and geocoded them in SARscape 5.5 using the approach outlined in Nelson et al. (2014b) to get normalised σ^o values (in dB). For the SLC products, we used the coherence change detection (CCD) processing chain of SARscape to produce geocoded coherence maps. The interferometric coherence (μ^o) ranging from 0-1 (1 being perfect coherence), is the amplitude of the complex correlation coefficient between two SAR images (s_1 and s_2) and is mathematically defined as:

$$\mu^o = \frac{|(s_1 s_2^*)|}{\sqrt{\langle (s_1 s_1^*) \rangle \langle (s_2 s_2^*) \rangle}} \quad (5.3)$$

where s^* is the complex conjugate of s ; and $\langle \rangle$ is the ensemble average (Touzi et al., 1999). We calculated μ^o ($\mu^{o_{VV}}$ and $\mu^{o_{VH}}$) between every adjacent image pair (e.g. date-1, date-2; date-2, date-3; ...; date-n-1, date-n) to achieve the lowest temporal baseline (i.e. six days).

Table 5.3. Satellite specifications for Sentinel-1 data. Note that the range of the incidence angle is specific to the location of the study site within the swath.

Parameter	Specification
Wavelength	C-band
Frequency	5.405 GHz
Product type	GRD, SLC
Acquisition mode	IW
Incidence angle	39.7-40.4°
Pass	ASC
Polarisation	VH, VV
Spatial resolution (resampled)	15m
Repeat cycle	6 days
No. of looks (range× azimuth)	7×1

We obtained standard Sentinel-2 (hereafter referred to as S-2) Level-2A products in UTM/WGS84 projection with bottom of atmosphere (BOA) reflectance from COA hub. The S-2 Multispectral Imager (MSI) has 13 spectral bands in the

visible (VIS), red edge, NIR and SWIR domains. Table 5.4 provides an overview of the 13 bands. Pre-processing of the S-2 spectral data included eliminating B1, B9 and B10 since they were not relevant for this work and resampling of the bands to 10 m in SNAP toolbox 5.0.

Table 5.4. Specifications of the Multi-Spectral Imager (MSI) onboard the Sentinel-2 satellite.

Spectral band	Centre wavelength (nm)	Bandwidth (nm)	Spatial resolution (m)
B1 Coastal aerosol	443	20	60
B2 Blue	490	65	10
B3 Green	560	35	10
B4 Red	665	30	10
B5 Red edge1 (RE1)	705	15	20
B6 Red edge2 (RE2)	740	15	20
B7 Red edge3 (RE3)	783	20	20
B8 NIR1	842	115	10
B8a NIR2	865	20	20
B9 Water vapor	940	20	60
B10 SWIR Cirrus	1375	30	60
B11 SWIR1	1610	90	20
B12 SWIR2	2190	180	20

For the lodged field samples, we selected the images that were available on the same date or immediately after the field observation date (not earlier, since lodging may not have happened). For the healthy samples, we selected the images which belonged to the same or earlier than the field observation time (not later since lodging may have happened). In our study, we could acquire only eight cloud-free S-2 images (as opposed to 19 Sentinel-1 images) available during the observation period. Thus, only 120 samples could be used for the spectral analysis of S-2 data while for S-1 data, all samples ($n=228$) were analysed.

5.2.3 Data analysis

For every plot, we extracted the mean σ^o , μ^o and reflectance values from S-1 and S-2 images and grouped them based on their lodging score. We performed the following time-series analysis from S-1 and S-2 data to understand the difference between He and lodged wheat plots and possibly detect the incidence of initial lodging event.

Using S-2 data, we first studied the influence of phenological stage and cultivar differences on the reflectance spectra and the continuum removed spectra of only He plots. We then analysed the reflectance spectra and the continuum removed spectra of He in comparison to other lodging severity classes for two scenarios: from stem elongation to ripening stage (i.e. for the entire observation period) and at the milking phenological stage (i.e. for a specific phenological stage). We tested the second scenario to disentangle the effect of the crop growth on the spectral curve from the lodging effect. Continuum removal normalises the reflectance spectra to a common baseline by fitting a convex hull over the top of the spectrum so that individual absorption features can be compared (Kokaly and Clark, 1999). The reflectance at a particular wavelength is divided by the values of the hull at that wavelength, giving a relative absorption value between 0 and 1 (Clark and Roush, 1984). We also calculated the absorption band depth (BD) at each wavelength by subtracting one from the continuum-removed value and used this to compare the difference between *He* and lodging severity classes. Similarly, for S-1, we generated five metrics (σ°_{VV} , σ°_{VH} , $\sigma^{\circ}_{VH/VV}$, μ°_{VH} and μ°_{VV}) and analysed the time-series for *He* and other lodging severity classes for the two scenarios.

We used the Kruskal Wallis rank-sum test (Kruskal and Wallis, 1952) to assess the statistical differences of the sample means among the lodging classes. This test is particularly useful for comparing statistical differences among more than two groups (four in our case) with respect to a dependent variable (MacFarland and Yates, 2016). We then used a post hoc Tukey's Honest Significant Difference (HSD) test to find significant pairwise differences among the classes. Tukey's HSD (equation 5.4) compares all possible pairs of group's means with each other to find out which specific group means are different.

$$HSD = \frac{M_i - M_j}{\sqrt{\frac{MS_w}{n_h}}} \quad (5.4)$$

where $M_i - M_j$ is the difference between the pair of means given $M_i > M_j$; MS_w is the mean square within and n is the number of groups.

5.3 Results and Discussion

5.3.1 Spectral analysis from Sentinel-2 data

5.3.1.1 Influence of phenological stage and cultivar differences on the spectra of healthy wheat

The average spectral profile and continuum removed spectra of *He* plots are shown in Fig. 5.5a and 5.5b, respectively. The lowest reflectance values in the NIR spectral region were observed in the early vegetative stage (stem elongation), where LAI (2.2) and FB (stems and leaves) were low (1.69 t/ha) and soil had a dominant effect on the reflectance. With the increase in FB and LAI to 3.62 t/ha and 3.78, respectively in the booting stage, the NIR reflectance also increased (which is related to an increase in leaf intercellular spaces and change of the dry leaf mass). The highest absorption peak at ~665 nm also characterised the booting stage (Fig. 5.5b) (BD = 0.83), which could correspond to the presence of high chlorophyll content (SPAD = 44.58). Maximum reflectance in the NIR was observed in the flowering stage, which is coincident with the highest average values of LAI (5.23) and peak FB values (3.9 t/ha) (composed of stems, leaves and heads). In the NIR region, the reflectance decreased due to the probable increase in the number of senescent leaves which causes the mesophyll structure to collapse into more compact horizontal layers (Bunnik, 1978). As the crop approached maturity, the crop reflectance spectra lost the typical vegetation features with a continuous increase in the VIS range similar to that of soil. During ripening, as the plants began to senesce, the chlorophyll concentration (SPAD = 24.24) along with moisture content declined (PWC = 49.50%), which might have increased the reflectance in visible (pigment reduction) and SWIR (drying processes) regions (Fig. 5.5a). The absorption peaks in the entire spectrum were almost non-existent (maximum BD = 0.07) (Fig. 5.5a). These results are consistent with the observations made by Leamer et al. (1980), Miglani et al. (2011), Sun et al. (2010) and Xavier et al. (2006).

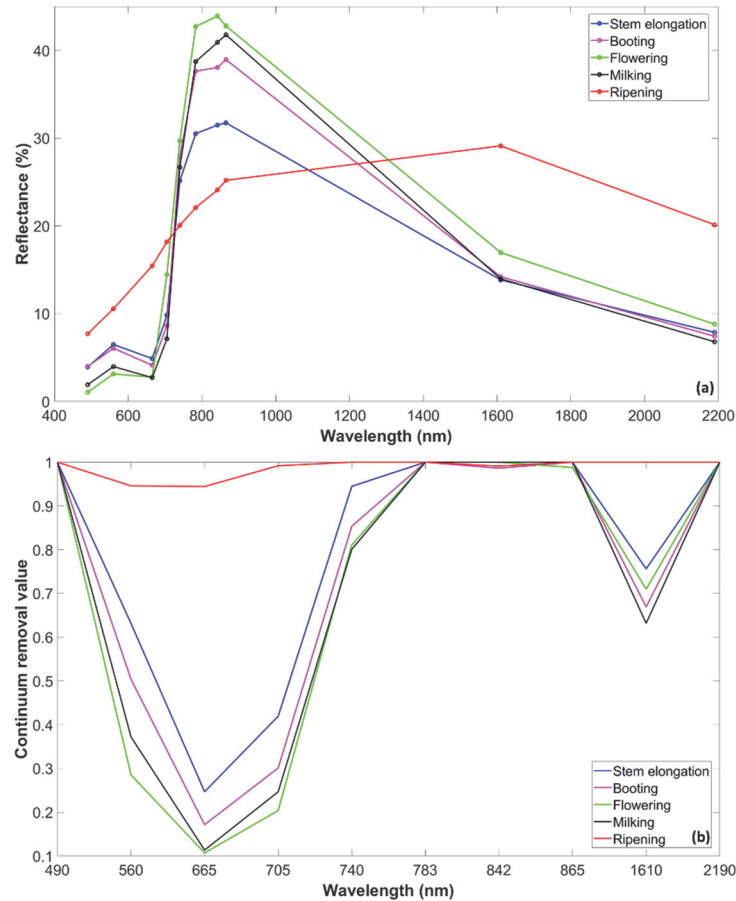


Fig. 5.5. (a) Average spectral reflectance variation and (b) continuum removed spectra for healthy wheat plots at the stem elongation (n=15), booting (n=15), flowering (n=5), milking (n=15) and ripening (n=9) phenological stages.

Fig. 5.6a and 5.6b show the average spectral reflectance and the continuum removed spectra of major *He* wheat cultivars at the milking phenological stage. We chose the milking phenological stage since the highest lodging incidence rates were recorded at this stage. The profiles have been physically interpreted as a function of the differences in biophysical/biochemical properties at the milking phenological stage (see Table 5.5) for four different wheat cultivars: PR22D66, Odisseo, Monastir and Marco Aurelio.

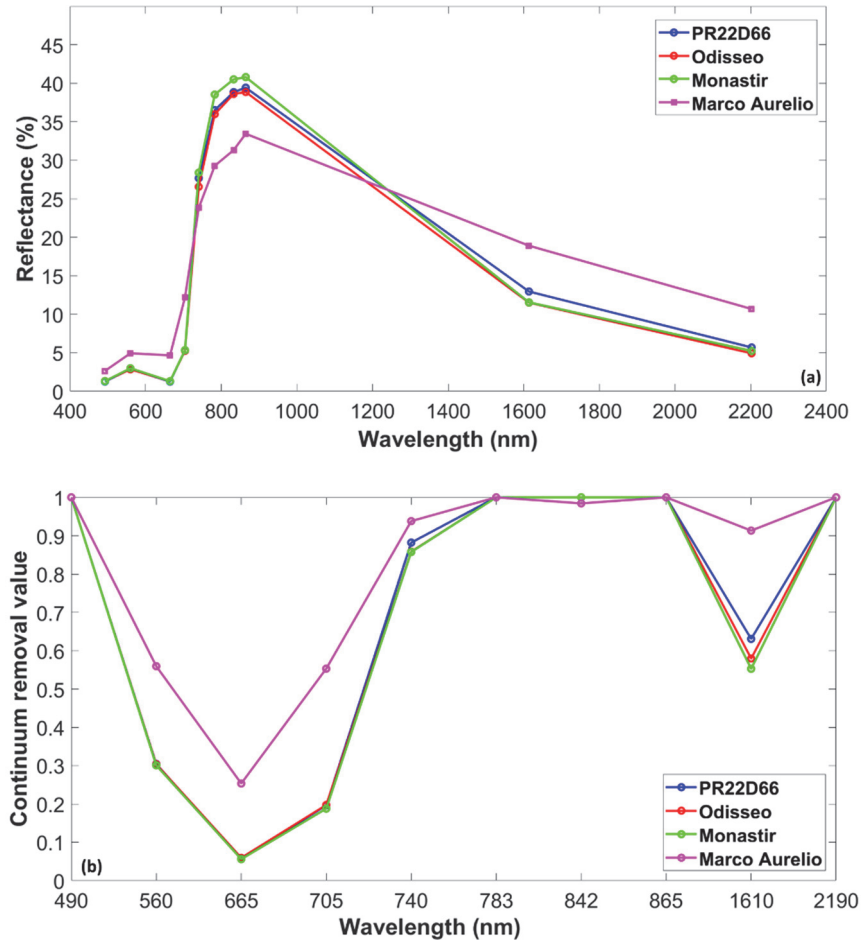


Fig. 5.6. (a) Average spectral reflectance variation and (b) continuum removed spectra for plots with healthy wheat cultivars: PR22D66 ($n=5$), Odisseo ($n=2$), Monastir ($n=4$) and Marco Aurelio ($n=4$), at the milking phenological stage.

Table 5.5. Average biophysical/biochemical properties of plots with healthy wheat cultivars: PR22D66 ($n=5$), Odisseo ($n=2$), Monastir ($n=4$), and Marco Aurelio ($n=4$), at the milking phenological stage. The maximum values are in bold for each plant/soil parameter.

Cultivar	Plant height (m)	LAI	FB (t/ha)	SPAD reading	PWC (%)	Soil moisture (%)
PR22D66	0.75	2.93	4.95	43.95	74.13	40.00
Odisseo	0.91	3.72	5.26	45.51	79.61	44.05
Monastir	0.71	4.81	6.05	49.73	77.87	37.24
Marco Aurelio	0.81	2.76	3.50	34.69	59.68	43.17

In the visible region, the mean reflectance of PR22D66, Odisseo and Monastir are almost similar (1.8%) while for Marco Aurelio, it went up to 5.7% (with the lowest absorption in red region-665 nm) (Fig. 5.6a, b). Since chlorophyll content has a significant effect on the reflectance of visible light, we observed that this effect is in agreement with the chlorophyll (SPAD readings) of the investigated cultivars (Table 5.5). Several studies have shown that a linear or curvilinear relationship exists between SPAD readings and wheat chlorophyll content (James et al., 2002; Wood et al., 1993). In the NIR region, the interaction of incident radiant flux with the crop canopy is primarily related to the intercellular scattering within the leaves and hence is governed by the crop structural parameters such as LAI, canopy cover (fCover) and crop FB/DB (Bunnik, 1978). The lowest reflectance of Marco Aurelio in the NIR region (32.4%) corresponds to lower LAI and lower FB values of this cultivar (Table 5.5). Monastir, on the other hand, has the highest reflectance (45.7%) in this region, which can be explained with high LAI (4.81) and high FB (6.05 t/ha). The vegetation reflectance in SWIR region (1400-2500 nm), particularly the reflectance at 1530 and 1720 nm wavelengths are influenced by several factors such as PWC, dry matter content, LAI, FB/DB, MLA and CAI (Ali et al., 2015; Darvishzadeh et al., 2019b, 2019a; Faurtyot and Baret, 1997). In Fig. 5.6, the high reflectance for the Marco Aurelio cultivar in the SWIR region is mainly explained by low PWC (59.68%), lower FB (3.5 t/ha) and LAI (2.76) compared to the others (Table 5.5).

5.3.1.2 Spectral behaviour of healthy and lodged wheat throughout the observation period

Fig. 5.7 shows the spectral behaviour of He and different lodging severities from stem elongation until the ripening stage. He represents the average spectra of the healthy plots that remained healthy throughout the observation period. Similarly, ML, SL and VSL correspond to the average spectra of the lodged plots which were observed to be moderately, severely and very severely lodged, respectively at the end of the ripening stage. Table 5.6 and Table 5.7 provides the overall and pairwise *p*-value statistics, respectively, for the differences in the reflectance values across the spectral regions for different classes.

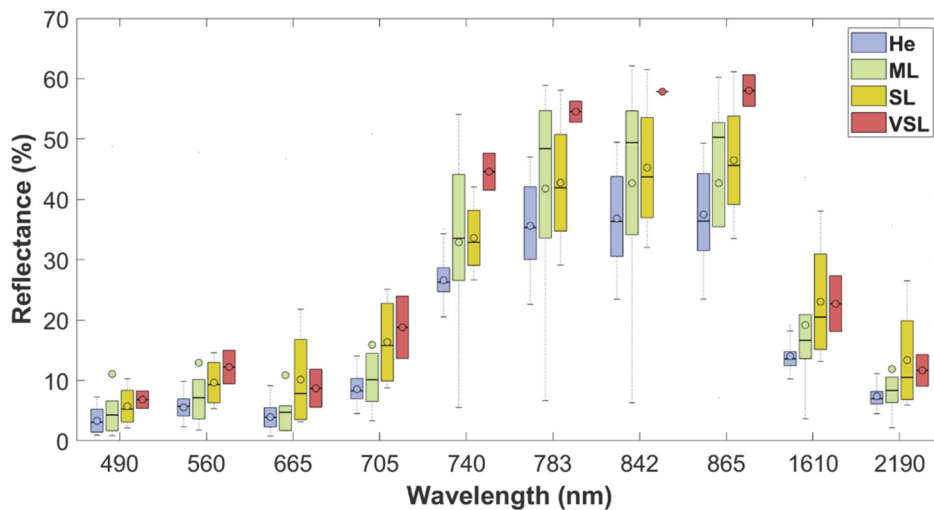


Fig. 5.7. Box plots presenting the reflectance variation in Sentinel-2 bands for healthy wheat plots (He ($n=50$)) and wheat plots with different lodging severities (ML ($n=8$); SL ($n=7$) and VSL ($n=8$)). Observations were taken from the stem elongation stage until the ripening stage.

Differences in the spectra are clearly visible in Fig. 5.7. The overall magnitude of reflectance increased with the increase in lodging severity. In the visible region (447-683 nm), the mean reflectance of He wheat varied between 3.3 and 5.5% while it ranged from 6.8 to 12.2% for VSL (Fig. 5.7). The effect was more pronounced in the red edge (695-796 nm) and NIR (800-880 nm) regions (Fig. 5.7). However, for ML and SL, the mean reflectances were quite similar (~31%). In the NIR region, the mean reflectance increased from 37% for He to 42%, 46%, and 58% for ML, SL, and VSL wheat respectively. In the SWIR region (1542-2324 nm), the mean reflectance initially increased from 10% (He) to 18% (SL), and then saturated (Fig. 5.7). Overall, a clear upward trend was observed from He to VSL in all the spectral bands, which can be explained as follows.

The changes in vegetation due to lodging become evident by an immediate or slow change in its biophysical/biochemical properties (e.g. uneven biomass accumulation in different parts of the plant, reduction in plant height, change in CAI, etc.). These changes in the biophysical/biochemical properties which are manifested in the reflectance characteristics (Darvishzadeh et al., 2008; Gitelson et al., 2003) of He and lodged plants are apparent in our results. The increase in the magnitude of overall reflectance after lodging in the VIS region is mainly due

Table 5.6. Kruskal Wallis *p*-value statistics for Sentinel-2 spectral bands. * and ** indicate 0.05 and 0.01 levels of significance.

Band	<i>p</i> -value
Blue (490 nm)	0.0983
Green (560 nm)	0.0275*
Red (665 nm)	0.1557
RE1 (705 nm)	0.0204*
RE2 (740 nm)	0.0053**
RE3 (783 nm)	0.0264*
NIR1 (842 nm)	0.0211*
NIR2 (865 nm)	0.0127*
SWIR1 (1610 nm)	0.0215*
SWIR2 (2190 nm)	0.1213

Table 5.7. Post-hoc Tukey's HSD *p*-value statistics of different lodging severities for Sentinel-2 spectral bands. *, **, and *** indicate 0.05, 0.01 and 0.001 levels of significance.

Class pairs	blue	green	red	RE1	RE2	RE3	NIR1	NIR2	SWIR1	SWIR2
H ML	0.022*	0.022*	0.056	0.043*	0.095	0.412	0.486	0.561	0.131	0.126
H SL	0.866	0.520	0.224	0.089	0.137	0.444	0.326	0.247	0.010*	0.074
H VSL	0.850	0.378	0.704	0.116	0.0009***	0.028*	0.016*	0.015*	0.122	0.580
ML SL	0.522	0.810	0.997	0.999	0.997	0.998	0.974	0.918	0.676	0.959
ML VSL	0.824	0.998	0.972	0.940	0.102	0.326	0.211	0.180	0.848	0.999
SL VSL	0.996	0.953	0.993	0.968	0.177	0.448	0.419	0.467	0.999	0.973

to the reduction of plant chlorophyll content (VIS) as photosynthesis is disrupted due to self-shading (Alberda, 1977). This decrease progressively manifests with the number of days after lodging. In the NIR-SWIR region, the change of canopy structure (significant reduction of CAI) and consequent increase in the fCover and FB (in the NIR-SWIR region) and reduction of PWC (in the SWIR region) are major factors affecting the spectra.

Furthermore, the blue and redshift of the red edge area is a critical component of spectral analysis of vegetation. A blue shift is visible in the red edge region, accompanied by an increase in overall reflectance (Fig. 5.7) which also suggests reduced chlorophyll concentrations in the lodged canopy. However, Fig. 5.7 also reveals that ML had abnormally high mean reflectance (even higher than VSL in some cases) in the visible and red edge region. Our field records show that at least 50% of the healthy wheat in most of these ML plots had turned yellow, while the lodged patches suffered from a phenological delay (these patches were relatively underdeveloped). This might have increased the reflectance.

The Kruskal Wallis test showed that majority of the spectral bands (green, RE1, RE2, RE3, NIR1, NIR2 and SWIR1) had statistically significant differences among different classes, with RE2 (central wavelength 740 nm) and NIR2 (central wavelength 865 nm) being the most significant (Table 5.6). Additionally, the posthoc Tukey HSD (pairwise) comparison identified significant differences between He and ML (for blue, green and RE1), between He and SL (for SWIR1) and between He and VSL wheat (for RE2, NIR1, NIR2 and NIR3) (Table 5.7).

5.3.1.3 Spectral behaviour of healthy and lodged wheat at the milking phenological stage

We further analysed the average spectral reflectance of He plots and plots with different lodging severities across different spectral bands at a single (milking) phenological stage. Fig. 5.8 displays the average spectral reflectance curve and continuum removed spectra of He and lodged wheat plots at the milking phenological stage. We observed that lodging caused the red edge to shift towards shorter wavelengths (blue shift) (Fig. 5.8a) and there was an increase in the overall reflectance. He wheat plots had a higher BD at 665 nm (0.88) than ML (0.62), SL (0.63) and VSL (0.75) plots (Fig. 5.8b). In the SWIR region, which is sensitive to the variation in PWC, the highest absorption peak was observed at ~1610 nm for He plots (BD = 0.37) (Fig. 5.8b). The SWIR reflectance for ML

(BD = 0.25), SL (BD = 0.18) and VSL (BD = 0.29) plots was higher than that from He plots. (Fig. 5.8a, b).

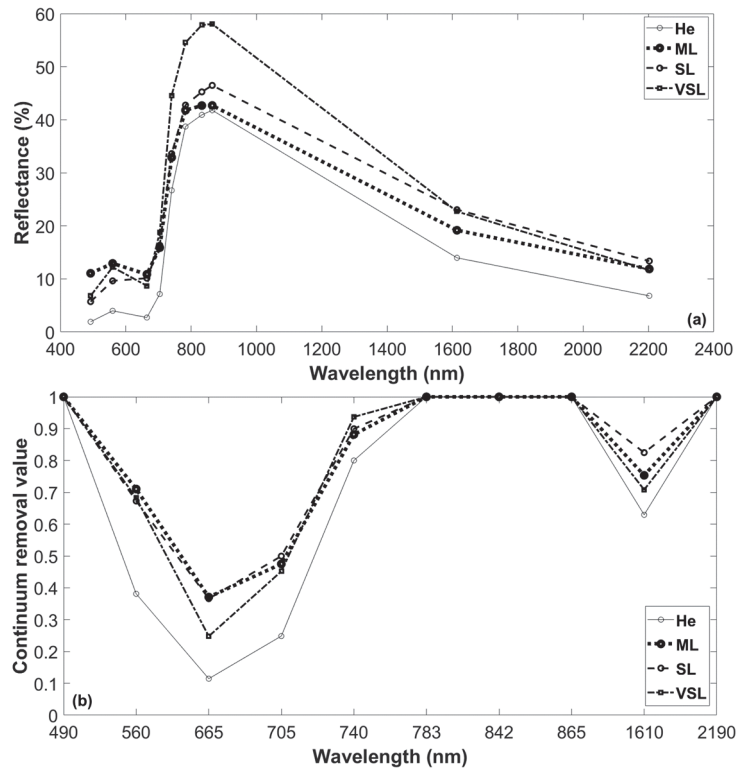


Fig. 5.8. (a) Average spectral reflectance variation and (b) continuum removed spectra for healthy wheat plots (He ($n=15$)) and wheat plots with different lodging severities: ML ($n=6$), SL ($n=6$), and VSL ($n=5$) at the milking phenological stage.

An in-depth analysis of the spectra of He plots for different wheat cultivars and lodged plots at the milking stage showed that change in mean reflectance due to cultivar differences is less than that due to lodging (Fig. 5.9). For instance, in the NIR region, the reflectance of He plots for different cultivars ranges from 32.4 to 40.6% (encircled green in Fig. 5.9) while for the lodged classes, the reflectance range increases to 42.7-58% (encircled red in Fig. 5.9). In the VIS region, the average reflectance at 665 nm increased from 2.13 (He) to 8.10% (lodged), which is consistent with the reduction in SPAD readings from 43.47 to 34.21. However, in the SWIR region, the reflectance of the Marco Aurelio cultivar in He plots (18.9%) and ML plots (19.2%) at 1610 nm was similar (Fig. 5.9). Furthermore, the mean reflectance of SL (calculated from different cultivars) (23.03%) and VSL (calculated from different cultivars) (22.7%) classes were also similar at

1610 nm (Fig. 5.9). The comparison of average PWC values for He (72.89%), ML (72.11%), SL (65.83%) and VSL (54.45%) plots (not shown) indicates that PWC is probably not the only driver of the existing variation in SWIR region. Therefore, other factors such as variation in MLA (He: 54° and ML: 51°; SL: 44° and VSL: 41°) and increase in FB (He: 1.3 and ML: 1.5; SL: 1.6 and VSL: 2.3 t/ha) might have had a bigger effect on the SWIR reflectance.

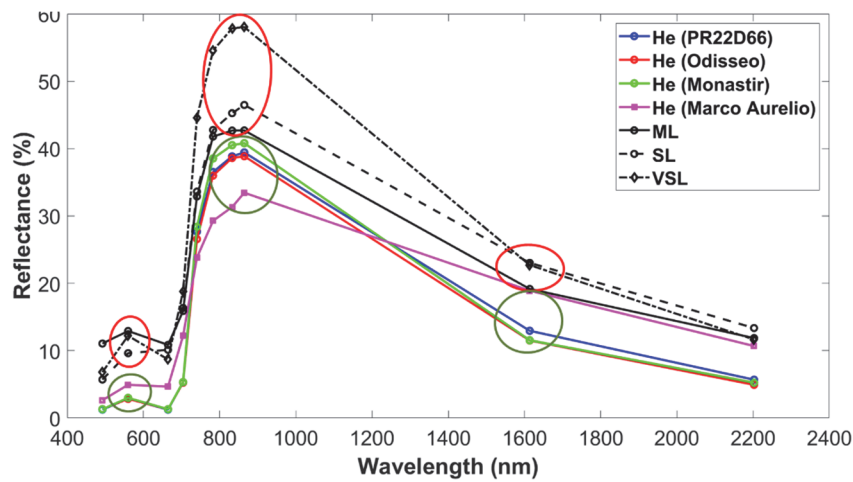


Fig. 5.9. (a) Average spectral reflectance of plots with healthy wheat cultivars: PR22D66 ($n=5$), Odisseo ($n=2$), Monastir ($n=4$) and Marco Aurelio ($n=4$) and those with different lodging severities (ML ($n=6$), SL ($n=6$), and VSL ($n=5$)) across multiple cultivars at the milking phenological stage. The green circle corresponds to the range of reflectance for the plots with healthy wheat cultivars while the red circle represents the range for plots with different lodging severities in the visible and NIR regions.

5.3.1.4 Sentinel-2 time-series analysis to identify the time of lodging incidence

We also analysed the time-series S-2 data as a function of time (DoY) for different lodging severities to see if we could identify the plausible time of lodging incidence. In this section, we only present the results for RE2 and NIR2 spectral bands, since they were highly significant in distinguishing He and lodged wheat (Table 5.7). The average temporal reflectance (of RE2 and NIR2) for He and different lodging severities is presented in Fig. 5.10 along with the distribution of rainfall and wind speed for the same period. In both spectral

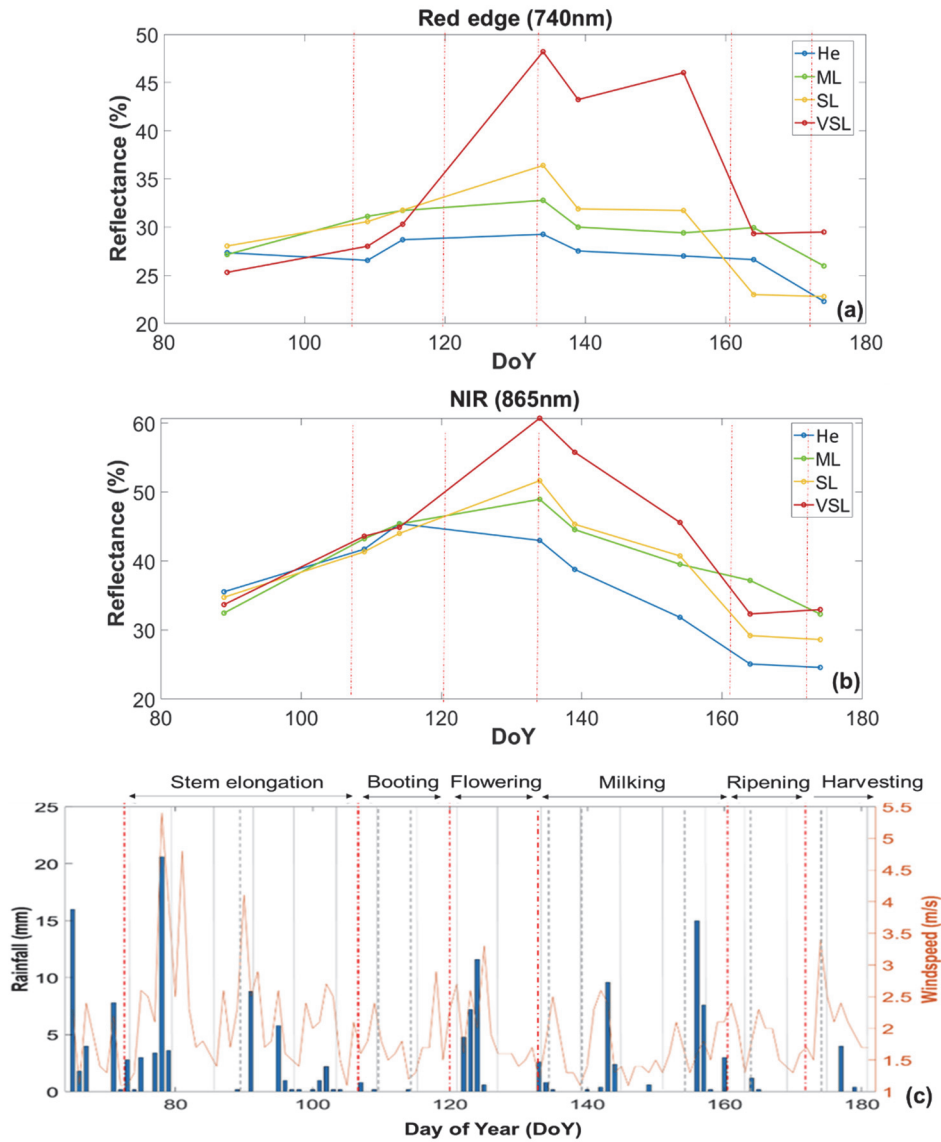


Fig. 5.10. Temporal average reflectance of healthy and lodged wheat plots in (a) red edge (740 nm) and (b) NIR (865 nm) spectral bands, and (c) rainfall and wind speed over Bonifiche Ferraresi farm where wheat was cultivated in 2017-2018. The blue profile in (a)-(b) correspond to healthy plot samples ($n=59$), the green profile is moderately lodged ($n=12$), the yellow profile is severely lodged ($n=21$), and the red profile is very severely lodged ($n=28$). In figure (c), the blue bars represent the daily-cumulated rainfall (mm). The daily average wind speed measured at 10 m from the ground (m/s) is displayed in the orange line. Vertical solid and dashed grey lines indicate Sentinel-1 and Sentinel-2 acquisition days, respectively while dotted red bars represent the wheat phenological stage intervals.

regions, the temporal reflectance of He and lodging severity classes followed a similar pattern until DoY 115, after which some abrupt variations were observed. In the RE2 spectral band, the reflectance of VSL wheat increased considerably from 29% to 48% with respect to He post-DoY 115 while for ML and SL wheat, reflectance increased by only 4 and 8%, respectively (Fig. 5.10). A similar change was noticeable for the temporal reflectance in NIR2 band; however, it was less pronounced. Post DoY 115, the reflectance increased from 43 to 61% for VSL wheat (with respect to He) while for ML and SL wheat, it increased by 6 and 7.5% respectively.

The field records confirmed that all the plots were healthy prior to DoY 115 (end of booting), and a few plots were VSL close to DoY 115. Overall, from the temporal analysis of S-2 data, we can infer that the wheat plots might have lodged post-DoY 115, i.e. when the crop was approaching the end of the booting stage. The meteorological data (Fig. 5.10c) also reports a period of wind and heavy rain after DoY 120 that are likely to be the cause of further lodging events as detected by the change in reflectance after that (Fig. 5.10a, b). Our field records are consistent with this observation. However, due to the unavailability of (cloud-free) satellite and field data every five days, it is difficult to state the exact date when the maximum (or all) number of plots had lodged. The results agree with the posthoc analysis presented in Table 5.7, which shows that He and VSL wheat can be distinguished in these spectral regions. Overall, we can say that different severity classes could be discriminated to some extent with the multispectral time-series data over the selected observation period.

5.3.2 Backscatter and coherence analysis from Sentinel-1 data

5.3.2.1. Backscatter and coherence analysis for healthy and lodged wheat

The box plots in Fig. 5.11a and 5.11b show the change in backscatter and coherence metrics, respectively for He and lodging severity classes during the entire observation period. Fig. 5.11a shows a clear linear trend of increasing σ°_{VH} and σ°_{VV} with the increase in the lodging severity (from He to VSL). The inverse relationship of μ°_{VH} and μ°_{VV} with lodging score is apparent in Fig. 5.11b as these metrics decreased from He to VSL. However, no clear trend was noticeable, especially with μ°_{VV} (Fig. 5.11b).

Furthermore, Kruskal Wallis tests demonstrated significant differences between He and lodging severity classes with all the five metrics (as shown in Table 5.8).

However, the post-hoc Tukey test showed that while *He* could be distinguished from VSL using any of the five SAR metrics (Table 5.9), σ°_{VH} outperformed the other metrics as it could discriminate five class pairs (out of six). With σ°_{VV} , the difference between the lodging severity classes (ML, SL and VSL) was significant with respect to *He* (Table 5.9), but it failed to differentiate within the lodged classes (such as ML-SL, ML-VSL, and SL-VSL). σ°_{VV} and $\sigma^{\circ}_{VH/VV}$ however, seemed to provide complementary information since together, they could discriminate five class pairs (Table 5.9). Similar behaviour in the backscattering coefficients was evident among the classes at the milking stage (Fig. 5.11c).

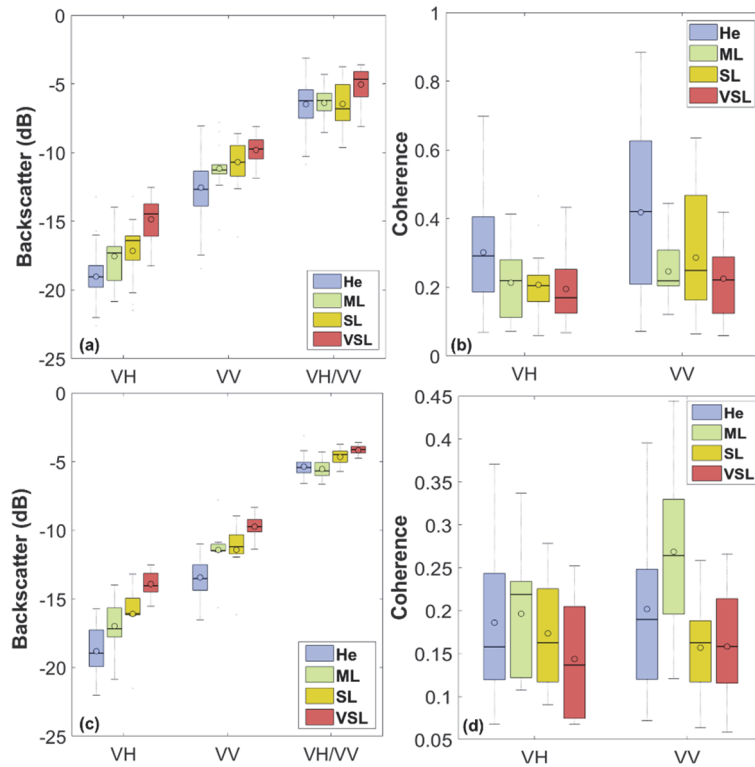


Fig. 5.11. Boxplots presenting the variation in (a) σ°_{VH} , σ°_{VV} , $\sigma^{\circ}_{VH/VV}$ and (b) μ°_{VH} and μ°_{VV} for healthy wheat plots (*He* ($n=160$)) and wheat plots with different lodging severities using Sentinel-1 data: ML ($n=12$); SL ($n=25$) and VSL ($n=31$) throughout the stem elongation-ripening phenological stages. (c) σ°_{VH} , σ°_{VV} , $\sigma^{\circ}_{VH/VV}$ and (d) μ°_{VH} and μ°_{VV} corresponds to healthy wheat plots (*He* ($n=21$)) and wheat plots with different lodging severities: ML ($n=6$); SL ($n=6$) and VSL ($n=8$) at the milking phenological stage.

Table 5.8. Kruskal Wallis p -value statistics for Sentinel-1 metrics. *** indicates a 0.001 level of significance

Parameter	p -value
σ°_{VH}	6.18e-18***
σ°_{VV}	8.07e-13***
$\sigma^{\circ}_{VH/VV}$	2.65e-05***
μ°_{VH}	1.82e-05***
μ°_{VV}	7.85e-06***

Table 5.9. Post-hoc Tukey's HSD p -value statistics of different lodging severities for Sentinel-1 metrics. *, ** and *** indicates 0.05, 0.01 and 0.001 levels of significance.

Class pairs		σ°_{VH}	σ°_{VV}	$\sigma^{\circ}_{VH/VV}$	μ°_{VH}	μ°_{VV}
He	ML	0.005***	0.049*	0.996	0.082	0.015*
He	SL	1.27e-07***	2.50e-05***	0.999	0.003**	0.012*
He	VSL	3.76e-09***	3.76e-09***	1.14e-05***	0.0002***	7.88e-06***
ML	SL	0.881	0.886	0.999	0.999	0.937
ML	VSL	1.08e-06***	0.134	0.0377*	0.975	0.988
SL	VSL	2.82e-07***	0.306	0.0031**	0.985	0.673

5.3.2.2 Sentinel-1 time series analysis to identify the time of lodging incidence

We further interpreted the trend of S-1 time-series for He and lodged wheat while accounting for ancillary rainfall and wind speed information, as well as with the *in situ* observations. The corresponding S-1 time series are shown in Fig. 5.12 with respect to DoY. The backscatter and coherence of the plots that were lodged later in the season (or remained healthy until the harvest) have been plotted from March 14, 2018 onwards, when they were still in a healthy state.

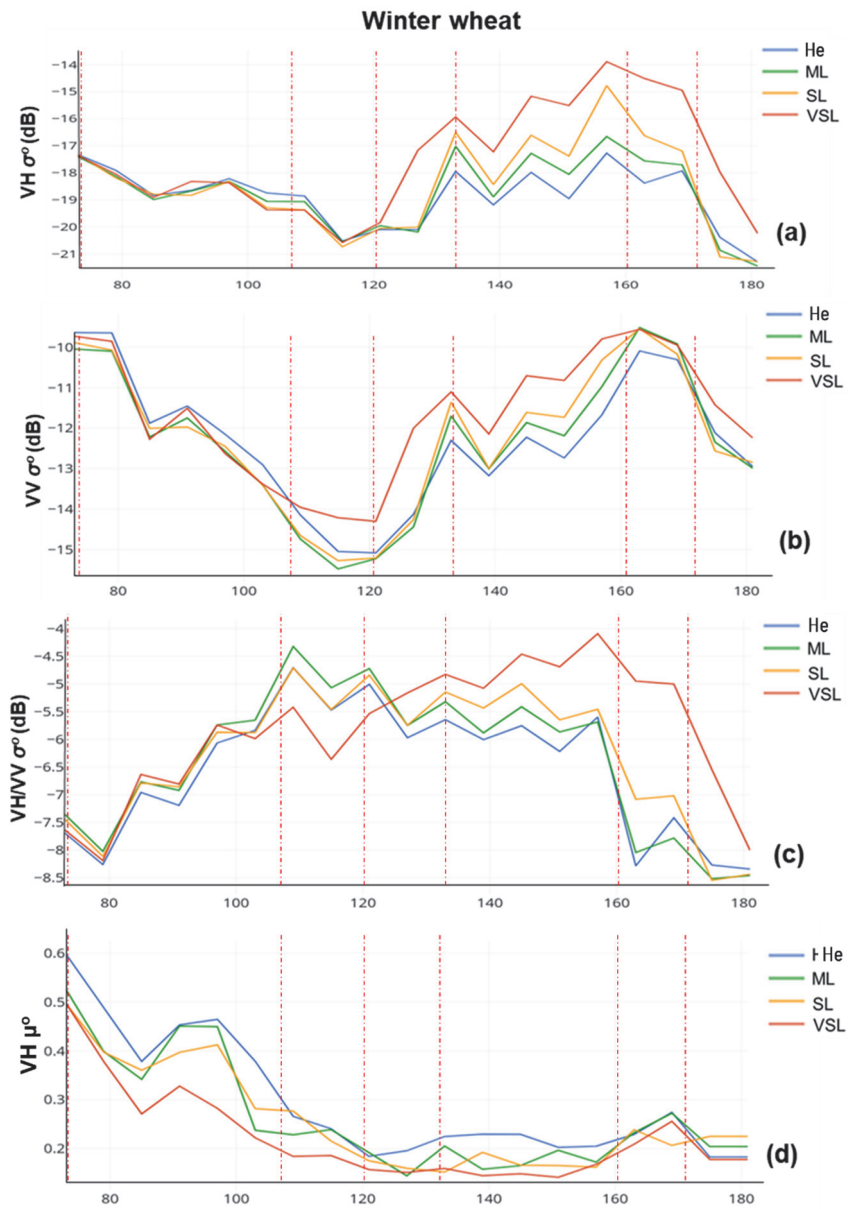
Most of the variability in the backscatter profiles (Fig. 5.12) can be explained physically through changes in physical plant properties. The most striking feature is the sensitivity of σ°_{VH} to lodging (Fig. 5.12a). There is no distinct difference in σ°_{VH} profile until DoY 120 (end of booting), even though there was a constant increase in plant height, FB and LAI. In the initial phenological stages (early stem elongation), the vegetation was short (LAI = 2.6); hence soil σ° (driven by soil moisture and roughness) might have been the dominant contributor to the total σ°_{VH} and σ°_{VV} . For the majority of the plots, the average soil moisture during stem elongation ranged from 34 to 82%, except for a few plots in which the soil was fully saturated (soil moisture >100%). The slight increase in σ°_{VH} , which is observed on DoY 103 (Fig. 5.12a), is mostly the result of an increase in attenuated double bounce and volume scattering mechanisms (as LAI and FB increased to

4.1 and 4.59 t/ha, respectively). This is characteristic of narrow-leaf crops such as wheat (with small plant constituents or scatterers, i.e. stems and leaves) where absorption by the canopy elements appears to be a dominant factor in backscattering from the plant (Macelloni et al., 2001; Tsang et al., 1985). However, a significant increase in the backscatter of lodged wheat is observed around the beginning of May, when wheat is at the end of the booting period or the beginning of the flowering phenological stage. While there is an increase in the magnitude of $\sigma^{\circ}_{\text{VH}}$ for ML, SL, and VSL, the overall σ° trend follows the same behaviour as He. On DoY 121, the increase in $\sigma^{\circ}_{\text{VH}}$ by almost 1.8 dB with respect to He is consistent with the field observations made in VSL plots. The increase in $\sigma^{\circ}_{\text{VH}}$ for ML and SL plots (with respect to He) was close to 0.14 and 0.21 dB respectively, which is well below the radiometric resolution of the sensor (1 dB) and hence might be considered as noise. As reported in the interpretation of S-2 data, the heavy rain and windy period after DOY 120, can justify the observed change in $\sigma^{\circ}_{\text{VH}}$.

The increase in $\sigma^{\circ}_{\text{VV}}$ is also evident in Fig. 5.12b as lodging became severe. $\sigma^{\circ}_{\text{VV}}$ initially decreased until DoY 120, which suggests that the differential extinction (wave attenuation as it propagates through the vegetation volume) is significant due to the vertical stems while the plant is growing. Studies show that cereal stems play an important role in both scattering and attenuation as they represent a significant part of the fresh aboveground biomass (Picard and Toan, 2002). The contribution of the stems is even more important for V polarised waves because of their vertical structure. However, this vertical structure is destroyed after lodging, causing an increase in the magnitude of $\sigma^{\circ}_{\text{VV}}$ (and even $\sigma^{\circ}_{\text{VH}}$) for ML, SL and VSL classes (see Fig. 5.12a, b). The extent of σ° extinction, however, seems to depend on the CAI and LA (i.e. LS). For instance, with severe lodging, as we can see in Fig. 5.12a and 5.12b, there is a higher attenuation than that with very severe lodging, resulting in higher $\sigma^{\circ}_{\text{VH}}$ and $\sigma^{\circ}_{\text{VV}}$ in the latter case. $\sigma^{\circ}_{\text{VV}}$ increased steeply for all lodging severities, except for VSL where the backscatter increased by 0.3 dB (with respect to He) from DoY 114 onwards (end of booting). The wind and rainfall events (see Fig. 5.12f) also explain some of the variations. For instance, the strong wind on DoY 124 (see Fig. 5.12f) could have pronounced the increase in radar backscatter (Pichierri et al., 2018; Skrunes et al., 2018) through its effect on the orientation of the canopy elements. The high wind (5.4 m/s) and rainfall (20.6 mm) events on DoY 78 just before the second S-1 image acquisition could explain the slight increase in $\sigma^{\circ}_{\text{VV}}$ (assuming that the antecedent soil moisture condition may still affect the σ° few days later) (Fig. 5.12f). Then, a

prominent decrease in σ°_{VV} by 2.2 dB (Fig. 5.12b) was observed during the vegetative growth until it saturated (-15.1 dB). Overall, from the field observations of soil moisture and crop biophysical parameters (Table 5.2) of He and lodged plots as well as the temporal analysis of radar backscatter (σ°_{VH} and σ°_{VV}), it can be inferred that the change in the soil/biophysical properties due to lodging is manifested in the backscatter response.

$\sigma^{\circ}_{VH/VV}$ remained relatively unstable throughout the season with an overall increase during the stem elongation stage, around the beginning of April (Fig. 5.12c). The change in coherence values (in both μ°_{VH} and μ°_{VV} polarisations) was moderate across different lodging severities. As can be seen from Fig. 5.12d and 5.12e, the μ° in both channels decreased steadily until DoY 120 and then became stable, followed by a slight increase after crop harvest. The μ°_{VH} and μ°_{VV} of the *He* wheat were slightly higher than that of ML, SL and VSL (Fig. 5.12d), probably because the lodged crop screens the ground more effectively, causing higher backscatter return from the vegetation that decorrelates quickly than that from the underlying soil (Engdahl et al., 2001). However, due to limited field data (every six days) and lack of literature, it is difficult to comment on the role of soil scattering from He and lodged plots. Thus, we cannot wholly attribute the change in μ° values to lodging (Fig. 5.12d, e) even though the statistical analyses revealed a significant difference between He and SL/VSL (Table 5.9). This makes it challenging to consider that any decorrelation observed in the interferogram is solely due to lodging-induced structural changes in vegetation.



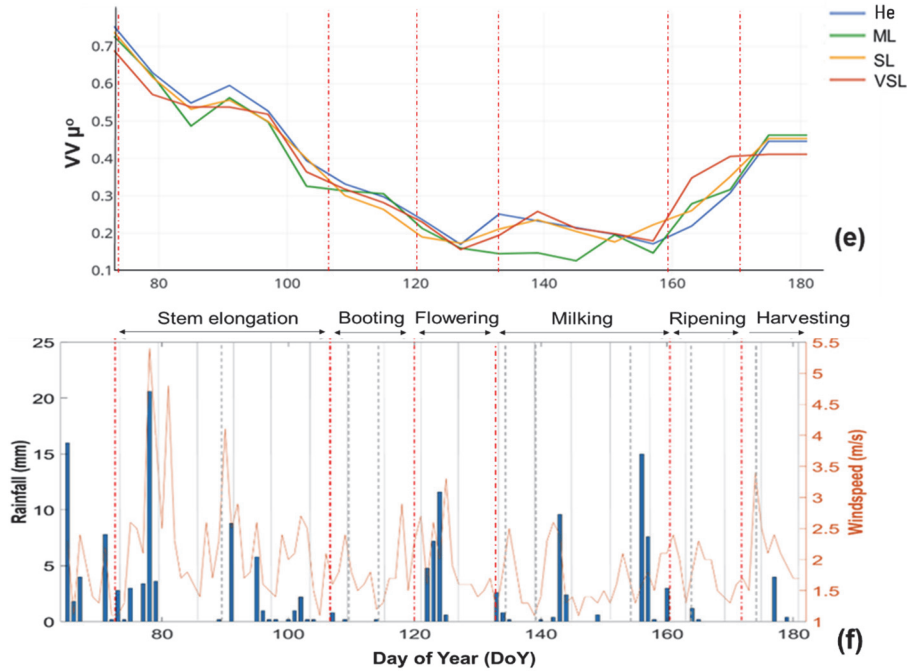


Fig. 5.12. Temporal average signatures of healthy and lodged wheat plots for (a) σ_{VH}^0 , (b) σ_{VV}^0 , (c) $\sigma_{VH/VV}^0$, (d) μ_{VH}^0 and (e) μ_{VV}^0 and (f) rainfall and wind speed over Bonifiche Ferraresi farm where wheat was cultivated in 2017-2018. The blue profile in (a)-(e) corresponds to healthy plot samples ($n=160$), the green profile is moderately lodged ($n=12$), the yellow profile is severely lodged ($n=25$), and the red profile is very severely lodged ($n=31$). In figure (f), the blue bars represent the daily-cumulated rainfall (mm). The daily average wind speed measured at 10 m from the ground (m/s) is displayed in the orange line. Vertical solid and dashed grey lines indicate Sentinel-1 and Sentinel-2 acquisition days, respectively while dotted red bars represent the wheat phenological stage intervals.

5.3.3 Comparison of Sentinel-1 and Sentinel-2 data for identifying the time of lodging incidence

The statistical analysis and time-series interpretation of S-1 and S-2 data in the above sections leads to recommendations of the best features in the context of lodging incidence identification. This is in accordance with the physical processes that are involved in the plants and their effect on plant parameters as measured in the field. As observed in Fig. 5.7 and Fig. 5.11, red edge (740 nm), NIR (865 nm), $\sigma_{VH/VV}^0$ together with σ_{VV}^0 , and lastly σ_{VH}^0 are able to clearly separate *He* and different lodging severities when lodging occurs between the stem elongation and ripening phenological stages (from March to June). Lodging resulted in a shift in the red edge to the shorter wavelengths (blue shift) and

increased the reflectance in this region (Fig. 5.7) possibly due to reduction in chlorophyll content as revealed by SPAD measurements (Table 5.2). The lodging effect was pronounced in the NIR region as well, mainly due to structural changes and an increase in crop surface cover, with the highest reflectance in the VSL class (Fig. 5.7). Moreover, reduction of PWC in the lodged canopy, as observed in the field data (Table 5.2), might have increased the reflectance in the SWIR region (Fig. 5.7). σ°_{VH} outperformed all the other metrics while the information provided by σ°_{VV} and $\sigma^{\circ}_{VH/VV}$ seemed to be complementary as they could discriminate the maximum number of lodging severity class pairs (five out of six). On the other hand, red edge and NIR bands could discriminate only between He and VSL classes.

Thus, in this study, the changes in crop biochemical and structural parameters due to lodging are detected either by optical or SAR data which shows that these datasets provide complementary and convergent information on lodging event. Although, our results showed that both datasets could reproduce the changes in wheat growth status and temporal dynamics, the benefit of having regular S-1 acquisitions versus the rather sparse dates of S-2 was apparent. One of the most critical challenges associated with optical data is the lack of spatial/temporal continuity caused by differential cloud cover, which can greatly affect the accuracy of time-series analysis. (Kovalskyy and Roy, 2013). In this study, we could acquire only eight S-2 images as opposed to 19 S-1 images during the same observation period. This advantage means that SAR-based information can be more reliable than optical information for supporting crop management decisions. The availability of *a priori* information such as sowing dates, crop cultivar, soil type and cultivation practices from the farm managers, can help with the interpretation of SAR data in agricultural applications (Moran et al., 2002).

Our findings suggest that the availability of dense-time series data is important for identifying the time of lodging incidence in wheat since the phenomenon is very dynamic and can occur at any time after the booting stage. Despite gaps in the S-2 time-series, our study highlights the potential of S-2 data due to its high spectral sensitivity and the presence of red edge bands. Indeed, in this study, optical data served as an additional information source to identify lodging severity and most importantly, identify the time of lodging incidence. With the time-series analysis of both datasets together, we could select the best features that could identify the time of lodging incidence (somewhere between DoY 115-121). The unprecedented free availability of dense time-series of S-1 and S-2 data

at high spatial resolution and the further expansion of S-1 and S-2 to four satellites per constellation (A and B, will soon be joined by C and D satellites) presents a new opportunity for operational detection of crop lodging in NRT.

5.4 Conclusions

We assessed the potential of Sentinel-1 and Sentinel-2 time-series data for identifying the time of lodging incidence in wheat and understanding the effect of lodging on the backscatter/coherence and spectral response. The time series of the radar backscatter ($\sigma^{\circ}_{\text{VH}}$, $\sigma^{\circ}_{\text{VV}}$ and $\sigma^{\circ}_{\text{VH/VV}}$), coherence and reflectance were analysed and interpreted in healthy and lodged field conditions, together with meteorological data (rainfall and wind speed data) and in situ measurements of crop parameters (LAI, biomass, CAI, etc.). We showed that the use of S-1 and S-2 data could distinguish *He* from different lodging severities throughout the stem elongation and ripening phenological stages in wheat while the (dense) time-series of Earth Observation data can be used to identify the time of lodging incidence.

We studied the spectral reflectance behaviour of *He* and different lodging severity classes (derived from lodging score) throughout the stem elongation to ripening phenological stages as well as at the milking stage. We further analysed the influence of phenological stages and cultivar differences on the spectral curves of *He* wheat to understand the change in spectra from factors other than lodging. In the event of lodging, we observed that the magnitude of reflectance increased with increasing lodging severity as a consequence of changes in structural and biochemical parameters (e.g. photosynthetic reduction and drying process). We also found that the effect of the phenological stage and cultivar differences on the spectra was far less than that due to lodging. This evidence confirms the capability of optical data in detecting changes that are diagnostic of lodging event. The temporal analysis of the spectra in the red edge (740 nm) and NIR (865 nm) spectral regions showed that lodging might have occurred after DoY 115. However, more than 20 days of missing satellite data did not allow more precise estimates.

In the case of S-1, $\sigma^{\circ}_{\text{VH}}$ was the most reliable discriminator to separate *He* from other lodging severity classes. $\sigma^{\circ}_{\text{VV}}$ and $\sigma^{\circ}_{\text{VH/VV}}$ metrics were complementary as together they could distinguish maximum class pairs. The temporal analysis of $\sigma^{\circ}_{\text{VV}}$ confirmed that the lodging event started somewhere after DoY 115 (same as what was observed with Sentinel-2 data). However, the analysis of $\sigma^{\circ}_{\text{VH}}$ provided

hints of lodging incidence around DoY 121. Since the reflectance/backscatter profiles were averaged across different He and lodged plots with different cultivars and also due to the unavailability of field data every five or six days, it is difficult to point out a precise date when the maximum number (or all) of the plots had lodged. However, with the temporal analysis of both S-1 and S-2 data, it was possible to indicate a plausible window of the main lodging event (i.e. between DoY 115-121); even though lodging continues throughout the season as was observed in the field and mapped by Chauhan et al. (2020a) and Chauhan et al. (2020b). This suggests the complementary nature of the two Sentinel sensors. The change in coherence metrics due to lodging was significant in some cases, but the change could not be wholly attributed to lodging alone. Overall, this study has demonstrated the potential of dense time-series of SAR and optical data in identifying the time of lodging incidence and distinguishing different lodging severities, which has been poorly documented in the literature

Chapter-6

Mapping of wheat lodging susceptibility with Synthetic Aperture Radar data*

*This chapter is based on:

Chauhan, S., Darvishzadeh, R., van Delden, S.H., Boschetti, M., & Nelson, A. (2020d). Mapping of wheat lodging susceptibility with Synthetic Aperture Radar data. *Remote Sensing of Environment* (revisions submitted)

Abstract

Crop lodging reduces yield quantity and grain quality of cereal crops. Understanding seasonal variation in crop lodging susceptibility enables lodging risk assessments and predictions of associated crop yield losses. We demonstrate a novel remote sensing-based approach, using sparse field observations and widely available synthetic aperture radar (SAR) satellite imagery, to map a safety factor against root lodging (SF_A) in wheat. SF_A quantifies the ability of the rooting system to support the self-weight moment of the whole plant and can be used as an indicator of in-season root lodging susceptibility. SAR satellite images, from Sentinel-1 and RADARSAT-2, were acquired synchronously with field measurements in Jolanda di Savoia, Ferrara, Italy during the 2018 winter wheat growing season. The field data included measurements from non-lodged (healthy) wheat such as plant height, height at the centre of gravity, self-weight moment of the whole plant, soil anchorage strength, SF_A and those from lodged wheat such as crop angle of inclination, lodged area and the point of plant failure (stem or root). Field measurements confirmed that SF_A decreased progressively through the season and was consistent with the observed lodging. Strong and significant correlations through the season were observed between SF_A and SAR satellite image metrics. The validated regression models showed a strong relationship between field-measured SF_A and the metrics from RADARSAT-2 ($R^2_{CV} = 0.84$, $RMSE_{CV} = 0.54$) and Sentinel-1 data ($R^2_{CV} = 0.73$, $RMSE_{CV} = 0.59$). Our study, for the first time, demonstrates the use of remote sensing SAR data for lodging susceptibility assessment. Current and planned satellite platforms have the potential for large scale, operational assessment of lodging susceptibility in cereal crops.

6.1 Introduction

Crop lodging, which is the permanent displacement of the crop's stem from its vertical position (Pinthus, 1974), can cause severe yield reductions by up to 75% in cereals (Berry and Spink, 2012). Lodging is also associated with delayed harvest, increased drying costs, deterioration in grain quality and increased susceptibility to mycotoxins (Fischer and Stapper, 1987). Accurate spatio-temporal information about crop lodging and its susceptibility during the growing season are critical for improving yield estimates, increasing productivity and targeting lodging control interventions.

Lodging is caused by either stem failure (stem lodging) or anchorage failure (root lodging) and the most probable form of lodging is governed by genetic, management and environmental factors (Berry et al., 2003a). For instance, high plant population density increases the susceptibility of root lodging over stem lodging, while the early application of nitrogen fertilizer may favour stem lodging (Berry et al., 2000). Root lodging is more predominant in wheat than stem lodging (Crook and Ennos, 1993). For example, an extensive study Berry et al. (2003a) examining 15 winter wheat cultivars at three UK sites between 2000 and 2002 showed that root lodging varied between 2-47%, while stem lodging was observed in only 0-19% of the wheat cultivars.

Before we proceed, it is important to understand the conceptual differences between the two terms: susceptibility and risk. In the case of lodging, susceptibility means the degree to which the crop is prone to lodging. It captures the fact that the host (the plant) reacts variably to lodging, some plants do better than others even if the exposure to a certain external factor is the same. Heavy rain increases the risk of lodging, but the amount and severity of lodging that occurs will be (partially) determined by how susceptible each plant is to lodging. The cultivar, environment, management practices and their complex interactions, strongly influence these factors due to their effects on the crop structure (Berry et al., 2004). A study of all these factors together can form part of a comprehensive lodging risk assessment.

Conventional measures to assess lodging susceptibility are primarily based on visual inspection of the crop (Caldicott and Nuttall, 1979). Visual assessments are sparse, subjective, time-consuming and costly (Bock et al., 2010). Alternatively, mathematical models based on the underlying physics of plant structure might be used to assess lodging (Berry et al., 2003b). Although these

mechanistic models facilitate an in-depth understanding of the lodging phenomenon, the detailed measurements required to parameterize these models make them input-intensive; therefore, mechanistic models are challenging to apply on a large scale. In this regard, some efforts have been made to develop “simple” lodging susceptibility indicators (Crook and Ennos, 1995, 1993).

A safety factor against root lodging (SF_A) has been conceptualized as a “simple” indicator of root lodging susceptibility (Crook and Ennos, 1994). The SF_A is the ratio between the root anchorage strength (S_A) and the self-weight moment of the whole plant (M_P) generated by all the aerial parts, *i.e.* stems, leaves and heads (Fig. 6.1). SF_A correlates well with lodging in the field, with lodging resistant cultivars having greater SF_A (>1) than susceptible cultivars (≤ 1) (Crook and Ennos, 1994, 1993; van Delden et al., 2010). Accurate information about the variability of SF_A and its distribution can enable assessment of root lodging susceptibility and help mitigate lodging impacts (e.g., lodging controls).

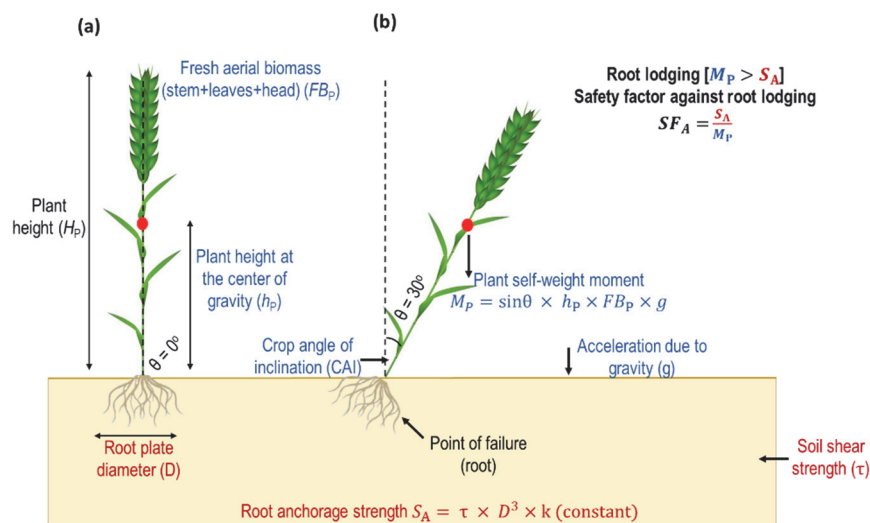


Fig. 6.1. Schematic diagram of the safety factor against root lodging. Crop and soil parameters are governing the safety factor against root lodging (SF_A) for two scenarios (A) healthy/non-lodged wheat with $\theta = 0^\circ$ and (B) root lodged wheat with $\theta = 30^\circ$. An SF_A is a ratio of the plant self-weight moment (M_P , N-m) and root anchorage strength (S_A , N-m). M_P is a function of crop angle of inclination (CAI, θ°), height at the center of gravity (h_p , m), fresh aerial biomass (FB_P , kg) and acceleration due to gravity (g , $N\ kg^{-1}$). S_A is a function of root plate diameter (D), soil shear strength (τ) and a dimensionless constant (k).

Satellite-based remote sensing (RS) data, with its ability to cover large geographic areas with repeated observations, offer a promising alternative for lodging monitoring and susceptibility assessment. So far in the context of lodging assessment using satellite RS data, only three research avenues have been investigated: i) discrimination between lodged and non-lodged areas (Chen et al., 2016), ii) detection of when lodging occurs (Chauhan et al., 2020c), and iii) classification of lodging severity (Chauhan et al., 2020b). These studies diagnose lodging events after they have occurred and emphasise the need for precise and timely Earth observation data for improving lodging assessment. These studies have emphasised that cloud contamination in optical RS data can substantially decrease the number of suitable observations over a region of interest. At the same time, synthetic aperture radar (SAR) sensors can create gap-free datasets for continuous lodging monitoring.

A sound theoretical basis for RS-based lodging susceptibility assessment and the underlying estimation of lodging susceptibility indicators is still missing. Seasonal assessment of lodging susceptibility is important in many aspects - for optimal resource utilization in risk-prone areas, effective decision-making in selecting remedial measures (e.g., nitrogen or plant growth regulator application at critical growth stages), for decreasing crop production costs and reducing the impact on crop yield and grain quality.

This study aims to address this gap and contribute to future lodging risk prediction studies by estimating SF_A as a simple measure of in-season root lodging susceptibility using SAR data. For seasonal susceptibility, we assess the actual plant condition that can influence lodging due to the interaction between genetic, environment and management factors that can amplify or reduce the inherent propensity of different cultivars to lodging. In this study, we compare the performance of RS-based metrics derived from multi-temporal Sentinel-1 (dual-polarized) and RADARSAT-2 (quad-polarized) datasets representing state-of-the-art observational platforms for agricultural monitoring. We also discuss the performance of field-measured SF_A in detecting root lodging susceptibility throughout the growing season and analyse the lodging susceptibility of nine different cultivars.

6.2 Materials and Methods

6.2.1 Experimental design and field measurements

We used stratified random sampling with information derived from six raster layers (sowing date, soil pH, soil type, elevation, seed density and crop cultivar) to obtain spatially distributed sampling points and represent the heterogeneity of the research area. We selected a total of 61 plots (size 60×60 m per plot) on the basis of a *t*-test based power analysis (with a power of 0.95). These plots are overlaid on the satellite image in Fig. 6.2. To capture the variability of crop growth in each plot, we selected three subplots (2×2 m) and averaged the readings to get plot-level measurements. We revisited each plot three times in 2018 between March 14 and June 30 to measure crop biophysical and structural variables: i) we took measurements for plant height (H_P in m); root anchorage strength (S_A in N-m); plant height at the center of gravity (h_P in m); self-weight moment of the whole plant (M_P in N-m); fresh aerial biomass (FB_P in kg) and determined the crop phenological stage using the Biologische Bundesanstalt, Bundessortenamt and CHEMical industry (BBCH) scale (Bleiholder et al., 2001).

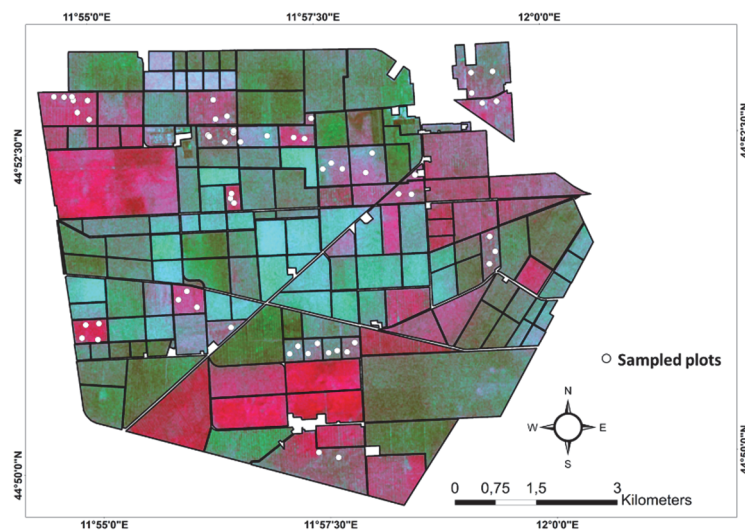


Fig. 6.2. An RGB composite of a Sentinel-1 (R: VH/VV, G: VV, B: VH) scene acquired on April 19, 2018 containing the study area (Bonifiche Ferraresi farm) overlaid with the sampled plots (white dots) over the wheat sown fields and the farm boundary (black outline).

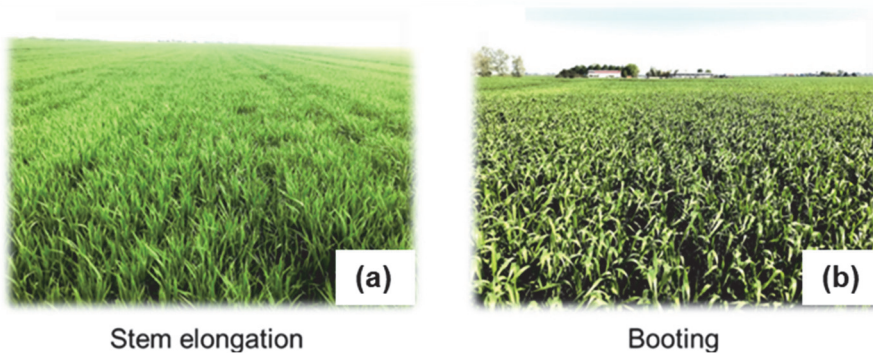
During the entire duration of the field campaign, 30 plots had lodged at one point or the other while the others remained healthy until the end of the season. To see

if SF_A can actually be used as an indicator of root lodging susceptibility in wheat, it was first important to analyze how field measured SF_A values vary in both lodged and non-lodged scenarios. Therefore, the field measurements were used for two different purposes:

(i) First, we aimed at demonstrating how field measured SF_A vary with lodging susceptibility scores (LSS) and observed lodging in the field. The results of this preliminary analysis would establish if SF_A in fact, could be used as an indicator to map lodging susceptibility.

(ii) Secondly, we investigated the potential of SAR derived metrics to estimate SF_A , through regression analysis. For the model development and validation to predict SF_A , we only used the samples from healthy wheat (non-lodged wheat). The rationale behind using only healthy samples to predict SF_A is that SF_A should be able to indicate the susceptibility of the healthy samples to lodge in the future early in the season (when the plants are still healthy) or even at later growth stages.

Overall, the sampled observations covered four major crop phenological stages – stem elongation, booting, flowering, and milking (Fig. 6.3).



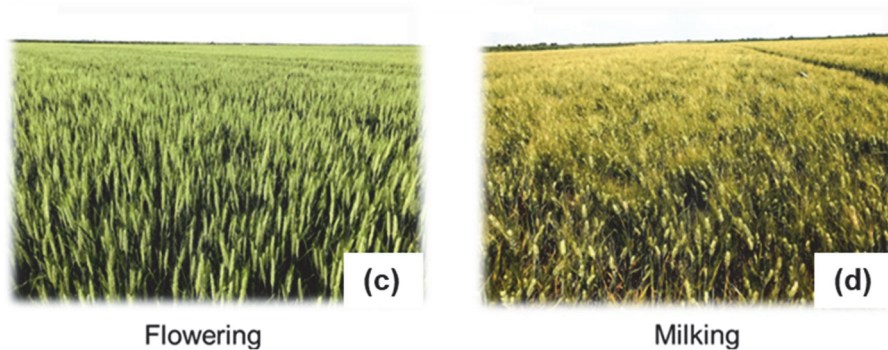


Fig. 6.3. Field photographs of wheat in different phenological stages: (a) stem elongation, (b) booting, (c) flowering and (d) milking.

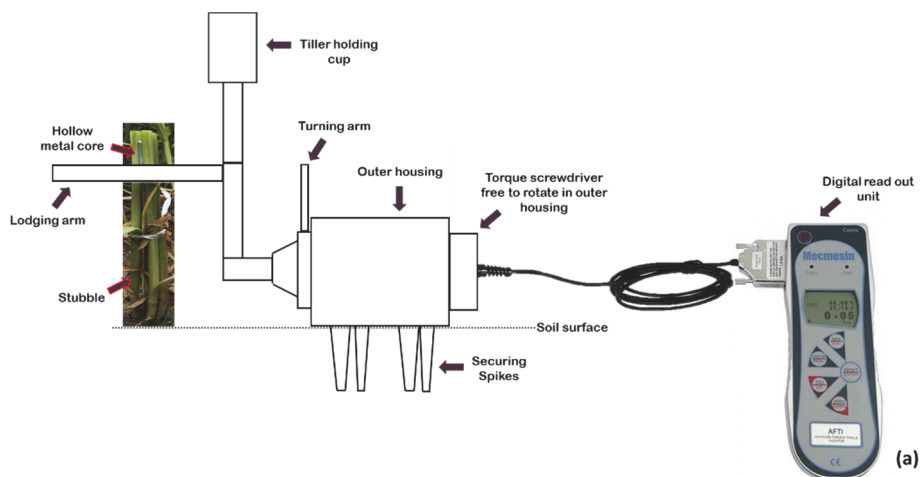
The field measurement protocol was as follows: first, we recorded plant height (H_p), defined as the distance from the soil surface to the tip of the head of the longest tiller; then S_A was measured by subjecting the plants to lodging using a custom-built, handheld lodging meter (Fig. 6.4). The lodging meter was built using a sensitive digital torque screwdriver (reading up to 6 N-m with 0.001 N-m intervals; Mecmesin Ltd., UK) fitted with an integrated tiller holding cup, a lodging arm and an outer casing with four spikes similar to (Crook and Ennos, 2000; van Delden et al., 2010) (Fig. 6.4a). To estimate S_A the following steps were taken: i) Stubbles were created by cutting all stems at 10 cm above soil level, the upper mass was preserved to measure (h_p) and fresh aerial biomass (FB_p). ii) To make the stubbles behave like a rigid beam and avoid bending, lightweight hollow metalcore was inserted in the middle of the stubbles and the stubble-pin combination was tied together with a fastener (Fig. 6.4b). iii) The lodging meter was inserted into the soil such that the setup could deliver a rotational force around the base of the plant stem (Fig. 6.4b). iv) Using the lodging meter, the stubble-pin combination was pushed over to create different angles of inclination (AIs) from the vertical, i.e., 10°, 20°, 30°, 40°, 45° and 60° and at each angle, we recorded the maximum root resistance, i.e., root anchorage strength (S_A) (Fig. 6.4c). This is basically the force needed to create an angle of inclination of the stubbles (the reading on the display was recorded). We also recorded the angle of inclination at which the roots break. This is noticeable when the force suddenly drops because the crown roots break (one can even hear a click) and the stubbles become easy to move around.

We ensured that the neighboring plants did not interfere with these measurements and the readings were corrected for the self-weight moment of the stubble-pin combination and the pushing device. We then cut off the stubble at soil level and tied the stubble together with the remaining section of the plant (with lightweight tape) and measured the h_P of the whole plant using a balancing method. We balanced the plant on a thin (3 mm), smooth metal tube to find the balance point of the whole plant, while the leaves and ears were still attached. h_P was defined as the distance between the balance point and the stem base. Then FB_P was measured using a high-precision digital scale. Lastly, we calculated the self-weight moment of the whole plant (M_P in N-m) and the safety factor against root lodging (SF_A) using equation 6.1 and equation 6.2 (Crook and Ennos, 1994), respectively.

$$M_P = \sin\theta \times h_P \times FB_P \times g \quad (6.1)$$

$$SF_A = \frac{S_A}{M_P} \quad (6.2)$$

where M_P (N-m) is the self-weight moment of the whole plant at 10° , 20° , 30° , 40° , 45° , 60° from the vertical, h_P (m) is the plant height at the center of gravity, FB_P (kg) is the fresh aerial biomass, g (N kg^{-1}) is the acceleration due to gravity; g is $\sim 9.81 \text{ N kg}^{-1}$, SF_A is the safety factor against root lodging and S_A (N-m) is the maximum root anchorage strength. The summary statistics of the field measured variables are in Table 6.1.



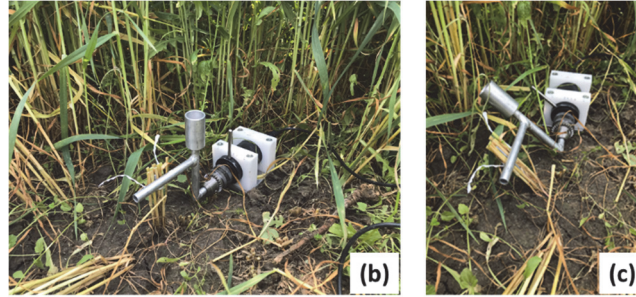


Fig. 6.4. Basic layout of the lodging meter and its demonstration in the field. (a) Schematic illustration of the lodging meter connected with a portable digital unit, (b) shows the setup of the lodging meter in the soil. The stubble (stem base cut 10 cm from the soil surface) with a hollow metal core inserted in between and tied with a fastener is shown. The lodging meter is placed level with the soil at a distance such that the lodging arm touches the stubble-pin combination and (c) illustrates the procedure to measure the root anchorage strength at different crop angles of inclination.

Table 6.1. Summary statistics of field measurements. A statistical summary (mean, minimum, maximum, standard deviation and coefficient of variation) of the field measurements are provided for non-lodged (healthy) wheat across the wheat-growing period ($n=90$). *CAI* is the crop angle of inclination. The measurements were taken from 61 plots with different wheat cultivars.

Parameter	Mean	Min.	Max.	Std. Dev.	COV
Plant height (m)	0.50	0.20	1.01	0.27	0.54
Height at the centre of gravity (m)	0.21	0.04	0.65	0.16	0.79
Fresh biomass (kg m^{-2})	0.33	0.05	1.01	0.22	0.65
Self-weight moment of the whole plant (N-m) ($\text{CAI}=30^\circ$)	0.46	0.013	2.57	0.55	1.21
Root anchorage strength (N-m) ($\text{CAI}=30^\circ$)	0.18	0.013	1.80	0.23	1.34
Safety factors ($\text{CAI}=30^\circ$)	0.98	0.056	2.90	0.79	0.81

6.2.2 Remote sensing data acquisition

We acquired remote sensing images synchronously with the field observations (Table A6.1). We downloaded ten Sentinel-1A/B (in Interferometric Wide swath mode) images in ascending mode between March 14 and June 30, 2018 via the Copernicus Open Access Hub. The Interferometric Wide swath mode provides data in dual-polarization mode (VV: Vertical-Vertical and VH: Vertical-Horizontal). We acquired the images in both ground range detected (GRD) and single look complex (SLC) formats to facilitate the extraction of backscattering

coefficients and polarimetric/coherence parameters, respectively. The incidence angle over the surveyed study site ranged between 39.7° to 40.4°. The spatial resolution was resampled to 15 m.

We also obtained five SLC RADARSAT-2 images in fine quad-polarization mode through the Canadian Science and Operational Applications Research Program (SOAR). We selected the fine-polarization mode for its high spatial resolution and quad-polarized configuration that permits the derivation of various polarimetric parameters. We procured the images in different beam modes with incidence angles ranging from 26.9-28.7° to 40.2-41.6°. The nominal spatial resolution of the images was resampled to 10 m.

Table 6.2. The dates for the acquisition of Sentinel-1 and RADARSAT-2 images over Bonifiche Ferraresi farm, Jolanda di Savoia, Italy during the wheat growing season March-June 2018 are outlined. The images were selected synchronous to the field measurements.

Acquisition date	Satellite data	
Mar 14	Sentinel-1	
Mar 20	Sentinel-1	RADARSAT-2
Mar 26	Sentinel-1	
Apr 1	Sentinel-1	
Apr 2		RADARSAT-2
Apr 19	Sentinel-1	RADARSAT-2
Apr 26		RADARSAT-2
May 1	Sentinel-1	
May 7	Sentinel-1	RADARSAT-2
May 13	Sentinel-1	
May 31	Sentinel-1	RADARSAT-2
June 24	Sentinel-1	RADARSAT-2

6.2.3 Remote sensing data pre-processing

6.2.3.1 Sentinel-1

We pre-processed Sentinel-1 images in SARscape 5.5 to extract backscattering coefficients (σ^0) and coherence (μ^0) metrics and carried out polarimetric decomposition in SNAP 6.0. After applying the precise orbit correction on the GRD images, we extracted the backscattering coefficients (σ^0_{VH} , σ^0_{VV} , $\sigma^0_{VH/VV}$) in dB units using the methodology outlined by Nelson et al. (2014b). In addition,

we also applied orientation angle correction to remove the azimuth slope variations. The Radar Vegetation Index (RVI) for dual-pol data proposed by Charbonneau, Trudel, & Fernandes (2005) was later derived using equation 6.3:

$$RVI = \frac{4\sigma_{VH}^0}{(\sigma_{VH}^0 + \sigma_{VV}^0)} \quad (6.3)$$

where σ_{VH}^0 and σ_{VV}^0 are the backscattering coefficients (in dB) in VH and VV polarizations.

We used the coherence module of SARscape to generate geocoded coherence maps. Unlike SAR, which utilizes the amplitude information of a complex SAR signal, InSAR utilizes phase information to calculate interferometric coherence (that includes both, the interferometric correlation coefficient and interferometric phase). Coherence is a function of the change in phase or amplitude of an image pixel and is defined as the systemic spatial or scene de-correlation that occurs between two acquired dates. These changes in the backscatter can be due to differences in dielectric properties (e.g. wet or dry soil), due to natural processes (e.g. growth of crop) or abrupt changes (e.g. crop harvesting or lodging) all of which can cause coherence loss. γ is formulated as the amplitude of the complex correlation coefficient between two SAR scenes,

$$\gamma = \frac{|(s_1 s_2^*)|}{\sqrt{\langle (s_1 s_1^*) (s_2 s_2^*) \rangle}} \quad 0 \leq \gamma \leq 1 \quad (6.4)$$

where, γ is the interferometric coherence, $|\cdot|$ represents the absolute values, $\langle \cdot \rangle$ denotes the averaging operation, $*$ is the complex conjugate product, and s_1 and s_2 are the complex pixel values from the two image dates (Touzi et al., 1999). The processing steps for coherence estimation include i) Orbit file and orientation angle correction, (ii) interferogram generation. This step resamples the slave image onto the geometry of the master image, applies multilooking and generates a coregistered output. The coregistration accuracy was improved (in the order of 1/1000th of a pixel) using an external DEM (10 m resolution) as an additional input and spectral diversity techniques, iii) interferogram flattening using the external DEM and topographic phase removal, iv) adaptive phase filtering to reduce noise and coherence estimation, v) geocoding.

SARscape, based on the master input data resolution, suggests the azimuth and range multi-looking factors. The multi-looking factors of 4 (looks in range

direction) \times 1 (looks in azimuth direction), leading to the pixel size of $13.27 \text{ m} \times 13.8 \text{ m}$, was used for Sentinel-1 to increase the signal-to-noise ratio (SNR) of the interferograms and obtain squared pixels. A similar approach was also used by Darvishi et al. (2018) and Khabbazan et al. (2019) for coherence estimation. We also filtered the interferograms for visual inspection, and to identify fringe patterns and coherence estimation using a Goldstein filter. Additionally, we used the SARscape Sentinel-1 SLC data processing guidelines, which recommends setting the cartographic grid size for Sentinel-1 SLC data as 15m. The resampling parameters were estimated from the orbital data information and exploited cross-correlation and coherence maximization techniques. The accuracy of the results was further improved using a very high-resolution data DEM (10 m) as an additional input to the process. In order to achieve the lowest temporal baseline (six days), we estimated γ between every adjacent image pair (e.g. between date 1 and date 2; between date 2 and date 3; and so on). The coherence (γ) reported for a given date indicates the coherence between the image on that date (or the closest available later date, i.e. N) and its predecessor, i.e. N-1. The in-situ observations were matched to the coherence image pairs based on the N image date. The coherence value $\gamma_{N-1,N}$ was assigned to the in-situ observation if the date of the latter was either close to N or if it fell between N-1 and N.

We also applied a dual-pol $H/\alpha/A$ polarimetric decomposition to the SLC images using the Graph Builder and Batch processing capabilities of SNAP. The processing chain consisted of six steps: i) orbit file correction, ii) Terrain Observation with Progressive Scan (TOPS) Split to extract the sub-swath with our region of interest, iii) radiometric calibration, iv) TOPS Deburst to remove the demarcation zones between the bursts, v) Refined Lee polarimetric speckle filter with 5×5 window, and vi) $H/\alpha/A$ decomposition to produce entropy (H), alpha angle (α) and anisotropy (A) parameters. $H/\alpha/A$ decomposition, proposed by (Cloude and Pottier, 1996), is an eigenvector-eigenvalue based decomposition. H [0,1] accounts for the heterogeneity of the scattering, α [0,90°] indicates the type of scattering (surface, double-bounce or volume) and A provides information on the relative importance of the secondary mechanisms occurring in the pixel. The anisotropy may reach 0 value for a dominant scattering mechanism. We processed all the SLC images in a batch mode to produce the decomposed outputs and then co-registered and terrain corrected them. Thus, for each Sentinel-1 acquisition, we computed nine metrics: i) σ_{VH}^o , ii) σ_{VV}^o , iii) $\sigma_{VH/VV}^o$, iv) RVI, v) γ_{VH} vi) γ_{VV} , vii) H , viii) α and ix) A .

6.2.3.2 RADARSAT-2

Similar to S-1 data, we pre-processed RADARSAT-2 images in SARscape 5.5 to extract σ^0 and carried out polarimetric processing in SNAP 6.0. We used definitive orbit files obtained from the MacDonald Dettwiler Associates Ltd. FTP repository to update the orbital information in the RADARSAT-2 images. We used the approach outlined in Nelson et al. (2014b) to get normalized σ^0 values (dB). The backscatter was normalized for the incidence angle induced variations using the cosine law of incidence angle, and an orientation angle correction was applied to remove the variations due to azimuth slope. For polarimetric decomposition, we applied a Refined Lee polarimetric speckle filter (5×5 window) on the calibrated images to eliminate speckle noise while preserving the complex information. We then used different polarimetric decomposition methods: i) Sinclair decomposition, ii) Pauli decomposition, iii) $H/a/A$ decomposition, iv) Freeman-Durden decomposition, v) Yamaguchi decomposition, vi) Cloude decomposition, vii) Touzi decomposition and viii) Van Zyl decomposition to decompose the radar scattering matrix into components that could be physically interpreted in terms of the scattering mechanisms. The detailed description of these methods can be found in Chauhan et al. (2020a).

In addition to the decomposition parameters, we also computed simple SAR polarimetric parameters such as span, biomass index, RVI, pedestal height, volume scattering index, canopy scattering index, radar forest degradation index, co-pol ($\sigma_{HH}^0/\sigma_{VV}^0$) ratio and cross-pol ($\sigma_{HH}^0/\sigma_{HV}^0$) ratio from the radiometrically calibrated images. The detailed description of these parameters can be found in Chauhan et al. (2020a). Lastly, we co-registered and geocoded the images and extracted 39 metrics (Table A6.3) from them.

6.2.4 Statistical analysis

In this study, we performed two different kinds of statistical analyses: (i) Pearson correlation coefficient analysis aimed at understanding the correlation between the predictors, i.e. remote sensing metrics derived from Sentinel-1 and RADARSAT-2 data (Table A6.2, A6.3) and the safety factor against root lodging (SF_A); and (ii) an Extreme Gradient Boosted Tree Ensemble for regression (XGB) model to estimate SF_A using the remote sensing predictors. Pearson correlation coefficient, also referred to as Pearson's r [-1,1], is a statistic to measure the linear correlation between the two variables. It is an established way to provide insights

into the black-box machine learning algorithms as it can indicate the relative performances of different predictor variables.

XGB is a non-parametric regularized extension of traditional boosting techniques (Chen & Guestrin, 2016). It iteratively applies tree-based approximation to varying gradient descent by predicting a new membership value after each iteration to minimize the overall loss (Torres-Barrán et al., 2019). The overall loss is depicted by a cost function that measures the difference between the observed and the predicted output from the model. Boosting works on the principle of the ensemble, which means that a set of weak learners are combined to improve the prediction accuracy. This is achieved by weighing the outcome of the model at an instant t based on the outcome of the previous model at instant $t-1$ and capitalizing on the error. XGB simplifies the objective functions by combining the training loss and regularization terms to prevent overfitting (Zhang et al., 2020). The training loss measures the predictive capability of the model with regard to the training data while the regularization term accounts for the model complexity. The aim is to develop a simple, yet predictive model and the tradeoff between the two is known as a bias-variance tradeoff.

In this study, we implemented an extreme gradient boosting tree ensemble regression model to estimate safety factor parameter using the XGBoost package in MATLAB in the partial least square toolbox v8.7 from Eigenvector Research, Inc., with the Multivariate Image Analysis toolbox v3.0 add-on (in MATLAB 2018b). We trained and cross-validated the models separately with the input metrics from Sentinel-1 and RADARSAT-2 data separately. The input metrics derived from each sensor data are mentioned in Table A6.2 and A6.3. We used a cross-validated grid-search to tune the hyperparameters and select the optimal parameter values to build the models. We used $RMSE_{CV}$ as the evaluation measure of the model performance, with the model parameters yielding the lowest $RMSE_{CV}$ being chosen as the best performing model. We used a five-fold Venetian blinds cross-validation procedure to divide the datasets into training and validation subsets. This method guarantees that both training and validation sets span across the entire data range (Allison et al., 2009). This involved dividing the datasets randomly into five subgroups, performing five iterations such that each subgroup could be used once as a validation set and giving an average output. We then used the final cross-validated models to generate SF_A maps of all the wheat fields in the study area. The methodological flowchart of the study is shown in Fig. 6.5.

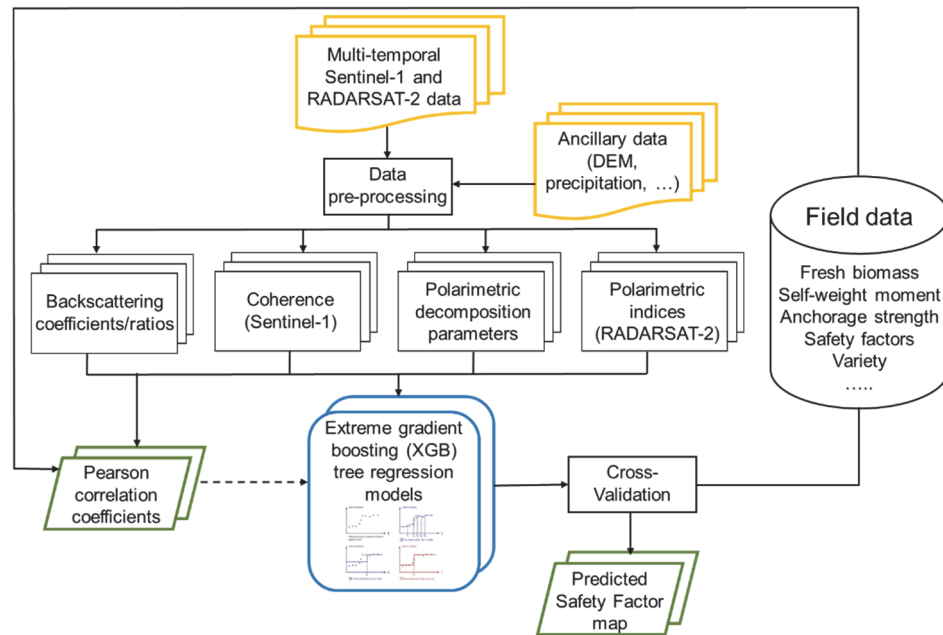


Fig. 6.5. Process flowchart for the estimation of safety factor against root lodging. The inputs are colour-coded in yellow, the model used is in blue, and primary/intermediate outputs are in green. The dashed line signifies that the output is used for interpretation.

6.3 Results

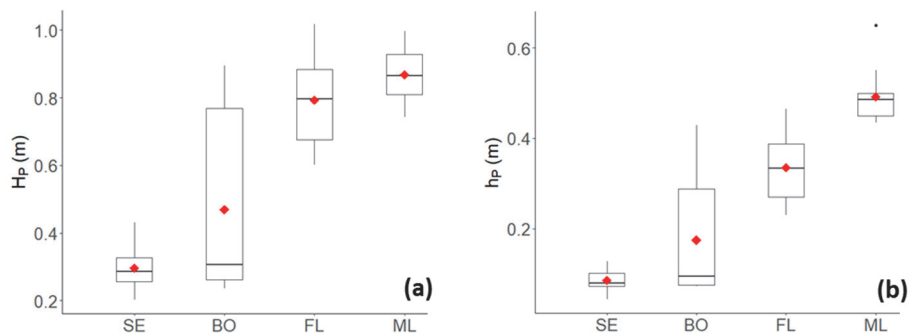
6.3.1 Temporal variation of field-measured parameters

Field measurements on biophysical and structural parameters (Table 6.1) of nine winter wheat (*Triticum aestivum*) cultivars were performed between March 14 (early stem elongation stage: BBCH 30) and June 23, 2018 (crop maturity: BBCH 99). We limit our interpretation of the temporal variation in field-measured parameters from non-lodged (healthy) wheat to four phenological stages: stem elongation (BBCH 30-39), booting (BBCH 40-49), flowering (BBCH 60-69), and milking (BBCH 70-77). Samples from later phenological stages (BBCH>80) were mostly lodged and were excluded from the analysis but were used for validating the performance of SF_A for assessing root lodging susceptibility.

Plant height (H_p) and height at the centre of gravity of the whole plant (h_p) (Fig. 6.6a) changed from a mean of 0.30 and 0.08 m during stem elongation stage to 0.86 and 0.49 m in the milking stage, respectively (Fig. 6.6a, b). They exhibited a similar pattern of change across the season and were found to correlate with each other positively ($r = 0.96, p < 0.001$). During early grain filling, h_p was almost

half of H_P but increased as the grains matured (Fig. 6.6a, b). Overall, H_P and h_P were significantly different between cultivars throughout the period ($p < 0.05$) (Fig. A6.1a, b). The high variation in H_P and h_P at the booting stage was mainly due to the samples from Senatore Capelli, a traditional and tall cultivar with H_P up to 1.1 m.

After both H_P (Fig. 6.6a) and fresh aerial biomass of the whole plant (FB_P) (Fig. 6.1) plateaued (Fig. 6.6c), h_P still increased (Fig. 6.6b) due to grain filling, i.e., the continued accumulation of dry biomass in the plant head. Large variation existed in the FB_P of different cultivars ($p < 0.001$), with cultivars such as Senatore Capelli, Odisseo and Marco Aurelio having relatively higher FB_P (Fig. A6.1c). The self-weight moment of the whole plant (M_P) was measured (using equation 6.1) at six different crop angles of inclination (CAI) from the vertical - 10°, 20°, 30°, 40°, 45° and 60°. During our analysis we found, that both M_P and S_A values increased linearly with increasing crop angle before levelling (slight decline) out at CAI of 30°, which was also consistent with the findings of Crook & Ennos (1994). The moment of decline is the maximum resistance and a good measure for root anchorage failure, after that moment the plants will lodge for sure. Therefore, we selected the measurements made at CAI = 30° for subsequent analyses. M_P continued to rise after flowering, reaching its maximum at the milking stage (mean of 1.34 N-m) (Fig. 6.6d) when the plant ears were the heaviest (late May/beginning of June). The high M_P of Senatore Capelli, Odisseo and Marco Aurelio can be attributed to high h_P and FB_P (Fig. A6.1d).



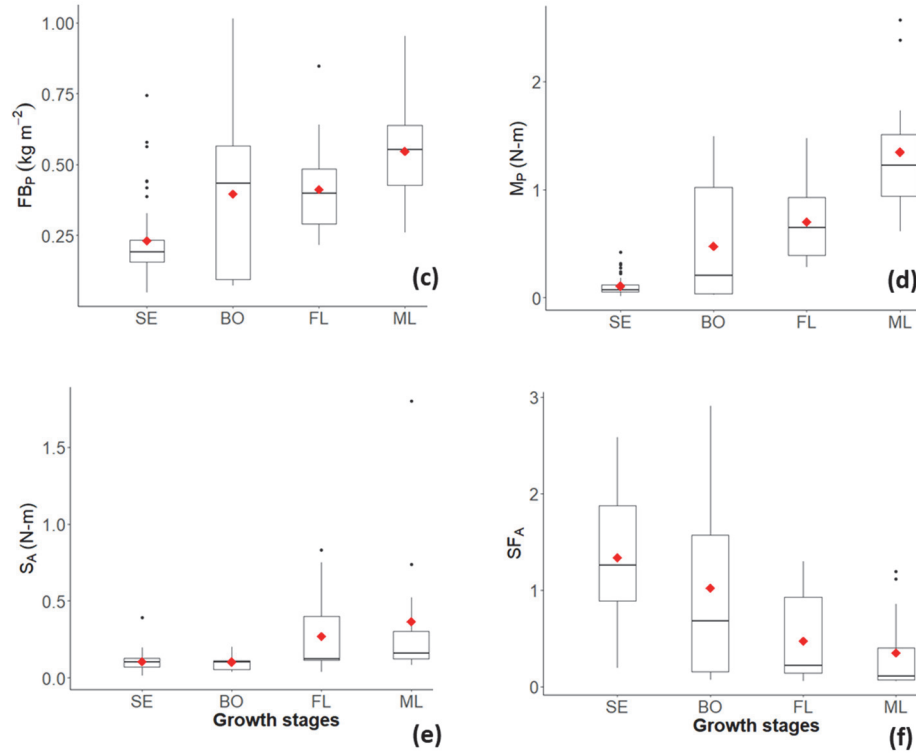


Fig. 6.6. Variation of measured crop biophysical parameters across the growing season. Boxplots illustrate plot-level variation in field-measured crop biophysical parameters: (a) plant height (H_p , m), (b) plant height at the center of gravity (h_p , m), (c) fresh aerial biomass (FB_p , kg m^{-2}), (d) self-weight moment of the whole plant at the crop angle of inclination of 30° (M_p , N-m), (e) anchorage strength at a crop angle of inclination of 30° (S_A , N-m) and (f) safety factor against root lodging at a crop angle of inclination of 30° (SFA) across different growth stages ($n=90$): stem elongation (SE), booting (BO), flowering (FL) and milking (ML). Boxplots display data distribution from bottom to top: lower whisker as a minimum, first quartile, median, third quartile and upper whisker as maximum. The black dots represent outliers, and red diamonds are mean values.

From the early stem elongation stage to crop maturation, mean root anchorage strength (S_A) increased from 0.11 to 0.36 N-m (Fig. 6.6e). In general, from the booting stage onwards, the mean S_A of the observed samples was lower than the mean M_p resulting in a mean crop safety factor against root lodging (SFA) below 1 (Fig. 6.6e, Fig. A6.1e). There were minor differences in the M_p and S_A for different cultivars. For example, at the flowering stage, Massimo Meridio required the largest moment to push the plant over (mean $S_A = 0.45$ N-m)

compared to other cultivars (mean $S_A = 0.20$ N-m) (Fig. A6.1e); still, Massimo Meridio's S_A was lower than its M_p . The maximum S_A of all cultivars over the entire observation period did not exceed 1 N-m, except for one Marco Aurelio sample (1.8 N-m at the milking stage) (Fig. A6.1e). The variation of SF_A across different growth stages is shown in Fig. 6.6f. The values of SF_A demonstrated a statistically significant decreasing trend as the crop matured ($p < 0.001$, Fig. 6.6f). SF_A was lowest during the flowering and grain filling phenological stages. The mean SF_A from the booting stage onwards was ≤ 1 , which indicated that root lodging might have occurred from any point thereon.

6.3.2 Field-measured safety factor versus lodging susceptibility score of different cultivars

We further assessed the correlation between cultivar lodging susceptibility score (LSS) and SF_A (Fig. 6.7). Based on the LSS, we categorized the cultivars as “low score” (< 4.5) and “high score” (≥ 4.5) where the cultivars falling in the “high score” group were highly susceptible to lodging. A total of 44 out of 47 (i.e., 94%) samples were observed to be lodged in the study site and 30% of the samples falling in the “low score” group still lodged, showing that the cultivars with low LSS were, to some extent, still prone to lodging. This observation is not surprising because “cultivar susceptibility” is only one of the components of lodging risk that is strongly dependent on i) site-specific crop growth (i.e. seasonal susceptibility - SF_A) and ii) external driving forces (e.g. wind and rain).

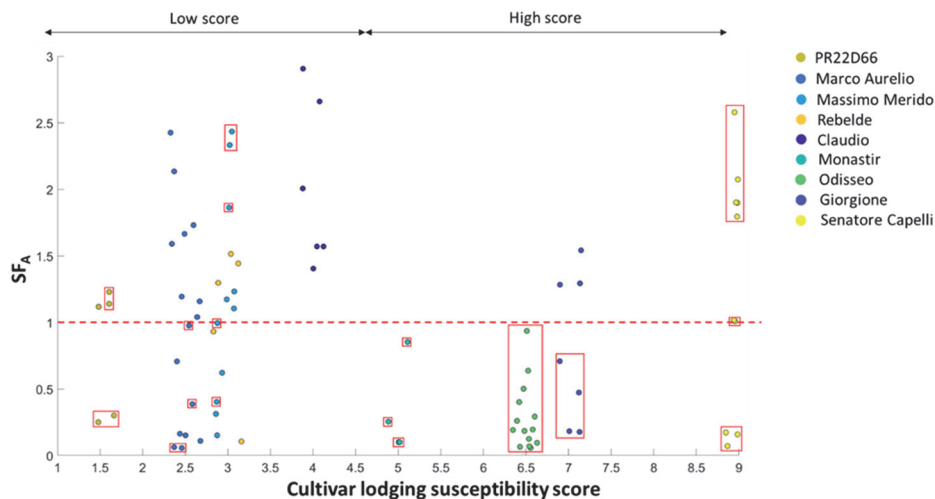


Fig. 6.7. Variation of the field-measured SF_A for different cultivar lodging susceptibility scores along the season ($n=90$). Cultivars are categorized into low (< 4.5) and high score (≥ 4.5) groups. The observed lodged samples are highlighted with red boxes. The dashed

red line represents the critical threshold at $SF_A=1$. Plots with $SF_A \leq 1$ signify that the crop is at high risk of being root lodged due to the self-weight moment while the ones with $SF_A > 1$ are at relatively lower root lodging risk.

6.3.3 Correlation analyses between remote sensing-based metrics and SF_A

Pearson correlation coefficients were used to quantify the relationship between RS-based metrics and SF_A and to identify the best performing metrics. Sentinel-1 has a shorter revisit time than RADARSAT-2 resulting in more images in the time-series. Therefore, 90 and 71 field samples were measured across the season for the analysis of Sentinel-1 and RADARSAT-2 data, respectively. Six out of nine Sentinel-1 metrics and 23 out of 39 RADARSAT-2 metrics had statistically significant correlations with SF_A (Fig. 6.8, Table A6.2, A6.3).

For Sentinel-1, the coherence in VV polarization (γ_{vv}) showed the highest positive correlation with SF_A ($r = 0.64$) (Fig. 6.8a), suggesting that γ_{vv} provided the most reliable information for monitoring SF_A over the study area. Strong negative correlations were observed between SF_A and the $\sigma_{VH/VV}$, Anisotropy and Radar Vegetation Index (RVI) ($-0.57 < r < -0.60$) (Fig. 8a). High anisotropic scattering (>0.5) corresponded to low SF_A values (<1) while higher SF_A values (>1) exhibited low anisotropic scattering (<0.3).

For RADARSAT-2, the volume scattering component derived from Pauli decomposition (Pauli_vol) had the highest correlation with SF_A ($r = 0.71$) (Fig. 6.8b). The Span, biomass index and surface scattering component derived from Cloude decomposition (Cloude_surf) showed the same trend in correlation with SF_A ($r = 0.69$) (Fig. 6.8b). The correlation of SF_A with double-bounce scattering components derived from Pauli (Pauli_dbl, $r = 0.51$), Freeman-Durden (FD_dbl, $r = 0.37$) and Yamaguchi (Yama_dbl, $r = 0.24$) decomposition were statistically significant but lower than the other metrics (Table A6.3).

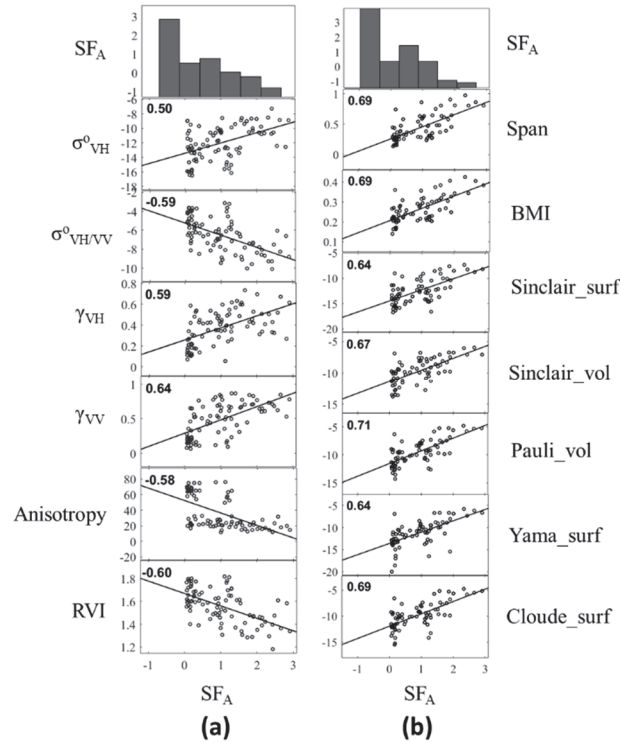


Fig. 6.8. Pearson correlation scatterplots of field measured SF_A against satellite metrics. Pearson correlation scatter plots of the most significant satellite metrics derived from (a) Sentinel-1 ($n=90$), (b) RADARSAT-2 ($n=71$) data and the field measured safety factor against root lodging (SF_A). The variation in the number of samples (n) for Sentinel-1 and RADARSAT-2 data is due to the difference in image availability between the two. All shown correlation coefficients between SF_A and satellite metrics are statistically significant at $p = 0.01$. σ^0_{VH} is the backscattering coefficient in VH polarization, $\sigma^0_{VH/VV}$ is the ratio of the backscattering coefficients in VH and VV polarizations, γ_{VH} , γ_{VV} are the interferometric coherences in VH and VV polarizations, RVI is the radar vegetation index, BMI is the biomass index, Sinclair_vol and Pauli_vol are the volume scattering components derived from Sinclair and Pauli decomposition respectively, and Yama_surf and Cloude_surf are the surface scattering components derived from Yamaguchi and Cloude decomposition respectively.

6.3.4 Estimation and mapping of the safety factor

The XGB regression models were trained and validated using a five-fold Venetian blinds cross-validation. Fig. 6.9 displays the scatterplots between measured and predicted SF_A values, the cross-validated coefficient of determination (R^2_{CV}) and root mean square error ($RMSE_{CV}$) based on a regression analysis of SF_A against RS-based metrics. The predicted SF_A values were in strong agreement with the measured values when the backscattering coefficients,

coherence, and polarimetric metrics (listed in Table A6.2) derived from Sentinel-1 were used as inputs, ($R^2_{CV} = 0.73$) (Fig. 6.9a). However, the results were penalized by some degree of underestimation for the high SF_A values (>2), resulting in an $RMSE_{CV}$ of 0.59. This is evident from the dispersion of the samples around the 1:1 line in Fig. 6.9a. The degree of underestimation reduced when backscattering coefficients and polarimetric metrics derived from RADARSAT-2 were used, resulting in an $RMSE_{CV}$ of 0.54 (Fig. 6.9b). The predicted SF_A correlated strongly with the measured SF_A ($R^2_{CV} = 0.84$).

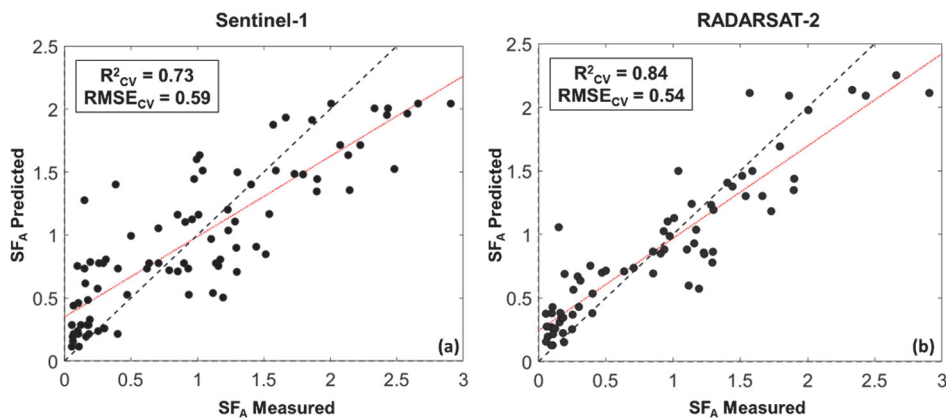


Fig. 6.9. Relationships between measured and predicted SF_A for Sentinel-1 and RADARSAT-2. Scatterplots show the relations between measured and predicted SF_A values obtained using cross-validated regression models for (a) Sentinel-1 ($n=90$) and (b) RADARSAT-2 ($n=71$) data. The variation in the number of samples (n) for Sentinel-1 and RADARSAT-2 data is due to the difference in the image availability for each sensor. The field data has been compiled for the entire season for different wheat cultivars. The black dashed line is the 1:1 line, while the red dotted line is the modeled regression line. The R^2_{CV} is the cross-validated coefficient of determination, and $RMSE_{CV}$ is the cross-validated root mean square error for each model.

Cross validated XGB models were applied over the study site to map the spatial and temporal variability of SF_A . Fig. 6.10 illustrates the predicted SF_A maps derived from Sentinel-1 (March 26) and RADARSAT-2 (April 2) datasets over the wheat fields. These dates were selected to demonstrate the potential of indicating root lodging susceptibility early in the season (early spring) when the crop is in the stem elongation growth stage. The underestimation of high SF_A values is apparent in the Sentinel-1 map (Fig. 6.10a). However, the spatial distribution of predicted SF_A in both maps shows that areas where SF_A is 1 (or less), it is likely that the gravitational forces due to M_P of the whole plant alone

could cause lodging. The areas with $SF_A > 1$ indicate that M_P alone may not cause lodging.

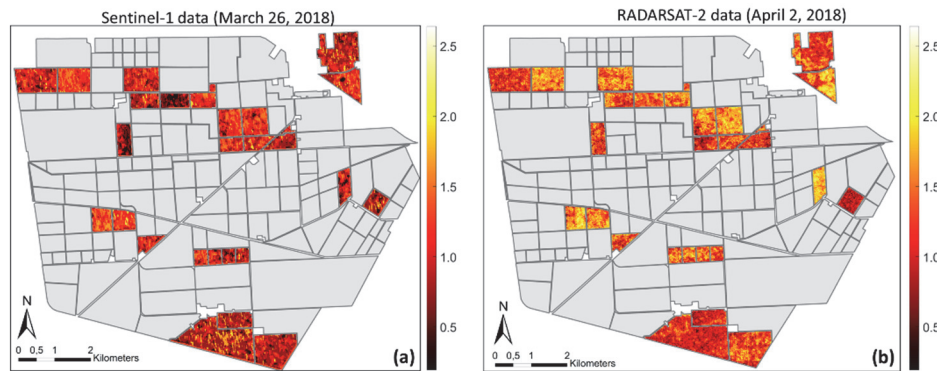


Fig. 6.10. Spatial distribution of SF_A in the study area. SF_A in wheat fields in study site obtained from the cross-validated regression models using inputs from (a) Sentinel-1 (image on March 26, 2018) and (b) RADARSAT-2 (image on April 2, 2018). Wheat was in the stem elongation growth stage. The farm boundaries are also overlaid on the maps. Non-wheat fields are gray. “RADARSAT-2 Data and Products. MacDonald, Dettwiler and Associates Ltd. (2018) – All Rights Reserved. RADARSAT is an official trademark of the Canadian Space Agency.”

6.4 Discussion

6.4.1 Safety factor prediction using Sentinel-1 and RADARSAT-2 data

Microwave scattering is mainly governed by crop macrostructure (such as plant density or row spacing), plant dielectric properties and canopy structure (shape, size and orientation of plant constituents) (Wang et al., 2019). C-band SAR, to a certain degree, can penetrate the crop canopy, which also results in a contribution from the soil in the total backscatter signal (soil roughness and moisture). This is especially true in the early growth stages when the crop cover is less dense. Polarimetric decomposition parameters can be used to separate the vegetation contributions from the total backscatter. The better performance of the RADARSAT-2 (quad-polarization mode with HH, HV, VH and VV channels) model can be attributed to a rich set of polarimetric decomposition metrics. Sentinel-1 has a higher revisit time, but its data is available only in the dual-polarization mode, which restricts the usage to just one cross-polar (VH) and one copolar channel (VV). This results in fewer metrics and lower SF_A retrieval accuracy. However, the synergic use of backscattering coefficients and

interferometric coherence in Sentinel-1 enhanced the estimation of SF_A ($R^2_{CV} = 0.73$, $RMSE_{CV} = 0.59$), over using backscattering coefficients alone.

Even though the scattering from crop and attenuation effects are complexly coupled in wheat (Ferrazzoli, 2002; Wang et al., 2019), the XGB models were able to capture the coupling pattern, resulting in a robust SF_A retrieval ($R^2_{CV} > 0.70$; $RMSE_{CV} < 0.60$) (Fig. 6.9). However, there are two issues that should be mentioned here. Firstly, the underestimation of both models at high SF_A values (> 2) can perhaps be explained by the saturation of the backscatter and polarimetric parameters with high plant height and fresh aerial biomass values due to pronounced scattering from wheat heads (Bouman and van Kasteren, 1989; Harfenmeister et al., 2019; Yan et al., 2019). Moreover, the general tendency of the regression models to underestimate large magnitudes cannot be neglected. This phenomenon has been reported in diverse experimental settings and is likely to represent a general response bias under uncertainty (Karolis et al., 2011). Despite this, the critical SF_A value (close to 1) required to assess root lodging susceptibility in wheat could be detected by both Sentinel-1 and RADARSAT-2-based models (Fig. 6.9). Hence, the identified underestimation is not considered critical for highlighting spatially explicit zones of potential lodging susceptibility that can occur later in the crop season. The predicted SF_A maps demonstrate the capability of SAR data for geospatial mapping SF_A in wheat and can consequently be used as an indicator of root lodging susceptibility early in the season. Secondly, it is possible that the relationship between SF_A and SAR parameters may potentially be confounded by the variations in crop biomass, which is highly correlated with SF_A ($r = -0.63$). The correlation of biomass with SF_A may also largely reflect the sensitivity of the radar measurements to SF_A . The accuracy may further be improved by reducing the effects of such confounding factors and will be addressed in our further work.

6.4.2 Relationship between satellite metrics and SF_A

The correlation analyses between the RS-based metrics and field measured SF_A identified the most significant parameters for estimating SF_A from satellite data. In general, the r values were higher for RADARSAT-2 derived metrics (Fig. 6.8b). The microwave signal is highly sensitive to the structure and geometry of the canopy and is a function of size, orientation and density of the scatterers/target (Chauhan et al., 2018). As a microwave signal hits the crop canopy, there are three forms of scattering mechanisms that can occur: surface/single-bounce, double-bounce, and volume scattering. The higher relative correlation of the

volume scattering components such as Pauli_vol ($r = 0.71$) and Sinclair_vol ($r = 0.67$) (Fig. 8b) with SF_A possibly indicates the dominance of the volume scattering mechanism as the crop grows. The decrease in SF_A across different growth stages (Fig. 6f) indicates the increasing susceptibility of root lodging during the season as the M_P exceeded S_A in our study site. However, we would like to emphasize that the decreasing trend of SF_A (Fig. 6f) over the season is not always the case (as observed in our study site). If the root structure is strong enough to compensate for the increased M_P , the safety factor may show an increasing trend (Crook and Ennos, 1994). The decrease in SF_A with the crop growth in our case is because the rate of increase in M_P is much higher than the increase in S_A (Fig. 6d, 6e). And since the increase in M_P (which is composed of biomass, crop height and crop angle of inclination) is the main factor here governing the SF_A trend, the volumetric component is increasing due to increasing crop volume.

It should also be emphasized here that the contribution of azimuth slope and soil roughness on elevated cross-polarized response can be considered negligible here since (i) we applied orientation angle correction to remove the orientation angle shift caused by azimuth slopes from the polarimetric SAR data, (ii) unlike lower frequencies (such as L-band), higher frequency PolSAR responses (such as from C-band) are less sensitive to azimuth slope variations, because electromagnetic waves with shorter wavelengths are less penetrative and more sensitive to small scatterers (Lee and Pottier, 2017) and lastly (iii) wheat fields had similar soil roughness, approximately 1 cm in average, with minimal changes during the entire crop development.

We also found evidence of a certain degree of surface scattering from the wheat fields, which is depicted by a moderate correlation between SF_A and the Cloude_surf metric ($r = 0.69$) (Fig. 6.8b). The presence of surface scattering confirms some degree of backscatter contribution from the soil attenuated by vegetation canopy. Typically, either of the scattering mechanisms dominates, however for distributed targets (such as an agricultural field), secondary or tertiary scattering mechanisms can also occur (Steele-Dunne et al., 2017). At the beginning of the season when the crop cover is less dense, surface scattering dominates (soil is the dominant contributing factor) and with the development of crop canopy volume scattering becomes more dominant, although the surface scattering is still evident, due to a quite probable horizontal orientation resulting from the bending of leaves (Chauhan et al., 2018). Furthermore, SF_A is a

parameter that is sensitive to both crop (M_P) and soil components (S_A). Therefore, our analyses showed that a mixture of volume and surface scattering types characterized the crop canopy. Similar observations were also made by Kar et al. (2017).

For Sentinel-1 data, the interferometric coherence in the VV polarization showed the highest positive correlation with SF_A ($r = 0.64$) (Fig. 6.8a). Interferometric coherence at any polarization is not only sensitive to the dielectric properties, orientation and shape of plant constituents but also the vertical structure of the plant (Lopez-Sanchez and Ballester-Berman, 2009). Studies have shown that a strong linear relationship exists between plant height and coherence (Khabbazan et al., 2019; Vreugdenhil et al., 2018). At the same time, at VV polarization, the contribution from the upper canopy dominates for incidence angles $>37^\circ$, due to the presence of flag leaves and ears (Brown et al., 2003). With the increasing plant height (Fig. 6.6a) and fresh biomass (Fig. 6.6c), the SF_A decreases (Fig. 6.6f). As plant height is inversely proportionate to the interferometric coherence (Engdahl et al., 2001), a positive correlation emerged between SF_A and VV coherence values. We should also emphasize here that based on the insights gained from previous studies (Ghosh et al., 2020; Khabbazan et al., 2019; Shang et al., 2020), we assumed that the changes in vegetation structure between the two Sentinel-1 SAR acquisitions resulted in temporal decorrelation. The negative correlation of SF_A with RVI and $\sigma_{VH/VV}^\circ$ (Fig. 6.8a) could be attributed to the increase in RVI and $\sigma_{VH/VV}^\circ$ from booting to flowering as the plant biomass accumulates. The increasing RVI and $\sigma_{VH/VV}^\circ$ at the beginning of the vegetation period indicates the attenuation of the radar signal by growing vegetation. Similar results have also been reported by Mandal et al. (2020) for wheat crop during these growth stages. Furthermore, a high anisotropic scattering (>0.5) for low SF_A values (<1) indicates two dominant scattering mechanisms with almost equal probability and a less significant third scattering mechanism. Lower anisotropic scattering (<0.3) for higher SF_A values (>1), on the other hand, shows that there is only one dominant scattering mechanism with two non-negligible secondary mechanisms with equal importance. However, it is difficult to point out which scattering mechanism is dominant and which is not solely based on dual-polarimetric Sentinel-1 data. The polarimetric parameters derived from RADARSAT-2 quad-pol data complement these observations (as shown above).

Furthermore, there are studies that explain the effect of soil moisture, roughness and texture on SAR backscatter (Balenzano et al., 2010; Srivastava et al., 2003),

there is limited knowledge on the how SAR data is responsive to soil structural properties such as soil shear strength and root plate diameter (factors that govern root anchorage strength). An analysis in this regard is beyond the scope of this study and should be researched in future studies. A study done by Rabus et al. (2010) does shed some light on how backscatter and interferometric phase information can infer near soil structural parameters such as vertical gradients and inhomogeneities, the research is in a very nascent stage and was performed in simulated conditions. However, the results are promising and must be explored further to study other soil structural traits (such as root anchorage strength).

Overall, although both Sentinel-1 and Radarsat-2 sensors operate at the same frequency C-band, differences in other sensor characteristics such as polarization (dual and quad-pol), incidence angle (40° and 27° - 41°), radiometric accuracy (1 dB and <1 dB) and spatial resolution (15×15 m and 10×10 m) resulted in varying performances of the two sensors. The r values for RVI (radar vegetation index) (Table A6.2, A6.3) are particularly different for Sentinel-1 and RADARSAT-2. This could be attributed to different polarization channels that are used in the formulation of RVI for Sentinel-1 ($RVI = 4 \sigma_{VH}^o / (\sigma_{VH}^o + \sigma_{VV}^o)$) and RADARSAT-2 ($RVI = 8 \sigma_{HV}^o / (\sigma_{HH}^o + \sigma_{VV}^o + 2 \sigma_{HV}^o)$).

6.4.3 Variability in the field measured crop biophysical parameters

Plant height (H_P) and height at the center of gravity (h_P) are important factors influencing lodging susceptibility in wheat (Berry et al., 2000). h_P is influenced by both H_P and ear biomass (Berry et al., 2000). With grain filling, ear biomass increases, and straw biomass reduces, thus raising h_P . The self-weight moment of the whole plant (M_P), which approximates the wind-induced base bending moment that a plant experiences, increased as the crop matured (Fig. 6.6d). This could be due to the increase in both h_P and FB_P .

Root system architecture plays an essential role in anchoring the plant to soil. It has been demonstrated that S_A is a function of mechanical properties such as root plate diameter and soil shear strength (van Delden et al., 2010) (Fig. 6.1). S_A increased as the crop matured, which is possibly due to the increase in the depth and spread of the root plate diameter (Berry et al., 2000) The susceptibility of root lodging increases if M_P exceeds S_A (Crook and Ennos, 1993) and can be quantified using SF_A (equation 6.2). In most cases, S_A was less than M_P (Fig. 6.6d, e). A relatively high S_A (1.8 N-m) for one of Marco Aurelio samples can be explained by the low seed rate in this plot, which might have increased the S_A by

increasing the root plate spread (Berry et al., 2000). The decrease in SF_A across different growth stages (Fig. 6.6f) indicated the increasing susceptibility of root lodging during the season due to the plant self-weight moment alone as M_P exceeded S_A . Lower S_A resulted in a lower SF_A later in the season, implying that root-soil anchorage may not be able to resist the overturning moments produced by the plant's self-weight, even though only gravitational forces were considered. Therefore S_A should be improved to increase root lodging resistance (Wu et al., 2019). A rigid root system can be developed by enabling enlarged root spread through low seed rate, increasing soil shear strength and stimulating greater proportion of assimilates to be partitioned into the roots (Li et al., 2018; Wu et al., 2012). SF_A does not account for the forces generated by wind, which can further intensify the overturning moments and can progressively weaken the root-soil anchorage (Coutts, 1983).

6.4.4 Field measured safety factor versus observed lodging

The observed rate of lodging was high throughout the growing season, with most cases coinciding with grain filling when the ears were heaviest. Root lodging was the primary cause of failure (80% of cases). The measured SF_A was largely consistent with field recorded observations of lodging (Fig. 6.11). The time when SF_A dropped to the absolute critical value of 1, coincided with the observed onset of lodging in the field (i.e., at the end of the booting stage) (Fig. 6.6f); 32 samples were non-lodged while 58 samples had lodged with different degrees of severity. Furthermore, as shown in Fig. 11, 24 out of 32 healthy samples corresponded to $SF_A > 1$, i.e. 75% of the samples were correctly identified as having no root lodging susceptibility using the SF_A while 42 out of 58 lodged samples corresponded to $SF_A \leq 1$, meaning that 73% of the samples were correctly identified as susceptible to root lodging using the SF_A (Fig. 6.11). A comparison within and across different wheat cultivars at specific growth stages is also presented in the appendix (Table A6.3) demonstrating how the root lodging susceptibility (high/low) predicted using SF_A correlate with the actual crop condition (lodged/non-lodged) observed on the field around the harvest time. Based on the analysis, we can say that the SF_A assessment resulted in an overall agreement with the observed lodging phenomena.

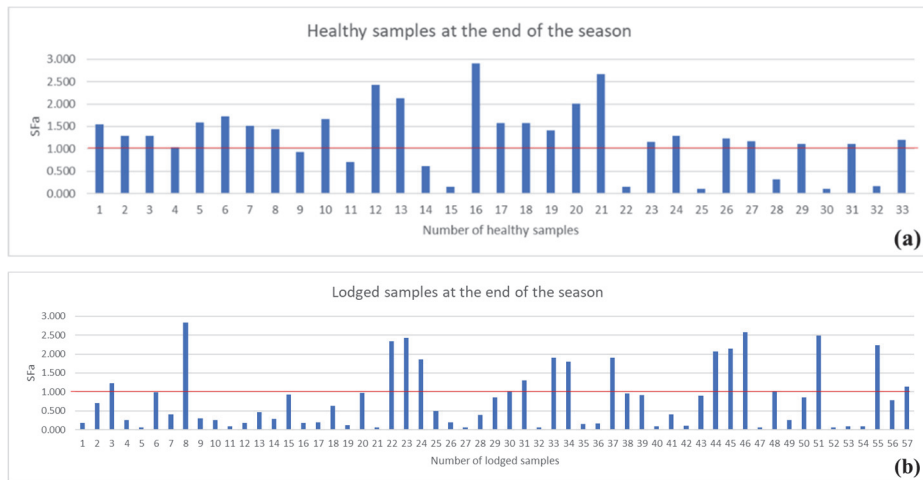


Fig. 6.11. Distribution of the field measured samples that remained (a) healthy and (b) were lodged at the end of the season versus the field-measured safety factor values. The red line indicates the safety factor lodging threshold (i.e. $SF_A=1$) considered in this study.

Currently, LSS serves as the only measure for farmers to indicate the theoretical relative lodging susceptibility for each cultivar. However, LSS does not explain the reason for a high or low susceptibility of a cultivar. The relative strength of the stem base and the roots as depicted by M_P and S_A (see Fig. A6.1d, e) can explain the variation in LSS for each cultivar. For instance, the high LSS (6.5) of the cultivar Odisseo is probably explained by very low root anchorage strength (S_A) and safety factor (SF_A), resulting from poor root structure (Fig. A6.1). Similarly, a very low self-weight moment (M_P) for the cultivar Senatore Capelli, indicates that poor stem structure might explain a high LSS (9) (Fig. A6.1). This information can be beneficial as it gives a better idea to the farmers about which section of the plant to target for lodging control. In this context, for a cultivar such as Odisseo, it might be more important to take measures to boost the soil/root structure (e.g. through lower seed rate or rolling), while for Senatore Capelli with weaker stem structure, using plant growth regulators can be useful. For cultivars with a good root and stem structure (such as Monastir), careful management along with low plant growth regulator input could be sufficient to reduce lodging susceptibility. Thus, an understanding in the variation of SF_A (and its components), in addition to a cultivar LSS, can result in informed cultivar choice.

6.4.5 Recommendations and perspectives

The primary advantage of using a safety factor against root lodging (SF_A) as an indicator of crop lodging susceptibility is that it is simple, allows quantitative analysis of the variation in root lodging resistance and, above all, is detectable over large areas using operational remote sensing platforms. The RS model can be applied to other locations under similar conditions, but this will require model validation using a small number of SF_A field measurements. The SF_A measure thus constitutes a state-of-the-art approach for the assessment of root lodging susceptibility early in the season. Information about SF_A can be used to develop optimum crop management practices in almost real-time, for instance, adjusting the use of plant growth regulators later in the season, as the maps can be generated early in the spring when the crop completes the stem elongation period. The use of SF_A as an indicator to guide nitrogen fertilizer applications and mitigate lodging susceptibility would further validate the effectiveness of the SF_A method.

SF_A does not directly account for wind or rain-induced forces; neither does SF_A explicitly consider the environmental or other management-related parameters, SF_A is simply a measure of lodging susceptibility. This study provides a basis for future research efforts that could benefit from the incorporation of the SF_A parameter in lodging risk assessments. For example, SF_A could be combined with long term climate averages (for baseline risks), forecasts of precipitation and wind gusts, soil properties and other remotely sensed crops biophysical and biochemical parameters (such as plant area index and plant nitrogen) to provide more accurate and timely risk assessments. Also, despite the diverse dataset used in this work, the robustness and reproducibility must be assessed further in other environmental, soil and management conditions for wheat as well as other crops using a multi-season and more contrasted dataset. Although stem lodging was almost neglectable for the cultivars in our study area (only 15 plots showed an occurrence of stem lodging contrary to 30 plots with root lodging), an RS-based investigation of the safety factors against stem lodging is another potential topic of research. Regardless of the assumptions behind the formulation of SF_A , our study demonstrates that time-series of RS data can be used effectively to estimate root lodging susceptibility at the field scale and offers a preview of further opportunities in making lodging risk analysis more robust and accurate.

6.5 Conclusions

This study aims to quantify the utility of fine spatial resolution SAR imagery as acquired from commercial and open-access satellite platforms for the estimation of SF_A in wheat crop. First, we analyzed and interpreted the temporal trend of the

field measurements across different growth stages. A suite of RS-based metrics was also correlated with the field measured SF_A for different plots to understand the strength of correlation and enable interpretation of the regression models. Lastly, we developed two XGB regression models using the inputs from Sentinel-1 and RADARSAT-2 data to estimate SF_A and map its spatial distribution across the study site. We also validated field measured SF_A with the occurrence of lodging in the field. The key conclusions are summarized below:

- a) The SF_A showed a decreasing trend as the crop matured, with the lowest values during the flowering and grain filling period when the lodging risk is the highest.
- b) In general, most of the RS-based metrics showed a statistically significant correlation with SF_A values, particularly the biomass index, VV coherence, span, Pauli volume scattering component and Cloude surface scattering components ($r > 0.60$).
- c) The cross-validated XGB model using the inputs from RADARSAT-2 data ($R_{CV}^2 = 0.84$, $RMSE_{CV} = 0.54$) outperformed the Sentinel-1 model ($R_{CV}^2 = 0.73$, $RMSE_{CV} = 0.59$), with some degree of underestimation at high SF_A (> 2) values. The resulting maps also successfully captured the spatial variation in SF_A .
- d) The field measured SF_A correlated well with the lodging observed on the field. The time when SF_A reached the critical threshold of 1, coincided with the time when the first few instances of lodging were observed in the field (i.e. during the booting stage). 70% of the actual healthy samples corresponded to $SF_A > 1$ while 74% of the lodged samples had $SF_A \leq 1$, which indicates the utility of RS-derived SF_A as an early measure of root lodging risk.

The SF_A measure constitutes a state-of-the-art approach in the RS community for the assessment of root lodging susceptibility early in the season. However, we emphasise that SF_A does not account for the external wind or rain-induced forces and neither the environmental and other management-related parameters are considered in this study. These parameters when incorporated in a model can provide more robust lodging risk estimates. This study provides a basis for future research efforts which could benefit from the incorporation of SF_A parameter along with other lodging sensitive parameters in a lodging risk model. The investigation of the assessment of RS-based stem lodging susceptibility using safety factors against stem lodging is another potential topic of research.

Mapping of wheat lodging susceptibility with Synthetic Aperture Radar data

Nevertheless, this study demonstrates that the time-series RS data from different sources can be used effectively for detecting root lodging susceptibility at the field scale.

Appendix

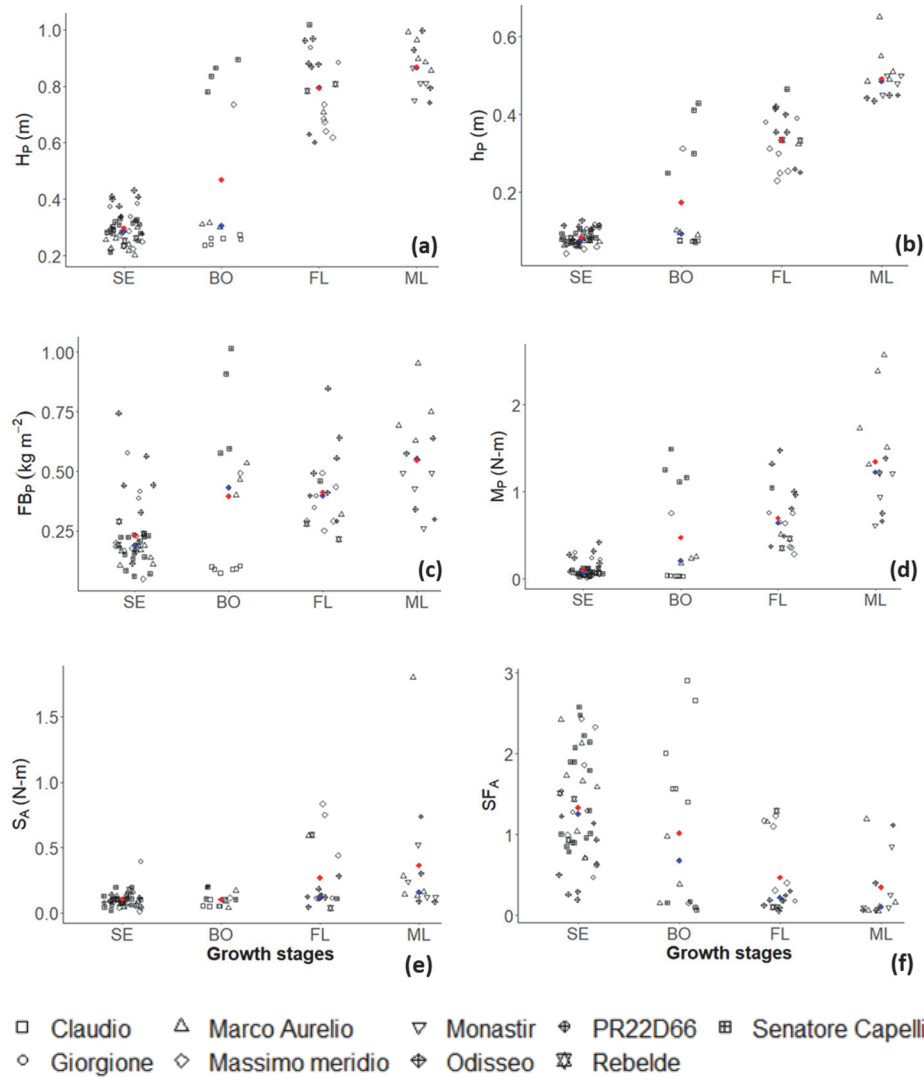


Fig. A6.1. Variation of crop biophysical parameters across the growing season for different wheat cultivars. Boxplots illustrate plot-level variation in field-measured crop biophysical parameters: (a) plant height (H_P , m), (b) plant height at the centre of gravity (h_P , m), (c) fresh biomass (FB_P , kg m^{-2}), (d) self-weight moment of the whole plant at the crop angle of inclination of 30° (M_P , N-m), (e) anchorage strength at a crop angle of inclination of 30° (S_A , N-m) and (f) safety factor against root lodging at a crop angle of inclination of 30° (SF_A) across different growth stages ($n=90$): stem elongation (SE), booting (BO), flowering (FL) and milking (ML). The blue and red diamonds are the median and mean values, respectively.

Table A6.1. Pearson correlation coefficients (r) and p -values between metrics derived from Sentinel-1 data ($n=90$) and the safety factor against root lodging at a crop angle of inclination of 30°. *** indicates values are significant at $p=0.001$ level of significance.

	Satellite metrics	r	p -value
1	VH backscattering coefficient	0.50	5.90e-03***
2	VV backscattering coefficient	0.09	0.4113
3	Ratio of VH and VV backscattering coefficient (VH/VV)	-0.59	9.49e-06***
4	VH coherence	0.59	1.40e-05***
5	VV coherence	0.64	2.13e-07***
6	Entropy	-0.11	0.3236
7	Alpha	0.10	0.3349
8	Anisotropy	-0.58	2.78e-05***
9	Radar vegetation index (RVI)	-0.60	5.42e-06***

Table A6.2. Pearson correlation coefficients (r) and p -values between metrics derived from RADARSAT-1 data ($n=71$) and the safety factor against root lodging at a crop angle of inclination of 30°. *** indicates values are significant at $p=0.001$ level of significance.

	Satellite metrics	r	p -value
1	HH backscattering coefficient	0.51	5.03e-06***
2	HV backscattering coefficient	0.54	1.02e-06***
3	VV backscattering coefficient	0.56	3.39e-07***
4	Span	0.69	2.29e-11***
5	Pedestal height	-0.22	0.0672
6	Radar vegetation index (RVI)	-0.31	0.9140
7	Radar forest degradation index (RFDI)	0.04	0.7096
8	Canopy scattering index (CSI)	0.14	0.2549
9	Volume scattering index (VSI)	-0.13	0.2930
10	Biomass index (BMI)	0.69	3.88e-11***
11	Ratio of HH and VV backscattering coefficient	-0.11	0.3578
12	Ratio of HH and HV backscattering coefficient (HH/HV)	0.10	0.4274
13	Ratio of VH and VV backscattering coefficient (VH/VV)	-0.58	5.87e-04***
14	Sinclair surf	0.64	1.53e-09***
15	Sinclair dbl	0.51	5.67e-06***
16	Sinclair vol	0.67	1.52e-10***
17	Pauli surf	0.44	1.34e-04***
18	Pauli dbl	0.51	5.67e-06***

19	Pauli_vol	0.71	2.82e-12***
20	Freeman Durden_dbl	0.37	0.001***
21	Freeman Durden_vol	0.51	6.83e-06***
22	Freeman Durden_surf	0.48	2.75e-05***
23	Yamaguchi_dbl	0.24	0.0469*
24	Yamaguchi_vol	0.53	1.59e-06***
25	Yamaguchi_surf	0.64	2.28e-09***
26	Yamaguchi_hlx	0.42	3.04e-04***
27	Van Zyl_dbl	0.15	0.2277
28	Van Zyl_vol	0.51	4.38e-06***
29	Van Zyl_sur	0.58	9.35e-08***
30	Cloude_dbl	-0.004	0.9732
31	Cloude_vol	0.11	0.3800
32	Cloude_surf	0.69	2.95e-11***
33	Entropy	-0.26	0.0311*
34	Anisotropy	-0.11	0.3730
35	Alpha	-0.34	0.0032**
36	Psi	-0.004	0.9684
37	Tau	-0.02	0.9010
38	Alpha_touzi	-0.30	0.0109**
39	Phi	0.15	0.2266

Table A6.3. Comparisons within and across wheat cultivars demonstrating the agreement of lodging susceptibility (in bold) predicted based on safety factor (high/low) and the actual crop condition (lodged/non-lodged) observed on the field at specific growth stages.

Cultivar: Odisseo, Growth stage: Stem elongation

Field measured safety factor value	Lodging susceptibility based on the safety factor	Crop condition as observed on the field
0.260	High	Lodged
0.292	High	Lodged
0.936	High	Lodged
0.637	High	Lodged
0.501	High	Lodged
0.195	High	Lodged

Cultivar: Marco Aurelio, Growth stage: Stem elongation

Field measured safety factor value	Lodging susceptibility based on the safety factor	Crop condition as observed on the field
1.665	Low	Non-Lodged
1.040	Low	Non-Lodged
1.590	Low	Non-Lodged
2.425	Low	Non-Lodged
2.134	Low	Non-Lodged

Mapping of wheat lodging susceptibility with Synthetic Aperture Radar data

Cultivar: Senatore Capelli, **Growth stage:** Stem elongation

Field measured safety factor value	Lodging susceptibility based on the safety factor	Crop condition as observed on the field
0.960	High	Lodged
0.909	High	Lodged
0.851	High	Lodged
1.008	Low	Lodged
0.899	High	Lodged
1.017	Low	Lodged
0.788	High	Lodged

Cultivar: Claudio, **Growth stage:** Booting

Field measured safety factor value	Lodging susceptibility based on the safety factor	Crop condition as observed on the field
2.906	Low	Non-Lodged
1.570	Low	Non-Lodged
1.570	Low	Non-Lodged
1.404	Low	Non-Lodged
2.006	Low	Non-Lodged
0.659	High	Non-Lodged

Cultivar: Massimo Meridio, **Growth stage:** Stem elongation

Field measured safety factor value	Lodging susceptibility based on the safety factor	Crop condition as observed on the field
2.332	Low	Lodged
2.433	Low	Lodged
1.863	Low	Non-Lodged
0.621	High	Lodged
1.229	Low	Lodged

Chapter-7

Synthesis: Remote sensing of wheat lodging and its susceptibility

7.1 Summary/Introduction

A quantitative understanding of the spatio-temporal variability of crop lodging over synoptic scales is important for targeted crop management and reducing yield losses. In situ methods to assess crop lodging are sparse, subjective and costly and therefore not sufficient for monitoring the heterogeneous distribution of lodging in vast agricultural fields. High-resolution time-series RS data is highly beneficial for crop lodging monitoring as it provides timely and precise information on the change in crop biophysical traits.

This research aimed to investigate and formulate a robust methodology for lodging detection, characterisation and susceptibility mapping in wheat using RS techniques. The research is summarised in Fig. 7.1. We first carried out an extensive literature review in Chapter-2 that enabled us to understand the state-of-the-art and identify unanswered research questions in the area of crop lodging assessment. Subsequently, we characterised lodging using RS in three ways: through i) quantification of the crop angle of inclination (CAI) as a measure of wheat lodging stages (Chapter-3); ii) classification of wheat crop lodging severity using a lodging score (Chapter-4) and; iii) identifying the time of lodging incidence in wheat using time-series image analysis based on lodging score (Chapter-5). Finally, in Chapter-6, we mapped lodging susceptibility in wheat with a safety factor against root lodging. In this context, we analysed the performances of freely available Copernicus data (Sentinel-1, Sentinel-2) as well as commercial (RADARSAT-2) satellite data sources to examine the trade-offs between temporal, spatial and spectral (or polarimetric) resolution associated with crop lodging assessment. We made temporal field measurements in Bonifiche Ferraresi farm, Italy covering the critical wheat phenological stages from stem elongation (GS30) until ripening (GS99) between March-June 2018. To analyse the field and RS data, we further used different machine learning algorithms such as support vector regression, partial least square discriminant analysis and extreme gradient boosting tree regression.

The main findings of this research are discussed in this chapter and summarised as follows: a) the scientific consensus on crop lodging assessment using RS data is in the nascent stage and is still evolving. Very few studies (22) published between 1951-2018 demonstrated the potential of RS data for crop lodging

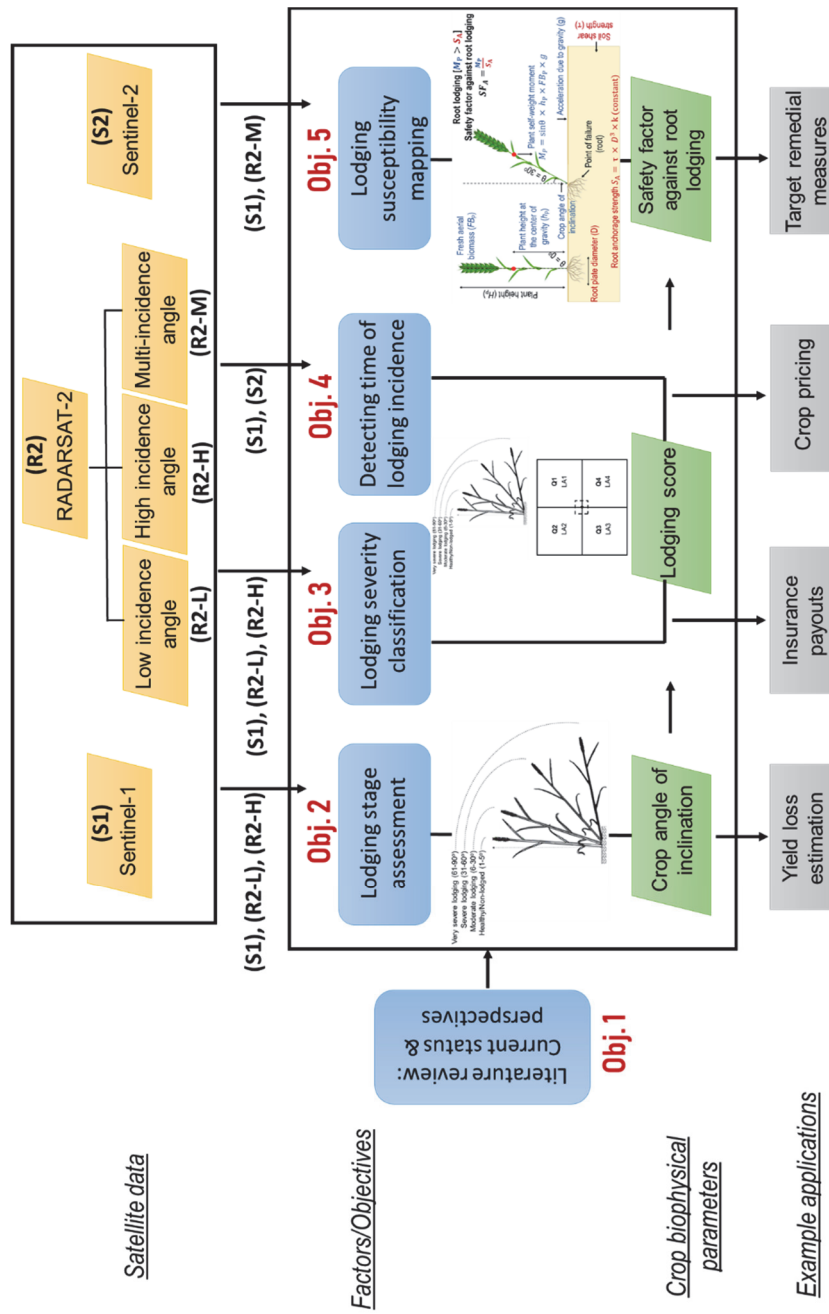


Fig. 7.1. Flowchart illustrating the research summary. The satellite data used as input is colour coded as yellow, the objectives are in blue, the crop biophysical parameters retrieved/used are in green and the example applications are in grey.

assessment, particularly at regional scales using high-resolution satellite data (see section 7.2); b) low incidence angle ($\sim 27^\circ$) quad-polarimetric RADARSAT-2 data with a spatial resolution of 10 m was found to be sufficient in estimating crop lodging-related structural parameters such as CAI ($R^2_{CV}=0.87$, $RMSE_{CV}=8.89^\circ$) (see section 7.3) and classifying lodging severity-based on lodging score (overall accuracy=72%, Kappa=0.60) (see section 7.4); c) the use of dense-time series Sentinel-1 SAR data in combination with multispectral Sentinel-2 data enabled the identification of a plausible time of lodging incidence and could distinguish between different degrees of lodging severity in wheat (moderate, severe and very severe) (see section 7.5) and d) multi-incidence angle RADARSAT-2 data enabled root lodging susceptibility mapping through the estimation of safety factor with an R^2_{CV} of 0.84 and $RMSE_{CV}$ of 0.54 (see section 7.6). Finally, in this chapter, we discuss the future opportunities for crop lodging assessment using RS data (see section 7.7) and implications of the research for technology transfer to potential end-users (see section 7.8).

7.2 Advances in remote sensing of crop lodging

Our capacity to monitor the Earth's surface with satellite-based Earth observation platforms has expanded rapidly in the past three decades. During this time, RS has proved to be a promising tool for crop lodging assessment (Bouman, 1991b; Hufkens et al., 2019; Ogden et al., 2002). While RS methods for lodging assessment have not yet reached sufficient maturity, a vast array of studies already exists on the use of field-/lab-based methods and approaches (Crook and Ennos, 1995; Sterling et al., 2003). These well-established field-/lab-based methods have enabled a deep understanding of lodging mechanics and the factors that cause lodging as well as how lodging severity impacts crop yield.

In Chapter 2, for the first time, we provided a detailed overview of some of these field-/lab-based studies (49 studies) and showed how RS could contribute to lodging-based applications. The chapter also characterised the strengths and limitations of RS-based crop lodging studies. It laid out a solid foundation for subsequent research on this topic by identifying research gaps and providing perspectives on the untapped potential of RS for crop lodging assessment. The review showed that there were only 22 ISI publications between 1951-2018 that used RS for crop lodging assessment. We have summarised the number of RS-based publications (and their citations) that were reviewed in Chapter-2 and the subsequent (22) studies performed post-2018 in Fig. 7.2. Research on RS-based lodging progressed at a slow pace until 2010 and increased rapidly after that, with

much of this increase taking place after 2018 (Fig. 7.2). This increase is mainly due to the rapid advancement in airborne and satellite-based sensors together with promising developments in machine learning research, which have led to new RS opportunities for lodging assessment. About 22 RS-based studies on crop lodging assessment have been published post-2018, including the outputs from this research, resulting in a total of 44 RS-based lodging publications to date. The number of citations of these studies has also increased dramatically, with approximately 400 citations of the studies published between 2011-2020. The increasing number of publications exhibit that a preliminary level of knowledge now exists on the use of RS for lodging assessment and that the interest of the scientific RS community in lodging is growing rapidly (Fig. 7.2).

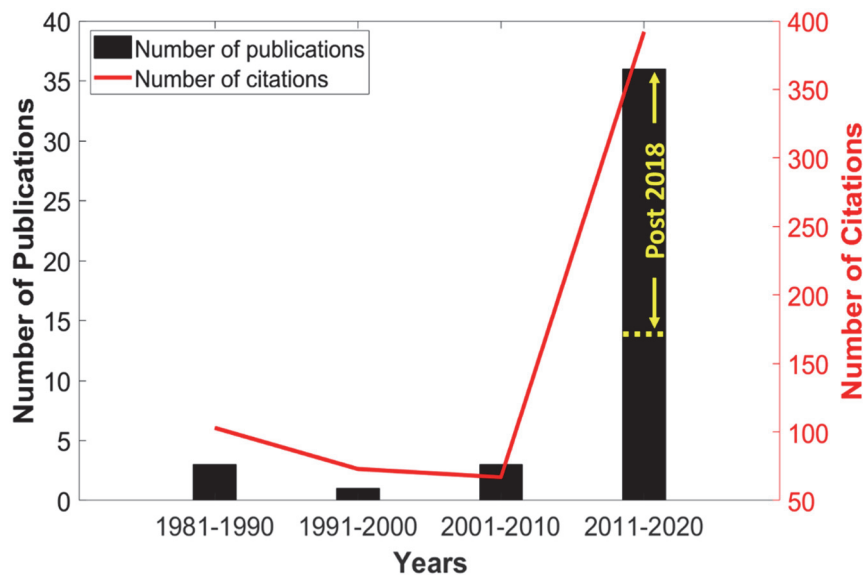


Fig. 7.2. The total number of publications and citations from the RS-based crop lodging studies throughout 1980-2020. This includes the studies reviewed in Chapter-2 and the ones published subsequently (post-2018).

Lodging detection in wheat using airborne UAV data acquired in the VNIR (visible-near infrared) region continues to be a hot topic of RS-based lodging research. A substantial part of the efforts (80% of the studies) has been dedicated to the categorical classification of crop lodging stages (non-lodged and lodged) using optical RS data while the remaining studies have focused mainly on understanding the impact of lodging on the RS signal. However, most of these studies merely detect lodging while replacing the existing technology but do little to advance it or show the unique capabilities of RS methods. The findings of the

review pointed out four major research gaps that were taken up as the objectives of this study: we proposed the i) estimation of crop angle of inclination (CAI) as a proper measure of wheat lodging stages, ii) classification of lodging severity using RS-based assessment of lodging score, iii) identifying the time of lodging incidence in wheat and understanding the effect of lodging on the RS signal using lodging score, and iv) estimation of a “safety factor against root lodging” as a measure of root lodging susceptibility in wheat.

7.3 Potential of remote sensing data in detecting crop lodging stages

It is important to characterise the intensity of lodging as it is a prerequisite to calculate crop yield losses and plan harvesting operations. SAR satellite data has shown to be valuable for crop lodging assessment due to its sensitivity to crop vertical structure, the ability of the SAR signal to resolve the scattering within the crop canopy into separate scattering mechanisms and data availability irrespective of weather conditions (Wang et al., 2019). When the plant is lodged, the stem moves from the upright position, and there is a change in the crop’s morphological status. It can be reasonably assumed that this change is manifested in the backscatter/polarimetric response of the canopy. Multiple metrics derived from SAR satellite data have shown to detect crop lodging successfully (e.g. detection of lodging stages) (Yang et al., 2015; Zhao et al., 2017). However, it was important to compare these diverse set of metrics to form a more mechanistic understanding of the probable variabilities produced by each of them. Moreover, it was not known how the incidence angle of the sensor affects the interaction of the microwave signal with the lodged canopy.

In Chapter-3, we investigated the role and contribution of a range of RS-based metrics derived from Sentinel-1 and RADARSAT-2 data (low and high incidence angle) to estimate crop angle of inclination (CAI [0, 90°]), as a measure of crop lodging stages (moderate, severe and very severe). CAI is the angle made by the crop stem with respect to the vertical. During lodging, a crop undergoes a series of stages (referred to as lodging stages in this study) starting with a slight lean from the vertical (CAI ~ 0°) and ending with the crop lying close to horizontal (CAI ~ 90°). We demonstrated how CAI is a better quantitative indicator of lodging stage than plant height (that had been used in most of the studies), as the variation in CAI is independent of the differences in crop cultivars and phenological stages. In general, higher accuracy was achieved with low incidence angle (~27°) RADARSAT-2 data ($R^2_{CV} = 0.87$) especially for CAI > 60°.

Moreover, the cross-polarised backscattering coefficients and volume scattering metrics were highly sensitive to CAI at a low incidence angle, suggesting that volume scattering was dominant at low incidence angles. The double bounce scattering metrics were highly correlated (negatively) with CAI at a high incidence angle. The analysis also revealed the potential of backscattering coefficients in distinguishing different lodging stages. For instance, the cross-polarised (VH or HV) backscattering coefficient values between healthy (He, non-lodged) and severely lodged (SL), He and very severely lodged (VSL), moderately lodged (ML) and VSL, and SL and VSL stages were all significantly different. The CAI maps, generated for the first time in this study, showed widespread lodging in the study area and its progression over time.

To better understand the utility of CAI for lodging detection and for classifying lodging stages, Chauhan et al. (2019b) also analysed multispectral very fine-resolution unmanned aerial vehicle (UAV) data (5 cm) (not included in this thesis). The UAV data with nine spectral bands (390-950 nm) was acquired over two wheat fields (18.6 ha each) on May 29, 2018 (Fig. 7.3a, b) parallel with CAI and plant height measurements in 51 plots (2×2 m spatial extent). The lodging stages were classified with a high overall classification accuracy (90%), with some degree of confusion between VSL and other lodging stages (Fig. 7.3c).

Overall, the results underlined the significance of very fine-spatial resolution data in lodging detection and mapping lodging stages. CAI maps generated in NRT can be used to predict yield losses and to design in-field navigation routes for autonomous driving vehicles so that the speed can be adjusted depending on the lodging condition, thus reducing harvest losses.

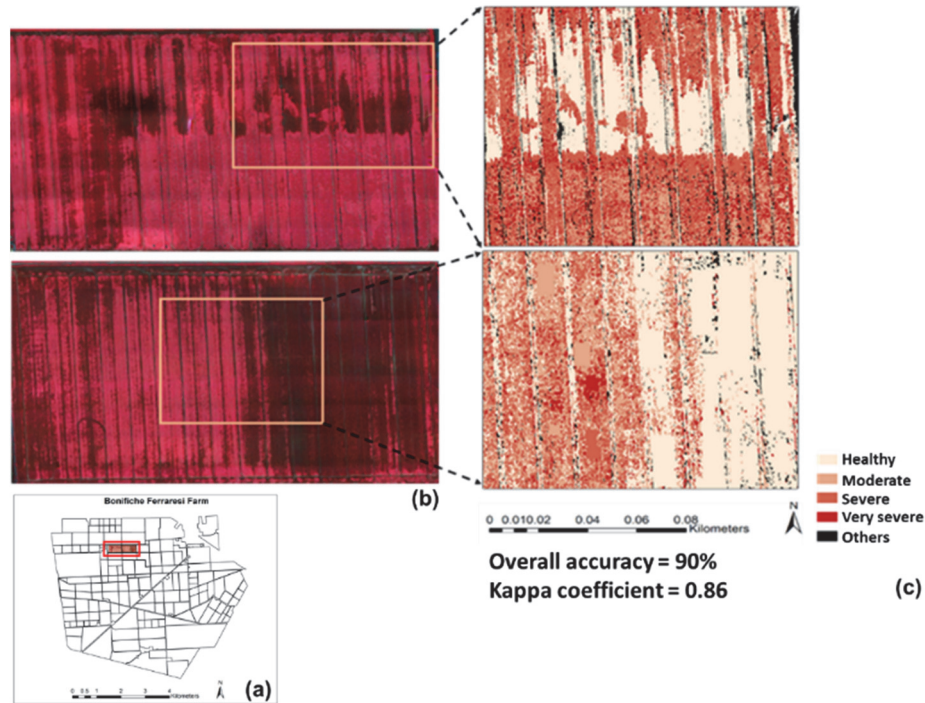


Fig. 7.3. The red polygon in (a) shows the location of the wheat fields in the Bonifichè Ferraresi farm where UAV data was acquired, (b) shows the false colour-composite (R:865 nm, G:665 nm, B:560 nm) of the scenes acquired from the UAV platform on May 29, 2018 and in (c) are the UAV images classified into different lodging stages using a supervised nearest neighbour algorithm.

7.4 Exploring the information capacity of SAR remote sensing for lodging severity mapping

One of the primary findings of our review (Chapter-2) was the absence of a standard reference/scale and terminology to represent lodging condition. Therefore, based on the gathered insights, we differentiated between three terms in the context of lodging characterisation: lodging stage, lodging severity and detecting when lodging occurs (or identifying lodging incidence). Crop biophysical parameters, such as CAI or plant height, were defined as measures for lodging stage assessment, whilst lodged area (LA), CAI and the phenological stage under observation govern lodging severity (Acreche and Slafer, 2011; Easson et al., 1993; Lang et al., 2012) and in turn, the extent of yield loss.

In Chapter-4, building upon our previous chapter, we carried out a discriminant analysis for classifying different degrees of lodging severity using Sentinel-1 and

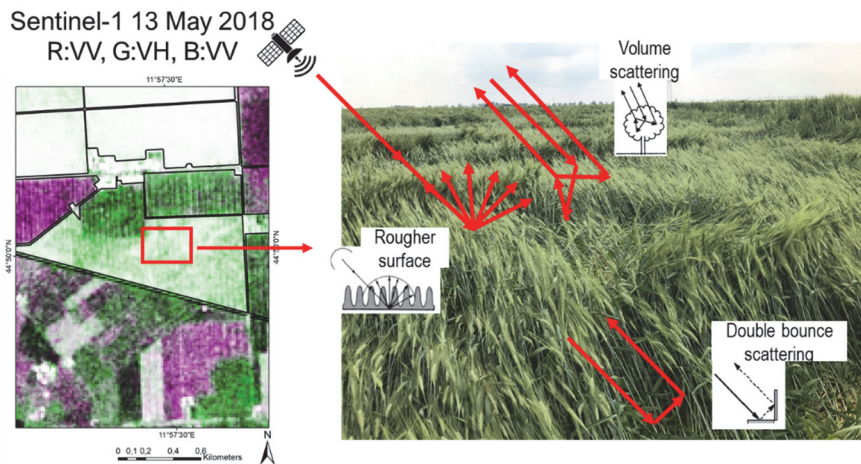
RADARSAT-2 data (low and high incidence angle). We proposed an index, modified after Caldicott and Nuttall (1979) called *lodging score*, that combines LA and CAI, as a simple measure of lodging severity. We hypothesised that an assessment of lodging score delivers a more comprehensive evaluation of lodging-induced crop damage than using CAI alone. In this regard, we analysed the correlation between the proposed lodging score and various satellite metrics. We then classified lodging severity-based on the lodging score using PLS discriminant analysis. As was the case with CAI estimation (Chapter-3), the low incidence angle RADARSAT-2 based model (overall accuracy of 72%) outperformed the high incidence angle RADARSAT-2 and Sentinel-1 models.

Furthermore, correlation analysis indicated the dependency of backscattering mechanisms on the satellite incidence angle and the polarimetric information content of Sentinel-1 and RADARSAT-2 data. The backscattering coefficients and polarimetric parameters responsive to the volume scattering mechanism (e.g. σ_{HV}^o , Yama_vol, biomass index) were highly sensitive to lodging severity for low incidence angle RADARSAT-2 data. The double bounce and surface scattering were more prevalent for high incidence angle RADARSAT-2 data. In the case of Sentinel-1, different backscattering mechanisms were prevalent in varying proportions. This is further explained in Fig. 7.4 for high angle of incidence ($\sim 40^\circ$) Sentinel-1 data acquired at different dates. The two wheat fields are in ML (Fig. 7.4a right) and VSL (Fig. 7.4b right) severity states. The Sentinel-1 backscattering intensities in VV and VH polarisations are also shown on the left. In essence, the higher the backscattering intensity, the rougher the surface being imaged. The polarised return from the target provides information on structure orientation and penetration depth. The visual interpretation of both wheat fields in Fig. 7.4a, b (right) shows varying levels of crop surface roughness that is being imaged. The VSL field in Fig. 7.4b (right) appears slightly less rough than the ML field in Fig. 7.4a (right), resulting in decreased backscatter. Although both VV and VH backscatter are evident in both image dates, the dominance of VV backscatter in the VSL condition is mainly due to increased surface scattering (smoother surface). Contrarily, in the ML scenario, VH is dominant (Fig. 7.4a left) indicating more volume scattering. The moderate to very severe destruction of the vertical plant structure could have resulted in a corresponding decrease in double bounce scattering (stem-soil returns).

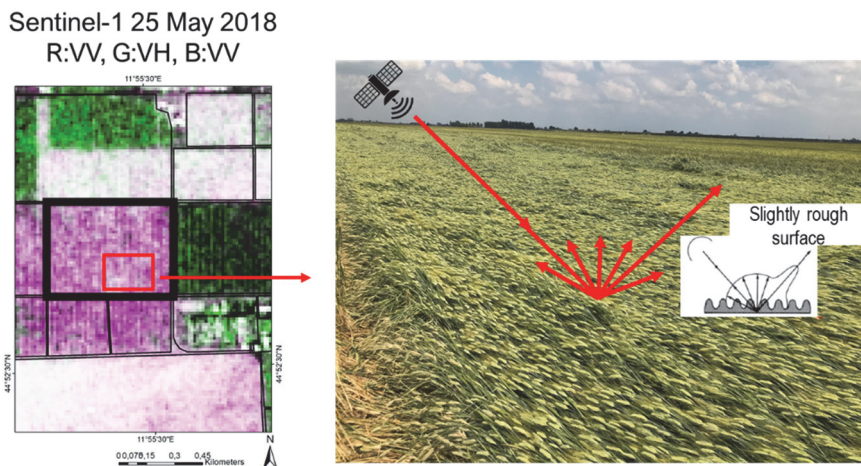
This study is the first demonstration that satellite-based SAR RS data can detect and characterise the lodging severity of staple crops like wheat. Our research

Synthesis

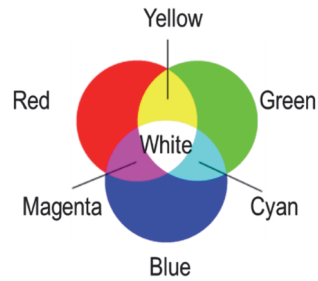
shows that accurate, synoptic-scale assessment of lodging severity in wheat is feasible and can form part of timely, data-driven approaches for crop management at farm level and food security monitoring systems at a regional level. The classified lodging severity maps can also be used for insurance payouts and settling insurance compensation disputes.



(a)



(b)



(c)

Fig. 7.4. RGB composites (R: VV, G: VH, B: VV) of the two Sentinel-1 images acquired on (a) May 13, 2018 (moderately lodged) and (b) May 25, 2018 (very severely lodged) showing the variation in the backscattering intensity for the two wheat fields. The photographs from the fields taken on the same date as the acquired satellite images are shown on the left. An example of the backscattering mechanisms caused due to different degree of lodging severities is also illustrated in the field photographs. (c) shows the colour scale for interpreting the satellite image colour composites.

7.5 Contribution of time-series SAR and optical remote sensing data in identifying the time of lodging incidence in wheat

Monitoring the seasonal variations of vegetation is important for many applications such as crop yield and net primary productivity estimation, detecting the time of crop harvest or supporting decisions about water supply (Sakamoto et al., 2005). Time-series RS data constitutes a valuable tool for NRT monitoring of crop growth by providing precise and timely information on vegetation status and development. While optical data provide a link between the biochemical and photosynthetic properties of crops, SAR data is useful for analysing the structural attributes of plants. The free and openly available dense time-series of Sentinel-1 and Sentinel-2 data have stimulated a shift in recent years towards studying the temporal behaviour of different crop types (Schlund and Erasmi, 2020; Veloso et al., 2017). However, these time series had not been exploited to detect the changes in crop development that are informative of when lodging occurs.

In Chapter-5, we addressed this gap and our time series analysis indicated that a plausible window of the first main lodging event in our experimental dataset could be identified (between DoY 115-121) using Sentinel-1 and Sentinel-2 data together. However, >20 days of missing Sentinel-2 satellite data (primarily due to cloud cover), did not allow for as accurate estimates as with Sentinel-1 data (with data available every six days). We also demonstrated the capability and

complementarity of the metrics derived from different polarisations and spectral bands to distinguish between different degrees of lodging severity. For instance, the red-edge and NIR regions with central wavelengths of 740 nm and 865 nm, respectively were the most important spectral regions for distinguishing He and other lodging severity classes, while $\sigma^{\circ}_{\text{VH}}$ backscattering coefficient and the complementarity of $\sigma^{\circ}_{\text{VV}}$ and $\sigma^{\circ}_{\text{VH/VV}}$ backscattering coefficients also played a major role in distinguishing the lodging severity classes. The change in reflectance spectra due to crop cultivar differences and crop growth (or change in phenological growth stages) was much less than the variation due to lodging. The results are promising given the complexity (heterogeneous and random distribution of lodging) and level of detail (different degree of lodging severities) in the lodged wheat considered in the study.

The results observed from the analysis of Sentinel-2 data were further confirmed by Chauhan et al. (2019b) (not included in this thesis). They also noted that the mean reflectance obtained from UAV acquired data increased as the lodging progressed from He to VSL stage (Fig. 7.5). The change was more pronounced in the green (560 nm), NIR (842 nm) and red-edge (740nm) regions (Fig. 7.5). This effect is mainly due to the change in structural characteristics of the plant and leaves from their vertical position to a horizontal flat condition. Moreover, the increase of reflectance in VIS is also an indicator of plant stress (e.g. reduced chlorophyll absorption in red region).

The identification of when lodging occurs and the knowledge about how lodging affects the RS signal could contribute to in-season yield loss estimates, crop management decision support systems, setting crop retail prices and enabling algorithm development for operational crop lodging detection.

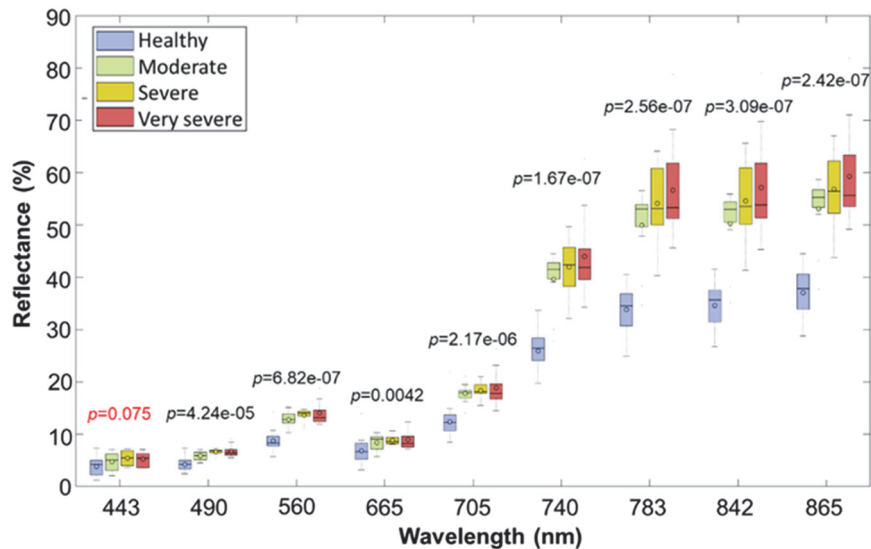


Fig. 7.5. Boxplot depicting the UAV reflectance at various wavelengths for healthy, moderate, severe and very severe crop lodging stages. The Kruskal Wallis p -values at the end of each box plot indicate if the differences between group means are significant (at 0.01 level of significance). The p -value in red indicates that the difference between group means is insignificant at 0.01 level of significance.

7.6 Role of SAR remote sensing in lodging susceptibility mapping

RS serves as a valuable tool for monitoring the changes in crop canopy that are too subtle to be noticed at the local scale but maybe distinct when summarised at synoptic scales. Susceptibility indicators that can be quantitatively measured using RS are often used to depict the degree to which crops are susceptible to being influenced by future change (Kim et al., 2014). RS has been widely used to assess crop trajectories following the damage caused due to lodging (lodging detection), as seen in section 7.2 and Chapter-2. However, lodging susceptibility mapping using RS data is still mostly unexplored.

In Chapter-6, we addressed this gap by demonstrating the use of RS-based metrics derived from Sentinel-1 and multi-incidence angle RADARSAT-2 data to estimate safety factor against root lodging (SF_A) as a simple quantitative measure of root lodging susceptibility. Root lodging is a result of the failure of the root-soil anchorage system due to weak soil shear strength and a small root plate diameter (Crook and Ennos, 1994). It is a ratio of the self-weight moment

of a plant (measured using crop angle of inclination, plant height at the centre of gravity, fresh aerial biomass and acceleration due to gravity) to the anchorage strength of the root-soil system.

The results obtained in this chapter showed that the SF_A is detectable from high-resolution SAR satellite data with up to 73-84% accuracy at the field level, although the backscattering coefficients and polarimetric features saturated at high safety factor values (>2). Despite this, the critical SF_A value (close to 1) required to assess root lodging susceptibility in wheat could be reliably detected by both models; with higher accuracy for fully polarimetric multi-incidence angle RADARSAT-2 data ($R^2_{CV} = 0.84$, $RMSE_{CV} = 0.54$). In the case of Sentinel-1 data, the interferometric coherence combined with backscattering coefficients seemed promising for estimating the safety factor (for non-lodged wheat). This is probably due to the well documented high correlation of coherence with the plant height of non-lodged wheat. We also found that the safety factor was largely consistent with the real lodging events observed during the field visits and that the crop condition in early spring (stem elongation growth stage [GS30-40]) can indicate future lodging susceptibility. In Chapter-6, we also emphasised that a safety factor against root lodging, when combined with other crop biophysical (such as plant density) and environmental (such as rainfall and wind speed) parameters sensitive to root lodging susceptibility, would result in more comprehensive and timely lodging risk estimates.

This study is the first demonstration that presents a replicable and scalable method of assessing the susceptibility of globally relevant yield-reducing factor to staple crop production. Lodging susceptibility mapping is important in several aspects, e.g. for efficient nitrogen fertiliser management during the growing season and formulating the subsequent plant growth regulator programme. Our research shows that accurate, synoptic-scale assessment of the susceptibility of the wheat crop to lodging is feasible and can form part of timely, data-driven approaches for crop management at farm level and food security monitoring systems at a regional level.

7.7 Future opportunities

This study has advanced the use of RS for characterising crop lodging using current operational satellite-based sensors and field observations. In this section, we share some insights into research avenues that can be explored in future studies.

7.7.1 Crop lodging detection and characterisation

Crop lodging detection and the characterisation of lodging stages, lodging severity and lodging incidence remain challenging, despite the growth in the number of lodging-based RS studies. Although our research had promising findings, it is limited to one season in a single test site with limited field observations. We believe the following five issues should be considered to achieve major improvements in the existing methodologies for lodging detection and characterisation i) availability of a statistically significant temporal sample size before and at the time of the lodging event for proper validation, ii) minimising the image gap, especially after lodging occurs, iii) exploiting hyperspectral data in the VIS-SWIR range to identify the absorption features diagnostic of lodging, iv) utilising textural features in combination with existing RS-based satellite metrics and v) a larger-scale study, covering different environments and management practices and using information from a broader set of current and near-future EO platforms. Future studies can benefit from a combination of current and upcoming satellite sensors such as multi-temporal NISAR, ALOS2/PALSAR-2, RADARSAT Constellation Mission (RCM), Sentinel-1, Sentinel-2, ICEYE, Capella, EnMap and PRISMA for operational multi-sensor monitoring of crop lodging.

In order to increase the availability of field data close to the lodging events, a network of phenological cameras (phenocams), spread over multiple sites and climate zones, can be installed in agricultural fields to provide hourly to daily information from which the timing of lodging events can be determined. This could also assist in subsequent planning of timely collection of ground truth data of lodging events and crop parameters. A network of phenocams is already expanding globally, covering different ecosystems (Brown et al., 2016). Recent developments in the EO sector can also improve the efficacy of crop lodging assessment across the globe. The (almost) daily availability of ICEYE and RCM data (with limited polarimetric information) and the increased frequency of the optical observations from hyperspectral systems such as EnMap and PRISMA (in combination with multispectral Sentinel-2 and Landsat-OLI acquisitions further complemented by Sentinel-1 SAR data) would help overcome the problem of the image gap. Since lodging can occur any time after the booting or flowering phenological stages, the (almost) daily time-series of ICEYE and RCM data could be useful to accurately identify the timing of a lodging event by analysing temporal changes in the RS signal. The rich spectral information of EnMap (228 spectral bands) and PRISMA (237 spectral bands) data may allow understanding

of how lodging-induced change in the crop parameters affect the spectral reflectance of wheat fields, which absorption features are diagnostic of lodging and how different degrees of lodging severity can be discriminated.

Textural analysis of very high-resolution satellite images has shown promising results in the retrieval of crop biophysical parameters in non-lodged conditions (Colombo et al., 2003). In general, texture analysis provides an estimate of the spatial distribution of grey levels in an image by reflecting the contrast between the areas lit by the sun and those that are in shadow (Ploton et al., 2017). This, in turn, provides information about the size and distribution of the crop canopy and intercrop gaps, given the spatial resolution is very high. Our review study (Chapter 2) revealed that there is a lack of understanding about how canopy texture features in contrasted lodging and environmental conditions vary with respect to the crop structural attributes such as CAI or lodging score. Feature extraction methods such as grey-level co-occurrence matrix (GLCM) can be used (Singha and Sarmah, 2019) to derive textural features related to contrast (homogeneity, dissimilarity and contrast), orderliness (angular moment, maximum probability and entropy) and statistical (mean, variance and correlation) features.

7.7.2 Quantification of lodging impact on crop yield and grain quality

Accurate crop yield estimates allow farmers to interpret how management strategies affect crop productivity and can help guide future practices (Lobell, 2013). Existing RS-based methods of wheat yield estimation (Barbouchi et al., 2016) have been applied to homogeneous non-lodged wheat fields. Despite the recognised impact that lodging has on crop yield (with losses up to 75%), to our knowledge, the use of RS for assessing the effects of lodging on the accuracy of these methods for yield estimation remains unknown. The mechanisms by which lodging results in yield loss (such as inefficient use of radiation by the canopy resulting in reduced photosynthesis) is well understood and has been postulated in the literature (Berry and Spink, 2012; Setter et al., 1997). The knowledge of these mechanisms can help build RS-based algorithms to predict lodging-induced yield losses. For instance, RS can contribute to estimating the absorbed photosynthetic active radiation (APAR) as a direct proxy of the dry matter productivity and final yield of the lodged canopy. RS-derived parameters such as photochemical reflectance index (Barton and North, 2001) and solar-induced chlorophyll fluorescence (Meroni et al., 2009) have shown to have a consistent

relationship with the light use efficiency of a non-lodged canopy. Future studies should focus on the use of these remotely sensed parameters to characterise the light use efficiency of lodged crops in combination with crop growth models (such as Crop Estimation through Resource and Environment Synthesis or CERES-Wheat) driven by weather data to quantify the crop yield losses. In this context, the upcoming Fluorescence Explorer (FLEX) satellite mission (2022) intended for rapid improvement in solar-induced chlorophyll fluorescence sensing capabilities will play an important role.

Moreover, the use of RS-derived biophysical parameters such as crop angle of inclination (CAI) and lodging score should also be explored for yield loss assessments. For example, the RS-derived lodging score can be assimilated into a simple equation (Eqn. 7.1) formulated by Berry and Spink (2012), that can predict the extent of yield loss (Y_{loss}) for any lodged crop:

$$Y_{loss} = \frac{\sum_i^f (LA_{90^\circ} \times 0.7 + LA_{65^\circ} \times 0.3 + LA_{25^\circ} \times 0.1)}{n} \quad (7.1)$$

where, i and f are the 1st and last days of grain filling, LA_{90° , LA_{65° and LA_{25° is the extent of the lodged area at the CAI of 85-90° (very severely lodged), 46-84° (severely lodged) and 5-45° (moderately lodged) from the vertical, respectively and n is the number of days of grain filling.

As discussed in Chapter-2, lodging can have a significant impact on grain quality too. The use of RS to quantify the impact of lodging on grain quality indicators such as grain protein content is still largely unexplored. An assessment of grain protein content in cereal crops is important to meet varying commodity needs. For instance, a grain protein content above 12.5% is needed in wheat to provide sufficient gluten for bread making. Studies show that the nitrogen content of wheat at the flowering growth stage is indicative of grain protein content (Zhao et al., 2005, 2019). An RS model based on hyperspectral data estimating plant nitrogen content for lodged canopy can be integrated – in future studies- with process-based models such as SiriusQuality (Martre et al., 2006) or STICS (Brisson et al., 2003) to quantify lodging impact on grain protein.

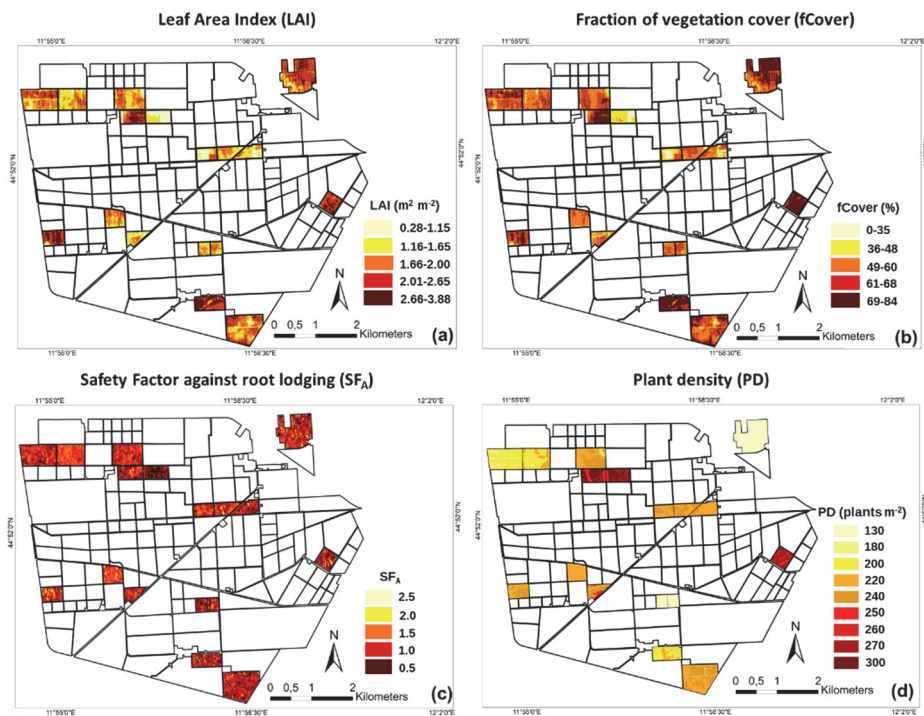
7.7.3 Lodging risk mapping using remote sensing retrieved soil and crop parameters

The findings stemming from this work could eventually result in more accurate and timely lodging risk estimates. As mentioned earlier, the mapping of susceptibility indicators is an essential component of a comprehensive risk assessment of lodging. A comprehensive lodging risk assessment entails the inclusion of long term climate averages (baseline risks exposure), forecasts of precipitation and wind gusts (hazard) and susceptibility indicators such as soil nitrogen, soil moisture or other remotely sensed crops biophysical and biochemical parameters into a model. The status of the crop at the beginning of the stem elongation stage (GS 30-31) is a crucial determinant of lodging susceptibility in wheat. Just like the crop safety factor, other estimates of biophysical parameters such as leaf area index (LAI), fraction of vegetation cover (fCover) and plant density at GS30-31 can also be used as lodging susceptibility indicators (HGCA, 2005).

Our study showed that a remotely sensed safety factor against root lodging could serve as a reliable lodging susceptibility indicator during the growing season. It would be useful to further extend and validate the use of RS-based safety factor for assessing lodging susceptibility at several test sites with contrasting agricultural landscapes. A more detailed experimental investigation combining the crop safety factor with other environmental and crop/soil biophysical parameters is also needed. This could substantially improve and upscale lodging risk assessment capabilities using RS, as a major step towards a complete and comprehensive evaluation of lodging over large areas. In order to fully integrate quantitative lodging risk assessment in modern agriculture, future studies should make the model compliant with the standards of decision support schemes such as DESSAC (DEcision Support System for Arable Crops) so that farmers can use the knowledge in a practical and applied way. Future studies can also explore the application of RS in investigating lodging risk in other staple cereals such as rice, oats and barley.

Lastly, we demonstrate two approaches that could form a basis for future studies for lodging risk mapping. The first approach presents a lodging susceptibility map derived by combining different crop biophysical parameters. We combined the thresholds of safety factor against root lodging (SF_A) derived in Chapter-6 (Fig. 7.6c) with those of LAI (Fig. 7.6a), fCover (Fig. 7.6b) and plant density (Fig. 7.6d) to produce an “in season” lodging susceptibility map (Fig. 7.6e). We derived the LAI and fCover maps from Sentinel-2 data using the Biophysical processor in SNAP toolbox while the plant density map (Fig. 7.6d) was provided

by Bonifiche Ferraresi farm (study site). According to HGCA (2005) guidelines, $LAI > 2$ or $fCover > 60\%$ at GS30-31 increases stem lodging susceptibility. Furthermore, an increase in plant density above 200 plants per square meter can increase root lodging susceptibility (as it weakens the soil anchorage). As shown in Chapter-6, the $SFA \leq 1$ increases the root lodging susceptibility. A combined (stem+root) lodging susceptibility map combining these four parameters ($LAI > 2$ AND $fCover > 60\%$ AND $SFA \leq 1$ AND $PD > 200$) is shown in Fig. 7.6e. Future studies should develop models to produce accurate and fully validated products of LAI, fCover and plant density, should validate the thresholds that can indicate the lodging risk and carry out a sensitivity analysis to study the influence of each of these parameters together with environmental parameters on the lodging risk.



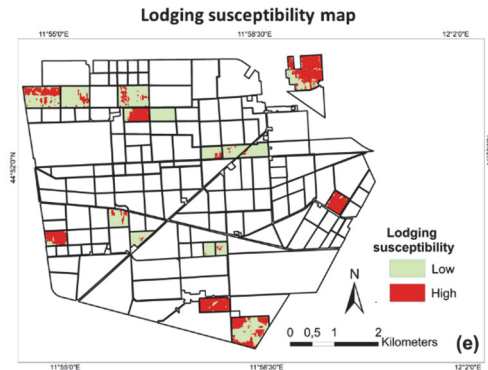


Fig. 7.6. (a) Leaf area index (LAI $\text{m}^2 \text{m}^{-2}$), (b) fraction of vegetation cover (fCover %) maps derived from the Sentinel-2 image acquired on March 30, 2018. The maps are derived using the biophysical processor in SNAP. The safety factor against root lodging (SF_A) map shown in (c) is derived from Sentinel-1 data (dated March 26) using extreme gradient boosting regression. The plant density (PD plants m^{-2}) map shown in (d) is provided by the Bonifiche Ferraresi farm. The lodging susceptibility map in (e) showing high risk is derived by combining the thresholds of $\text{LAI} > 2$, $\text{fCover} > 60\%$, $SF_A \leq 1$ and $\text{PD} > 200 \text{ plant m}^{-2}$. The wheat fields shown in the maps are at GS30-31.

The second approach that we demonstrate here is a proof of concept can contribute to developing an RS-based model independent of physical field-based measurements. We demonstrate a simple and cost-effective approach for getting a preliminary estimate of stem wheat lodging susceptibility using RGB photographs (acquired in nadir position) of a field. Based on the RGB photographs, a visual assessment can be made regarding the relative LAI or fCover values. Fig. 7.7 shows different stem lodging susceptibility scenarios in our study site based on the RGB photographs of the wheat plots at GS30-31 and the relative LAI/fCover values of wheat estimated visually. Although qualitative, such visual estimates can be useful in the absence of field measurements for assessing relative lodging susceptibility on a smaller scale (field level) and for validating the RS-based estimates. The accuracy of the relative LAI and fCover estimates can be further improved through object-based segmentation.

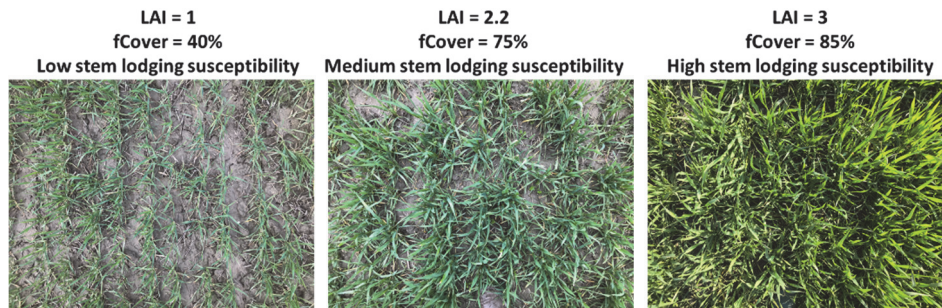


Fig. 7.7. Different stem lodging susceptibility scenarios based on a visual estimate of leaf area index (LAI $\text{m}^2 \text{m}^{-2}$) and the fraction of vegetation cover (fCover %) measured from the RGB photographs of the wheat plots at the beginning of stem elongation growth stage (GS30-31). The highest stem lodging susceptibility is for the scenario where the green canopy cover is highest (LAI>2, fCover>60%).

7.8 Research implications

7.8.1 Implications for technology and knowledge transfer to end-users: Market potential of the research

An increased focus on crop monitoring is a major factor fuelling the smart precision farming RS market today. One of the biggest growth prospects in smart precision farming is the web/mobile applications segment, which is growing at a much higher rate than the market average growth rate. Roland (2015) estimated the worldwide total available market of the software and hardware for precision farming to be €4.5 billion in 2020 which has been growing at a compound annual growth rate (CAGR) of 12% from 2014 through 2020 (Fig. 7.8). The demonstrated potential of using RS for crop lodging assessment has created a new market niche. Therefore, it is envisaged that an easy-to-use web/mobile-based application or a decision support tool that uses satellite data to notify the end-user about possible lodging risk and the extent of lodging-induced crop damage in NRT could be developed. This would allow optimal resource utilisation for affected areas and adequate decision-making in selecting remedial measures.

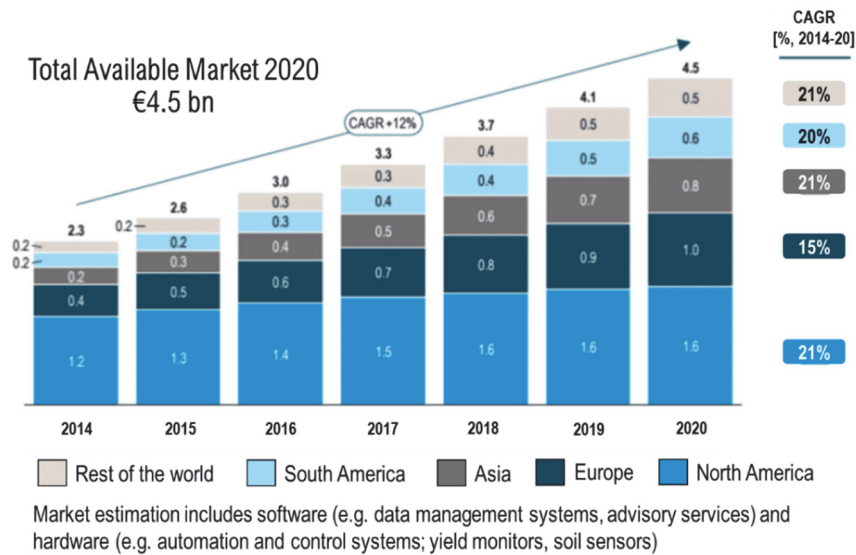


Fig. 7.8. The market estimation (grouped by the continents) for precision smart farming 2014-2020 is shown. The figures are in billion euros; CAGR is the compound annual growth rate (Roland, 2015).

Through a combination of expertise in RS data and algorithms, GIS analysis and agronomy, the application can serve as a useful tool for crop lodging monitoring. A scheme for RS-based lodging detection and risk mapping of wheat is proposed in Fig. 7.9. There are seven key steps: 1) acquiring satellite images at critical growth stages such as GS30-31 for lodging risk analysis and after GS60 for lodging detection in wheat; 2) a processing chain for processing the satellite images; 3) intermediate crop biophysical data products such as LAI maps, soil moisture maps, etc. as indicators for lodging susceptibility; 4) assimilation of intermediate products, such as climate data as well as meteorological conditions from sowing to harvest date into a crop lodging model to generate precision maps (such as a lodging risk map); 5) the precision maps can be delivered to the end-user through a web platform or mobile application; 6) the end-user also receives suggestions regarding the remedial measures in high-risk/highly-lodged areas, and 7) providing customised support from technicians for follow-up queries. Through a co-development process with the necessary stakeholders, it can be ensured that the RS-based information meets requirements for local and regional assessments of crop production and losses.

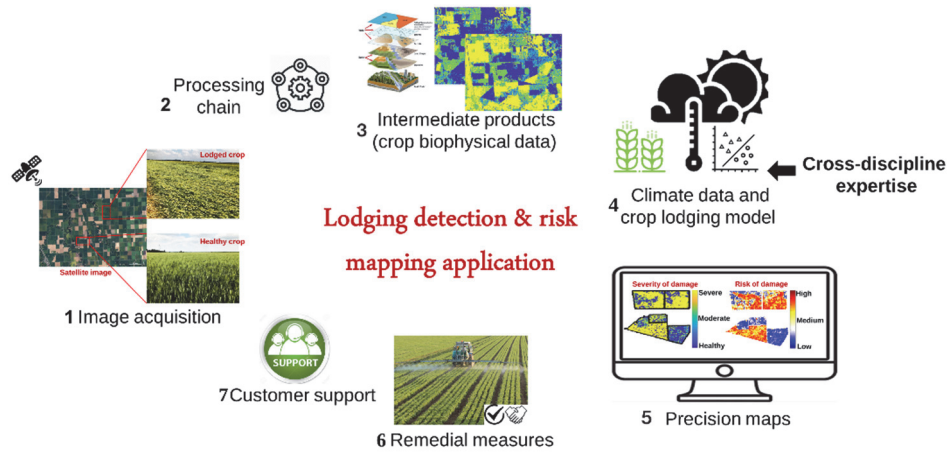


Fig. 7.9. The proposed framework for developing a web/mobile-based application for lodging detection and risk mapping.

In order to develop a web/mobile-based interface, two important considerations can be made for the NRT availability of information to the end-user. Firstly, freely available satellite data has high potential in creating an NRT, localised crop lodging tracking and risk mapping system that can provide immediate value to the end-user with negligible human involvement. A framework can be developed for processing free satellite data (using Google Earth Engine, for example) by leveraging computational devices in combination with cloud infrastructures (such as Google Cloud). Second is the availability of information irrespective of the weather conditions. A model that uses weather-independent satellite data (e.g. microwave data) as the data source will be useful.

7.8.2 Potential end-users

The agri-food Bonifiche Ferraresi company in Italy could be the primary tester and early adopter of the application or the recommendations generated from this study. For a long time, the main problem for the Bonifiche farm was their inability to detect the timing and severity of a lodging event, quantify its impact and foresee where lodging was expected to occur. We identified the problem and realised that if this information was available in time, it could help the farm take proper actions during the crop season and prevent/lessen the extent of the damage.

The other potential end-users of the research could be crop insurance companies, agronomists, agricultural retailers, policymakers and most importantly, farmers.

Farmers, loss adjusters from the insurance companies and even Bonifiche face this huge challenge to get an accurate estimation of crop damage and decide upon the compensation claims. Upon receiving a claim, it may take weeks for a loss adjuster to assess the farm as large as 5000 ha to validate the claim and assess the crop damage. High claim rates during the season make it even more challenging. For agricultural retailers, it is important to get an estimate of the damage to set the crop retail prices. For policymakers, delivering accurate crop lodging inventories with consistency and reliability at the regional or national scales can be important.

7.8.3 The relevance of the results to the attainment of the Sustainable Development Goals

The Sustainable Development Goals (SDGs) laid out by the United Nations spell out the commitment to address global challenges and attain sustainable development in three dimensions: economic, environmental and social. The 17 goals are associated with critical sectors, including clean water, responsible consumption/production and climate action, among others. Geospatial datasets from EO satellites have been recognised as feasible replacements or complementary data source to survey or to get census-based statistics that often form the basis for assessing and reporting on these goals (Holloway and Mengersen, 2018). In this context, the objectives and the successive results of this work are directly relevant and applicable for the accomplishment of two targets (2.3 and 2.4) under SDG 2 (“Zero hunger-Achieve food security and improved nutrition and promote sustainable agriculture”), though implicit links exist with five other SDGs (9, 12, 13, 15 and 17).

The Inter-agency Expert Group on SDG Indicators (IAEG-SDGs) has proposed indicators to examine progress towards sustainable agriculture management (SAM) (indicators 2.3.1 and 2.4.1). These indicators correspond to increasing crop production volume per unit area (2.3.1) and monitoring the proportion of agricultural land under productive and sustainable agriculture (2.4.1). Inter-year comparison of these indicator values at regional or national scales can help quantify the advancements being made towards SAM. Thus, stable or increasing crop yields per hectare over time due to the timely assessment of lodging can indicate SAM while a long-term decrease in crop production volumes could imply otherwise. The demonstrated feasibility of using freely available satellite data to map crop lodging and assess its susceptibility can greatly aid in accurately estimating, observing and reporting on SDG indicators 2.3.1 and 2.4.1.

Bibliography

- Abdullah, H., Darvishzadeh, R., Skidmore, A.K., Groen, T.A., Heurich, M., 2018. European spruce bark beetle (*Ips typographus*, L.) green attack affects foliar reflectance and biochemical properties. *Int. J. Appl. earth Obs. Geoinf.* 64, 199–209.
- Acorsi, M.G., Martello, M., Angnes, G., 2019. Identification of maize lodging: a case study using a remotely piloted aircraft system. *Eng. Agrícola* 39, 66–73.
- Acreche, M.M., Slafer, G.A., 2011. Lodging yield penalties as affected by breeding in Mediterranean wheats. *F. Crop. Res.* 122, 40–48.
- AHDB, 2005. Avoiding lodging in winter wheat – practical guidelines [WWW Document]. URL [https://projectblue.blob.core.windows.net/media/Default/Imported Publication Docs/Avoiding lodging in winter wheat - practical guidelines.pdf](https://projectblue.blob.core.windows.net/media/Default/Imported%20Publication%20Docs/Avoiding%20lodging%20in%20winter%20wheat%20-%20practical%20guidelines.pdf) (accessed 5.1.17).
- Alatorre, L.C., Sánchez-Andrés, R., Cirujano, S., Beguería, S., Sánchez-Carrillo, S., 2011. Identification of mangrove areas by remote sensing: The ROC curve technique applied to the northwestern Mexico coastal zone using Landsat imagery. *Remote Sens.* 3, 1568–1583.
- Alberda, T., 1977. Crop photosynthesis: methods and compilation of data obtained with a mobile field equipment. Pudoc, Centre for Agricultural Publishing and Documentation.
- Ali, A.M., Darvishzadeh, R., Skidmore, A.K., van Duren, I., 2015. Effects of canopy structural variables on retrieval of leaf dry matter content and specific leaf area from remotely sensed data. *IEEE J. Sel. Top. Appl. earth Obs. Remote Sens.* 9, 898–909.
- Allison, G.G., Morris, C., Hodgson, E., Jones, J., Kubacki, M., Barraclough, T., Yates, N., Shield, I., Bridgwater, A.V., Donnison, I.S., 2009. Measurement of key compositional parameters in two species of energy grass by Fourier transform infrared spectroscopy. *Bioresour. Technol.* 100, 6428–6433.
- Asrar, G., Kanemasu, E.T., Yoshida, M., 1985. Estimates of leaf area index from spectral reflectance of wheat under different cultural practices and solar angle. *Remote Sens. Environ.* 17, 1–11.
- Atzberger, C., 2013. Advances in remote sensing of agriculture: Context description, existing operational monitoring systems and major information needs. *Remote Sens.* 5, 949–981.
- Baker, C.J., 1995. the Development of a Theoretical-Model for the Windthrow of Plants. *J. Theor. Biol.* 175, 355–372.
- Baker, C.J., Berry, P.M., Spink, J.H., Sylvester-Bradley, R., Griffin, J.M., Scott, R.K., Clare, R.W., 1998. A method for the assessment of the risk of wheat lodging. *J. Theor. Biol.* 194, 587–603.
- Baker, C.J., Sterling, M., Berry, P.M., 2014. A generalised model of crop lodging. *J. Theor. Biol.* 363, 1–12.
- Balenzano, A., Mattia, F., Satalino, G., Davidson, M.W.J., 2010. Dense temporal series of C-and L-band SAR data for soil moisture retrieval over agricultural crops. *IEEE J. Sel. Top. Appl. Earth Obs. Remote Sens.* 4, 439–450.
- Barbouchi, M., Chokmani, K., Abdelfattah, R., Ben Aissa, N., 2016. Yield estimation of the winter wheat using Radarsat 2 polarimetric SAR response, in: 2nd International

- Conference on Advanced Technologies for Signal and Image Processing, ATSIP 2016. Institute of Electrical and Electronics Engineers Inc., pp. 555–560. <https://doi.org/10.1109/ATSIP.2016.7523143>
- Baret, F., Houles, V., Guérif, M., 2007. Quantification of plant stress using remote sensing observations and crop models: the case of nitrogen management. *J. Exp. Bot.* 58, 869–880.
- Barton, C.V., North, P.R.J., 2001. Remote sensing of canopy light use efficiency using the photochemical reflectance index: Model and sensitivity analysis. *Remote Sens. Environ.* 78, 264–273.
- BASF, 2011. Managing lodging risk in winter wheat. Featuring the new Canopy Assessment Tool (CAT) [WWW Document]. URL <https://www.agricentre.basf.ie/Documents/Tools/CanopyAssessmentToolPocketGuide.pdf> (accessed 7.26.18).
- Battude, M., Al Bitar, A., Morin, D., Cros, J., Huc, M., Sicre, C.M., Le Dantec, V., Demarez, V., 2016. Estimating maize biomass and yield over large areas using high spatial and temporal resolution Sentinel-2 like remote sensing data. *Remote Sens. Environ.* 184, 668–681.
- Baylis, A.D., Wright, I.T.J., 1990. The effects of lodging and a paclobutrazol—chlormequat chloride mixture on the yield and quality of oilseed rape. *Ann. Appl. Biol.* 116, 287–295.
- Berberoglu, S., Lloyd, C.D., Atkinson, P.M., Curran, P.J., 2000. The integration of spectral and textural information using neural networks for land cover mapping in the Mediterranean. *Comput. Geosci.* 26, 385–396.
- Berry, P.M., 2013. New Advances in PGRs, in: BCPC 50 Year Anniversary Conference. Rothamsted, UK.
- Berry, P.M., Griffin, J.M., Sylvester-Bradley, R., Scott, R.K., Spink, J.H., Baker, C.J., Clare, R.W., 2000. Controlling plant form through husbandry to minimise lodging in wheat. *F. Crop. Res.* 67, 59–81.
- Berry, P.M., Spink, J.H., 2012. Predicting yield losses caused by lodging in wheat. *F. Crop. Res.* 137, 19–26.
- Berry, P.M., Spink, J.H., Gay, A.P., Craigon, J., 2003a. A comparison of root and stem lodging risks among winter wheat cultivars. *J. Agric. Sci.* 141, 191–202.
- Berry, P.M., Spink, J.H., Sylvester-Bradley, R., Pickett, A., Sterling, M., Baker, C.J., Cameron, N., 2002. Lodging control through variety choice and management. *Proc. 8th Home-Grown Cereal. Assoc. R D Conf. Cereal. Oilseeds 7.1-7.12.*
- Berry, P.M., Sterling, M., Baker, C.J., Spink, J.H., Sparkes, D.L., 2003b. A calibrated model of wheat lodging compared with field measurements. *Agric. For. Meteorol.* 119, 167–180.
- Berry, P.M., Sterling, M., Mooney, S.J., 2006. Development of a model of lodging for barley. *J. Agron. Crop Sci.* 192, 151–158.
- Berry, P.M., Sterling, M., Spink, J.H., Baker, C.J., Sylvester-Bradley, R., Mooney, S.J., Tams, A.R., Ennos, A.R., 2004. Understanding and reducing lodging in cereals. *Adv. Agron.* 84, 215–269.
- Berry, P.M., Sylvester-Bradley, R., Berry, S., 2007. Ideotype design for lodging-resistant wheat. *Euphytica* 154, 165–179.
- Berry, P.M., White, C., Sterling, M., Baker, C.J., 2013. Development of a model of lodging risk in oilseed rape to enable integrated lodging control to reduce PGR use. CRD Proj. PS2146, August.

- Bhatia, A.S., Yu-Wei, C.D.C., 2017. Machine learning with R cookbook: analyze data and build predictive models. Packt Publishing Ltd.
- Blaes, X., Defourny, P., 2003. Retrieving crop parameters based on tandem ERS 1/2 interferometric coherence images. *Remote Sens. Environ.* 88, 374–385.
- Blaes, X., Defourny, P., Wegmuller, U., Della Vecchia, A., Guerriero, L., Ferrazzoli, P., 2006. C-band polarimetric indexes for maize monitoring based on a validated radiative transfer model. *IEEE Trans. Geosci. Remote Sens.* 44, 791–800.
- Blanzieri, E., Melgani, F., 2008. Nearest neighbor classification of remote sensing images with the maximal margin principle. *IEEE Trans. Geosci. Remote Sens.* 46, 1804–1811.
- Bleiholder, H., Weber, E., Lancashire, P.D., Feller, C., Buhr, L., Hess, M., Wicke, H., Hack, H., Meier, U., Klose, R., 2001. Growth stages of mono- and dicotyledonous plants, BBCH monograph, Federal Biological Research Centre for Agriculture and Forestry, Berlin/Braunschweig, Germany.
- Board, S.S., NRC, 2007. Earth science and applications from space: national imperatives for the next decade and beyond. National Academies Press.
- Bock, C.H., Poole, G.H., Parker, P.E., Gottwald, T.R., 2010. Plant disease severity estimated visually, by digital photography and image analysis, and by hyperspectral imaging. *CRC. Crit. Rev. Plant Sci.* 29, 59–107.
- Boschetti, M., Busetto, L., Manfron, G., Laborte, A., Asilo, S., Pazhanivelan, S., Nelson, A., 2017. PhenoRice: A method for automatic extraction of spatio-temporal information on rice crops using satellite data time series. *Remote Sens. Environ.* 194, 347–365.
- Boulesteix, A.L., Strimmer, K., 2006. Partial least squares: a versatile tool for the analysis of high-dimensional genomic data. *Brief. Bioinform.* 8, 32–44.
- Bouman, B.A.M., 1991a. Linking X-band radar backscattering and optical reflectance with crop growth models. PhD Thesis. Wageningen Agric. Univ. Netherlands.
- Bouman, B.A.M., 1991b. Crop parameter estimation from ground-based x-band (3-cm wave) radar backscattering data. *Remote Sens. Environ.* 37, 193–205.
- Bouman, B.A.M., Hoekman, D.H., 1993. Multi-temporal, multi-frequency radar measurements of agricultural crops during the Agriscatt-88 campaign in The Netherlands. *Remote Sens.* 14, 1595–1614.
- Bouman, B.A.M., van Kasteren, H.W., 1990a. Ground-based X-band (3-cm wave) radar backscattering of agricultural crops. I. Sugar beet and potato; backscattering and crop growth. *Remote Sens. Environ.* 34, 93–105.
- Bouman, B.A.M., van Kasteren, H.W., 1990b. Ground-Based X-Band (3 cm Wave) Radar Backscattering of Agricultural Crops.2. Wheat, Barley and Oats; the Impact of canopy structure. *Remote Sens. Environ.* 34, 107–119.
- Bouman, B.A.M., van Kasteren, H.W.J., 1989. Ground based X-band radar backscatter measurements of wheat, barley and oats 1975-1981.
- Bovenga, F., Belmonte, A., Refice, A., Pasquariello, G., Nutricato, R., Nitti, D., Chiaradia, M., 2018. Performance analysis of satellite missions for multi-temporal SAR interferometry. *Sensors* 18, 1359.
- Branson, M., 2011. Using conservation agriculture and precision agriculture to improve a farming system, in: *Rainfed Farming Systems*. Springer, pp. 875–900.
- Brereton, R.G., Lloyd, G.R., 2010. Support vector machines for classification and regression. *Analyst* 135, 230–267.
- Brisson, N., Gary, C., Justes, E., Roche, R., Mary, B., Ripoche, D., Zimmer, D., Sierra,

Bibliography

- J., Bertuzzi, P., Burger, P., others, 2003. An overview of the crop model STICS. *Eur. J. Agron.* 18, 309–332.
- Brown, S.C.M., Quegan, S., Morrison, K., Bennett, J.C., Cookmartin, G., 2003. High-resolution measurements of scattering in wheat canopies-Implications for crop parameter retrieval. *IEEE Trans. Geosci. Remote Sens.* 41, 1602–1610.
- Brown, T.B., Hultine, K.R., Steltzer, H., Denny, E.G., Denslow, M.W., Granados, J., Henderson, S., Moore, D., Nagai, S., SanClements, M., Sánchez-Azofeifa, A., 2016. Using phenocams to monitor our changing Earth: toward a global phenocam network. *Front. Ecol. Environ.* 14, 84–93.
- Brune, P.F., Baumgarten, A., McKay, S.J., Technow, F., Podhiny, J.J., 2017. A biomechanical model for maize root lodging. *Plant Soil* 422, 397–408.
- Bunnik, N.J.J., 1978. The multispectral reflectance of shortwave radiation by agricultural crops in relation with their morphological and optical properties (Doctoral dissertation, Veenman). Veenman.
- Burkart, A., Aasen, H., Alonso, L., Menz, G., Bareth, G., Rascher, U., 2015. Angular dependency of hyperspectral measurements over wheat characterized by a novel UAV based goniometer. *Remote Sens.* 7, 725–746.
- Caldicott, J.J.B., 1966. The interaction of Cycocel 2-chloroethyltrimethylammonium chloride and nitrogen top dressing on the growth, lodging and yield of wheat, in: *Proc. 8th Brighton Weed Control Conf.*, November. pp. 229–239.
- Caldicott, J.J.B., Nuttall, A.M., 1979. A method for the assessment of lodging in cereal crops. *J. Natl. Inst. Agric. Bot.* 15, 88–91.
- Caldicott, J.J.B., Nuttall, A.M., 1968. The effects of combined applications of chlormequat and herbicides to cereals, in: *Proc. 9th Br. Weed Control Conf.* pp. 244–248.
- Campos-Taberner, M., García-Haro, F.J., Camps-Valls, G., Grau-Muedra, G., Nutini, F., Crema, A., Boschetti, M., 2016. Multitemporal and multiresolution leaf area index retrieval for operational local rice crop monitoring. *Remote Sens. Environ.* 187, 102–118.
- Canisius, F., Shang, J., Liu, J., Huang, X., Ma, B., Jiao, X., Geng, X., Kovacs, J.M., Walters, D., 2018. Tracking crop phenological development using multi-temporal polarimetric Radarsat-2 data. *Remote Sens. Environ.* 210, 508–518.
- Ceballos, F., Kramer, B., Robles, M., 2019. The feasibility of Picture-Based insurance (PBI): Smartphone pictures for affordable crop insurance. *Dev. Eng.* 4, 100042.
- Chalmers, A.G., Dyer, C.J., Sylvester-Bradley, R., 1998. Effects of nitrogen fertilizer on the grain yield and quality of winter oats. *J. Agric. Sci.* 131, 395–407.
- Chapman, S., Merz, T., Chan, A., Jackway, P., Hrabar, S., Dreccer, M., Holland, E., Zheng, B., Ling, T., Jimenez-Berni, J., 2014. Pheno-Copter: A low-altitude, autonomous remote-sensing robotic helicopter for high-throughput field-based phenotyping. *Agronomy* 4, 279–301.
- Charbonneau, F., Trudel, M., Fernandes, R., 2005. Use of Dual Polarization and Multi-Incidence SAR for soil permeability mapping. *Adv. Synth. Aperture Radar St-Hubert*, QC, Canada.
- Chauhan, S., Darvishzadeh, R., Boschetti, M., Nelson, A., 2020a. Estimation of crop angle of inclination for lodged wheat using multi-sensor SAR data. *Remote Sens. Environ.* 236, 111488.
- Chauhan, S., Darvishzadeh, R., Boschetti, M., Nelson, A., 2020b. Discriminant analysis for lodging severity classification in wheat using RADARSAT-2 and Sentinel-1

- data. *ISPRS J. Photogramm. Remote Sens.* 164, 138–151.
- Chauhan, S., Darvishzadeh, R., Boschetti, M., Pepe, M., Nelson, A., 2019a. Remote sensing-based crop lodging assessment: Current status and perspectives. *ISPRS J. Photogramm. Remote Sens.* 151, 124–140.
- Chauhan, S., Darvishzadeh, R., Lu, Y., Boschetti, M., Nelson, A., 2020c. Understanding wheat lodging using multi-temporal Sentinel-1 and Sentinel-2 data. *Remote Sens. Environ.* 243, 111804.
- Chauhan, S., Darvishzadeh, R., Lu, Y., Stroppiana, D., Boschetti, M., Pepe, M., Nelson, A., 2019b. Wheat lodging assessment using multispectral UAV data. *ISPRS - Int. Arch. Photogramm. Remote Sens. Spat. Inf. Sci. XLII-2/W13*, 235–240.
- Chauhan, S., Srivastava, H.S., Patel, P., 2019c. Crop Height Estimation Using RISAT-1 Hybrid-Polarized Synthetic Aperture Radar Data. *IEEE J. Sel. Top. Appl. Earth Obs. Remote Sens.* 12, 2928–2933.
- Chauhan, S., Srivastava, H.S., Patel, P., 2018. Wheat crop biophysical parameters retrieval using hybrid-polarized RISAT-1 SAR data. *Remote Sens. Environ.* 216, 28–43.
- Chen, J., Li, H., Han, Y., 2016. Potential of RADARSAT-2 data on identifying sugarcane lodging caused by typhoon. 5th Int. Conf. Agro-Geoinformatics, Agro-Geoinformatics 1–6.
- Chen, T., Guestrin, C., 2016. XGBoost: A scalable tree boosting system. *Proc. ACM SIGKDD Int. Conf. Knowl. Discov. Data Min.* 13-17-Aug, 785–794.
- Chu, T., Starek, M., Brewer, M., Murray, S., Pruter, L., 2017. Assessing lodging severity over an experimental maize (*Zea mays* L.) field using UAS images. *Remote Sens.* 9, 923.
- Clark, R.N., Roush, T.L., 1984. Reflectance spectroscopy: Quantitative analysis techniques for remote sensing applications. *J. Geophys. Res. Solid Earth* 89, 6329–6340.
- Clevers, J.G.P.W., 1986. Application of remote sensing to agricultural field trials. Clevers.
- Cloude, S.R., Pottier, E., 1997. An entropy based classification scheme for land applications of polarimetric SAR. *IEEE Trans. Geosci. Remote Sens.* 35, 68–78.
- Cloude, S.R., Pottier, E., 1996. A review of target decomposition theorems in radar polarimetry. *IEEE Trans. Geosci. Remote Sens.* 34, 498–518.
- Colombo, R., Bellingeri, D., Fasolini, D., Marino, C.M., 2003. Retrieval of leaf area index in different vegetation types using high resolution satellite data. *Remote Sens. Environ.* 86, 120–131.
- Comber, A., Fisher, P., Brunson, C., Khmag, A., 2012. Spatial analysis of remote sensing image classification accuracy. *Remote Sens. Environ.* 127, 237–246.
- Constantinescu, C.A., Herbei, M.V., Manea, D., Sala, F., 2017. Aanalysis of some deficiencies in crops of wheat and barley based on terrestrial and aerial images 49, 95–103.
- Coquil, B., 2004. FARMSTAR a fully operational system for crop management from satellite imagery, in: Mulla, D.J. (Ed.), *Proceedings of the 7th International Conference on Precision Agriculture and Other Precision Resources Management*, Hyatt Regency, Minneapolis, MN, USA, 25-28 July,.
- Coutts, M.P., 1983. Development of the structural root system of Sitka spruce. *For. An Int. J. For. Res.* 56, 1–16.
- Crook, M.J., Ennos, A.R., 2000. A field based method of quantifying the lodging

Bibliography

- resistance of wheat cultivars. *Plant Biomech.* 315–320.
- Crook, M.J., Ennos, A.R., 1995. The effect of nitrogen and growth-regulators on stem and root characteristics associated with lodging in 2 cultivars of winter-wheat. *J. Exp. Bot.* 46, 931–938.
- Crook, M.J., Ennos, A.R., 1994. Stem and root characteristics associated with lodging resistance in four winter wheat cultivars. *J. Agric. Sci.* 123, 167.
- Crook, M.J., Ennos, A.R., 1993. The mechanics of root lodging in winter wheat, *Triticum Aestivum* L. *J. Exp. Bot.* 44, 1219–1224.
- Cushnie, J.L., 1987. The interactive effect of spatial resolution and degree of internal variability within land-cover types on classification accuracies. *Int. J. Remote Sens.* 8, 15–29.
- Darvishi, M., Schlögel, R., Kofler, C., Cuozzo, G., Rutzinger, M., Zieher, T., Toschi, I., Remondino, F., Mejia-Aguilar, A., Thiebes, B., others, 2018. Sentinel-1 and ground-based sensors for continuous monitoring of the Corvara Landslide (South Tyrol, Italy). *Remote Sens.* 10, 1781.
- Darvishzadeh, R., Skidmore, A.K., Abdullah, H., Cherenet, E., Ali, A., Wang, T., Nieuwenhuis, W., Heurich, M., Vrieling, A., O'Connor, B., others, 2019a. Mapping leaf chlorophyll content from Sentinel-2 and RapidEye data in spruce stands using the invertible forest reflectance model. *Int. J. Appl. Earth Obs. Geoinf.* 79, 58–70.
- Darvishzadeh, R., Skidmore, A.K., Atzberger, C., van Wieren, S., 2008. Estimation of vegetation LAI from hyperspectral reflectance data: Effects of soil type and plant architecture. *Int. J. Appl. Earth Obs. Geoinf.* 10, 358–373.
- Darvishzadeh, R., Wang, T., Skidmore, A.K., Vrieling, A., O'Connor, B., Gara, T.W., Ens, B.J., Paganini, M., 2019b. Analysis of Sentinel-2 and RapidEye for retrieval of leaf area index in a saltmarsh using a radiative transfer model. *Remote Sens.* 11, 671.
- Davies, E.R., 2009. The application of machine vision to food and agriculture: a review. *Imaging Sci. J.* 57, 197–217.
- De Grandi, G.F., Leysen, M., Lee, J.S., Schuler, D., 1997. Radar reflectivity estimation using multiple SAR scenes of the same target: technique and applications, in: *IGARSS'97. 1997 IEEE International Geoscience and Remote Sensing Symposium Proceedings. Remote Sensing-A Scientific Vision for Sustainable Development.* pp. 1047–1050.
- Dente, L., Satalino, G., Mattia, F., Rinaldi, M., 2008. Assimilation of leaf area index derived from ASAR and MERIS data into CERES-Wheat model to map wheat yield. *Remote Sens. Environ.* 112, 1395–1407.
- Dickinson, J.L., Shirk, J., Bonter, D., Bonney, R., Crain, R.L., Martin, J., Phillips, T., Purcell, K., 2012. The current state of citizen science as a tool for ecological research and public engagement. *Front. Ecol. Environ.* 10, 291–297.
- Ding, Y., Zhao, X., Zhang, D., Liang, D., Wang, Z., Xi, S. hangjin., Du, S., 2019. Rice lodging area extraction based on YCbCr spatial and texture features, in: *IGARSS 2019-2019 IEEE International Geoscience and Remote Sensing Symposium.* pp. 9228–9231.
- Doraiswamy, P.C., Hatfield, J.L., Jackson, T.J., Akhmedov, B., Prueger, J., Stern, A., 2004. Crop condition and yield simulations using Landsat and MODIS. *Remote Sens. Environ.* 92, 548–559.
- Duy, P.Q., Abe, A., Hirano, M., Sagawa, S., Kuroda, E., 2004. Analysis of lodging-

- resistant characteristics of different rice genotypes grown under the standard and nitrogen-free basal dressing accompanied with sparse planting density practices. *Plant Prod. Sci.* 7, 243–251.
- Easson, D.L., White, E.M., Pickles, S.J., 1993. The effects of weather, seed rate and cultivar on lodging and yield in winter wheat. *J. Agric. Sci.* 121, 145–156.
- Eitel, J.U., Magney, T.S., Vierling, L.A., Greaves, H.E., Zheng, G., 2016. An automated method to quantify crop height and calibrate satellite-derived biomass using hypertechnical lidar. *Remote Sens. Environ.* 187, 414–422.
- Engdahl, M.E., Borgeaud, M., Rast, M., 2001. The use of ERS-1/2 Tandem interferometric coherence in the estimation of agricultural crop heights. *IEEE Trans. Geosci. Remote Sens.* 39, 1799–1806.
- Erten, E., Lopez-Sanchez, J.M., Yuzugullu, O., Hajnsek, I., 2016. Retrieval of agricultural crop height from space: A comparison of SAR techniques. *Remote Sens. Environ.* 187, 130–144.
- ESA, 2015. SENTINEL-2 User Handbook.
- Estes, L.D., Reillo, P.R., Mwangi, A.G., Okin, G.S., Shugart, H.H., 2010. Remote sensing of structural complexity indices for habitat and species distribution modeling. *Remote Sens. Environ.* 114, 792–804.
- Evans, D.L., Farr, T.G., Van Zyl, J.J., Zebker, H.A., 1988. Radar polarimetry: analysis tools and applications. *IEEE Trans. Geosci. Remote Sens.* 26, 774–789.
- Fang, H., Liang, S., Hoogenboom, G., Teasdale, J., Cavigelli, M., 2008. Corn-yield estimation through assimilation of remotely sensed data into the CSM-CERES-Maize model. *Int. J. Remote Sens.* 29, 3011–3032.
- Fang, H., Liang, S., Kuusk, A., 2003. Retrieving leaf area index using a genetic algorithm with a canopy radiative transfer model. *Remote Sens. Environ.* 85, 257–270.
- FAO, T., 2014. The state of food and agriculture: Innovation in family farming [WWW Document]. Rome FAO. URL <http://www.fao.org/publications/sofa/2014/en/> (accessed 5.6.19).
- Farghaly, D., Urban, B., Sörgel, U., Elba, E., 2019. Differentiating forest types using TerraSAR-X spotlight images based on inferential statistics and multivariate analysis. *Remote Sens. Appl. Soc. Environ.* 100238.
- Faurtyot, T., Baret, F., 1997. Vegetation water and dry matter contents estimated from top-of-the-atmosphere reflectance data: a simulation study. *Remote Sens. Environ.* 61, 34–45.
- Fawcett, T., 2006. An introduction to ROC analysis. *Pattern Recognit. Lett.* 27, 861–874.
- Ferrazzoli, P., 2002. SAR for agriculture: Advances, problems and prospects, in: *Retrieval of Bio-and Geo-Physical Parameters from SAR Data for Land Applications*. pp. 47–56.
- Ferrazzoli, P., Paloscia, S., Pampaloni, P., Schiavon, G., Sigismondi, S., Solimini, D., 1997. The potential of multifrequency polarimetric SAR in assessing agricultural and arboreal biomass. *IEEE Trans. Geosci. Remote Sens.* 35, 5–17.
- Fischer, R.A., Stapper, M., 1987. Lodging effects on high-yielding crops of irrigated semidwarf wheat. *F. Crop. Res.* 17, 245–258.
- Fitch, B.W., Walraven, R.L., Bradley, D.E., 1984. Polarization of light reflected from grain crops during the heading growth stage. *Remote Sens. Environ.* 15, 263–268.
- Forkuor, G., Conrad, C., Thiel, M., Ullmann, T., Zoungrana, E., 2014. Integration of

- optical and Synthetic Aperture Radar imagery for improving crop mapping in Northwestern Benin, West Africa. *Remote Sens.* 6, 6472–6499.
- Frazer, G.W., Magnussen, S., Wulder, M.A., Niemann, K.O., 2011. Simulated impact of sample plot size and co-registration error on the accuracy and uncertainty of LiDAR-derived estimates of forest stand biomass. *Remote Sens. Environ.* 115, 636–649.
- Freeman, A., Durden, S.L., 1998. A three-component scattering model for polarimetric SAR data. *IEEE Trans. Geosci. Remote Sens.* 36, 963–973.
- Freeman, A., Villasenor, J., Klein, J.D., Hoogeboom, P., Groot, J., 1994. On the use of multi-frequency and polarimetric radar backscatter features for classification of agricultural crops. *Int. J. Remote Sens.* 15, 1799–1812.
- Fritz, S., McCallum, I., Schill, C., Perger, C., Grillmayer, R., Achard, F., Kraxner, F., Obersteiner, M., 2009. Geo-Wiki. Org: The use of crowdsourcing to improve global land cover. *Remote Sens.* 1, 345–354.
- Funk, C., Budde, M.E., 2009. Phenologically-tuned MODIS NDVI-based production anomaly estimates for Zimbabwe. *Remote Sens. Environ.* 113, 115–125.
- Gallego, F.J., Kussul, N., Skakun, S., Kravchenko, O., Shelestov, A., Kussul, O., 2014. Efficiency assessment of using satellite data for crop area estimation in Ukraine. *Int. J. Appl. Earth Obs. Geoinf.* 29, 22–30.
- Gallego, J., Craig, M., Michaelsen, J., Bossyns, B., Fritz, S., 2008. Best practices for crop area estimation with remote sensing, Ispra: Joint Research Center.
- Galtier, O., Abbas, O., Le Dréau, Y., Rebufa, C., Kister, J., Artaud, J., Dupuy, N., 2011. Comparison of PLS1-DA, PLS2-DA and SIMCA for classification by origin of crude petroleum oils by MIR and virgin olive oils by NIR for different spectral regions. *Vib. Spectrosc.* 55, 132–140.
- Gao, F., Morisette, J.T., Wolfe, R.E., Ederer, G., Pedelty, J., Masuoka, E., Myneni, R., Tan, B., Nightingale, J., 2008. An algorithm to produce temporally and spatially continuous MODIS-LAI time series. *IEEE Geosci. Remote Sens. Lett.* 5, 60–64.
- Gao, S., Niu, Z., Huang, N., Hou, X., 2013. Estimating the Leaf Area Index, height and biomass of maize using HJ-1 and RADARSAT-2. *Int. J. Appl. Earth Obs. Geoinf.* 24, 1–8.
- Gerten, D.M., Wiese, M.V., 1987. Microcomputer-assisted video image analysis of lodging in winter wheat. *Photogramm. Eng. Remote Sens.* 53, 83–88.
- Gherboudj, I., Magagi, R., Berg, A.A., Toth, B., 2011. Soil moisture retrieval over agricultural fields from multi-polarized and multi-angular RADARSAT-2 SAR data. *Remote Sens. Environ.* 115, 33–43.
- Ghosh, S.M., Behera, M.D., Paramanik, S., 2020. Canopy Height Estimation Using Sentinel Series Images through Machine Learning Models in a Mangrove Forest. *Remote Sens.* 12, 1519.
- Gitelson, A.A., Gritz, Y., Merzlyak, M.N., 2003. Relationships between leaf chlorophyll content and spectral reflectance and algorithms for non-destructive chlorophyll assessment in higher plant leaves. *J. Plant Physiol.* 160, 271–282.
- Gorelick, N., Hancher, M., Dixon, M., Ilyushchenko, S., Thau, D., Moore, R., 2017. Google Earth Engine: Planetary-scale geospatial analysis for everyone. *Remote Sens. Environ.* 202, 18–27.
- Green, C.F., Ivins, J.D., 1985. Time of sowing and the yield of winter wheat. *J. Agric. Sci.* 104, 235–238.
- Gu, X., Sun, Q., Yang, G., Song, X., Xu, X., 2019. Monitoring maize lodging disaster

- via multi-temporal remote sensing images, in: IGARSS 2019-2019 IEEE International Geoscience and Remote Sensing Symposium. pp. 7302–7305.
- Han, D., Yang, H., Yang, G., Qiu, C., 2017. Monitoring model of corn lodging based on Sentinel-1 radar image, in: SAR in Big Data Era: Models, Methods and Applications (BIGSAR DATA), 2017. pp. 1–5.
- Han, L., Yang, G., Feng, H., Zhou, C., Yang, H., Xu, B., Li, Z., Yang, X., 2018. Quantitative identification of maize lodging-causing feature factors using unmanned aerial vehicle images and a nomogram computation. *Remote Sens.* 10, 1528.
- Hanley, F., Jarvis, R.H., Whitear, J.D., 1961. The effects of time of ploughing and time of drilling on the development and yield of the winter wheat crop following a clover ley. *J. Agric. Sci.* 56, 119–125.
- Hansen, P.M., Schjoerring, J.K., 2003. Reflectance measurement of canopy biomass and nitrogen status in wheat crops using normalized difference vegetation indices and partial least squares regression. *Remote Sens. Environ.* 86, 542–553.
- Harfenmeister, K., Spengler, D., Weltzien, C., 2019. Analyzing temporal and spatial characteristics of crop parameters using Sentinel-1 backscatter data. *Remote Sens.* 11, 1569.
- HGCA, 2005. Lodging in winter wheat-Practical guidelines.
- Hoekman, D.H., Bouman, B.A.M., 1993. Interpretation of C- and X-band radar images over an agricultural area, the Flevoland test site in the Agriscatt-87 campaign. *Int. J. Remote Sens.* 14, 1577–1594.
- Holloway, J., Mengersen, K., 2018. Statistical machine learning methods and remote sensing for sustainable development goals: A review. *Remote Sens.* 10, 1365.
- Holman, F.H., Riche, A.B., Michalski, A., Castle, M., Wooster, M.J., Hawkesford, M.J., 2016. High throughput field phenotyping of wheat plant height and growth rate in field plot trials using UAV based remote sensing. *Remote Sens.* 8, 1031.
- Hong, S., Lakshmi, V., Small, E.E., 2007. Relationship between vegetation biophysical properties and surface temperature using multisensor satellite data. *J. Clim.* 20, 5593–5606.
- Hosoi, F., Omasa, K., 2012. Estimation of vertical plant area density profiles in a rice canopy at different growth stages by high-resolution portable scanning lidar with a lightweight mirror. *ISPRS J. Photogramm. Remote Sens.* 74, 11–19.
- Huang, Y., Thomson, S.J., Ortiz, B.V., Reddy, K.N., Ding, W., Zablutowicz, R.M., Bright, J.R., 2010. Airborne remote sensing assessment of the damage to cotton caused by spray drift from aerially applied glyphosate through spray deposition measurements. *Biosyst. Eng.* 107, 212–220.
- Hufkens, K., Melaas, E.K., Mann, M.L., Foster, T., Ceballos, F., Robles, M., Kramer, B., 2019. Monitoring crop phenology using a smartphone based near-surface remote sensing approach. *Agric. For. Meteorol.* 265, 327–337.
- Hunt, E.R., Cavigelli, M., Daughtry, C.S.T., McMurtrey, J.E., Walthall, C.L., 2005. Evaluation of digital photography from model aircraft for remote sensing of crop biomass and nitrogen status. *Precis. Agric.* 6, 359–378.
- Islam, M.S., Peng, S., Visperas, R.M., Ereful, N., Bhuiya, M.S.U., Julfiquar, A.W., 2007. Lodging-related morphological traits of hybrid rice in a tropical irrigated ecosystem. *F. Crop. Res.* 101, 240–248.
- Jackson, R.D., 1986. Remote sensing of biotic and abiotic plant stress. *Annu. Rev. Phytopathol.* 24, 265–287.

Bibliography

- Jain, M., Srivastava, A.K., Joon, R.K., McDonald, A., Royal, K., Lisaius, M.C., Lobell, D.B., 2016. Mapping smallholder wheat yields and sowing dates using micro-satellite data. *Remote Sens.* 8, 860.
- James, R.A., Rivelli, A.R., Munns, R., von Caemmerer, S., 2002. Factors affecting CO₂ assimilation, leaf injury and growth in salt-stressed durum wheat. *Funct. plant Biol.* 29, 1393–1403.
- Jiao, X., Kovacs, J.M., Shang, J., McNairn, H., Walters, D., Ma, B., Geng, X., 2014. Object-oriented crop mapping and monitoring using multi-temporal polarimetric RADARSAT-2 data. *ISPRS J. Photogramm. Remote Sens.* 96, 38–46.
- Kar, S., Mandal, D., Bhattacharya, A., Adinarayana, J., 2017. Temporal analysis of Touzi parameters for wheat crop characterization using L-band AgriSAR 2006 data, in: 2017 IEEE International Geoscience and Remote Sensing Symposium (IGARSS). pp. 3909–3912.
- Karolis, V., Iuculano, T., Butterworth, B., 2011. Mapping numerical magnitudes along the right lines: Differentiating between scale and bias. *J. Exp. Psychol. Gen.* 140, 693.
- Keller, M., Schimel, D.S., Hargrove, W.W., Hoffman, F.M., 2008. A continental strategy for the National Ecological Observatory Network. *Front. Ecol. Environ.* 6, 282–284.
- Khabbazan, S., Vermunt, P., Steele-Dunne, S., Ratering Arntz, L., Marinetti, C., van der Valk, D., Iannini, L., Molijn, R., Westerdijk, K., van der Sande, C., 2019. Crop monitoring using Sentinel-1 data: a case study from The Netherlands. *Remote Sens.* 11, 1887.
- Kim, Y., Kimball, J.S., Didan, K., Henebry, G.M., 2014. Response of vegetation growth and productivity to spring climate indicators in the conterminous United States derived from satellite remote sensing data fusion. *Agric. For. Meteorol.* 194, 132–143.
- Kim, Y., van Zyl, J.J., 2009. A time-series approach to estimate soil moisture using polarimetric radar data. *IEEE Trans. Geosci. Remote Sens.* 47, 2519–2527.
- Kirby, E.J.M., 1967. The effect of plant density upon the growth and yield of barley. *J. Agric. Sci.* 68, 317–324.
- Kirby, E.J.M., Appleyard, M., Fellowes, G., 1985. Variation in development of wheat and barley in response to sowing date and variety. *J. Agric. Sci.* 104, 383–396.
- Kokaly, R.F., Clark, R.N., 1999. Spectroscopic determination of leaf biochemistry using band-depth analysis of absorption features and stepwise multiple linear regression. *Remote Sens. Environ.* 67, 267–287.
- Kong, E., Liu, D., Guo, X., Yang, W., Sun, J., Li, X., Zhan, K., Cui, D., Lin, J., Zhang, A., 2013. Anatomical and chemical characteristics associated with lodging resistance in wheat. *Crop J.* 1, 43–49.
- Kovalskyy, V., Roy, D.P., 2013. The global availability of Landsat 5 TM and Landsat 7 ETM+ land surface observations and implications for global 30 m Landsat data product generation. *Remote Sens. Environ.* 130, 280–293.
- Krogager, E., Boerner, W.M., Madsen, S.N., 1997. Feature-motivated Sinclair matrix (sphere/diplane/helix) decomposition and its application to target sorting for land feature classification, in: *Wideband Interferometric Sensing and Imaging Polarimetry*. pp. 144–155.
- Kruskal, W.H., Wallis, W.A., 1952. Use of ranks in one-criterion variance analysis. *J. Am. Stat. Assoc.* 47, 583–621.

- Kumar, P., Prasad, R., Gupta, D.K., Mishra, V.N., Vishwakarma, A.K., Yadav, V.P., Bala, R., Choudhary, A., Avtar, R., 2018. Estimation of winter wheat crop growth parameters using time series Sentinel-1A SAR data. *Geocarto Int.* 33, 942–956.
- Kumpumäki, T., Linna, P., Lipping, T., 2018. Crop lodging analysis from UAS orthophoto mosaic, Sentinel-2 image and crop yield monitor data, in: *IGARSS 2018-2018 IEEE International Geoscience and Remote Sensing Symposium*. pp. 7723–7726.
- Kussul, N., Skakun, S., Kravchenko, O., Shelestov, A., Gallego, J.F., Kussul, O., 2013. Application of satellite optical and SAR images for crop mapping and area estimation in Ukraine. *Int. J. Inf. Model. Anal.* 7, 203–211.
- Lang, Y.Z., Yang, X.D., Wang, M.E., Zhu, Q.S., 2012. Effects of lodging at different filling stages on rice yield and grain quality. *Rice Sci.* 19, 315–319.
- Larranaga, A., Alvarez-Mozos, J., Albizua, L., Peters, J., 2012. Backscattering behavior of rain-fed crops along the growing season. *IEEE Geosci. Remote Sens. Lett.* 10, 386–390.
- Laude, H.H., Pauli, A.W., 1956. Influence of lodging on yield and other characters in winter wheat1. *Agron. J.* 48, 452–455.
- Leamer, R.W., Noriega, J.R., Gerbermann, A.H., 1980. Reflectance of wheat cultivars as related to physiological growth stages 1. *Agron. J.* 72, 1029–1032.
- Lee, J.S., Pottier, E., 2017. *Polarimetric radar imaging: from basics to applications*. CRC press.
- Lemaire, G., Jeuffroy, M.H., Gastal, F., 2008. Diagnosis tool for plant and crop N status in vegetative stage. Theory and practices for crop N management. *Eur. J. Agron.* 28, 614–624.
- Li, P.F., Ma, B.L., Xiong, Y.C., 2018. Modern hexaploid wheat differs from diploid and tetraploid ancestors in the importance of stress tolerance versus stress avoidance. *Crop Pasture Sci.* 69, 265–277.
- Liu, H.Y., Yang, G.J., Zhu, H.C., 2014. The extraction of wheat lodging area in UAV's image using spectral and texture features. *Appl. Mech. Mater.* 651, 2390–2393.
- Liu, T., Li, R., Zhong, X., Jiang, M., Jin, X., Zhou, P., Liu, S., Sun, C., Guo, W., 2018. Estimates of rice lodging using indices derived from UAV visible and thermal infrared images. *Agric. For. Meteorol.* 252, 144–154.
- Liu, Z., Li, C., Wang, Y., Huang, W., Ding, X., Zhou, B., Wu, H., Wang, D., Shi, J., 2012. Comparison of Spectral Indices and Principal Component Analysis for Differentiating Lodged Rice Crop from Normal Ones, in: Li, D., Chen, Y. (Eds.), *Computer and Computing Technologies in Agriculture V*. Springer Berlin Heidelberg, Berlin, Heidelberg, pp. 84–92.
- Lobell, D.B., 2013. The use of satellite data for crop yield gap analysis. *F. Crop. Res.* 143, 56–64.
- Lopez-Sanchez, J.M., Ballester-Berman, J.D., 2009. Potentials of polarimetric SAR interferometry for agriculture monitoring. *Radio Sci.* 44, 1–20.
- Lopez-Sanchez, J.M., Cloude, S.R., Ballester-Berman, J.D., 2011. Rice phenology monitoring by means of SAR polarimetry at X-band. *IEEE Trans. Geosci. Remote Sens.* 50, 2695–2709.
- Macelloni, G., Paloscia, S., Pampaloni, P., Marliani, F., Gai, M., 2001. The relationship between the backscattering coefficient and the biomass of narrow and broad leaf crops. *IEEE Trans. Geosci. Remote Sens.* 39, 873–884.
- MacFarland, T.W., Yates, J.M., 2016. Kruskal–Wallis H-test for oneway analysis of

- variance (ANOVA) by ranks, in: *Introduction to Nonparametric Statistics for the Biological Sciences Using R*. Springer, pp. 177–211.
- Maes, W.H., Steppe, K., 2012. Estimating evapotranspiration and drought stress with ground-based thermal remote sensing in agriculture: a review. *J. Exp. Bot.* 63, 4671–4712.
- Mandal, D., Kumar, V., Ratha, D., Dey, S., Bhattacharya, A., Lopez-Sanchez, J.M., McNairn, H., Rao, Y.S., 2020. Dual polarimetric radar vegetation index for crop growth monitoring using sentinel-1 SAR data. *Remote Sens. Environ.* 247, 111954.
- Manfron, G., Delmotte, S., Busetto, L., Hossard, L., Ranghetti, L., Brivio, P.A., Boschetti, M., 2017. Estimating inter-annual variability in winter wheat sowing dates from satellite time series in Camargue, France. *Int. J. Appl. earth Obs. Geoinf.* 57, 190–201.
- Mardanisamani, S., Maleki, F., Hosseinzadeh Kassani, S., Rajapaksa, S., Duddu, H., Wang, M., Shirliffe, S., Ryu, S., Josuttis, A., Zhang, T., others, 2019. Crop lodging prediction from UAV-acquired images of wheat and canola using a DCNN augmented with handcrafted texture features, in: *Proceedings of the IEEE Conference on Computer Vision and Pattern Recognition Workshops*.
- Marinho, E., Vancutsem, C., Fasbender, D., Kayitakire, F., Pini, G., Pekel, J.F., 2014. From remotely sensed vegetation onset to sowing dates: Aggregating pixel-level detections into village-level sowing probabilities. *Remote Sens.* 6, 10947–10965.
- Martre, P., Jamieson, P.D., Semenov, M.A., Zyskowski, R.F., Porter, J.R., Triboi, E., 2006. Modelling protein content and composition in relation to crop nitrogen dynamics for wheat. *Eur. J. Agron.* 25, 138–154.
- Mascolo, L., Lopez-Sanchez, J.M., Vicente-Guijalba, F., Nunziata, F., Migliaccio, M., Mazzarella, G., 2016. A complete procedure for crop phenology estimation with PolSAR data based on the complex Wishart classifier. *IEEE Trans. Geosci. Remote Sens.* 54, 6505–6515.
- Mattia, F., Le Toan, T., Picard, G., Posa, F.I., D'Alessio, A., Notarnicola, C., Gatti, A.M., Rinaldi, M., Satalino, G., Pasquariello, G., 2003a. Multitemporal C-band radar measurements on wheat fields. *IEEE Trans. Geosci. Remote Sens.* 41, 1551–1560.
- Mattia, F., Le Toan, T., Picard, G., Posa, F.I., D'Alessio, A., Notarnicola, C., Gatti, A.M., Rinaldi, M., Satalino, G., Pasquariello, G., 2003b. Multitemporal C-band radar measurements on wheat fields. *IEEE Trans. Geosci. Remote Sens.* 41, 1551–1560. <https://doi.org/10.1109/TGRS.2003.813531>
- McNairn, H., Brisco, B., 2004. The application of C-band polarimetric SAR for agriculture: a review. *Can. J. Remote Sens.* 30, 525–542.
- McNairn, H., Champagne, C., Shang, J., Holmstrom, D., Reichert, G., 2009. Integration of optical and Synthetic Aperture Radar (SAR) imagery for delivering operational annual crop inventories. *ISPRS J. Photogramm. Remote Sens.* 64, 434–449.
- McNairn, H., Duguay, C., Brisco, B., Pultz, T.J., 2002. The effect of soil and crop residue characteristics on polarimetric radar response. *Remote Sens. Environ.* 80, 308–320.
- Meroni, M., Rossini, M., Guanter, L., Alonso, L., Rascher, U., Colombo, R., Moreno, J., 2009. Remote sensing of solar-induced chlorophyll fluorescence: Review of methods and applications. *Remote Sens. Environ.* 113, 2037–2051.
- Mi, C., Zhang, X., Li, S., Yang, J., Zhu, D., Yang, Y., 2011. Assessment of

- environment lodging stress for maize using fuzzy synthetic evaluation. *Math. Comput. Model.* 54, 1053–1060.
- Miglani, A., Ray, S.S., Vashishta, D.P., Parihar, J.S., 2011. Comparison of two data smoothing techniques for vegetation spectra derived from EO-1 Hyperion. *J. Indian Soc. Remote Sens.* 39, 443–453.
- Mitchard, E.T.A., Saatchi, S.S., White, L., Abernethy, K., Jeffery, K.J., Lewis, S.L., Collins, M., Lefsky, M.A., Leal, M.E., Woodhouse, I.H., 2012. Mapping tropical forest biomass with radar and spaceborne LiDAR in Lopé National Park, Gabon: overcoming problems of high biomass and persistent cloud. *Biogeosciences* 9, 179–191.
- Moran, M.S., Clarke, T.R., Inoue, Y., Vidal, A., 1994. Estimating crop water deficiency using the relation between surface minus air temperature and spectral vegetation index. *Remote Sens. Environ.* 49, 246–263.
- Moran, M.S., Hymer, D.C., Qi, J., Kerr, Y., 2002. Comparison of ERS-2 SAR and Landsat TM imagery for monitoring agricultural crop and soil conditions. *Remote Sens. Environ.* 79, 243–252.
- Moran, M.S., Inoue, Y., Barnes, E.M., 1997. Opportunities and limitations for image-based remote sensing in precision crop management. *Remote Sens. Environ.* 61, 319–346.
- Murakami, T., Yui, M., Amaha, K., 2012. Canopy height measurement by photogrammetric analysis of aerial images: Application to buckwheat (*Fagopyrum esculentum* Moench) lodging evaluation. *Comput. Electron. Agric.* 89, 70–75.
- Mutanga, O., Skidmore, A.K., 2004. Narrow band vegetation indices overcome the saturation problem in biomass estimation. *Int. J. Remote Sens.* 25, 3999–4014.
- Nafziger, E.D., Wax, L.M., Brown, C.M., 1986. Response of five winter wheat cultivars to growth regulators and increased nitrogen. *Crop Sci.* 26, 767–770.
- Narkhede, S., 2018. Understanding AUC-ROC Curve. *Towar. Data Sci.* 26.
- Nebiker, S., Annen, A., Scherrer, M., Oesch, D., 2008. A light-weight multispectral sensor for micro UAV—Opportunities for very high resolution airborne remote sensing. *Int. Arch. Photogramm. Remote Sens. Spat. Inf. Sci.* 37, 1193–1199.
- Neenan, M., Spencer-Smith, J.L., 1975. An analysis of the problem of lodging with particular reference to wheat and barley. *J. Agric. Sci.* 85, 495–507.
- Nelson, A., Boschetti, M., Manfron, G., Holecz, F., Collivignarelli, F., Gatti, L., Barbieri, M., Villano, L., Chandna, P., Setiyono, T., 2014a. Combining moderate-resolution time-series RS data from SAR and optical sources for rice crop characterisation: examples from Bangladesh, in: *Land Applications of Radar Remote Sensing*. InTech: Rijeka, Croatia, pp. 121–147.
- Nelson, A., Setiyono, T., Rala, A.B., Quicho, E.D., Raviz, J.V., Abonete, P.J., Maunahan, A.A., Garcia, C.A., Bhatti, H.M., Villano, L.S., Thongbai, P., Holecz, F., Barbieri, M., Collivignarelli, F., Gatti, L., Quilang, E.J.P., Mabalay, M.R.O., Mabalot, P.E., Barroga, M.I., Bacong, A.P., Detoito, N.T., Berja, G.B., Varquez, F., Wahyunto, Kuntjoro, D., Murdiyati, S.R., Pazhanivelan, S., Kannan, P., Nirmala Mary, P.C., Subramanian, E., Rakwatin, P., Intrman, A., Setapayak, T., Lertna, S., Minh, V.Q., Tuan, V.Q., Duong, T.H., Quyen, N.H., Van Kham, D., Hin, S., Veasna, T., Yadav, M., Chin, C., Ninh, N.H., 2014b. Towards an operational SAR-based rice monitoring system in Asia: Examples from 13 demonstration sites across Asia in the RIICE project. *Remote Sens.* 6, 10773–

- 10812.
- Niu, L., Feng, S., Ding, W., Li, G., 2016. Influence of speed and rainfall on large-scale wheat lodging from 2007 to 2014 in China. *PLoS One* 11, e0157677.
- Norberg, O.S., Mason, S.C., Lowry, S.R., 1988. Ethephon influence on harvestable yield, grain quality, and lodging of corn. *Agron. J.* 80, 768–772.
- Nottingham, T., User, N.E., 1998. Griffin, Jonathan Michael (1998) Understanding and assessing lodging risk in winter wheat. PhD thesis, University of Nottingham.
- Ogden, R.T., Miller, C.E., Takezawa, K., Ninomiya, S., 2002. Functional regression in crop lodging assessment with digital images. *J. Agric. Biol. Environ. Stat.* 7, 389–402.
- Oplinger, E.S., Wiersma, D., Grau, C.R., Kelling, K.A., 1967. Intensive wheat management.
- Oplinger, E.S., Wiersma, D.W., 1984. Belgian lodging rating system. *F. Crop.* 26, 7.
- Ozdogan, M., Yang, Y., Allez, G., Cervantes, C., 2010. Remote sensing of irrigated agriculture: Opportunities and challenges. *Remote Sens.* 2, 2274–2304.
- Pacifici, F., Chini, M., Emery, W.J., 2009. A neural network approach using multi-scale textural metrics from very high-resolution panchromatic imagery for urban land-use classification. *Remote Sens. Environ.* 113, 1276–1292.
- Patel, P., Srivastava, H.S., Panigrahy, S., Parihar, J.S., 2006. Comparative evaluation of the sensitivity of multi-polarized multi-frequency SAR backscatter to plant density. *Int. J. Remote Sens.* 27, 293–305.
- Peerbhay, K.Y., Mutanga, O., Ismail, R., 2013. Commercial tree species discrimination using airborne AISA Eagle hyperspectral imagery and partial least squares discriminant analysis (PLS-DA) in KwaZulu-Natal, South Africa. *ISPRS J. Photogramm. Remote Sens.* 79, 19–28.
- Picard, G., Toan, T.L., 2002. A multiple scattering model for C-band backscatter of wheat canopies. *J. Electromagn. Waves Appl.* 16, 1447–1466.
- Pichierri, M., Hajsek, I., Zwieback, S., Rabus, B., 2018. On the potential of Polarimetric SAR Interferometry to characterize the biomass, moisture and structure of agricultural crops at L-, C- and X-Bands. *Remote Sens. Environ.* 204, 596–616.
- Piñera-Chavez, F.J., Berry, P.M., Foulkes, M.J., Molero, G., Reynolds, M.P., 2016. Avoiding lodging in irrigated spring wheat. II. Genetic variation of stem and root structural properties. *F. Crop. Res.* 196, 64–74.
- Pinthus, M.J., 1974. Lodging in wheat, barley, and oats: the phenomenon, its causes, and preventive measures. *Adv. Agron.* 25, 209–263.
- Ploton, P., Barbier, N., Coutron, P., Antin, C.M., Ayyappan, N., Balachandran, N., Barathan, N., Bastin, J.-F., Chuyong, G., Dauby, G., others, 2017. Toward a general tropical forest biomass prediction model from very high resolution optical satellite images. *Remote Sens. Environ.* 200, 140–153.
- Pope, K.O., Rey-Benayas, J.M., Paris, J.F., 1994. Radar remote sensing of forest and wetland ecosystems in the Central American tropics. *Remote Sens. Environ.* 48, 205–219.
- Pope, K.O., Sheffner, E.J., Linthicum, K.J., Bailey, C.L., Logan, T.M., Kasischke, E.S., Birney, K., Njogu, A.R., Roberts, C.R., 1992. Identification of central Kenyan Rift Valley fever virus vector habitats with Landsat TM and evaluation of their flooding status with airborne imaging radar. *Remote Sens. Environ.* 40, 185–196.

- Potgieter, A.B., Lawson, K., Huete, A.R., 2013. Determining crop acreage estimates for specific winter crops using shape attributes from sequential MODIS imagery. *Int. J. Appl. Earth Obs. Geoinf.* 23, 254–263.
- Prasad, R., Pandey, A., Singh, K.P., Singh, V.P., Mishra, R.K., Singh, D., 2012. Retrieval of spinach crop parameters by microwave remote sensing with back propagation artificial neural networks: A comparison of different transfer functions. *Adv. Sp. Res.* 50, 363–370.
- Rabus, B., Wehn, H., Nolan, M., 2010. The importance of soil moisture and soil structure for InSAR phase and backscatter, as determined by FDTD modeling. *IEEE Trans. Geosci. Remote Sens.* 48, 2421–2429.
- Reynolds, M., Foulkes, J., Furbank, R., Griffiths, S., King, J., Murchie, E., Parry, M., Slafer, G., 2012. Achieving yield gains in wheat. *Plant. Cell Environ.* 35, 1799–1823.
- Roland, B., 2015. Business opportunities in Precision Farming: Will big data feed the world in the future? *Strateg. Consult. GmbH Automot. Competence Cent.*
- Sakamoto, T., Shibayama, M., Takada, E., Inoue, A., Morita, K., Takahashi, W., Miura, S., Kimura, A., 2010. Detecting seasonal changes in crop community structure using day and night digital images. *Photogramm. Engineering Remote Sens.* 76, 713–726. <https://doi.org/10.14358/PERS.76.6.713>
- Sakamoto, T., Yokozawa, M., Toritani, H., Shibayama, M., Ishitsuka, N., Ohno, H., 2005. A crop phenology detection method using time-series MODIS data. *Remote Sens. Environ.* 96, 366–374.
- Sangoi, L., Gracietti, M.A., Rampazzo, C., Bianchetti, P., 2002. Response of Brazilian maize hybrids from different eras to changes in plant density. *F. Crop. Res.* 79, 39–51.
- Schaepman, M.E., Ustin, S.L., Plaza, A.J., Painter, T.H., Verrelst, J., Liang, S., 2009. Earth system science related imaging spectroscopy-An assessment. *Remote Sens. Environ.* 113, S123–S137.
- Schlund, M., Erasmi, S., 2020. Sentinel-1 time series data for monitoring the phenology of winter wheat. *Remote Sens. Environ.* 246, 111814.
- Serrano-Cinca, C., Gutiérrez-Nieto, B., 2013. Partial least square discriminant analysis for bankruptcy prediction. *Decis. Support Syst.* 54, 1245–1255.
- Setter, T.L., Laureles, E.V., Mazaredo, A.M., 1997. Lodging reduces yield of rice by self-shading and reductions in canopy photosynthesis. *F. Crop. Res.* 49, 95–106.
- Shah, S.S., Chang, X., Martin, P., 2017. Effect of dose and timing of application of different plant growth regulators on lodging and grain yield of a Scottish landrace of barley (Bere) in Orkney, Scotland. *Int. J. Environ. Agric. Biotechnol.* 2.
- Shang, J., Liu, J., Poncos, V., Geng, X., Qian, B., Chen, Q., Dong, T., Macdonald, D., Martin, T., Kovacs, J., others, 2020. Detection of Crop Seeding and Harvest through Analysis of Time-Series Sentinel-1 Interferometric SAR Data. *Remote Sens.* 12, 1551.
- Sher, A., Khan, A., Ashraf, U., Liu, H.H., Li, J.C., 2018. Characterization of the effect of increased plant density on canopy morphology and stalk lodging risk. *Front. Plant Sci.* 9, 1047.
- Shiferaw, B., Smale, M., Braun, H.J., Duveiller, E., Reynolds, M., Muricho, G., 2013. Crops that feed the world 10. Past successes and future challenges to the role played by wheat in global food security. *Food Secur.* 5, 291–317.
- Shu, M., Zhou, L., Gu, X., Ma, Y., Sun, Q., Yang, G., Zhou, C., 2019. Monitoring of

- maize lodging using multi-temporal Sentinel-1 SAR data. *Adv. Sp. Res.* 65, 470–480.
- Sims, D.A., Gamon, J.A., 2002. Relationships between leaf pigment content and spectral reflectance across a wide range of species, leaf structures and developmental stages. *Remote Sens. Environ.* 81, 337–354.
- Singha, M., Sarmah, S., 2019. Incorporating crop phenological trajectory and texture for paddy rice detection with time series MODIS, HJ-1A and ALOS PALSAR imagery. *Eur. J. Remote Sens.* 52, 73–87.
- Sisler, W.W., Olson, P.J., 1951. A study of methods of influencing lodging in barley and the effect of lodging upon yield and certain quality characteristics. *Sci. Agric.* 31, 177–186.
- Skrunes, S., Brekke, C., Jones, C.E., Espeseth, M.M., Holt, B., 2018. Effect of wind direction and incidence angle on polarimetric SAR observations of slicked and unslicked sea surfaces. *Remote Sens. Environ.* 213, 73–91.
- Sorenson, P.T., Small, C., Tappert, M.C., Quideau, S.A., Drozdowski, B., Underwood, A., Janz, A., 2017. Monitoring organic carbon, total nitrogen, and pH for reclaimed soils using field reflectance spectroscopy. *Can. J. Soil Sci.* 97, 241–248.
- Soria-Ruiz, J., Fernandez-Ordonez, Y., McNairn, H., 2009. Corn monitoring and crop yield using optical and microwave remote sensing, in: *Geoscience and Remote Sensing*. IntechOpen.
- Spink, J.H., Whaley, J., Wade, A., Sparkes, D., Foulkes, J., 2000. Prediction of optimum plant population in winter wheat. *HGCA Proj. Rep.* 234, 53.
- Sposaro, M.M., Berry, P.M., Sterling, M., Hall, A.J., Chimentì, C.A., 2010. Modelling root and stem lodging in sunflower. *F. Crop. Res.* 119, 125–134.
- Srivastava, H.S., Patel, P., Manchanda, M.L., Adiga, S., 2003. Use of multiincidence angle RADARSAT-1 SAR data to incorporate the effect of surface roughness in soil moisture estimation. *IEEE Trans. Geosci. Remote Sens.* 41, 1638–1640.
- Srivastava, H.S., Patel, P., Sharma, Y., Navalgund, R.R., 2009. Large-area soil moisture estimation using multi-incidence-angle RADARSAT-1 SAR data. *IEEE Trans. Geosci. Remote Sens.* 47, 2528–2535.
- Stanca, A., Jenkins, G., Hanson, P., 1979. Varietal responses in spring barley to natural and artificial lodging and to a growth regulator. *J. Agric. Sci. Cambridge* 93, 449–456.
- Stapper, M., Industry, C.P., Box, G.P.O., Act, C., 2007. High-Yielding Irrigated Wheat Crop Management. *Management* 1–30.
- Steele-Dunne, S.C., McNairn, H., Monsivais-Huertero, A., Judge, J., Liu, P.W., Papathanassiou, K., 2017. Radar remote sensing of agricultural canopies: A review. *IEEE J. Sel. Top. Appl. Earth Obs. Remote Sens.* 10, 2249–2273.
- Sterling, M., Baker, C.J., Berry, P.M., Wade, A., 2003. An experimental investigation of the lodging of wheat. *Agric. For. Meteorol.* 119, 149–165.
- Stiles, J.M., Sarabandi, K., Ulaby, F.T., 2000. Electromagnetic scattering from grassland. II. Measurement and modeling results. *IEEE Trans. Geosci. Remote Sens.* 38, 349–356.
- Stroppiana, D., Villa, P., Sona, G., Ronchetti, G., Candiani, G., Pepe, M., Busetto, L., Migliazzi, M., Boschetti, M., 2018. Early season weed mapping in rice crops using multi-spectral UAV data. *Int. J. Remote Sens.* 39, 5432–5452.
- Sullivan, D.G., Fulton, J.P., Shaw, J.N., Bland, G., 2007. Evaluating the sensitivity of an unmanned thermal infrared aerial system to detect water stress in a cotton

- canopy. *Trans. ASABE* 50, 1963–1969.
- Sun, C., Bian, Y., Zhou, T., Pan, J., 2019. Using of Multi-Source and Multi-Temporal Remote Sensing Data Improves Crop-Type Mapping in the Subtropical Agriculture Region. *Sensors* 19, 2401.
- Sun, H., Li, M.Z., Zhao, Y., Zhang, Y.E., Wang, X.M., Li, X.H., 2010. The spectral characteristics and chlorophyll content at winter wheat growth stages. *Spectrosc. Spectr. Anal.* 30, 192–196.
- Swets, J.A., 1988. Measuring the accuracy of diagnostic systems. *Science* (80-). 240, 1285–1293.
- Sylvester-Bradley, R., Scott, R.K., Wright, C.E., others, 1990. Physiology in the production and improvement of cereals. *HGCA Res. Rev.* 156.
- Tamm, T., Zalite, K., Voormansik, K., Talgre, L., 2016. Relating Sentinel-1 interferometric coherence to mowing events on grasslands. *Remote Sens.* 8, 802.
- Tarquini, S., Isola, I., Favalli, M., Mazzarini, F., Bisson, M., Pareschi, M.T., Boschi, E., 2007. TINITALY/01: a new triangular irregular network of Italy. *Ann. Geophys.* 50, 407–425.
- Thenkabail, P.S., Smith, R.B., De Pauw, E., 2000. Hyperspectral vegetation indices and their relationships with agricultural crop characteristics. *Remote Sens. Environ.* 71, 158–182.
- Torres-Barrán, A., Alonso, Á., Dorronsoro, J.R., 2019. Regression tree ensembles for wind energy and solar radiation prediction. *Neurocomputing* 326, 151–160.
- Touzi, R., 2007. Target scattering decomposition in terms of roll-invariant target parameters. *IEEE Trans. Geosci. Remote Sens.* 45, 73–84.
- Touzi, R., Lopes, A., Bruniquel, J., Vachon, P.W., 1999. Coherence estimation for SAR imagery. *IEEE Trans. Geosci. Remote Sens.* 37, 135–149.
- Tripathi, S.C., Sayre, K.D., Kaul, J.N., 2005. Planting systems on lodging behavior, yield components, and yield of irrigated spring bread wheat. *Crop Sci.* 45, 1448–1455.
- Tripathi, S.C., Sayre, K.D., Kaul, J.N., Narang, R.S., 2003. Growth and morphology of spring wheat (*Triticum aestivum* L.) culms and their association with lodging: effects of genotypes, N levels and ethephon. *F. Crop. Res.* 84, 271–290.
- Tsang, L., Kong, J.A., Shin, R.T., 1985. Theory of microwave remote sensing.
- Tuia, D., Verrelst, J., Alonso, L., Pérez-Cruz, F., Camps-Valls, G., 2011. Multioutput support vector regression for remote sensing biophysical parameter estimation. *IEEE Geosci. Remote Sens. Lett.* 8, 804–808.
- Ulaby, F.T., Allen, C.T., Eger Iii, G., Kanemasu, E., 1984. Relating the microwave backscattering coefficient to leaf area index. *Remote Sens. Environ.* 14, 113–133.
- van Delden, S.H., Vos, J., Ennos, A.R., Stomph, T.J., 2010. Analysing lodging of the panicle bearing cereal teff (*Eragrostis tef*). *New Phytol.* 186, 696–707.
- Van Roekel, R.J., Coulter, J.A., 2011. Agronomic responses of corn to planting date and plant density. *Agron. J.* 103, 1414–1422.
- Van Zyl, J.J., Arii, M., Kim, Y., 2011. Model-based decomposition of polarimetric SAR covariance matrices constrained for nonnegative eigenvalues. *IEEE Trans. Geosci. Remote Sens.* 49, 3452–3459.
- Vargas, J.Q., Khot, L.R., Peters, R.T., Chandel, A.K., Molaei, B., 2020. Low orbiting satellite and small UAS-based high-resolution imagery data to quantify crop lodging: A case study in irrigated spearmint. *IEEE Geosci. Remote Sens. Lett.* 17, 755–759.

Bibliography

- Veloso, A., Mermoz, S., Bouvet, A., Le Toan, T., Planells, M., Dejoux, J.-F., Ceschia, E., 2017. Understanding the temporal behavior of crops using Sentinel-1 and Sentinel-2-like data for agricultural applications. *Remote Sens. Environ.* 199, 415–426.
- Vreugdenhil, M., Wagner, W., Bauer-Marschallinger, B., Pfeil, I., Teubner, I., Rüdiger, C., Strauss, P., 2018. Sensitivity of Sentinel-1 backscatter to vegetation dynamics: An Austrian case study. *Remote Sens.* 10, 1396.
- Wang, C., Wu, J., Zhang, Y., Pan, G., Qi, J., Salas, W.A., 2009. Characterizing L-band scattering of paddy rice in southeast China with radiative transfer model and multitemporal ALOS/PALSAR imagery. *IEEE Trans. Geosci. Remote Sens.* 47, 988–998.
- Wang, D., Su, Y., Zhou, Q., Chen, Z., 2015. Advances in research on crop identification using SAR, in: 2015 Fourth International Conference on Agro-Geoinformatics (Agro-Geoinformatics). pp. 312–317.
- Wang, H., Magagi, R., Goniita, K., Trudel, M., McNairn, H., Powers, J., 2019. Crop phenology retrieval via polarimetric SAR decomposition and Random Forest algorithm. *Remote Sens. Environ.* 231, 111234.
- Wang, J.-J., Ge, H., Dai, Qigen, Ahmad, I., Dai, Qixing, Zhou, G., Qin, M., Gu, C., 2018. Unsupervised discrimination between lodged and non-lodged winter wheat: a case study using a low-cost unmanned aerial vehicle. *Int. J. Remote Sens.* 39, 2079–2088.
- Webster, J.R., Jackson, L.F., 1993. Management practices to reduce lodging and maximize grain yield and protein content of fall-sown irrigated hard red spring wheat. *F. Crop. Res.* 33, 249–259.
- Werness, S.A., Stuff, M.A., Fienup, J.R., 1990. Two-dimensional imaging of moving targets in SAR data, in: 1990 Conference Record Twenty-Fourth Asilomar Conference on Signals, Systems and Computers, 1990. p. 16.
- Whelehan, O.P., Earll, M.E., Johansson, E., Toft, M., Eriksson, L., 2006. Detection of ovarian cancer using chemometric analysis of proteomic profiles. *Chemom. Intell. Lab. Syst.* 84, 82–87.
- White, E.M., 1991. Response of winter barley cultivars to nitrogen and a plant growth regulator in relation to lodging. *J. Agric. Sci.* 116, 191–200.
- Wilke, N., Siegmann, B., Klingbeil, L., Burkart, A., Kraska, T., Muller, O., van Doorn, A., Heinemann, S., Rascher, U., 2019. Quantifying lodging percentage and lodging severity using a UAV-based canopy height model combined with an objective threshold approach. *Remote Sens.* 11, 515.
- Williams, G., 2011. Decision trees, in: *Data Mining with Rattle and R*. Springer, pp. 205–244.
- Wise, B.M., Gallagher, N.B., Bro, R., Shaver, J., Windig, W., Koch, R.S., 2007. PLS Toolbox 4.0. Eig. Res. Inc. Wenatchee, WA, USA 99–162.
- Wold, S., Sjöström, M., Eriksson, L., 2001. PLS-regression: a basic tool of chemometrics. *Chemom. Intell. Lab. Syst.* 58, 109–130.
- Wolter, P.T., Townsend, P.A., Sturtevant, B.R., 2009. Estimation of forest structural parameters using 5 and 10 meter SPOT-5 satellite data. *Remote Sens. Environ.* 113, 2019–2036.
- Wolter, P.T., Townsend, P.A., Sturtevant, B.R., Kingdon, C.C., 2008. Remote sensing of the distribution and abundance of host species for spruce budworm in Northern Minnesota and Ontario. *Remote Sens. Environ.* 112, 3971–3982.

- Wood, C.W., Reeves, D.W., Himelrick, D.G., 1993. Relationships between chlorophyll meter readings and leaf chlorophyll concentration, N status, and crop yield: a review, in: *Proceedings of the Agronomy Society of New Zealand*. pp. 1–9.
- Wood, D., McNairn, H., Brown, R.J., Dixon, R., 2002. The effect of dew on the use of RADARSAT-1 for crop monitoring: Choosing between ascending and descending orbits. *Remote Sens. Environ.* 80, 241–247.
- Wu, W., Huang, J., Cui, K., Nie, L., Wang, Q., Yang, F., Shah, F., Yao, F., Peng, S., 2012. Sheath blight reduces stem breaking resistance and increases lodging susceptibility of rice plants. *F. Crop. Res.* 128, 101–108.
- Wu, W., Ma, B.L., 2019. Erect leaf posture promotes lodging resistance in oat plants under high plant population. *Eur. J. Agron.* 103, 175–187.
- Wu, W., Ma, B.L., 2016. A new method for assessing plant lodging and the impact of management options on lodging in canola crop production. *Sci. Rep.* 6, 31890.
- Wu, W., Ma, B.L., Fan, J.J., Sun, M., Yi, Y., Guo, W.S., Voldeng, H.D., 2019. Management of nitrogen fertilization to balance reducing lodging risk and increasing yield and protein content in spring wheat. *F. Crop. Res.* 241, 107584.
- Xavier, A.C., Rudorff, B., Friedrich, T., Moreira, M.A., Alvarenga, B.S., Freitas, J.G., Salomon, M.V., 2006. Hyperspectral field reflectance measurements to estimate wheat grain yield and plant height. *Sci. Agric.* 63, 130–138.
- Xiao, Y., Liu, J., Li, H., Cao, X., Xia, X., Zhonghu, H.E., 2015. Lodging resistance and yield potential of winter wheat: effect of planting density and genotype. *Front. Agric. Sci. Eng.*
- Xu, J., Li, Z., Tian, B., Huang, L., Chen, Q., Fu, S., 2014. Polarimetric analysis of multi-temporal RADARSAT-2 SAR images for wheat monitoring and mapping. *Int. J. Remote Sens.* 35, 3840–3858.
- Xu, M.S., Zhang, F.L., Xia, Z.S., 2012. *The method and application in vegetation monitoring by radar*, Beijing: Science Press.
- Yamaguchi, Y., Moriyama, T., Ishido, M., Yamada, H., 2005. Four-component scattering model for polarimetric SAR image decomposition. *IEEE Trans. Geosci. Remote Sens.* 43, 1699–1706.
- Yan, W., Zhang, Y., Yang, T., Liu, X., 2019. A Microwave Scattering Model for Simulating the C-Band SAR Backscatter of Wheat Canopy. *Am. J. Remote Sens.* 7, 13–24.
- Yang, H., Chen, E., Li, Z., Zhao, C., Yang, G., Pignatti, S., Casa, R., Zhao, L., 2015. Wheat lodging monitoring using polarimetric index from RADARSAT-2 data. *Int. J. Appl. Earth Obs. Geoinf.* 34, 157–166.
- Yang, M.D., Huang, K.S., Kuo, Y.H., Tsai, H.P., Lin, L.M., 2017. Spatial and spectral hybrid image classification for rice lodging assessment through UAV imagery. *Remote Sens.* 9, 583.
- Yang, M.D., Tseng, H.H., Hsu, Y.C., Tsai, H.P., 2020. Semantic segmentation using deep learning with vegetation indices for rice lodging identification in multi-date UAV visible images. *Remote Sens.* 12, 633.
- Yuzugullu, O., Marelli, S., Erten, E., Sudret, B., Hajnsek, I., 2017. Determining rice growth stage with X-band SAR: A metamodel based inversion. *Remote Sens.* 9, 460.
- Zarco-Tejada, P.J., González-Dugo, V., Berni, J.A., 2012. Fluorescence, temperature and narrow-band indices acquired from a UAV platform for water stress detection using a micro-hyperspectral imager and a thermal camera. *Remote Sens. Environ.*

Bibliography

- 117, 322–337.
- Zeide, B., 1980. Plot size optimization. *For. Sci.* 26, 251–257.
- Zhang, C., Walters, D., Kovacs, J.M., 2014. Applications of low altitude remote sensing in agriculture upon farmers' requests-A case study in northeastern Ontario, Canada. *PLoS One* 9, 17–19.
- Zhang, L., Zhang, Z., Luo, Y., Cao, J., Tao, F., 2020. Combining optical, fluorescence, thermal satellite, and environmental data to predict county-level maize yield in China using machine learning approaches. *Remote Sens.* 12, 21.
- Zhang, M., Wang, H., Yi, Y., Ding, J., Zhu, M., Li, C., Guo, W., Feng, C., Zhu, X., 2017. Effect of nitrogen levels and nitrogen ratios on lodging resistance and yield potential of winter wheat (*Triticum aestivum* L.). *PLoS One* 12, e0187543.
- Zhang, X., Friedl, M.A., Schaaf, C.B., Strahler, A.H., Hodges, J.C.F., Gao, F., Reed, B.C., Huete, A., 2003. Monitoring vegetation phenology using MODIS. *Remote Sens. Environ.* 84, 471–475.
- Zhao, C., Liu, L., Wang, J., Huang, W., Song, X., Li, C., 2005. Predicting grain protein content of winter wheat using remote sensing data based on nitrogen status and water stress. *Int. J. Appl. Earth Obs. Geoinf.* 7, 1–9.
- Zhao, H., Song, X., Yang, G., Li, Z., Zhang, D., Feng, H., 2019. Monitoring of nitrogen and grain protein content in winter wheat based on Sentinel-2A data. *Remote Sens.* 11, 1724.
- Zhao, L., Yang, J., Li, P., Shi, L., Zhang, L., 2017. Characterizing lodging damage in wheat and canola using Radarsat-2 polarimetric SAR data. *Remote Sens. Lett.* 8, 667–675.
- Zhou, L., Cheng, S., Sun, Q., Gu, X., Yang, G., Shu, M., Feng, H., 2020. Remote sensing of regional-scale maize lodging using multitemporal GF-1 images. *J. Appl. Remote Sens.* 14, 1.
- Zhu, G., Li, G., Wang, D., Yuan, S., Wang, F., 2016. Changes in the lodging-related traits along with rice genetic improvement in China. *PLoS One* 11, e0160104.
- Zuo, R., Carranza, E.J.M., 2011. Support vector machine: a tool for mapping mineral prospectivity. *Comput. Geosci.* 37, 1967–1975.

Summary

Crop lodging: the permanent bending of the crop stem from its vertical position (stem lodging) or displacement of root anchorage (root lodging), is a major yield-reducing factor in cereal crops such as wheat. It can also delay harvest, increase drying costs and deteriorate grain quality in cereal crops, thus affecting the likelihood of achieving a premium price. Therefore, accurate spatio-temporal information about crop lodging and its susceptibility is critical for improving yield estimates, informing insurance loss adjusters and facilitate decision making.

The conventional measures to assess lodging are primarily based on visual inspection of crop health and the use of mechanistic mathematical models which can be time-consuming and challenging to apply over large areas. Remote sensing (RS) data can be a valuable supplement or even replacement to these conventional methods, delivering spatial and temporal information about crop lodging over synoptic scales. However, the use of RS for crop lodging assessment is still in a nascent stage. An understanding of the RS-based metrics derived from the satellite data and their utility for lodging detection, characterisation and susceptibility analysis was lacking in the literature. In this context, this PhD study aimed to address the problem of lodging assessment using RS satellite data from different sensors, including Sentinel-1, Sentinel-2 and multi-incidence angle RADARSAT-2 data.

We defined five objectives that aimed at investigating the potential of spaceborne RS data for lodging detection, its characterisation and susceptibility mapping in wheat. The first objective was to carry out a systematic literature review that could relate field/lab-based approaches to RS-based methods, review and identify the research gaps in existing RS-based crop lodging studies and provide perspectives for future research. Our review found only 22 peer-reviewed articles published between 1951-2018, most of which focused on qualitative analysis of lodging. The review also enabled us to identify several unanswered research questions. Building upon our findings from the review, the subsequent objectives characterized lodging in three ways: detecting lodging stages, classifying lodging severity and identifying the time of lodging incidence. The final objective dealt with susceptibility analysis. The second objective investigated the use of Sentinel-1, low incidence angle RADARSAT-2 and high incidence angle RADARSAT-2 data for estimating crop angle of inclination as an indicator of lodging stage (moderate, severe and very severe). Our results demonstrated the higher sensitivity of low incidence angle RADARSAT-2 data

($R^2_{cv} = 0.87$) for estimating crop angle of inclination and highlighted the importance of Sentinel-1 data for operational assessment of crop lodging stages. The third objective presented a SAR-based approach for the classification of lodging severity based on lodging score. We found that lodging severity was best classified using low incidence angle RADARSAT-2 (overall accuracy 72%) while the model developed using Sentinel-1 data could identify 60% of the lodging severity cases in the study site. The next objective examined the utility of dense time-series Sentinel-1 data in combination with multi-spectral Sentinel-2 data for identifying the time of lodging incidence in wheat. It also evaluated the effect of lodging on backscatter/coherence and spectral reflectance response. Our results showed that with the temporal analysis, it was possible to indicate a plausible window of the main lodging event and the red edge (740nm), NIR (865nm) and VH backscatter could best distinguish between healthy from lodged wheat. The last objective investigated the role of SAR data for estimating a safety factor against root lodging as an indicator of lodging susceptibility in wheat. We found that the safety factor correlated well with the lodging observed in the fields and was detectable using the satellite data (with 73-84% accuracy), confirming that it could be used as an early indicator of lodging susceptibility.

Overall, this study contributes to understanding and monitoring crop lodging using RS. Our findings show that SAR and optical satellite data-based metrics can capture a substantial proportion of the observed variation in lodging, which is important in the context of operational crop lodging assessment in particular, and sustainable agriculture in general.

Samenvatting

Gewassen-verbuiging: het permanent buigen van het gewas vanuit de verticale positie (stengelverbuiging) of verplaatsing van de wortelverbuiging (wortelverbuiging), is een belangrijke opbrengst-verlagende factor bij graangewassen zoals tarwe. Het kan ook de oogst vertragen, de droogkosten verhogen en de graankwaliteit in graangewassen verslechteren, waardoor de kans op het behalen van een premieprijs wordt aangetast. Daarom is nauwkeurige spatio-temporele informatie over gewas-verbuiging en de gevoeligheid ervan cruciaal voor het verbeteren van opbrengstschattingen, het informeren van schade-experts en het vergemakkelijken van besluitvorming.

De conventionele maatregelen om de gewassen-verbuiging te beoordelen zijn voornamelijk gebaseerd op visuele inspectie van de gezondheid van gewassen en het gebruik van mechanistische wiskundige modellen die tijdrovend en uitdagend kunnen zijn om toe te passen op grote oppervlakken. Remote sensing (RS) -gegevens kunnen een waardevolle aanvulling op of zelfs vervanging zijn van deze conventionele methoden, door ruimtelijke en tijdelijke informatie te leveren over de legering van gewassen op synoptische schalen. Het gebruik van RS voor de beoordeling van gewas-verbuiging bevindt zich echter nog in de kinderschoenen. In de literatuur ontbrak een begrip van de op RS gebaseerde metrieken die zijn afgeleid van de satellietgegevens en hun bruikbaarheid voor detectie, karakterisering en gevoeligheidsanalyse. In deze context was dit doctoraatsonderzoek gericht op het aanpakken van het probleem van verbuiging-beoordeling met behulp van RS-satellietgegevens van verschillende sensoren, waaronder Sentinel-1, Sentinel-2 en RADARSAT-2-gegevens met meerdere invalshoeken.

We hebben vijf doelstellingen gedefinieerd die gericht waren op het onderzoeken van het potentieel van RS-gegevens in de ruimte voor detectie van onderdak, de karakterisering ervan en het in kaart brengen van de gevoeligheid in tarwe. Het eerste doel was om een systematische literatuurstudie uit te voeren die veld / laboratorium-gebaseerde benaderingen zou kunnen relateren aan RS-gebaseerde methoden, de lacunes in het onderzoek in bestaande RS-gebaseerde gewas-verbuigingsstudies te beoordelen en te identificeren en perspectieven te bieden voor toekomstig onderzoek.

Onze review vond slechts 22 peer-reviewed artikelen gepubliceerd tussen 1951-2018, waarvan de meeste gericht waren op kwalitatieve analyse van verbuiging.

De review stelde ons ook in staat om enkele onbeantwoorde onderzoeksvragen te identificeren. Gebouwen op basis van onze bevindingen uit de beoordeling, kenmerkten de daaropvolgende doelstellingen het verbuiging op drie manieren: het detecteren van verbuigingsfasen, het classificeren van de ernst van het verbuiging en het identificeren van het tijdstip waarop het verbuiging plaatsvond. Het uiteindelijke doel betrof de gevoeligheidsanalyse. De tweede doelstelling onderzocht het gebruik van Sentinel-1, lage invalshoek RADARSAT-2 en hoge invalshoek RADARSAT-2 data voor het schatten van de hellingshoek van het gewas als een indicator van het verbuigingstadium (matig, ernstig en zeer ernstig). Onze resultaten toonden de hogere gevoeligheid aan van RADARSAT-2-gegevens met een lage invalshoek ($R2CV = 0,87$) voor het schatten van de hellingshoek van het gewas en benadrukten het belang van Sentinel-1-gegevens voor de operationele beoordeling van de stadia van de plaatsing van gewassen. De derde doelstelling presenteerde een SAR-gebaseerde benadering voor de classificatie van de ernst van de verbuiging op basis van de verbuiging-score. We ontdekten dat de ernst van de verbuiging het best werd geclassificeerd met behulp van de lage invalshoek RADARSAT-2 (totale nauwkeurigheid 72%), terwijl het model dat was ontwikkeld met behulp van Sentinel-1-gegevens 60% van de gevallen van de ernst van de verbuiging op de onderzoekslocatie kon identificeren.

De volgende doelstelling onderzocht het nut van dichte tijdreeksen Sentinel-1-gegevens in combinatie met multi-spectrale Sentinel-2-gegevens voor het identificeren van het tijdstip van verbuiging in tarwe. Het evalueerde ook het effect van verbuiging op backscatter / coherentie en spectrale reflectantierespons. Onze resultaten toonden aan dat het met de temporele analyse mogelijk was om een plausibel venster van de hoofdzakelijke verbuigings gebeurtenis aan te geven en dat de rode rand (740 nm), NIR (865 nm) en VH-terugverstrooiing het beste onderscheid konden maken tussen gezonde en ingediende tarwe. De laatste doelstelling onderzocht de rol van SAR-gegevens voor het schatten van een veiligheidsfactor tegen wortelvorming als indicator voor vatbaarheid voor verbuiging in tarwe. We ontdekten dat de veiligheidsfactor goed correleerde met de verbuiging die in de velden werd waargenomen en detecteerbaar was met behulp van de satellietgegevens (met een nauwkeurigheid van 73-84%), wat bevestigt dat deze factor kan worden gebruikt als een vroege indicator voor vatbaarheid voor verbuiging.

Over het algemeen draagt deze studie bij aan het begrijpen en monitoren van gewas-verbuiging met RS. Onze bevindingen tonen aan dat op SAR en optische satellietgegevens gebaseerde meetgegevens een substantieel deel van de waargenomen variatie in huisvesting kunnen vastleggen, wat belangrijk is in de context van de operationele beoordeling van gewas-verbuiging in het bijzonder en duurzame landbouw in het algemeen.

Multi-Author Declaration

Given below is a list of all the academic works (ISI journals and conference papers) that are the basis for this thesis. In all the publications, Sugandh Chauhan has been the primary author.

ISI Journal papers

1. **Chauhan, S., Darvishzadeh, R., Boschetti, M., Pepe, M., Nelson, A. (2019a). Remote sensing-based crop lodging assessment: Current status and perspectives. ISPRS J. Photogramm. Remote Sens. 151, 124–140. (Published)**

Sugandh Chauhan: Conceptualization, Methodology, Software, Validation, Formal analysis, Investigation, Data curation, Writing - Original Draft Preparation, Visualisation.

Roshanak Darvishzadeh: Conceptualization, Resources, Writing - Review & Editing, Project administration, Formal analysis, Supervision.

Mirco Boschetti: Conceptualization, Resources, Project administration, Writing - Review & Editing, Supervision.

Monica Pepe: Investigation, Writing - Review & Editing

Andrew Nelson: Conceptualization, Writing - Review & Editing, Project administration, Funding acquisition.

2. **Chauhan, S., Darvishzadeh, R., Boschetti, M., Nelson, A. (2020a). Estimation of crop angle of inclination for lodged wheat using multi-sensor SAR data. Remote Sens. Environ. 236, 111488. (Published)**

Sugandh Chauhan: Conceptualization, Methodology, Software, Validation, Formal analysis, Investigation, Data curation, Writing - Original Draft Preparation, Visualisation.

Roshanak Darvishzadeh: Conceptualization, Resources, Writing - Review & Editing, Project administration, Formal analysis, Supervision.

Mirco Boschetti: Conceptualization, Resources, Project administration, Writing - Review & Editing, Supervision.

Andrew Nelson: Conceptualization, Writing - Review & Editing, Project administration, Funding acquisition.

3. **Chauhan, S., Darvishzadeh, R., Boschetti, M., Nelson, A. (2020b). Discriminant analysis for lodging severity classification in wheat using RADARSAT-2 and Sentinel-1 data. ISPRS J. Photogramm. Remote Sens. 164, 138–151. (Published)**

Sugandh Chauhan: Conceptualization, Methodology, Software, Validation, Formal analysis, Investigation, Data curation, Writing - Original Draft Preparation, Visualisation.

Roshanak Darvishzadeh: Conceptualization, Resources, Writing - Review & Editing, Project administration, Formal analysis, Supervision.

Mirco Boschetti: Conceptualization, Resources, Project administration, Writing - Review & Editing, Supervision.

Andrew Nelson: Conceptualization, Writing - Review & Editing, Project administration, Funding acquisition.

4. **Chauhan, S., Darvishzadeh, R., Boschetti, M., Nelson, A. (2020c). Understanding wheat lodging using multi-temporal Sentinel-1 and Sentinel-2 data. Remote Sens. Environ. 243, 111804. (Published)**

Sugandh Chauhan: Conceptualization, Methodology, Software, Validation, Formal analysis, Investigation, Data curation, Writing - Original Draft Preparation, Visualisation.

Roshanak Darvishzadeh: Conceptualization, Resources, Writing - Review & Editing, Project administration, Formal analysis, Supervision.

Yi Lu: Formal analysis, Writing - Review & Editing.

Mirco Boschetti: Conceptualization, Resources, Project administration, Writing - Review & Editing, Supervision.

Andrew Nelson: Conceptualization, Writing - Review & Editing, Project administration, Funding acquisition.

5. **Chauhan, S., Darvishzadeh, R., van Delden, S.H., Boschetti, M., Nelson, A. (2020d). Mapping of wheat lodging susceptibility with Synthetic Aperture Radar data. Remote Sens. Environ. (Revisions Submitted)**

Sugandh Chauhan: Conceptualization, Methodology, Software, Validation, Formal analysis, Investigation, Data curation, Writing - Original Draft Preparation, Visualisation.

Roshanak Darvishzadeh: Conceptualization, Resources, Writing - Review & Editing, Project administration, Formal analysis, Supervision.

Sander H. van Delden: Conceptualization, Formal analysis, Writing - Review & Editing.

Mirco Boschetti: Conceptualization, Resources, Project administration, Writing - Review & Editing, Supervision.

Andrew Nelson: Conceptualization, Writing - Review & Editing, Project administration, Funding acquisition.

ISI conference papers

1. **Chauhan, S., Darvishzadeh, R., Lu, Y., Stroppiana, D., Boschetti, M., Pepe, M., Nelson, A. (2019b). Wheat lodging assessment using**

multispectral UAV data. ISPRS - *Int. Arch. Photogramm. Remote Sens. Spat. Inf. Sci.* XLII-2/W13, 235–240. (Published)

Sugandh Chauhan: Conceptualization, Methodology, Software, Validation, Formal analysis, Investigation, Data curation, Writing - Original Draft Preparation, Visualisation.

Roshanak Darvishzadeh: Conceptualization, Resources, Writing - Review & Editing, Project administration, Formal analysis, Supervision.

Yi Lu: Formal analysis, Writing - Review & Editing.

Daniela Stroppiana: Investigation, Writing - Review & Editing

Mirco Boschetti: Conceptualization, Resources, Project administration, Writing - Review & Editing, Supervision.

Monica Pepe: Investigation, Writing - Review & Editing

Andrew Nelson: Conceptualization, Writing - Review & Editing, Project administration, Funding acquisition.

2. **Chauhan, S., Darvishzadeh, R., Boschetti, M., Nelson, A. (2020e). Understanding of crop lodging induced changes in scattering mechanisms using RADARSAT-2 and Sentinel-1 derived metrics, in: *Int. Arch. Photogramm. Remote Sens. Spat. Inf. Sci.*, 43, 267-274. (Published)**

Sugandh Chauhan: Conceptualization, Methodology, Software, Validation, Formal analysis, Investigation, Data curation, Writing - Original Draft Preparation, Visualisation.

Roshanak Darvishzadeh: Conceptualization, Resources, Writing - Review & Editing, Project administration, Formal analysis, Supervision.

Mirco Boschetti: Conceptualization, Resources, Project administration, Writing - Review & Editing, Supervision.

Andrew Nelson: Conceptualization, Writing - Review & Editing, Project administration, Funding acquisition.

Biography



Sugandh was born on October 27, 1991 in the city Bijnor, Uttar Pradesh, India. She completed her Bachelor's degree (B.Tech.) in June 2014 in the field of Agricultural Information Technology from Anand Agriculture University, India. In August 2016, she received her Master's degree (M.Tech.) in Remote Sensing and Geographic Information Systems with the specialization in Sustainable Agriculture from Indian Institute of Remote Sensing (IIRS). In the same year, she was offered a four-year AiO doctoral position from the Faculty of Geo-Information Science and Earth Observation (ITC), University of Twente, the Netherlands. Her research interests lie in the use of SAR/optical remote sensing and geographic information systems for vegetation monitoring and she is continually striving for technological excellence in Earth Observation and providing sustainable solutions that address food security.